POLITECNICO DI MILANO

FACOLTÀ DI INGEGNERIA CIVILE, AMBIENTALE E TERRITORIALE

Corso di Laurea in Ingegneria per l'Ambiente e il Territorio

ANALISI DI INCERTEZZA DI UNA CASCATA DI MODELLI DA UN MODELLO AFFLUSSI-DEFLUSSI A UN MODELLO IDRAULICO MONODIMENSIONALE: IL CASO STUDIO DEL FIUME SENNE (BELGIO)

Relatore:
prof. ing. Rodolfo Soncini Sessa

Correlatori:
prof. ing. Ann van Griensven
prof. ing. Giuliano Di Baldassarre

Tesi di Laurea di:
Claudio AVELLA
Matr. 721010

Anno Accademico 2009/2010

9 CONCLUSIONS AND RECOMMENDATIONS 160

List of tables

List of figures

Abstract

Water utilization is influenced by water quality and quantity. Many hydraulic and hydrologic models have been developed to support water resources management and water quality analysis. In particular the need to integrate different aspects in one single project lead to the necessity of linking different models. Model output makes sense only if accompanied by a quantitative representation of the uncertainty. As hydrologic and water quality models are increasingly used to guide water resources policies, it is not appropriate to disregard the uncertainty in model performances. It is indeed important that decision makers appreciate the uncertainty in model output. Uncertainty sources are: model structure, parameter estimation, observed and unobserved input disturbances, uncertainty in output data used for calibration .When a model is linked to another, the uncertainty propagates and, because of that, it can become higher, in the passage from a model to the other. The uncertainty affecting models that are used to predict water quantity can, thus, propagate to water quality models that use the results of the former models.

This work is mainly focused on the analysis of the uncertainty affecting models. The objective is to find a simple and effective tool to represent the uncertainty and to propagate it through different models linked among each other. The case study is the Zenne river, Belgium, a highly polluted river that flows from the Walloon region to the Flemish region and Brussels. Innovative rehabilitation techniques are needed to improve its water quality. The outcomes of this work are: a model of a river basin that integrates hydrologic and hydraulic aspects to support the water quality modelling. Different models have been used (SWAT, HEC-RAS and KOSIM), each of them representing different parts of the system, where the description of different phenomena and systems is needed; a tool for the evaluation of the uncertainty in the model. In particular, the thesis focuses on the assessment of the observation uncertainty, uncertainty propagation and cascade of uncertainty from one model to another; a simple method to represent the uncertainty to propagate it.

1 ABSTRACT IN ITALIANO

Introduzione

L'uso di acqua a scopo potabile, industriale, per l'irrigazione o ricreazionale è influenzato sia dalla quantità di acqua disponibile che dalla qualità della stessa. La qualità dell'acqua è determinata sia dalla quantità che dalla tipologia e degli inquinanti rilasciati nei corpi idrici da sorgenti puntuali e/o diffuse. La modellazione idraulica e quella idrologica sono strumenti fondamentali per progetti di gestione delle risorse, difesa territoriale da eventi di piena, riabilitazione fluviale, miglioramento della qualità dell'acqua. Negli ultimi decenni molti modelli sono stati sviluppati con questo scopo. Inoltre la recente necessità di analizzare e valutare il comportamento dei sistemi sotto molteplici aspetti, al fine di ottenere una visione sistemica dei casi in analisi, ha portato, in molti casi, ad utilizzare diversi modelli, con funzioni diverse, accoppiandoli tra loro. Spesso accoppiare, integrare o combinare dei modelli significa utilizzare le serie di uscita di uno come dati in ingresso dell'altro. Questo porta inevitabilmente a propagare l'incertezza nel da un modello ad un altro: un modello è solo una rappresentazione della realtà, è dunque impossibile riuscire a tenere conto di tutti i processi che avvengono nel sistema reale e ricostruirli in modo completo. Questo si riflette in un errore dell'uscita del modello rispetto a quanto osservato nella realtà. Una quantificazione di questa incertezza diventa perciò fondamentale: i risultati di un modello hanno senso solo se accompagnati da un'analisi della loro affidabilità. Solo in tal modo risultano essere effettivamente credibili e utilizzabili dai decisori politici nei processi decisionali, visto l'uso crescente di modelli idrologici e di qualità dell'acqua per la gestione e regolazione della risorsa e per i piani di riabilitazione fluviale (Beck, 1987; Sharpley et al., 2002; Harmel and Smith, 2007).

Le fonti di incertezza che nei modelli idraulici, idrologici e di qualità dell'acqua sono:

Incertezza nella struttura del modello

Incertezza nella stima dei parametri

Incertezza nelle osservazioni, disturbi nei dati di input e incertezza dovuta a disturbi non osservati nel sistema.

Incertezza nelle osservazioni utilizzate per tarare il modello (e.g. dati di portata misurati) (Van Griensven, 2002; Shrestha, Solomatine, 2008).

Nel caso due o più modelli siano accoppiati o combinati, la rappresentazione dell'incertezza diventa ancora più importante, in quanto essa si propaga da un modello all'altro con il rischio che aumenti di magnitudine. L'incertezza risultante nei modelli di portata (idraulici e idrologici) si propaga poi a modelli di qualità dell'acqua.

Lo scopo di questo lavoro di tesi è quello di costruire due modelli, uno idrologico, afflussi-deflussi a scala di bacino, e uno idraulico monodimensionale ed effettuarne un'analisi di incertezza dei due modelli accoppiati. I due modelli sono accoppiati in modo che le serie di uscita del modello a scala di bacino vengano usate come serie di dati in ingresso al modello idraulico monodimensionale. Il caso di

studio è il fiume Zenne , in Belgio, un fiume altamente inquinato che scorre dalla regione vallona a quella fiamminga, attraverso la città di Bruxelles, prima di confluire nel fiume Dijle, un affluente del fiume Scheldt. Un progetto che coinvolge il centro UNESCO-IHE Institute for Water Education e l'Università Vrije di Bruxelles è stato avviato allo scopo di studiare tecniche innovative di miglioramento della qualità dell'acqua.

Gli obiettivi di questo lavoro possono perciò essere riassunti in:

Costruire un modello del bacino che integri aspetti idrologici e idraulici e che siano da supporto ad un modello di qualità dell'acqua.

Costruire uno strumento per la valutazione dell'incertezza del modello. In particolare la tesi è focalizzata sulla propagazione dell'incertezza in una cascata di modelli. Allo scopo si propone una rappresentazione semplice dell'incertezza, in modo da facilitare la propagazione da un modello al seguente.

I principali risultati del lavoro sono:

Un modello idrologico afflussi-deflussi a scala di bacino: il modello è stato costruito per tutti i sottobacini ubicati nella regione fiamminga. Come codice è stato utilizzato Soil and Water Assessment Tool (SWAT). Il modello riceve in ingresso dati di precipitazioni, portate in ingresso dal sistema fognario della città di Bruxelles e presenta una condizione al contorno di monte: portate in ingresso dai sottobacini ubicati nella regione vallona

Modello monodimensionale degli ultimi 25 km del fiume: un modello monodimensionale è una buona rappresentazione dell'ultimo tratto di fiume, che è pensile. È stato utilizzato il codice HEC-RAS. Questo modello riceve, come unico ingresso e come condizione al contorno di monte, le uscite del modello SWAT: la sezione di chiusura del modello SWAT è localizzata in corrispondenza del punto dove è localizzata la condizione al contorno di questo modello.

Identificazione delle fonti di incertezza: Le sorgenti di incertezza sono state individuate e quantificate. L'attenzione è stata particolarmente rivolta all'incertezza nella scelta dei parametri e quella da cui sono affetti i dati di input del modello. Un modello dell'errore presente nei dati di portate in ingresso è stato costruito.

Calibrazione dei modelli: la calibrazione dei modelli è basata sul concetto di equifinalità: non esiste un solo set di parametri soddisfacente, ma ne esistono molti. I set di parametri vengono campionati con metodo Monte Carlo nello spazio dei parametri. Le simulazioni vengono poi valutate attraverso una funzione obiettivo da minimizzare. Attraverso metodi statistici vengono scelte le simulazioni "buone".

Analisi dell'incertezza dei sue modelli: l'analisi ha tenuto conto dell'incertezza nei set di parametri e nei dati di input, focalizzando l'attenzione sui dati di afflussi:

Prima è stata calcolata l'incertezza dovuta ai parametri: le simulazioni "buone" sono state pesate attraverso il valore della loro funzione obiettivo e una banda di confidenza con probabilità pari al 95% è stata costruita.

L'incertezza dovuta ai dati di ingresso è stata valutata sporcando le serie in ingresso con l'errore valutato precedentemente. Tutti i set di parametri soddisfacenti sono stati utilizzati per simulare il

modello con un elevato numero di serie di ingresso "sporcate". La banda di confidenza è stata dunque aggiornata.

Il modello SWAT e quello HEC-RAS sono stati calibrati e la loro incertezza analizzata dapprima indipendentemente l'uno dall'altro. Il risultato è una rappresentazione semplificata dell'incertezza del modello afflussi-deflussi. Questa rappresentazione e quantificazione dell'incertezza ha permesso di propagare in maniera facile l'incertezza al modello idraulico, tenendo conto di diverse fonti di incertezza.

Analisi di sensitività del parametro di calibrazione del modello HEC-RAS: l'unico parametro di calibrazione del modello HEC-RAS è il coefficiente di scabrezza di Mannning. Un'analisi di sensitività di questo parametro rispetto all'errore nelle serie in ingresso mostra che il valore effettivo di questo parametro, che non corrisponde a quello del sistema reale, è in grado di compensare incertezze elevate sia nella rappresentazione geometrica del fiume che nei dati di ingresso al modello.

Calibrazione e analisi di incertezza del modello combinato: Il modello HEC-RAS è stato alimentato con le serie di uscita del modello SWAT. La simulazione migliore del modello SWAT è stata utilizzata per la calibrazione e la validazione del modello. L'incertezza è stata ricalcolata utilizzando i percentili della banda di incertezza calcolata nel modello SWAT.

Il risultato di questo lavoro verrà utilizzato per gli studi in corso all'Università Vrije di Bruxelles e all'UNESCO-IHE Institute for Water Education di Delft. Il modello SWAT dei sottobacini nella regione Fiamminga verrà integrato con i modelli della regione Vallona e con un nuovo modello della citèa di Bruxelles e degli impianti di trattamento delle acque di rifiuto. I modelli di qualità dell'acqua verranno aggiunti ai modelli quantitativi costruiti. Il modello idraulico verrà utilizzato per il supporto a uno studio sull'impatto di un distretto industriale a Nord di Bruxelles sulla qualità dell'acqua del fiume.

1.1 Il fiume Zenne

Il bacino del fiume Zenne si situa in Belgio a ridosso delle regioni vallona, fiamminga e di Bruxelles. Scorre in direzione Sud-Nord dalla regione vallona a quella fiamminga. Il fiume sbocca nel Dijle, affluente del fiume Scheldt.

Figure 1 Mappa del belgio - In evidenza il fiume Zenne

Il bacino si estende su un'area di circa 1011 km^2, di cui 564 km^2 nella regione vallona, 162 km^2 in quella di Bruxelles e 286 km^2 in quella fiamminga. Il bacino si trova ad un'altezza compresa tra i 9 e i 170 m sopra il livello del mare. La portata è mediamente di 8 m^3/s e la pendenza media del letto è circa 0.2-0.5% (Van Griensven, 2002). L'area del bacino ubicata nella regione vallona può essere suddivisa in 8 sottobacini, mentre quella nella regione fiamminga e nella regione di Bruxelles in 12. La regione fiamminga è prevalentemente agricola, mentre la città di Bruxelles è, ovviamente, urbanizzata. Il tipo di suolo è prevalentemente argilloso. In figura 2 è riportata una mappa dell'intero bacino. I sottobacini in verde sono quelli ubicati nella regione fiamminga. L'ultimo tratto di fiume, di circa 25 km è pensile perciò lo scorrimento superficiale non influisce sulle portate.

Il fiume riceve in afflusso, annualmente, tra i 650 mm e gli 800 mm di piogge e 0.17 km^3/anno di acqua dal sistema fognario di Bruxelles.

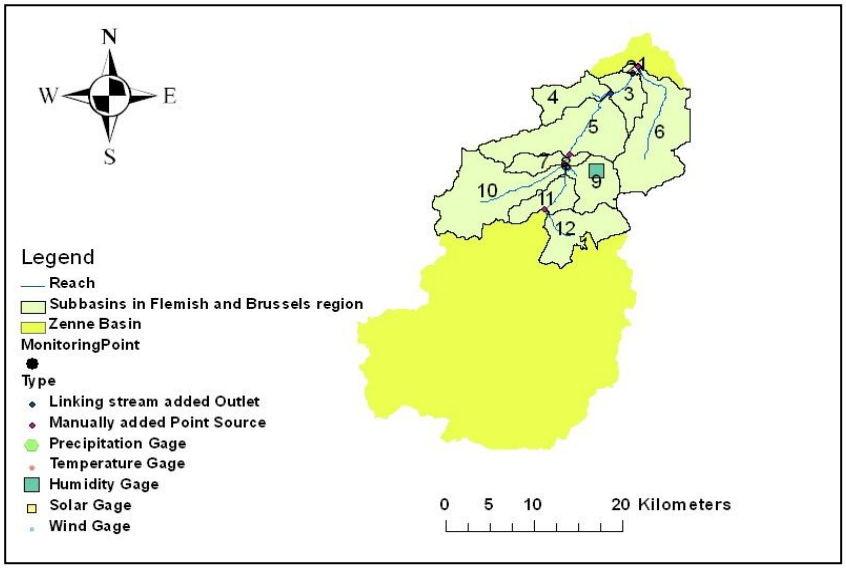

Figure 2 Il bacino del fiume Zenne

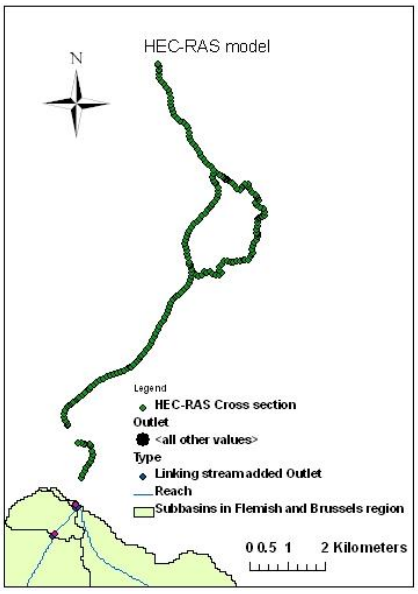

Figure 3 Ultimo tratto del fiume Zenne, 25km.

Nella regione di Bruxelles lo scorrimento superficiale viene generato soprattutto su suoli impermeabili urbanizzati e viene poi scaricato nel fiume attraverso il sistema fognario. Il sistema fognario di tipo misto è diviso in tre sottositemi: il sistema fognario Sud, quello Nord e Woluwe.

Le tre aree del bacino prese in considerazione in questo studio sono: i sottobacini ubicati nella regione fiamminga, quelli ubicati nella regione di Bruxelles e l'ultimo tratto di fiume, pensile. In figura 4 è riportata una rappresentazione schematica dei sottosistemi. I sottobacini nella regione fiamminga ricevono afflussi dalla regione vallona in corrispondenza della stazione Lot e in tre punti dal sistema fognario di Bruxelles. La sezione di chiusura di questa parte del bacino si trova in corrispondenza della stazione di Vilvoorde. In questa stazione è ubicato anche il punto in cui inizia il terzo sottosistema, il tratto di fiume pensile, dunque anche la sua condizione al contorno di monte.

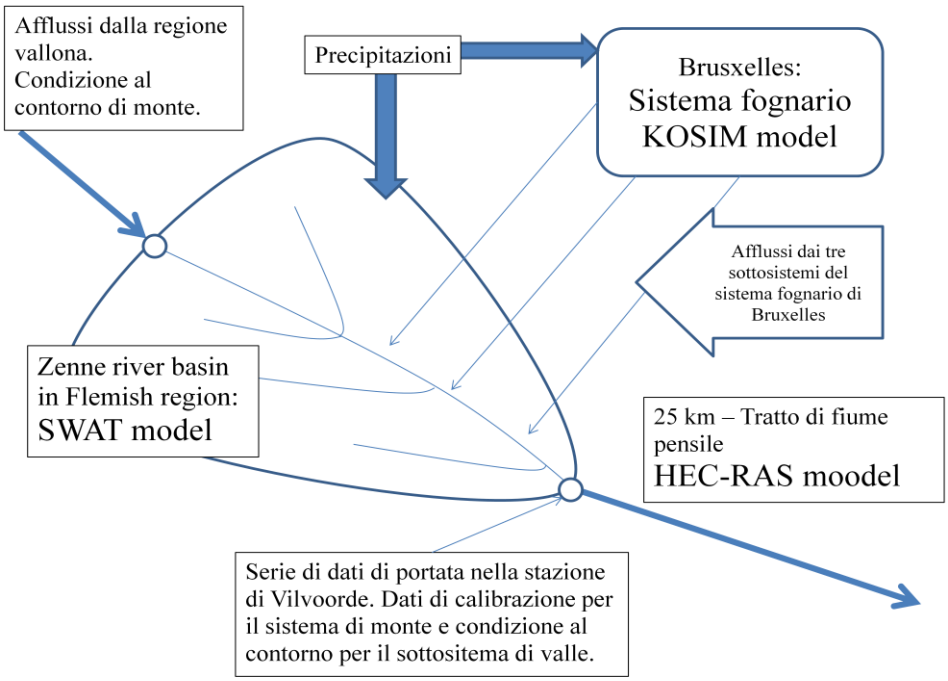

Figure 4 Rappresentazione schematica dei sottosistemi modellizzati e delle connessioni tra essi. Sono riportati sia i tre sottosistemi che le condizioni al contorno che i modelli utilizzati.

1.2 I modelli

Al fine di rappresentare i sottosistemi precedentemente descritti sono stati costruiti due modelli, uno per la regione fiamminga e uno per il tratto pensile. Un terzo modello, per il sistema fognario, già esistente, è stato utilizzato: essendo disponibili le serie di portate in uscita del, queste sono state utilizzate per alimentare il modello dei bacini nella regione fiamminga, che, come precedentemente spiegato, riceve in ingresso tali afflussi.

1.2.1 La regione fiamminga - il modello SWAT

Per costruire il modello dei sottobacini appartenenti alla regione fiamminga è stato utilizzato il modello SWAT (Soil and Water Assessment Tool).

SWAT è un modello tempo-continuo fisicamente basato con passo temporale giornaliero. Viene utilizzato per la predizione degli impatti della gestione delle risorse idriche, il trasporto di sedimenti e i carichi chimici di origine agricola sui bacini idrografici. È un modello semi-distribuito: suddivide il bacino imbifero, dapprima in sottobacini, attraverso l'uso di un modello digitale del terreno, e in seguito in Unità di Risposta Idrologica (Hydrologic Response Units - HRU), ovvero delle aree omogenee di territorio in base alla pendenza media, all'uso del territorio e il tipo di suolo, che vengono utilizzate per calcolare lo scorrimento superficiale del sottobacino attraverso una media pesata. Il modello riceve, come dati di ingresso: dati meteorologici (precipitazioni, temperatura. velocità media del vento, irraggiamento solare, umidità relativa) ed eventuali serie di portate e di dati di qualità da sorgenti puntuali. In figura 5 sono rappresentati i processi modellizzati da SWAT.

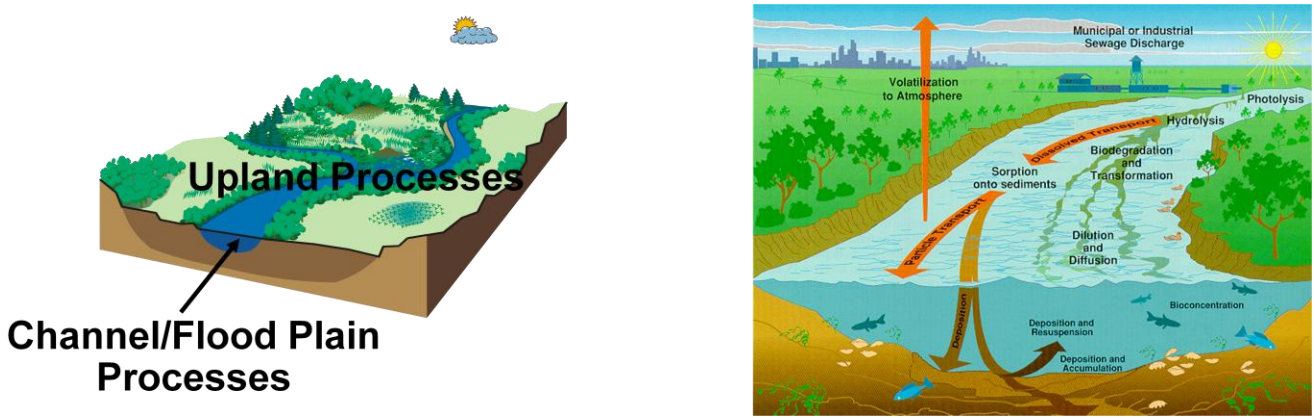

Figure 5 Processi modellizzati da SWAT

L'integrazione con il modello del sistema fognario di Bruxelles è stata effettuata ponendo uguali a zero le aree dei sottobacini in cui è ubicata la città (bacini 3,4,6 e 7 nella mappa in figura2): in questo modo lo scorrimento superficiale in tali aree non viene calcolato, vengono simulati solo i processi di trasporto nel fiume. Gli afflussi dalle aree urbane della città di Bruxelles sono stati aggiunti attraverso tre sorgenti puntuali aggiunte al modello SWAT.

1.2.2 Il tratto di fiume pensile - il modello HEC-RAS

HEC-RAS è un modello idraulico modimensionale basato sulla risoluzione delle equazioni De Saint Venant attraverso metodi alle differenze finite.

Il modello è in grado di effettuare:

1. Calcolo dei profili superficiali in regime stazionario
2. Simulazioni in regime variabile
3. Trasporto di sedimenti
4. Analisi di qualità dell'acqua

Tutte le componenti utilizzano una rappresentazione geometrica comune delle sezioni trasversali del fiume. Il modello può lavorare con un passo temporale minimo è di 1 secondo.

La rappresentazione geometrica degli ultimi 25 km del fiume Zenne è stata effettuata attraverso 211 sezioni trasversali distanti mediamente 125 m tra loro. La condizione al contorno di monte sono le serie orarie di afflussi registrate alla stazione di Lot. La condizione al contorno di valle sono serie orarie di altezza piezometrica presso la stazione di Hoombeek. Due stazioni in cui vengono registrati dati orari di altezza piezometrica vengono utilizzate per la calibrazione del modello a Eppegem e a Zemst.

Le stazioni di Lot (condizione al contorno di monte del modello SWAT) e di Vilvoorde, Eppegem, Zemst e Hoobeek sono rappresentate nella mappa in figura 6.

A valle il regime del fiume è fortemente influenzato dalla presenza delle maree. A causa delle maree gli afflussi provenienti dalla stazione di Vivoorde influenzano in maniera trascurabile i valori di altezza piezometrica nelle stazioni di Hoombeek e Zemst.

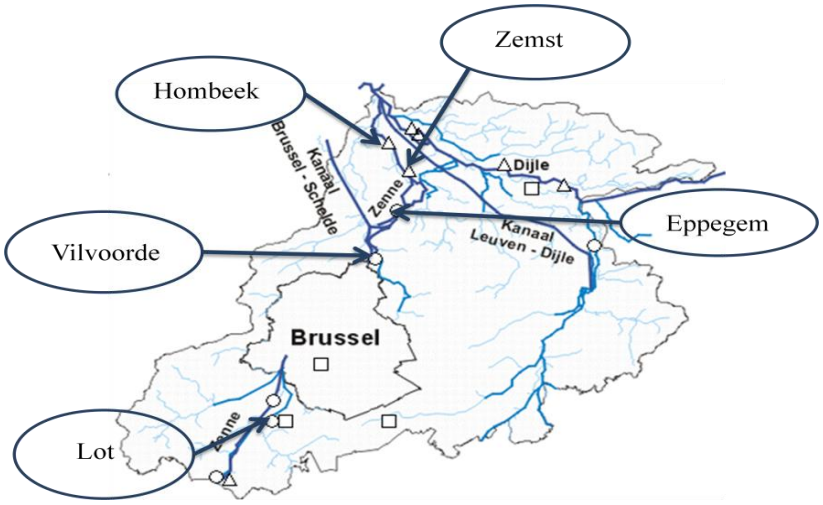

Figure 6 Visione di insieme delle staszioni idrologiche utilizzate in questo studio Immagine tratta da http://www.lin.vlaanderen.be/awz/waterstanden/hydra/images/hic_dijle04.gif

1.2.3 La città di Bruxelles - il modello KOSIM

KOSIM è un modello di simulazione per sistemi fognari misti sviluppato dall' ITWH, Hannover. È stato concepito per simulazioni di lungo periodo di portate e variabili di qualità dell'acqua dei sistemi fognari misti. Il modello riceve in ingresso dati di precipitazioni e, in base alla popolazione dell'area servita, simula i deflussi e le concentrazioni di inquinanti. Per questo studio vengono utilizzate delle serie di deflussi per gli anni 1995-1996 con cui viene alimentato il modello SWAT in tre punti di connessione tra i due modelli.

Un nuovo modello della città di Bruxelles e degli impianti di trattamento delle acque è in fase di sviluppo presso il gruppo di ricerca dell'Università Vrije di Bruxelles.

1.2.4 Il modello composto

Il modello composto è una cascata di modelli in cui l'uscita di uno alimenta quello successivo. Sia il modello KOSIM che il modello SWAT ricevono in ingresso dati di precipitazioni da una stazione (Ukkel) situata nella città di Bruxelles. I dati provenienti da questa stazione vengono considerati rappresentativi di tutto il bacino. Il modello KOSIM alimenta poi quello SWAT e quest'ultimo alimenta il modello HEC-RAS. In figura 7 è riportato uno schema della cascata di modelli con dati in ingresso e uscita da ciascuno. In particolare all'interno dei riquadri è riportata l'uscita del modello.

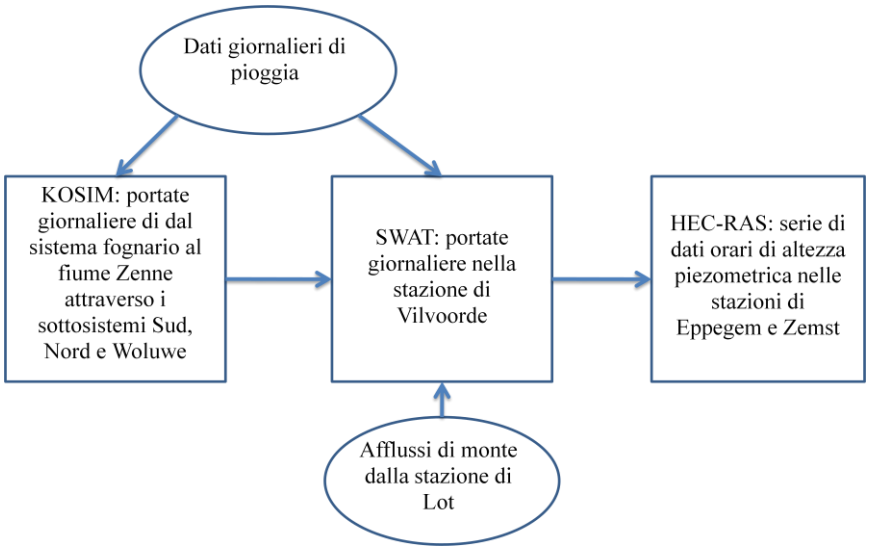

Figure 7 Struttura del modello composto e serie di input e output. All'interno dei riquadri sono riportati i dati di uscita dei modeli che alimentano i modelli successivi

1.3 Le fonti di incertezza

Le fonti di incertezza considerate in questo studio sono: quella dovuta ai set di parametri, quella dovuta all'uso di dati di afflussi calcolati attraverso l'uso di una scala di deflusso nelle stazioni di Lot e Vilvoorde e quella dovuta all'uso di dati di ingresso provenienti dal modello KOSIM nel modello SWAT. Non viene tenuta in conto l'incertezza nei dati di precipitazione poiché, essendo utilizzata solo una stazione meteorologica, la quantificazione dell'incertezza dovuta alla variabilità spaziale delle precipitazioni risulta perciò impossibile. Si raccomanda comunque che studi futuri sul caso di studio in questione tengano conto anche di questa importante fonte di incertezza. L'analisi di incertezza è stata conclusa propagando l'incertezza dal modello SWAT al modello HEC-RAS.

1.3.1 Incertezza nelle serie di afflussi nelle stazioni di misura di Lot e Vilvoorde

Le serie di afflussi dalle stazioni di Lot e Vilvoorde sono calcolate a partire da dati di altezza piezometrica attraverso l'uso di una scala di deflusso, una funzione polinomiale di terzo grado ricavata attraverso interpolazione a partire da dati misurati di altezza piezometrica e portate. Le portate per la stima della scala di deflusso sono calcolate attraverso il metodo area-velocità.

Il dato ricavato dalla scala di deflusso è affetto da un certo errore dovuto a (Di Baldassarre e Montanari, 2009):

$\varepsilon_1(Q(x,t))$: misurazioni delle portate ottenute con il metodo velocità-area: **4.4%**

$\varepsilon_2(Q(x,t))$: incertezza nella scala di deflusso stessa

$\varepsilon_{2.1}(Q(x,t))$: interpolazione ed estrapolazione della scala di deflusso: **1.14%**

$\varepsilon_{2.2}(Q(x,t))$: presenza di regime non stazionario (cappio di piena): **7.7%**

$\varepsilon_{2.3}(Q(x,t))$: variazioni stagionali della scabrezza: **10%**

Dove Q è la portata.

L'aggregazione, assumendo una distribuzione normale, di queste fonti di incertezza è

$$\varepsilon(Q(x,t)) = \varepsilon_1(Q(x,t)) + \varepsilon_2(Q(x,t)) \quad (1)$$

$$|\varepsilon_2(Q(x,t))| = |\varepsilon_{2.1}(Q(x,t))| + |\varepsilon_{2.2}(Q(x,t))| + |\varepsilon_{2.3}(Q(x,t))| \quad (2)$$

L'uso del valore assoluto è scelta in base a un approccio precauzionale, per cui si considera il caso in cui tutti abbiano lo stesso segno. Si ricava con questo approccio un valore della magnitudine dell'errore, che è mediamente intorno al **25%** del valore della portata stessa. Si assume poi, con ipotesi semplificativa e approccio precauzionale, che l'errore abbia distribuzione normale con media pari a zero e deviazione standard proporzionale al valore stesso della portata calcolata $\varepsilon \sim N(0, (0.25Q)^2)$.

Questo errore, casuale con distribuzione normale, assume un certo valore che si assume rimanga approssimativamente costante durante un certo evento di piena.

1.3.2 Incertezza nelle serie di afflussi dal sistema fognario di Bruxelles

L'errore nell'uscita del modello KOSIM si assume essere una variabile casuale con distribuzione uiforme e range di valore da $-\beta \cdot Q$ a $+\beta \cdot Q$, dove β è un coefficiente di proporzionalità peri a circa 0.25.

1.4 La calibrazione dei modelli

I modelli costruiti vengono calibrati dapprima indipendentemente l'uno dall'altro. L'analisi di incertezza viene effettuata per entrambi indipendentemente. In seguito i modelli in cascata vengono ricalibrati.

1.4.1 Calibrazione del modello SWAT

Il modello SWAT è stato calibrato utilizzando le serie di afflussi registrati alla stazione di Vilvoorde nell'anno 1995. La validazione è stata effettuata utilizzando la serie di afflussi dell'anno 1996. Un algoritmo già esistente, Parasol, è stato utilizzato per la taratura e per l'analisi di incertezza dovuta ai set di parametri. Il metodo è di tipo evolutivo e utilizza lo Shuffled Complex Evolution (SCE-UA) di Duan et al. (1994). Una volta che la procedura giunge a convergenza vengono selezionati i set di parametri soddisfacenti attraverso il metodo del χ^2. Tutte le simulazioni la cui funzione obiettivo da massimizzare sia superiore ad un certo valore limite, vengono considerate soddisfacenti e di conseguenza tutti i set di parametri utilizzati per tali simulazioni. Il valore limite è calcolato come.

$$c = OF(\theta^*) * \left(1 + \frac{\chi^2_{p,0.95}}{n-p}\right) \quad (3)$$

Veongono poi calcolate le bande di incertezza pesando le simulazioni attraverso la funzione obiettivo e calcolando, per ogni passo temporale della simulazione, i percentili al 2,5% e al 97.5%.

La funzione obiettivo utilizzata è 1 meno la varianza spiegata, che assume valore 1 per simulazioni che riproducono perfettamente le osservazioni e, nal caso di valore negativo, indica che la media delle osservazioni è una predizione migliore della simulazione. Il problema è perciò un problema di minimi quadrati:

$$E = 1 - \frac{\sum_{i=1}^{N}(O_i - P_i)^2}{\sum_{i=1}^{N}(O_i - \bar{O})^2} \quad (4)$$

La calibrazione di 13 parametri del modello ha dato luogo a 4830 set di parametri soddisfacenti, con funzione obiettivo compresa tra 0.89 e 0.9. Tramite essi è possibile costruire le bande di incertezza.

Nel periodo di validazione è stato fatto simulare il modello con tutti i set di parametri trovati in fase di calibrazione. In figura 8 e 9 sono riportati gli idrogrammi del periodo di calibrazione e validazione. Sono riportati sia la migliore simulazione, che le osservazioni e le bande di incertezza.

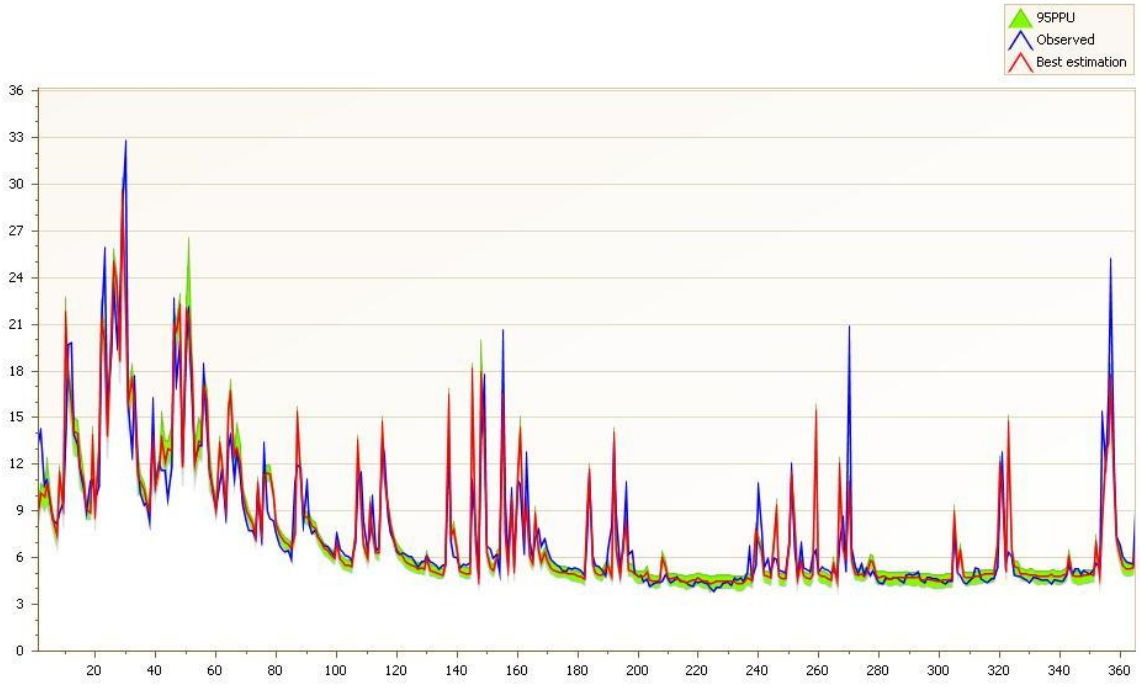

Figure 8 Calibrazione: Idrogramma delle osservazioni e delle simulazioni a Vilvoorde per l'anno 1995

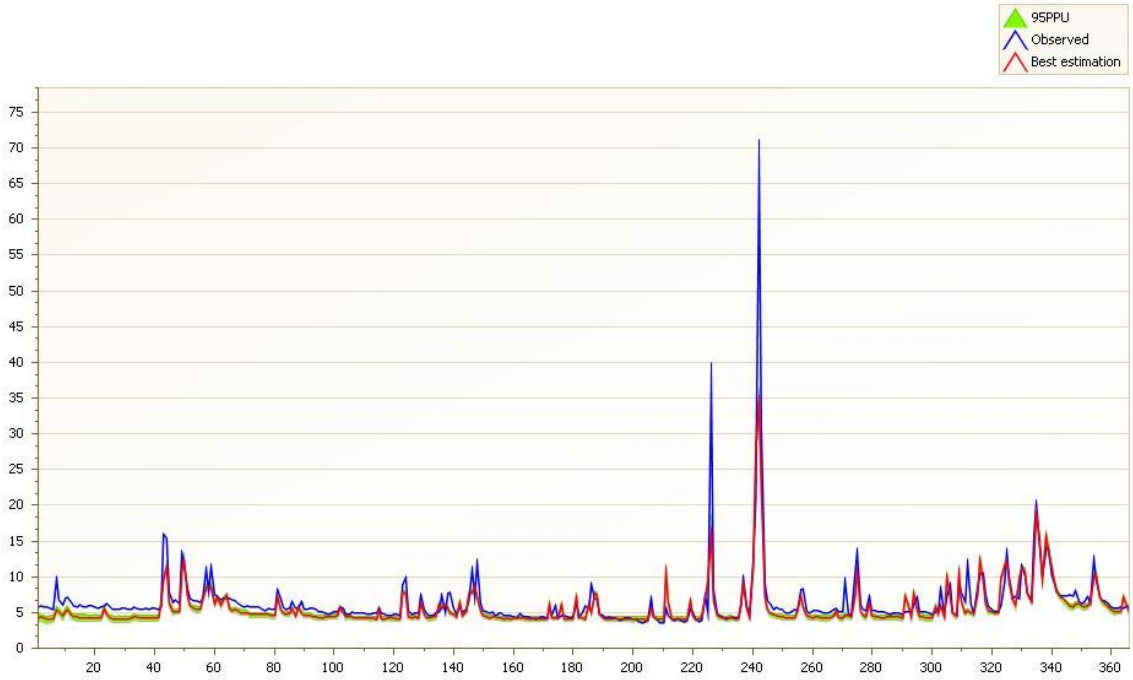

Figure 9 Validazione: Idrogramma delle osservazioni e delle simulazioni a Vilvoorde per l'anno 1995

Si nota soprattutto che le bande di incertezza sono molto strette. Questo può avere come conseguenza un percentuale di osservazioni non contenuta nelle bande di incertezza molto elevata. Nella tabella 1 sono riportati i risultati della calibrazione: i fattori p e r rappresentano la percentuale di osservazioni incluse nelle bande di incertezza e il rapporto tra l'ampiezza media delle bande di incertezza e la deviazione standard delle osservazioni. Al diminuire del fattore r diminuisce anche il fattore p. Questo spiega il suo basso valore.

	Green-Ampt
	Parasol
Numero di simulazioni buone	4830
NSE min	0.89
NSE max	0.9
p-factor [%]	5.40
r-factor [dm/s]	0.05
NSE min Validazione	0.62
NSE max Validazione	0.76

Table 1 Risultati della calibrazione, della validazione e dell'analisi di incertezza del modello

In figura 10 è riportato il grafico con i valori delle bande di incertezza in funzione della migliore simulazione. Quello che si nota è che due rette di regressione possono essere costruite a partire dai valori delle bande di incertezza in funzione della simulazione migliore ottenuta. Il coefficiente di determinazione, R^2, assume valori pari a circa 0.99, il che indica che le rette di regressione spiegano

molto bene i dati. Le due rette di regressione sono leggermente divergenti, il che significa che all'aumentare della portata simulata aumenta l'ampiezza della banda di incertezza. Questo effetto è però poco apprezzabile. Inserendo l'incertezza dovuta ai dati di ingresso questo effetto è molto più accentuato.

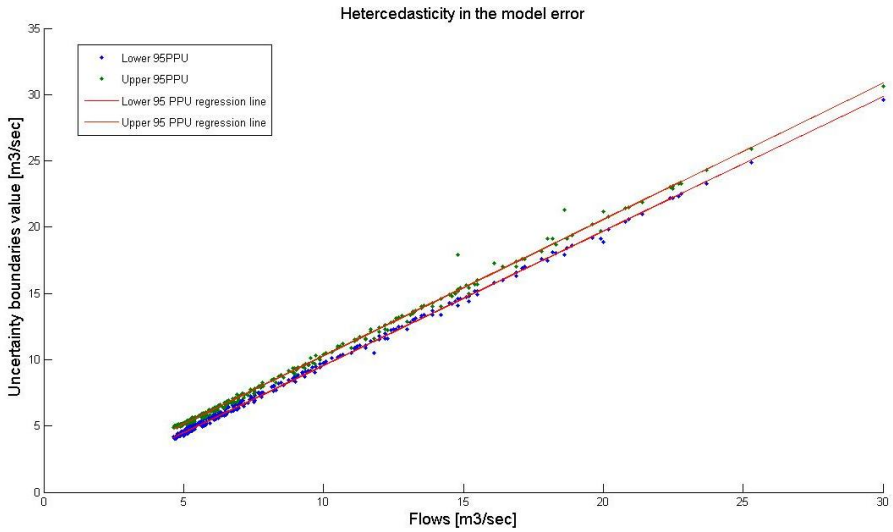

Figure 10 Modello dei limiti inferiore e superiore della banda di incertezza del modello SWAT

	Coefficiente angolare	Intercetta
Lower boundary	1.0135	-0.57419
Upper boundary	1.0276	0.022177

Table 2 Valori dei parametri delle rette di regressione dei limiti inferiore e superiore della banda di incertezza

1.4.2 Analisi di incertezza dovuta ai dati in ingresso nel modello SWAT

Per valutare l'incertezza dovuta agli ingressi, le serie di input sono state sporcate con un errore costruito a partire dalla distribuzione presentata in precedenza.

In particolare, per quanto riguarda l'errore presente nelle serie di afflussi dalla stazione di monte, Lot, ricavate dalla scala di deflusso, sono state create 20 serie, ognuna affetta da un errore il cui valore, per ogni passo temporale, ha la stessa probabilità cumulata. La prima serie sarà affetta interamente da un errore con probabilità cumulata pari a 0.025. Incrementando tale valore di 0.05 per ogni serie, sono state create 20 serie fino ad un valore della probabilità cumulata dell'errore pari a 0.975.

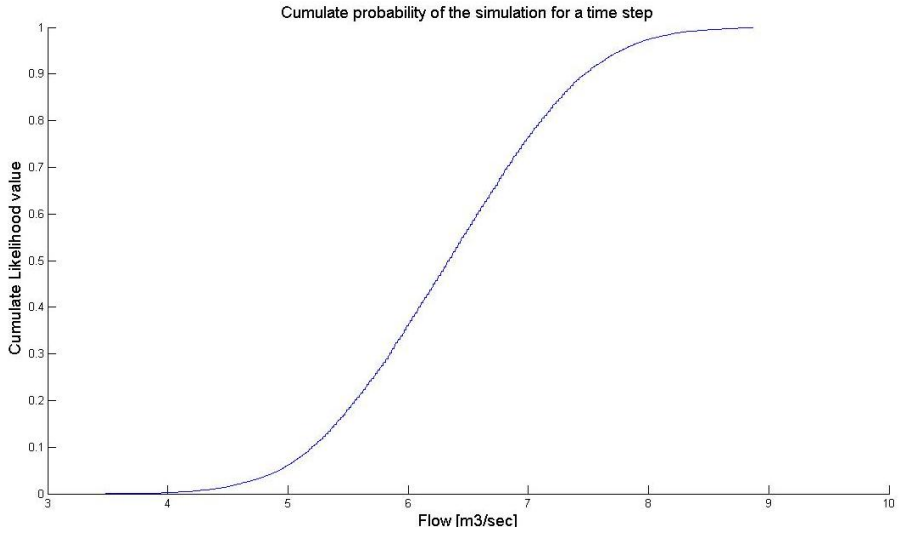

Figure 11 Probabilità cumulata del valore della portata per un time step delle serie sporcate da errore

Questa scelta è stata effettuata in quanto l'errore, casuale con distribuzione gaussiana, assume valore costante ad ogni evento di piena. Si può perciò semplificare la procedura di costruzione delle serie sporcate e diminuire il numero di simulazioni. Sono anche state crete 50 serie di afflussi dal sistema fognario a cui è stato applicato l'errore casuale descritto precedentemente. Tutte le serie sono state utilizzate per simulare il modello con 161 set di parametri rappresentativi dei 4830 trovati in fase di calibrazione.

Il risultato è che le bande di incertezza aumentano la propria ampiezza e, a causa della propagazione dell'errore, le rette di regressione mostrano un'elevata eteroschedasticità, come si vede in figura 11: la varianza dei valori simulati di portata non è costante, ma aumenta all'aumentare del valore della portata stessa. In figura 11 le rette di regressione sono state costruite in funzione della portata risultante dalla migliore simulazione. I valori del fattore r e p aumentano rispettivamente a 0.99 e 91.23%, visto l'aumento dell'ampiezza delle bande.

Attraverso la distribuzione delle uscite del modello trovate con queste simulazioni è, dunque, possibile costruire delle serie da utilizzare per l'analisi di incertezza del modello composto: 10 serie costruite a partire dai percentili delle serie pesate con le funzioni obiettivo sono utilizzate per tale analisi.

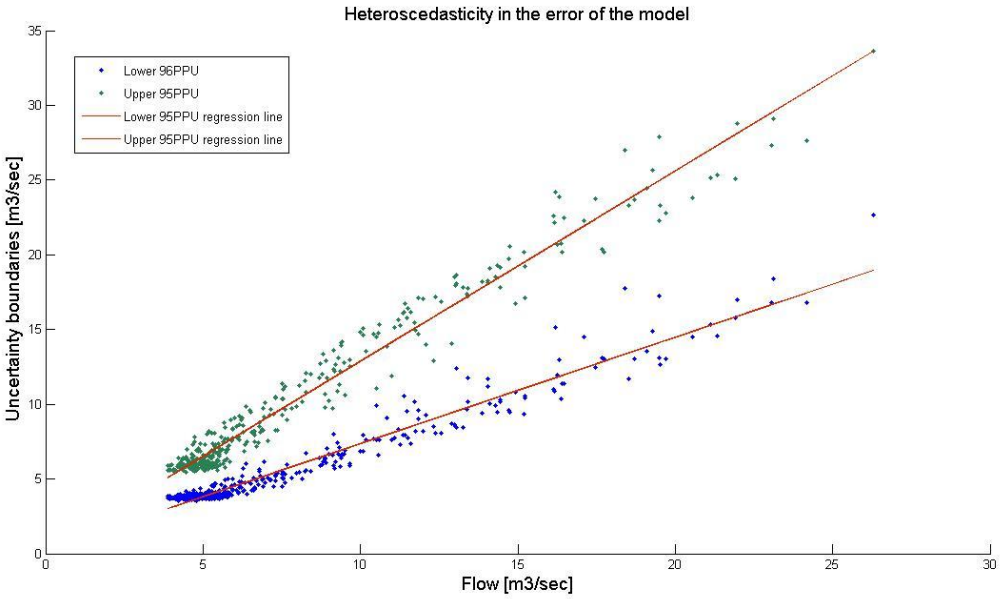

Figure 12 Bande di confidenza del 95% in funzione della migliore simulazione e rette di regressione.

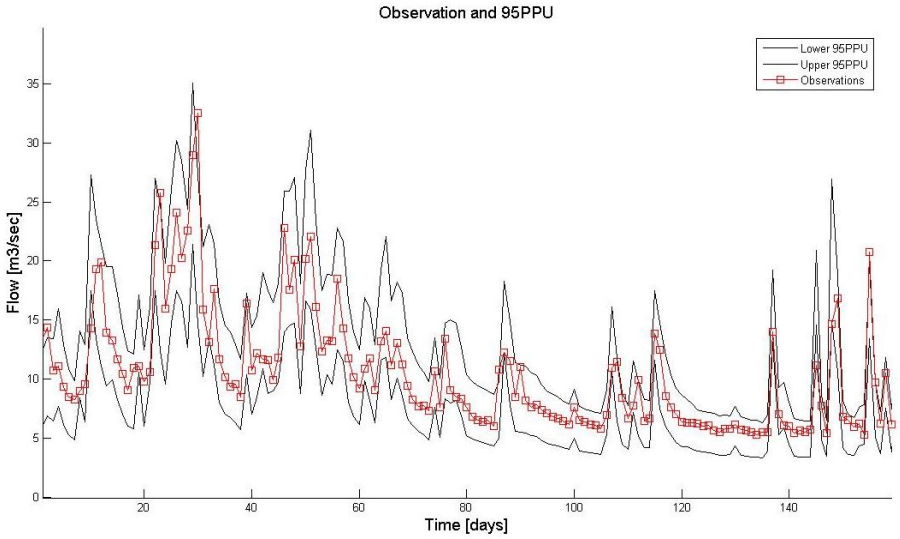

Figure 13 Nuova bande di confidenza aggiornata con l'incertezza docuta agli ingressi

1.4.3 Calibrazione del modello HEC-RAS

L'unico parametro di calibrazione del modello HEC-RAS è il coefficiente di scabrezza di Manning, n.

I valori soddisfacenti di questo parametro sono stati trovati tramite simulazione. Tutte le simulazioni con valore obiettivo della funzione obiettivo maggiore di 0.75, e i valori del parametro utilizzato, sono state considerate soddisfacenti. Una volta individuati i parametri soddisfacenti sono state calcolate le bande di incertezza come fatto per il modello SWAT: le simulazioni sono state pesate attraverso il valore della funzione obiettivo e i percentili 0.025 e 0.975 sono stati utilizzati per definire la banda di

incertezza. Sono stati trovati 5 valori soddisfacenti del parametro di calibrazione, da 0.042 a 0.044. In figure 12 e 13 sono riportati i grafici delle serie temporali di altezze piezometriche simulate e osservate nelle sue stazioni di misura, Eppegem e Zemst. da notare che in quest'ultima l'effetto delle maree rende assolutamente indipendente il valore di altezza piezometrica e di portata dalle portate di monte. In figura 14 è riportato l'idrogramma per l'evento di validazione in Eppegem.

Come fatto in precedenza le bande di incertezza sono state calcolate dapprima tenendo conto solo dell'incertezza nel parametro. In questo caso il fattore p e r assumono valori abbastanza elevati come si vede in tabella.

Numero di simulazioni buone	5
Set parametri ottimo	n=0.43
NSE min	0.77
NSE max	0.92
p-factor [%]	73.45
r-factor	0.65
NSE max Validazione	0.76

Table 3 Risultati della calibrazione e dell'analisi di incertezza dovuta ai parametri del modello HEC-RAS

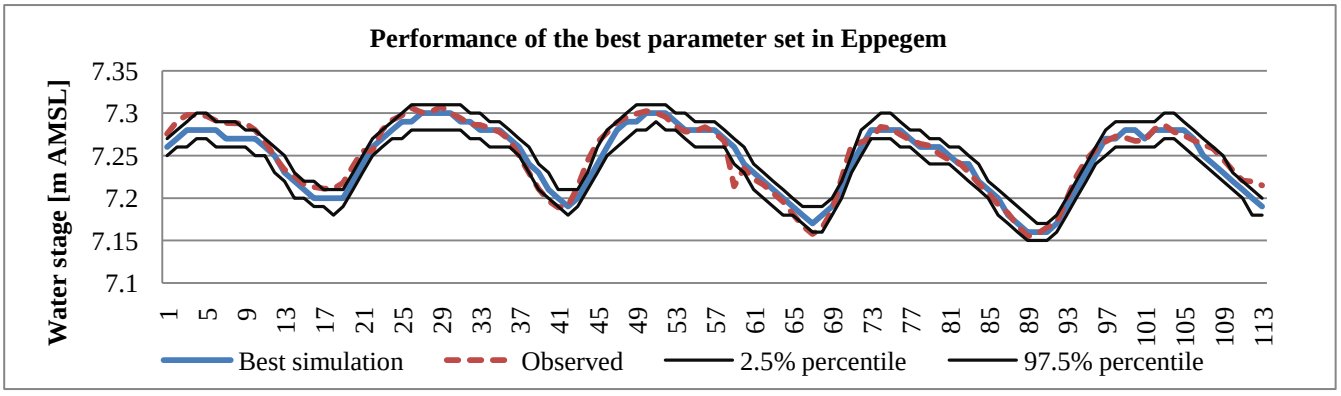

Figure 14 Miglior simulazione, bande di incertezza e osservazioni alla stazione di Eppegem.

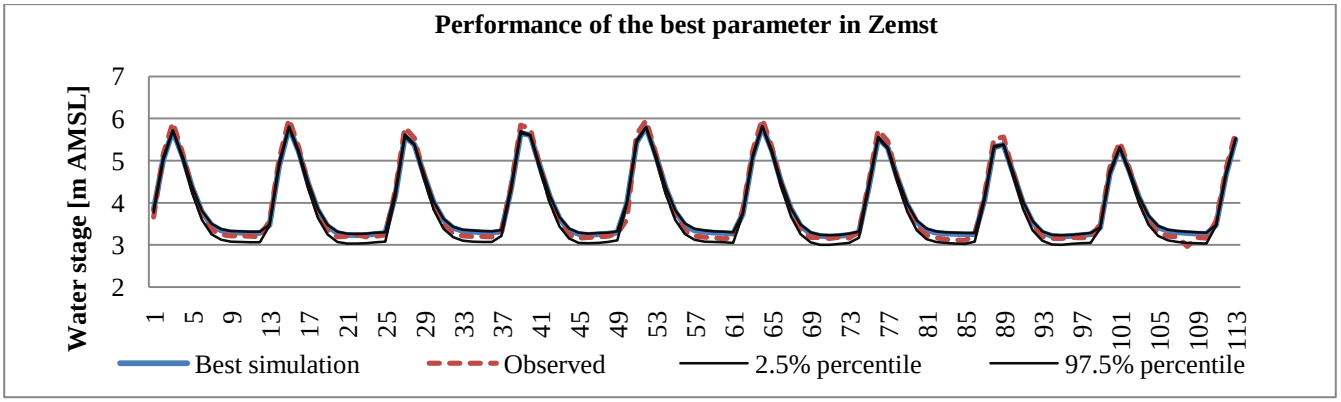

Figure 15 Miglior simulazione, bande di incertezza e osservazioni alla stazione di Zemst

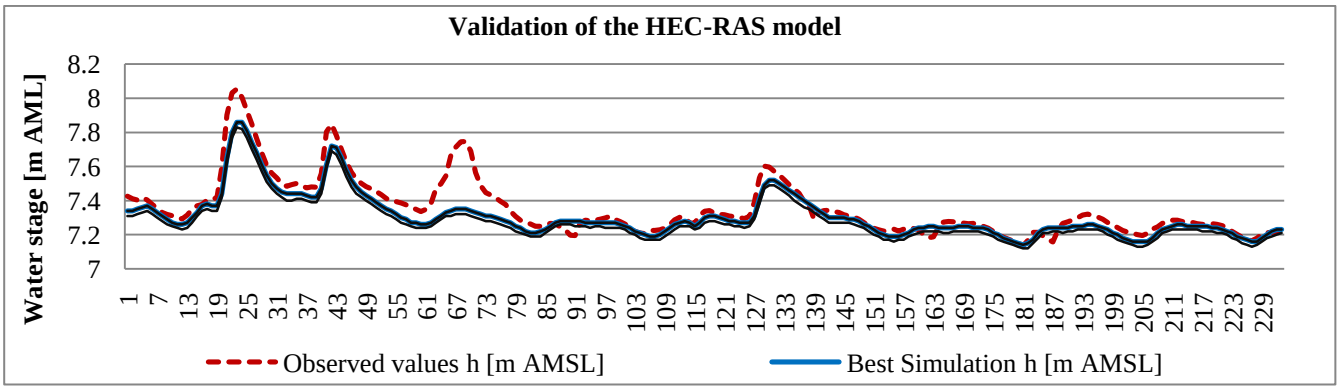

Figure 16 Miglior simulazione, bande di incertezza e osservazioni per il periodo di validazione nella stazione di Eppegem

1.4.4 Incertezza dovuta ai dati di ingresso

Come effettuato in precedenza l'incertezza dovuta ai dati in ingresso è stata calcolata simulando il modello con delle serie sporcati di afflussi in entrata. Le serie sono state sporcate come descritto per il modello SWAT, utilizzando i percentili della distribuzione cumulata dell'errore a partire da 0.025 fino a 0.975 con passo pari a 0.05. Sono state effettuate 1020 simulazioni combinando ciascuna delle venti serie di input costruite con 53 valori del coefficiente di Manning, da 0.028 a 0.081. Tutte le simulazioni con valore della funzione obiettivo superiore a 0.75 sono state utilizzate per costruire le nuove bande di incertezza.

Con le bande di incertezza aggiornate in questo modo la percentuale di osservazioni comprese nella banda passano dal 73.5% circa al 95%.

In questo caso nulla può essere detto sulla presenza di eteroschedasticità.

1.4.5 Analisi di sensitività del coefficiente di Manning

L'analisi di incertezza è stata accompagnata da un'analisi di sensitività del coefficiente di scabrezza: spesso il coefficiente di scabrezza viene utilizzato per compensare rappresentazioni incomplete della geometria del corpo idrico modellizzato. Attraverso simulazione del modello con serie di ingresso sporcate da errore risulta che il coefficiente di Manning è in grado anche di compensare eventuale incertezza nei dati di ingresso. Oltre alle serie create per l'analisi di incertezza sono state create serie analoghe con valori della deviazione standard differente, da 0.1Q a o.25Q, dove Q è la portata. Un totale di 5300 simulazioni è stato effettuato.

Il risultato dell'analisi di sensitività è che per errori dell'ordine del 5% della portata, i valori soddisfacenti del coefficiente di scabrezza non cambiano, per errori crescenti il range di valori entro cui il coefficeinte di scabrezza risulta soddisfacente aumenta, come si vede nella figura 17, dove i valori soddisfacenti del coefficiente di Manning sono riportati in funzione della deviazione standard nell'errore. Questo può indicare che simulando diversi episodi di piena, il valore del coefficiente di Manning potrebbe assumere valori molto differenti a seconda dell'entità dell'errore che casualmente agisce sulla scala di deflusso.

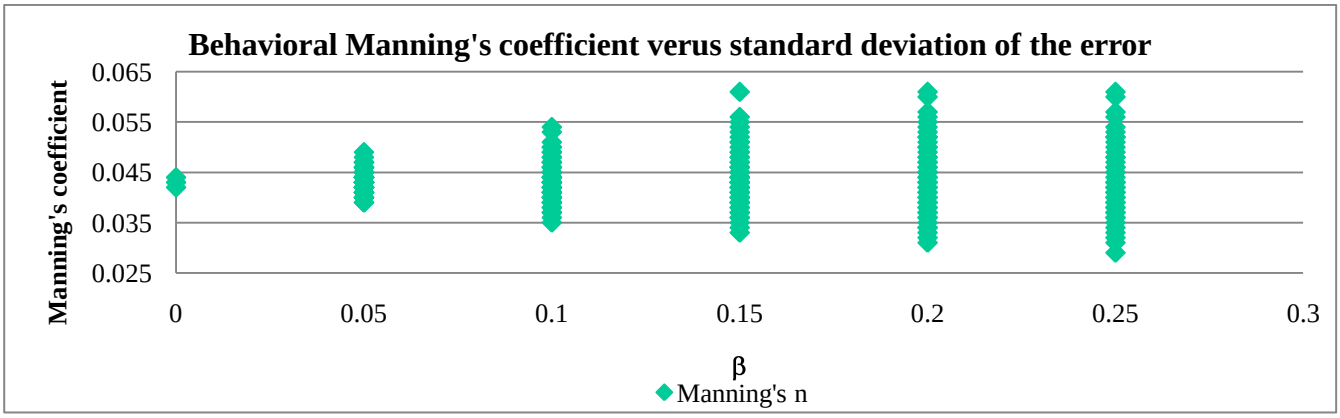

Figure 17 Valori soddisfacenti del coefficiente di Manning in funzione della deviazione standard dell'errore nella serie di ingresso

1.5 Il modello composto

Una volta effettuata la calibrazione e l'analisi di incertezza dei singoli modelli, il modello HEC-RAS è stato ricalibrato utilizzando in ingresso le uscite del modello SWAT.

La migliore simulazione del modello SWAT è stata utilizzata per ricalibrare il modello. Una volta ricalibrato il modello ed una volta individuati i paraetri che generano simulazioni soddisfacenti, l'incertezza dovuta ai dati di ingresso e al set di parametri viene valutata alimentando il modello con delle serie di uscita del modello SWAT ricavate dai percentili della banda di incertezza costruita pesando le simulazioni con i valori della funzione obiettivo. Il risultato è ancora una volta che la banda di incertezza si allarga rispetto a quella stimata in calibrazione e dovuta solo ai set di parametri. I limiti inferiore e superiore della banda possono essere espressi in funzione dei risultati della migliore simulazione tramite rette di regressione stimate a partire dai valori della banda di incertezza trovati tramite simulazione. In figura 94 sono riportate le rette di regressione stimate per l'incertezza dovuta solo ai parametri e dovuta sia ai parametri che ai dati di ingresso. In tabella 4 sono riportate le equazioni delle rette di regressione e il valore del coefficiente di determinazione delle stesse. Si nota che la regressione spiega molto bene i dati delle simulazioni.

	Calibrazione	Incertezza dovuta ai dati in gresso
Retta di regressione del limite inferiore della banda	0.972x+0.16	0.82x+1.2
R^2 della retta di regressione del limite inferiore	0.99	0.98
Retta di regressione del limite superiore della banda	x	1.12x-0.73
R^2 della retta di regressione del limite superiore	1.00	0.99

Table 4 Risultati della calibrazione dell'analisi di incertezza del modello in cascata

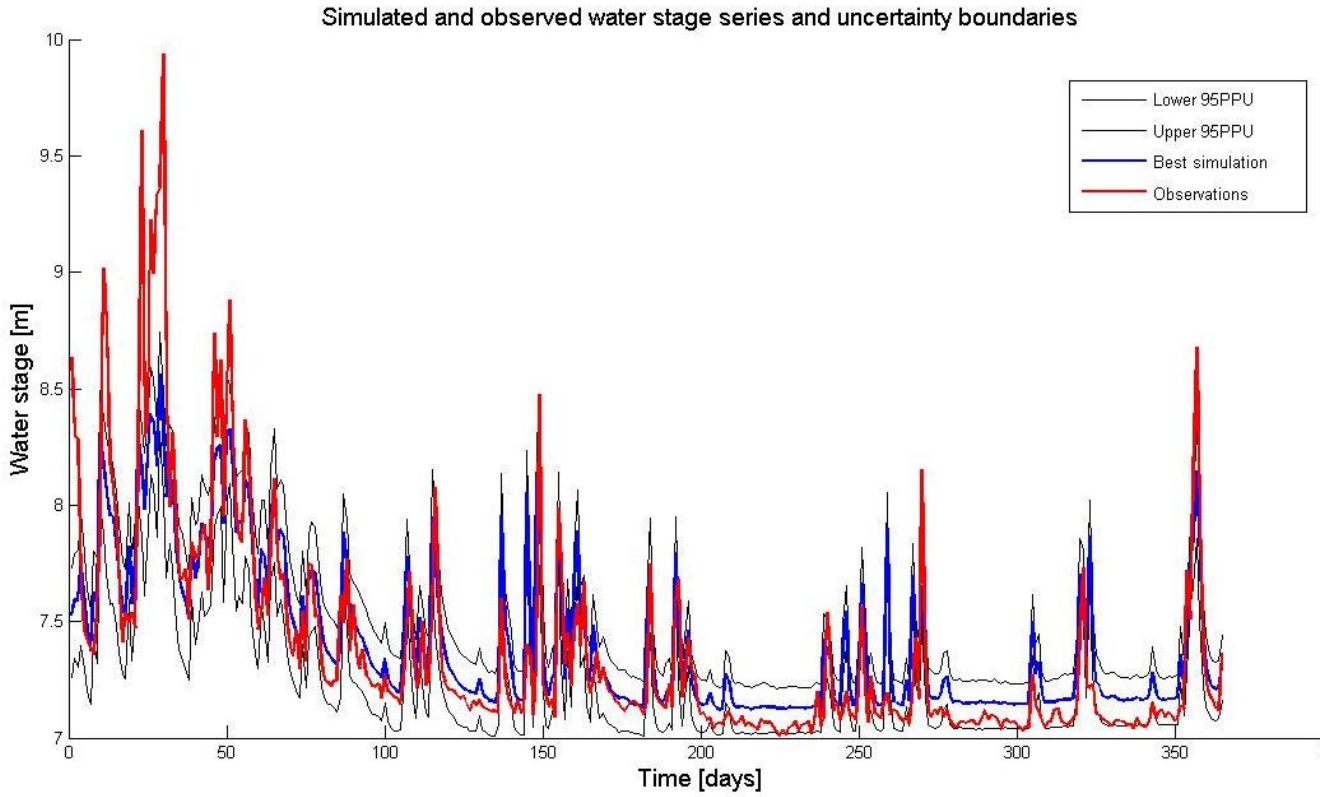

Figure 18 Serie di altezze piezometriche simulate e ossrvate e banda di incertezza dovuta a dati di ingresso e scelta dei parametri

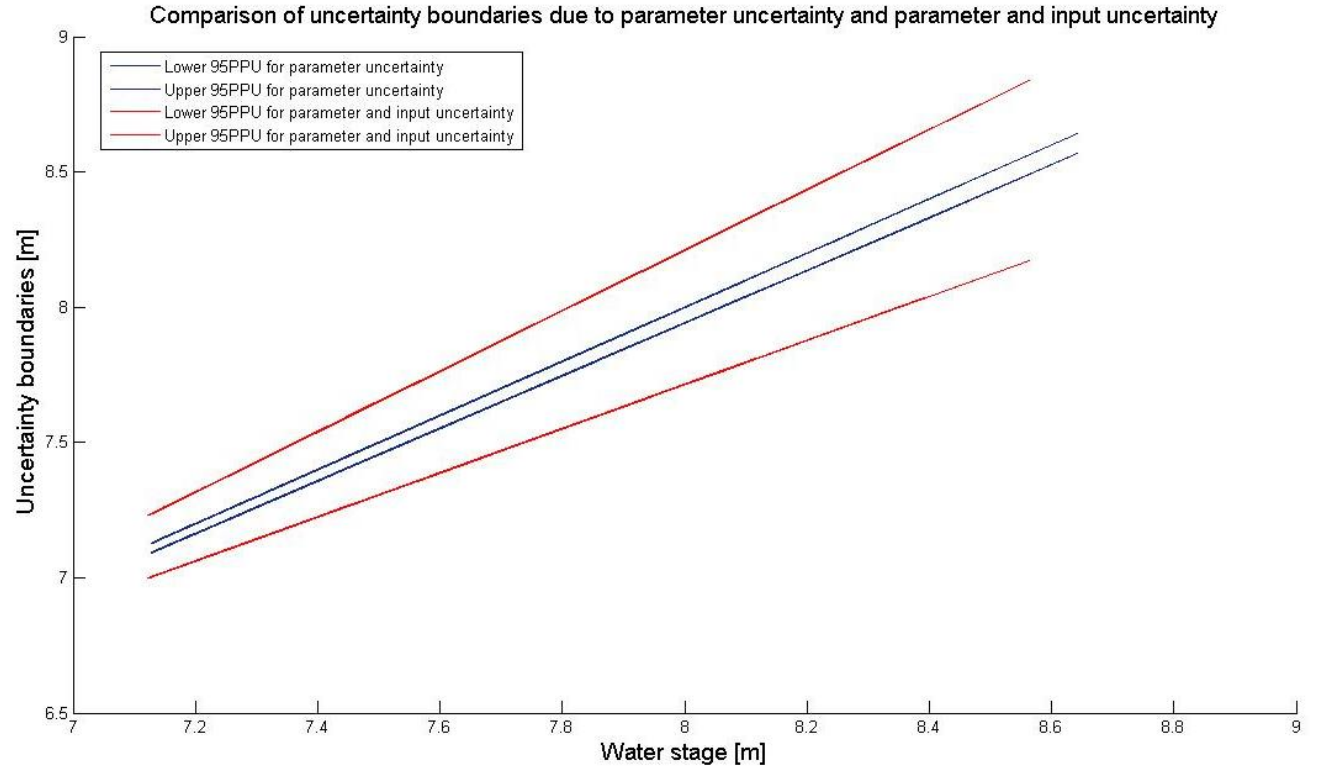

Figure 19 Comparazaione tra le rette di regressione dei limiti inferiore e superiore delle bande di incertezza dovute ai parametri e alla combinazione di parametri e dati di ingresso del modello

1.6 Conclusioni

Il seguente lavoro propone una procedura per la stima dell'incertezza dovuta ai dati in ingresso nei modelli applicandola al caso in cui questa incertezza si propaga attraverso più modelli.

Il metodo permette una rappresentazione semplificata dell'incertezza in modo da facilitare la propagazione attraverso i modelli.

La struttura dell'errore presente nei dati di ingresso al primo modello della cascata si propaga in maniera evidente attraverso i diversi modelli: l'errore, casuale e proporzionale al valore stesso dell'ossrvazione, propagandosi da un modello al successivo propaga la sua struttura stessa: le bande di incertezza risulatanti presentano eteroschedasticità, ovvero la varianza dei risultati delle simulazioni non è costante, ma aumenta all'aumentare del valore simulato dal modello. Il risultato più interessante del lavoro è che i limiti inferiore e superiore della banda di incertezza dei modelli possono essere essi stessi modellizzati attraverso delle rette di regressione che esprimono il valore dei limiti della banda in funzione del valore di uscita della simulazione stessa.

Il lavoro è in ogni caso da completare e integrare tenendo conto anche di altre fonti di incertezza di cui, per mancanza di tempo e dati, non si è tenuto conto: l'incertezza dovuta alla variabilità spaziale dei dati di pioggia e l'incertezza dovuta al cambio di uso del suolo nel bacino idrografico e alla risoluzione spaziale delle mappe usate per costruire il modello del bacino sono solo alcuni esempi.

Introduction

Water utilization, for drinking, industrial, irrigation or recreational purposes, is influenced by water quality and quantity. The water quality is determined both by the quantity and type of pollutants that are released in the water bodies from point or diffusive sources and the migration of them via run-off and groundwater towards water bodies. The current rehabilitation techniques are most of all intended to remove the sources of pollution and prevent their migration, but do not address the impact of the remedial actions on the whole water system. An integration of the remedial actions is, thus, needed.

In the last decades many hydraulic and hydrologic models have been developed to support water resources management, defense from flooding, land planning, fluvial rehabilitation projects, and water quality improvement. In particular the need to integrate different aspects in one single projects lead to the necessity of linking and integrating different models. The integration, linking and composition of different models consists often in using the output of one model to feed another one.

A model is anyway a representation of the real world. This means that the results of a model are affected by an error with respect to what actually happens in the real world. The results of a model thus make sense only if accompanied by a quantitative representation of the uncertainty. As hydrologic and water quality models are increasingly used to guide water resources policy, management and regulation, it is not appropriate to disregard the uncertainty in model calibration, validation and evaluation (Beck, 1987; Sharpley et al., 2002; Harmel and Smith, 2007). It is indeed important that decision makers appreciate the uncertainty in measured water (quality) data and its effect on model output. The main objective of the thesis is, thus, building a tool to represent uncertainty of hydrologic and water quality models that takes into account for different uncertainty sources.

Uncertainty sources in the model building are:

- Uncertainty of the model structure
- Uncertainty in the parameter estimation
- Uncertainty in the observed input disturbances and uncertainty arising from unobserved input disturbances in the system
- Uncertainty in output data used for calibration (e.g. streamflow) (Van Griensven, 2002; Shrestha, Solomatine, 2008).

The consequence is that, if a model is linked to another, the uncertainty propagates. In this case the representation of the uncertainty becomes even more important, as, because of the propagation, it can become higher, in the passage from a model to the other. The uncertainty affecting models that are used to predict water quantity can, thus, propagate to water quality models that use the results of the former models.

This work is mainly focused on the analysis of the uncertainty affecting models. The objective is to find a simple and effective tool to represent the uncertainty and propagate it through different models linked between each other. The case study is the Zenne River, Belgium, a highly polluted river that flows from the Walloon region to the Flemish region and Brussels. Innovative rehabilitation techniques are needed to improve its water quality taking into account of the land use and management, the type of

pollution sources, the pollutants discharged in the river and the availability of waste water treatment plants. A project involving the UNESCO-IHE institute and the Vrije Universiteit Brussel is working on this river with the purpose of integrating different techniques that act on the whole system.

The objectives of this thesis work, within this project, are:

- Building a model of a river basin, that integrates hydrologic and hydraulic aspects to support the water quality modelling. This objective is achieved using different models (SWAT, HEC-RAS and KOSIM). Each model is used to represent different parts of the system, where the description of different phenomena and systems (hydrologic, hydrodynamic, water quality, combined sewer system and WWTP) is needed.
- Building a tool for the evaluation of the uncertainty in the model. In particular, the thesis focuses on the assessment of the observation uncertainty, uncertainty propagation and cascade of uncertainty caused by the integration the three models.
- Finding a simple way to represent the uncertainty to propagate it from a model to another.

The main outcomes of the work done are:

Hydrologic, basin scale rainfall-runoff model of the subbasins of the Zenne River located in the Flemish region. The SWAT model has been used to represent the part of the basin located in the Flemish region. It receives, as input data, not only the rainfall, but also inflow data from the subbasins located in the Walloon region, upstream, and from the sewer system in the Brussels region.

One-dimensional model of the last 25 km of the river. A one-dimensional model is good representations of this part of the system, as the presence of levees prevent the runoff to enter the river. HEC-RAS model has been used to represent this stream of the river. This model receives, as inflow, the output of the SWAT model. The outlet of the SWAT model is actually located in the same point where the upstream boundary condition of the HEC-RAS model is.

Identification of the sources of uncertainty. The sources of uncertainty are identified and quantified. Particular attention is put on the uncertainty due to the parameter sets and due to the inflow series. A model of the error affecting the inflows is built.

Calibration of the models. The calibration of the two models is performed. The calibration is based on the concept of equifinality: it is not possible to identify only one optimum parameter set, but many parameter sets are considered to be behavioral. These parameter sets are found by means of a Monte Carlo sampling and in the parameter space. After the simulations the performance of the parameter sets is assessed by an objective function to be minimized. All the simulations whose performance is higher than a certain threshold, chosen by means of a statistics, are considered behavioral.

Uncertainty analysis of the two models. The uncertainty analysis takes into account for the uncertainty in the parameter sets and in the input data, focusing on the inflows.

- First of all, the uncertainty due to the parameters is computed. The simulations made using the good parameter sets are weighted by the objective function value and the 95% uncertainty boundaries are built from the 2.5% and 97.5% percentiles.

- The uncertainty due to the input data is assessed by corrupting the input series with the error computed previously. All the good parameter sets are run using an ensemble of corrupted input series. The 95% uncertainty boundaries are updated.

The outcome of this analysis is a simplified representation of the uncertainty: the uncertainty boundaries are represented as a function of the value of the output of the model. Thanks to this simplified representation, the propagation of the uncertainty can be computed quickly from one model to the other, taking into account for many sources of uncertainty in one quantitative result.

Sensitivity analysis of the calibration parameter of the one-dimensional hydraulic model, the Manning's roughness coefficient, with respect to the error affecting the input data.

Calibration and uncertainty analysis of the combination of the two models: the model representing the last 25 km of the river, the HEC-RAS model, is fed by the output of the upstream model, the SWAT model. The input series used to feed the model are built using the whole 95% prediction uncertainty boundaries. The HEC-RAS model is then recalibrated and the uncertainty boundaries are re-built.

The outcome of this work will be used in the work that is being done by the research group in the Vrije Universiteit Brussel and by other studies being developed in the research group of the UNESCO-IHE in Delft. In particular the SWAT model of the subbasins in the Flemish region will be integrated with another SWAT model representing the subbasins located in the Walloon region and the water quality model will be added to the water quantity model of the whole basin. The hydraulic model will be used in a study over the impact of an industrial district, in the North of Brussels, over the river water quality.

2 Literature review

2.1 Hydrologic and hydraulic modeling

Catchment models simulate the generation of runoff and pollutants from a land area to a water body. Not all the rainfall-runoff models incorporate both the runoff generation and the assessment of diffuse pollution generation. The first hydraulic computations and water balance algorithms on digital platforms have been made by hydrologist since the mid 60s with the advent of mainframe computers. During the 80's the spread and rapid advancement of personal computers resulted in numerous watershed modelling codes that still constitute the core of today's modelling technology, while in the 90s the development of GIS permitted the integration of those codes in geographical interfaces.

The increasing of the computer speed contributed at the progress in the understanding of runoff generation mechanisms in urban and rural areas and the modernisation of hydrometeorologic and hydrogeochemical measurement techniques.

Terminology-wise, a distinction is made between a model and a model code. A model is defined as a particular hydrological model established for a particular system (catchment, lake or river). A model code, however, is defined as a generalised software package, which, without program changes, can be used to establish a model with the same basic types of equations (but allowing different parameter values) (van Griensven, 2002)

Classification

Catchment models are classified as conceptual or physically based according to the process descriptions. Conceptual models describe the process in such a way that the parameters of the model are defined through calibration. Physically based models try to describe physical processes observed in the real world in the runoff generation process, so the values of the parameters are derived from physical data or by laboratory studies. Anyway no model is perfectly physical, so each model needs to be conditioned to match reality by optimizing the internal parameters (van Griensven, 2002).

Further classification distinguishes between distributed, semi-distributed and lumped models. In distributed models parameters and data vary spatially. Lumped models work in such a way so that the values of the parameters are averaged all over the area. Models which fall somewhere in the middle of the two kinds of models are termed semi-distributed models. Fully distributed models enable the spatial variation of the characteristics of the catchment, the hydro-meteorological data and the inputs to be described into a network of grid points or cells. The increasing usage of GISs has a fundamental role in the development of these kinds of models.

Physically-based distributed model codes are developed to predict the effect of land use change by integrating data such as topography, soil type and patterns and vegetation. They achieve this purpose using parameters that have a physical interpretation through the representation of their spatial distribution. However model can completely describe the processes that occur. Also scaling aspects and measurement errors have to be taken into account. Many studies have concluded that it is not possible to define a consistent effective parameter value to reproduce the responses of a spatially variable

pattern of parameters as this parameter is not able to represent these heterogeneous processes (Beven, 1989). The model codes labelled as physically based should thus rather be seen as distributed conceptual models. A true physically based model should at the minimum take into account effects such as heterogeneity by using input data with statistical distributions of parameter values instead of a single parameter value.

Semi-distributed models often use the same data (GIS maps) but aggregate grids to bigger units. These units are termed Hydrological Response Units (HRU). The subdivision of the catchment in HRUs can be done in many different ways. In the SWAT model (Arnold, 1998), the catchment is at first subdivided in subbasins, then the Hydrological Response Units are built in a statistical way, without further spatial determination, based on combinations of land use and soil type. The sub-basin outflow is then calculated as a weighted sum of the HRU outputs:

$$OUT\_subbasin\left[\frac{M}{L^2}\right] = \frac{\sum_{i=1,n} out\_HRU_i * area\_HRU_I}{\text{subbasin } area} \quad (5)$$

where n= number of HRU's in the sub-basin

OUT_HRU= output for a fictive area with a certain land use and soil type combination, and the geometrical characterisation of the sub-basin

Uncertainty analysis

Ones a model is built and calibrated it is crucial to accompany the results of the model with a quantitative description of the uncertainty that affects them. Many sources of uncertainty affect the models: the model structure itself and the description of the process is affected by uncertainty, as there is no model able to describe completely and exhaustively the real processes. The uncertainty in the parameter values is often evaluated in the modelling process. Less often the uncertainty affecting the input data and its influence on the results of the model are assessed.

The next two chapters present a description of typical techniques for assessing the uncertainty of models and a description of the model codes used for this work. These chapters will be followed by the description of the case study and of the system. Then a description of the models built is presented. After the description of the model a description and a quantitative assessment of the sources of uncertainties arising from the input of the models is reported. Finally a description of the calibration procedure is reported. The core of the study will be the assessment of the uncertainty affecting the calibrated models. The combination of the uncertainty rising from the parameters, the input data and due to the propagation from one model to another is assessed. A procedure to describe in a simple way the uncertainty and its propagation is proposed.

2.2 uncertainty estimation

2.2.1 Overview of uncertainty analysis methods

Due to the increasing interest in assessing the uncertainty in Rainfall-Runoff (R-R) and water quality models, in recent years many methods to estimate it have been developed. Shrestha and Solomatine (2008) distinguish them in six different classes:

1. Analytical methods: these methods compute the probability distribution function of the model output derived distribution method.
2. Approximation methods: these methods provide the moments of the distribution of the uncertain variable. Due to simplicity and low computational costs they are used in many complex R-R models.
3. Simulation and sampling based methods: These methods, can estimate the full distribution of the model for cases with non-linear and/or complex system relationship. The most common are based on Monte Carlo simulation (MCS) and Latin Hypercube sampling (LHS). The methods require a prior distribution of the input parameter to be propagated through deterministic R-R model to the output.
4. Bayesian methods: the methods belonging to this class combine the Bayes theorem and MCS to estimate or update the probability distribution function of the parameters of the model and consequently estimate the uncertainty of the model output. Beven and Binley (1992) introduced the generalized likelihood uncertainty estimation (GLUE). The premise of GLUE is that many different parameters, and not only one, sets can be considered as behavioral in reproducing the observed behavior. This concept is called equifinality.

The GLUE procedure consists in:

a) Define a generalized likelihood measure $L(\theta)$, then randomly sample a large number of parameter sets from the prior distribution. The likelihood measure must increase monotonously and have a value of zero for model considered non-acceptable or non-behavioral. Every parameter set is assessed as behavioral or non-behavioral through a comparison of the likelihood measure with a given threshold value.
b) Each behavioral parameter is given a likelihood weight according to:

$$w_i = \frac{L(\theta_i)}{\sum_{k=1}^{N} L(\theta_k)} \tag{6}$$

Where N is the number of behavioral parameter sets.
The distribution of the likelihood values is treated as a probabilistic weighting function for the predicted variables, therefore allows an assessment of the uncertainty associated with each prediction.

c) At any particular step the output values of the model of each behavioral parameter set are ranked in order of magnitude and, using the likelihood weights associated with each run a distribution of function of the predicted discharges is calculated.

d) Finally the prediction uncertainty is described as the prediction quantile from the cumulative distribution realized from the weighted behavioral parameter sets.

The most frequently used likelihood measure for GLUE is the *Nash-Sutcliff* coefficient (NS):

$$NS = 1 - \frac{\sum_{t_i=1}^{n}(y_{t_i}^{M}(\theta) - y_{t_i})^2}{\sum_{t_i=1}^{n}(y_{t_i} - \bar{y})^2} \quad (7)$$

Where n is the number of the observed data points and y_{t_i} and $y_{t_i}^{M}(\theta)$ represent the observations and the model simulations with parameter θ at time t_i, respectively, and $\bar{y}$ is the average value of the observations. The value of NS ranges from -∞ to 1. A value of NS smaller than 0 means that the average of the observation is a better representation of reality than the model, while a value of 1 means that the model perfectly reproduce the real system. NS is however overly sensitive to extreme case because it squares the value of paired differences (Legates and McCabe, 1999; Harmel and Smith, 2007).

1. Methods based on the analysis of model errors: These methods are intended to estimate the uncertainty by analyzing the model residuals resulting in reproducing the observed historical data. Some methods, as the meta-Gaussian model, intend to analyze and estimate the R-R model uncertainty by estimating the probability distribution of the model error conditioned by the value of the contemporary simulated river flow (Montanari and Brath, 2004; Kelly and Krzysztofovicz, 1997). The prediction bounds of the model error are computed using the procedure:
   a) Model residuals and simulated model outputs are transformed into Gaussian domain by normal quantile transform (NQT).
   b) The conditional mean and variance of the model error in the normalized space, as the cross dependence between the normalized series of residuals and simulation, is governed by the normal linear equation.
   c) Finally the inverse of the normal quantile transform is computed to calculate the prediction bounds of the model error in the original domain.

   These methods require assumption of the residuals as normality and homoschedasticity.
2. Fuzzy theory based-method: These methods provide a non probabilistic approach for modeling the kind of uncertainty associated with vagueness and imprecision.

As many sources of uncertainty are taken into account the tool should find a way to estimate the total and cumulate uncertainty of the model. The composite model of the basin is, furthermore, a cascade of three models: the KOSIM model for the city of Brussels, the SWAT model for the basin and the HEC-RAS model for the river downstream Brussels. SWAT receives as inputs the output of the KOSIM model, which consists in hourly flows and pollutants concentration from the combined sewer system. The output of the SWAT model is then used as input of the HEC-RAS model. Both KOSIM and SWAT receive, as input, observed rainfall data series.

Generally, while uncertainty in parameter estimation, when calibrating models, is taken into account, the same cannot be said for what concern the uncertainty in the observed input of the model and observation series used for calibrating the model. The result is that the scientific community still has not established an adequate understanding of the uncertainty in measured water quality data. It is estimated that cumulative probable uncertainty (±%) typically range from 6% to 19% for streamflow measurements and for what concern water quality measurements, from 4% to 48% for sample collection, from 2% to 16% for sample preservation/storage and from 5% to 21% for laboratory analysis. Errors in storm loads range from 8% to 104% for dissolved nutrients, from 8% to 110% for total N and P and from 7% to 53% for total suspended sediments (Harmel et al. 2006).

2.2.2 Uncertainty in observed data

Streamflow measurements are vital in water quality sampling programs, as concentration have to be coupled with streamflow data to evaluate transport mechanics and quantity mass loads. Streamflow data involve continuous stage observations that are converted to streamflow with an established stage discharge relationship (Harmel et al., 2006). The rating curve is estimated by using a set of stage and flow measurements, in this case the river discharge is calculated by using the velocity area method, based on the relationship

$$Q'(x,t) = A(x,t) \times v(x,t) \tag{8}$$

Where x is the river discharge, t is the sampling time, $Q'(x,t)$ is the measured river discharge, $A(x,t)$ is the cross sectional area and $v(x,t)$ is the average flow velocity. Hence uncertainties in $Q'(x,t)$ are originated by uncertainties in $A(x,t)$ and $v(x,t)$. An additional error is, then, induced by the imperfect estimation of the rating curve (Di Baldassarre and Montanari, 2009).

A proposal of model for the error structure, if the rating curve method in river discharges observations is used, is made by Di Baldassarre and Montanari (2009). The sources of error considered in the model are: $\varepsilon_1(Q(x,t))$ in the measurement of $Q'(x,t)$, obtained with the velocity-area method and $\varepsilon_2(Q(x,t))$ due to rating curve uncertainty, induced by: interpolation and extrapolation error, $\varepsilon_{2.1}(Q(x,t))$, presence of unsteady flow conditions, $\varepsilon_{2.2}(Q(x,t))$ and seasonal changes of roughness, $\varepsilon_{2.3}(Q(x,t))$. As $\varepsilon_1(Q(x,t))$ and $\varepsilon_2(Q(x,t))$ are independent, the global uncertainty is obtained by:

$$\varepsilon\big(Q(x,t)\big) = \varepsilon 1\big(Q(x,t)\big) + \varepsilon 2(Q(x,t)) \tag{9}$$

And

$$|\varepsilon 2(Q(x,t))| = |\varepsilon 2.1(Q(x,t))| + |\varepsilon 2.2(Q(x,t))| + |\varepsilon 2.3(Q(x,t))| \tag{10}$$

The major source of uncertainty in measured streamflow for natural channels is change in channel dimensions, which can be caused by bed scour/deposition, bank erosion, vegetation changes, and debris

deposition. Thus, also adjustments are frequently needed to minimize the uncertainty in measured streamflow data from unstable channels (Harmel et al., 2006).

For what concern water quality measurements the sources of uncertainty come mainly from sample collection, sample preservation/storage and laboratory analysis.

Harmel et al. (2006) used a root mean square method to compare the uncertainty introduced by different sources for best and worst case and a range of typical "data quality" scenarios and the error propagation method to calculate the cumulative probable uncertainty in measured streamflow, sediment and nutrient data for best and worst case and a range of typical "data quality" scenarios.

In further studies Harmel and Smith (2007) modified the goodness of fit indicators (Nash-Sutcliff coefficient of efficiency, Index of agreement, Root mean square error and Mean absolute error) to take into account for the probable error range and/or the probability distribution of the measured data. The methodology consists in modifying the error term in the indicators ($e_i=O_i-P_i$, where e is the deviation between paired observed, O, and predicted, P, values) taking into account for the uncertainty in measurements. Two modifications were introduced: Modification 1 applies when only the uncertainty boundaries, but not the distribution is known and Modification 2 applies when the probability distribution is known or assumed for each measured value.

A brief description of the goodness-of.fit indicators is presented:

The Nash-Sutcliff coefficient of efficiency (NS) has been already defined. And can be rewritten as:

$$E = 1 - \frac{\sum_{i=1}^{N}(O_i - P_i)^2}{\sum_{i=1}^{N}(O_i - \bar{O})^2} \tag{11}$$

Where O_i are the observed data, P_i are the modeled data, $\bar{O}$ is the mean of the measured data and N is the number of observed data points.

The index of agreement (d) (Willmott, 1981) is defined as:

$$d = 1 - \frac{\sum_{i=1}^{N}(O_i - P_i)^2}{\sum_{i=1}^{N}(|P_i - \bar{O}| + |O_i - \bar{O}|)^2} \tag{12}$$

Notation is the same as seen above. It is a measure of the degree to which the model's predictions are error free. This index is also overly sensitive to extreme values.

The root mean square error (RMSE) and mean square absolute error (MAE) are defined as:

$$RMSE = \sqrt{N^{-1}\sum_{i=1}^{N}(O_i - P_i)^2} \tag{13}$$

$$MAE = N^{-1} \sum_{i=1}^{N} (O_i - P_i)^2 \quad (14)$$

The modifications are made substituting the $ei = O_i - P_i$ with the new $eu1i$ and $eu2i$. The new deviation terms have the following characteristics:

- $ei = eu1i = eu2i$ if the uncertainty in observation is assumed to be 0.
- $eu1i \leq eu2i \leq ei$
- The modified deviation, $eu1i$ and $eu2i$, decrease as the measured data uncertainty increases for a given pair of measured and predicted values
- The modified deviation, $eu1i$ and $eu2i$, decrease as the absolute value of the difference between measured and predicted data decreases for a given uncertainty range or probability distribution for each measured value.

In case of **Modification 1** (no information about distribution of the error in the observation available), the deviation terms are:

$$eu1i = 0 \quad if\ UOi(l) \leq Pi \leq UOi(u) \quad (15)$$

$$eu1i = UOi(l) - Pi \quad if\ Pi < UOi(l) \quad (16)$$

$$eu1i = UOi(u) - Pi \quad if\ Pi > UOi(l) \quad (17)$$

Where $UOi(u)$ and $UOi(l)$ are the uncertainty boundaries for each measured value, upper and lower respectively:

$$UOi(u) = Oi + \frac{PER * Oi}{100} \quad (18)$$

$$UOi(l) = Oi - \frac{PER * Oi}{100} \quad (19)$$

Where PER is the probable error range ($\pm\%$). It can be determined by literature values or expert judgement or as the sum of the uncertainty of all the error sources:

$$PER = \sqrt{\sum_{i=1}^{n} E_i^2} \quad (20)$$

where E_i is the uncertainty associated with the *ith* potential error source.

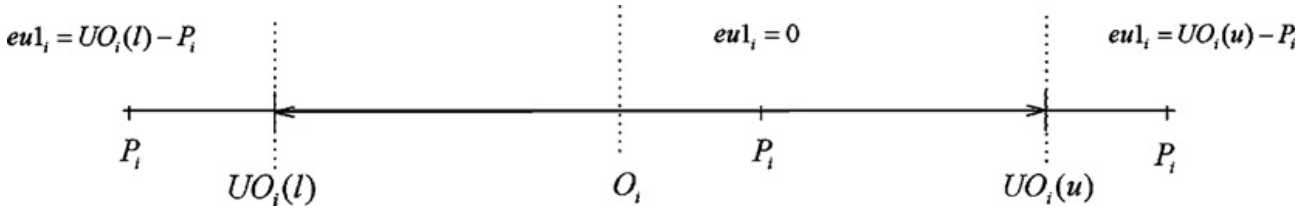

Figure 20 Graphical representation of Modification 1 to calculate the deviation between paired measured and predicted data based on the probable range of measured data but no distributional assumption (Harmel and Smith, 2006)

If the **Modification 2** is applied, then two distributions can be used: probability density function (pdf) in the case of normal distribution, or the continuous distribution function in case of the triangular distribution. A correction factor (CF) is calculated for each paired deviation and the new deviation term is calculated as:

$$eu2i = \frac{CFi}{0.5} * (Oi - Pi) \tag{21}$$

Modification 2 for measured data with a normal probability distribution:

When the probability distribution about data point is known or assumed to be represented by the normal distribution, then a CF is calculated from the standard normal distribution, so the mean and the variance are required: *Oi* is assumed to be the mean, μ, and median of the distribution, while the variance, σ^2 can be input directly, or can be calculated following the steps presented below:

1. Determine the PER for each data point using literature values or, expert judges, or the equation (20).
2. Uncertainty boundaries $UOi(u)$ and $UOi(l)$ are calculated:

$$UOi(l) = Oi - 3.9\sigma \text{ and } UOi(u) = Oi + 3.9\sigma \tag{22}$$

Where σ is the standard deviation about measured data value Oi:

$$\sigma^2 = \left(\frac{Oi - UOi(l)}{3.9}\right)^2 \text{ or } \sigma^2 = \left(\frac{UOi(u) - Oi}{3.9}\right)^2 \tag{23}$$

Where $\mu \pm 3.9\sigma$ contains the 99.99% of the normal probability distribution. The normal distribution is then transformed in the standard normal distribution:

$$Z_i = \frac{Xi - \mu_i}{\sigma_i}$$

$$Z_i = \frac{Pi - Oi}{\left(\frac{Oi - UOi(l)}{3.9}\right)^2} \text{ or } Z_i = \frac{Pi - Oi}{\left(\frac{UOi(u) - Oi}{3.9}\right)^2} \tag{24}$$

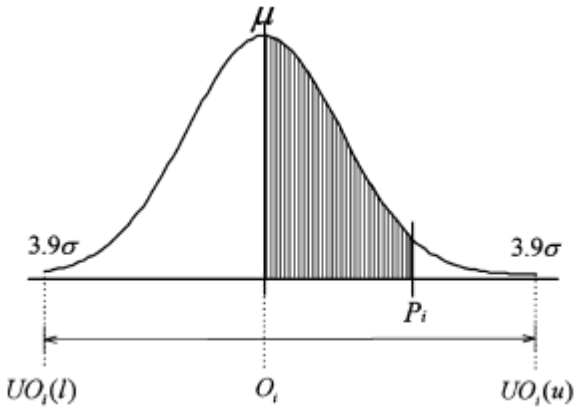

Figure 21 Graphical representation of Modification 2 to calculate the deviation between measured and predicted data for measured values with a normal probability distribution. (Harmel and Smith, 2007)

Modification 2 for measured data with a symmetric triangular probability distribution:

In this case the uncertainty boundaries are calculated with the eq. (13) and (14) while the CFs are calculated as:

$$CF = 0.5 - \frac{|Pi - UOi(l)|^2}{|UOi(u) - UOi(l)| * |Oi - UOi(l)|} \quad if\ UOi(l) \leq Pi \leq Oi \tag{25}$$

$$CF = 0.5 - \frac{|UOi(u) - Pi|^2}{|UOi(u) - UOi(l)| * |UOi(u) - Oi|} \quad if\ Oi \leq Pi \leq UOi(l) \tag{26}$$

$$CF = 0.5 \quad if\ Pi > UOi(u), Pi < UOi(l) \tag{27}$$

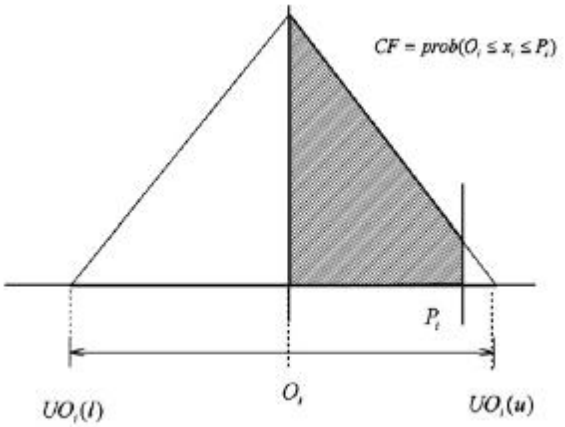

Figure 22 Graphical representation of Modification 2 to calculate the deviation between measured and predicted data for measured values with a triangular probability distribution. (Harmel and Smith, 2007)

Another source of error from observation is given by the assumption of spatial homogeneity of rainfall. Chaubey et al. (1998) describe the problem raising from a not proper representation of rainfall and asses the variability induced in calibrated model parameters solely due to rainfall spatial variability: they argue that spatial variability of rainfall should be captured and used in hydrologic/and water quality (H/WQ) models in order to accurately predict the hydrologic and water quality responses of watersheds. Their conclusion is that rainfall spatial pattern can be better captured using a network of rain gauges and radar rainfall data. They analyze the effect of using different rain gauges (17) over the same catchment and calculate the variation of rainfall comparing them with the average rainfall, resulting from an area weighted rainfall. They also compute the variability on parameter estimation due to rainfall with large variation and the correlation among the parameters and the input rainfall. They found a high correlation for example between the rainfall and the Curve Number, the slope, and the K factor of the Universal Soil Loss Equation.

To face the problem of uncertainty in rainfall data series and parameter values, Carpenter and Georgakakos (2004) use an approach based on prescribed probability distribution and a Monte Carlo simulation technique: a measure of the dispersion in the ensemble flow simulation was used to quantify the sensitivity of the flow simulation to parametric and radar rainfall uncertainty. The steps involved in the execution of the uncertainty sensitivity experiment are:

1. Calibration and validation of the R-R model based on adequate reproduction of observed stream flows at watershed gauged locations.
2. Definition of probabilistic uncertainty models for parameter error and radar rainfall input.
3. Identification of streamflow events to be modeled for each location.
4. Generation of ensemble simulated flows for each watershed location in a Monte Carlo experiment sampling from input probability distributions.
5. Computation of dispersion measures for each watershed location covering a range of spatial scales, for each event and for each uncertainty scenario.
6. Development of relationships between average dispersion measures and spatial scale for each scenario studied

Ensemble flow simulation were created for each event and watershed by introducing perturbations on model parameters and radar rainfall input through random sampling from prescribed probability distributions within a Monte Carlo simulation framework. Uncertainty was then introduced based on the prescribed distributions. Six uncertainty scenarios were considered and included:

a) Uncertainty in soil water parameters
b) Uncertainty in routing model parameters
c) Uncertainty in radar rainfall input using two different probability distributions and
d) Uncertainty in both model parameters and rainfall input

In each case the uncertainty is assessed by perturbing the parameters or the mean areal precipitation (MAP). The perturbation is performed considering a uniform distribution of the parameters or of the rainfall around the original value. So the parameters and the MAP are randomly changed:

$$P' = P * (1 + \alpha) \tag{28}$$

Where α ranges are [-0.5:0.5] and P and P' represent the original parameter or MAP and the perturbed ones respectively. For the precipitation they consider also an exponential distribution, so the perturbations are performed as:

$$P' = P10^{\varepsilon} \tag{29}$$

Where ε ranges from [-0.2: 0.2].

The uncertainty boundaries for rainfall are chosen assuming that no spatial or temporal correlation in sub-catchment hourly MAP errors. The simplification and the error ranges chosen are anyway consistent with other studies made (Georgakakos and Carpenter, 2003) that postulates general models for radar rainfall pixel errors. The uncertainty error found in the most of the cases is 50%.

2.2.3 Natural and epistemic uncertainty

When assessing the uncertainty it is also important to recognize two basic kinds of uncertainty that are fundamentally different from each other: natural and epistemic uncertainty. Natural uncertainty stems from variability of underlying modeled process, while the epistemic uncertainty results from incomplete knowledge about the process under study.

The main difference is that while the natural uncertainty cannot be reduced, the epistemic uncertainty, as it arises from model structure and expert judgment about an uncertain parameter, random sampling and measurement errors. The superposition of both types of uncertainty may lead to erroneous inferences (Cullern and Frey, 1999; Merz and Thieken, 2005).

2.2.4 Data-driven approaches for estimating uncertainty in R-R modeling

Shrestha and Solomatine (2008) propose a method, Uncertainty Estimation based on Local Errors and Clustering (UNEEC) for assessing the uncertainty in R-R models. This method is one of those based on the analysis of model errors. It assumes that the model error (mismatch between the observed and the modeled value) is an indication of total model uncertainty. The advantage of this method is that no assumption about the distribution of the parameters or of the residual is given. Unlike GLUE this method is based on the concept of *optimality* instead of *equifinality*: the first step of the method consist in finding the best parameter set of the model, then the uncertainty analysis is made analyzing the historical model residuals resulting from the optimal model. The uncertainty boundaries are then computed by two quantiles.

The three steps of the method are:

a) Clustering: the data set is partitioned in classes in which they share some common trait. Two different techniques are presented in the work of Shrestha and Solomatine, which are the *K-means* clustering and the *fuzzy C-means* clustering. The second one is a non exclusive clustering algorithm, in which every element is assigned to different clusters with different degree, so called fuzzy membership. The clustering in the UNEEC method is based on the assumption that "examples that are close in the input space correspond to similar real-life situation and will have similar values of model error". That means that small values of rainfall will produce small value of run-off and small error, while high values of rainfall will produce high values of rainfall with higher error.

b) Computing empirical error distribution: the computing of the prediction interval (PI) for each cluster are computed from empirical distributions of the corresponding historical residuals, computing the α/2*100 and the (1-. α/2)*100 percentiles in order to construct 100(1-α)% PIs. The method used depends on the clustering method used: the k-means is an exclusive method, so for every cluster the PIs are computed independently, while for the fuzzy C-means method each instance belongs to more than one cluster. In this case the PIs for every cluster are computed as:

$$PIC_i = e_j \quad j: \sum_{k=1}^{j} \mu_{i,j} < c_\alpha \sum_{j=1}^{n} \mu_{i,j} \tag{30}$$

Where *j* is the maximum integer value running from unity that satisfies the above inequality, e_j is the error associated with the instance *j* (instances are sorted with respect to the associated error), $\mu_{i,j}$ is the membership function of the *jth* instance to cluster *i*, $c_\alpha$equals to α/2 and 1-. α/2 for lower and upper PIs respectively.

c) Building uncertainty processor: the uncertainty processor compute the PIs for unseen input data. Different methods are presented:
   a. *Classification method:* used when the k-means clustering is used. It consists in attributing the input data to one of the cluster and querying in the lookup table including cluster labels and PIs.
   b. *Instance-based learning methods:* a distance function between the centers of the cluster and unseen input data is used to assign the data to particular cluster. The new data is assigned to the cluster which has the minimum distance between the cluster centre and it
   c. *Regression methods:* in this case the PIs for each training example have to be computed based on the PIs of each cluster.

Shrestha and Solomatine also compare the UNEEC method with GLUE and the Meta-Gaussian approach. The substantial difference among these methods is that while GLUE only accounts for the parameter uncertainty and the Meta-Gaussian method have strong assumption about the model residuals that should be Gaussian and homoscedastic and that model residuals are linearly dependent on simulated values, UNEEC take into account for all the sources of uncertainties and have no assumption

about the model residuals or the parameters distribution. Another criticism of GLUE is the selection of the appropriate threshold: the uncertainty boundaries depend much on it.

2.2.5 Cascading model uncertainty

The main purpose of this work is to assess the uncertainty that result from the cascading of the three models used to represent the Zenne river system: KOSIM, SWAT and HEC-RAS. Pappenberger et al. (2005) present a study about cascading model uncertainty from medium range forecast through a rainfall run-runoff model to flood inundation predictions. In their study they propagate the uncertainty from an atmospheric model to an R-R model to a flood inundation model (see figure 23).

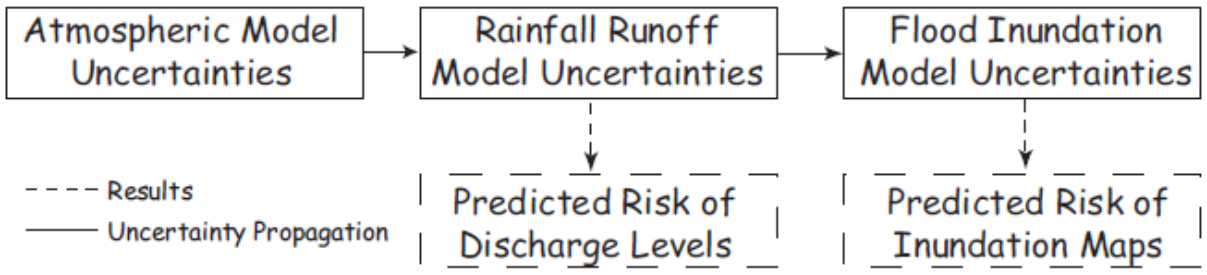

Figure 23 Sketch of the uncertainty cascade. Pappenberger et al., 2005

The rainfall forecast used are based on the European Centre for Medium Range Weather Forecasting control and ensemble forecast and consist in one deterministic, one control and 50 ensemble of 10-day ahead forecast of rainfall. Then these 52 rainfall forecast are fed to the R-R model.

The R-R model used is LisFlood (de Roo, 2000; de Roo et al. 2000, 2001). It is a distributed model with a water balance version (LiFlood-WB) that provides initial storage conditions for a flood prediction version (LisFlood-FF). The calibration is performed using a GLUE analysis through which 6 different data set are identified as behavioral. The uncertainty arising from model parameters and structure of the R-R model is thus evaluated from all the behavioral simulation.

The uncertainty in the hydraulic model (LisFlood-FP, Bates and De Roo, 2000), a simplified routing model that combines a one dimensional kinematic representation of the main channel flow with a grid square representation of the flood plain, is then assessed by a similar approach. The roughness values on the flood plain are varied by increments and the simulations are compared with observed patterns of flood inundation derived from aerial photography and satellite Synthetic Aperture Radar imagery.

To assess the resulting uncertainty from cascading the models, every forecast rainfall should be run through all the behavioral realization of the runoff generation model to provide upstream discharge for all the behavioral flood wave routing models. To reduce the number of runs required, a concept arising from the idea of equifinality within the GLUE methodology is applied, the functional similarity of parameter sets: particular parameter sets can be identified within which the difference between the

simulated hydrographs are small. The behavioral simulations are classified into functional types, so that only representative parameter sets for each functional type in the forecasting are used. The classification of the functional hydrographs predicted by the R-R model at a given point in the river network is made by a cluster analysis, in which the hydrographs are compared to each other by a similarity measure. Each class of behavioral hydrographs can be represented in prediction by a single (or a small number of) models weighted by the sum of the likelihood weights of all the behavioral parameter sets in that class.

The uncertainty is assessed computing the percentiles from 3120 inundation distributions: 52 rainfall forecast are used as inputs into the R-R model, which is represented by 6 parameter sets. These likelihood weighted outflow hydrographs are the upstream conditions for the inundation model, which is represented by 10 different parameter sets.

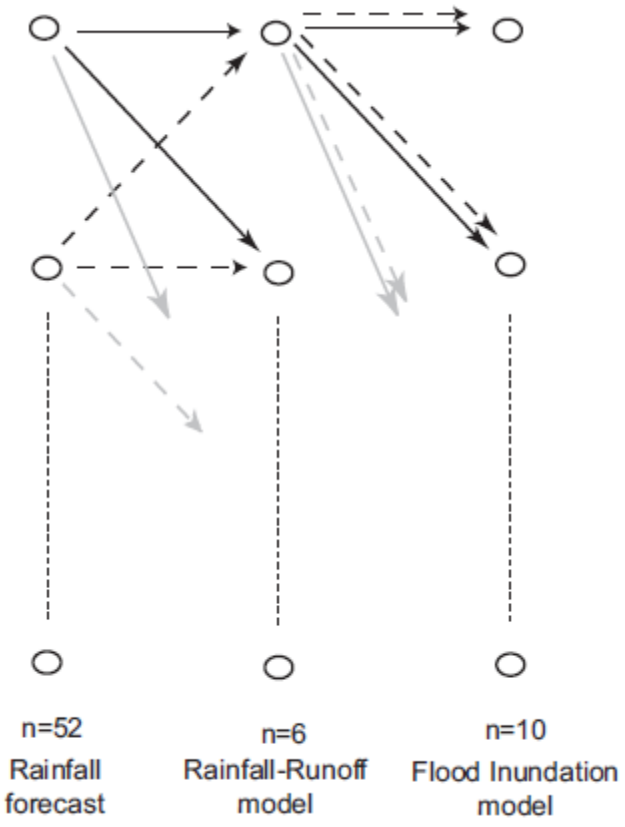

Figure 24 Sketch representing the uncertainty propagation and the implementation. (Pappenberger et al., 2005)

2.2.6 Calibration of SWAT models

As there is no method to quantify model concept uncertainty (Lei and Schilling, 1996; Van Griensven 2002), in this study, the model uncertainty will be assessed taking into account for parameter estimation uncertainty and observed data uncertainty. Many automatic methods exist to assess the

uncertainty of parameter estimation, such as ParaSol (Van Griensven and Meixner, 2006), SUFI-2 (Abbaspuor et al., 2004, 2007). These two algorithms can be used to calibrate the SWAT model.

The procedure for the calibration of SWAT consists in two steps:

- Selection of the most sensitive parameters to be calibrated.
- Performing of the calibration and uncertainty analysis.

The purpose of a sensitivity analysis is to assess the dependence of value of the output of the model, y, on the value of the parameter, x. It can be expressed as partial derivate $\partial y/\partial x$ (Lenhart et al, 2001) or by finite difference as:

$$I' = \frac{y_2 - y_1}{2\Delta x} \tag{31}$$

Where $y_1$and y_2 are the results of the perturbation of the parameter x from the initial value x_0 to the values $x_1 = x_0 - \Delta x$ and$x_2 = x_0 + \Delta x$. They classify the parameters as sensitive according to the table:

Class	Index	Sensitivity
I	0:00 $\leq$ | I | < 0:05	Small to negligible
II	0:05 $\leq$ | I | < 0:20	Medium
III	0:20 $\leq$ | I | < 1:00	High
IV	| I | $\geq$ 1:00	Very high

Table 5 Sensitivity classes. Lenhart et al. 2002

The sensitivity analysis in SWAT is performed automatically by an algorithm that combines a Latin Hypercube sampling (LHS) and a One factor At a Time (OAT) sampling procedure, the procedure is called Latin Hypercube - One-factor-At-a-Time (LH-OAT).

The Latin Hypercube is a procedure to perform random sampling such as Monte Carlo sampling. The concept behind the Latin Hypercube (McKay et al., 1979; McKay, 1988) is based on the Monte Carlo Simulation, but, instead of purely selecting the samples within the parameter space randomly, it uses a stratified sampling approach that allows efficient estimation of the output statistics. It subdivides the distribution of every parameter into N ranges, each with a probability of occurrence equal to 1/N. The parameters are then randomly sampled such a way that every range is sampled only once (van Griensven et al., 2006). The main strength of the LHS is that, if compared with the random sampling (Monte Carlo sampling), it is much more efficient. Helton and Davis (2003) made a comparison between the LHS and the random sampling and found that the former produces much more stable cumulate distribution (CDF) estimates of two function (a monotonic and a non-monotonic function) whose parameter ranges are within pre-established intervals. Yu et al. (2001) argued that LHS and MCS produce similar uncertainty boundaries, but the LHS require a number of run ten times smaller.

Compared with the random sampling the LHS has the advantage to determine the sensitivity over the entire parameter space in a computational efficient way. Also the parameter correlation can be included. The disadvantage lay in the assumption of linearity in multiple regressions and the incapacity of attributing the sensitivity to one particular model parameter.

The One-factor-At-a-Time (Morris 1991) is an example of an integration of a local into a global sensitivity method. For each run of the model only one parameter is changed, so that the sensitivity can be attributed only to the parameter that has been changed. For a model that has *n* parameters, *n+1* model runs are necessary to estimate the partial sensitivity of the model to each parameter.

The combination of the two methods (LH-OAT) ensures that the full range of the parameter value is sampled thanks to robustness of the Latin Hypercube sampling. It starts taking *N* Latin Hypercube sampling points, one for each LH interval, and then varying each LH sample point *P* times, where *P* is the number of parameters. The method operates by loops: around each LH point the effect of the variation of each parameter is computed. The final effect is calculated by averaging the partial effect of each loop.

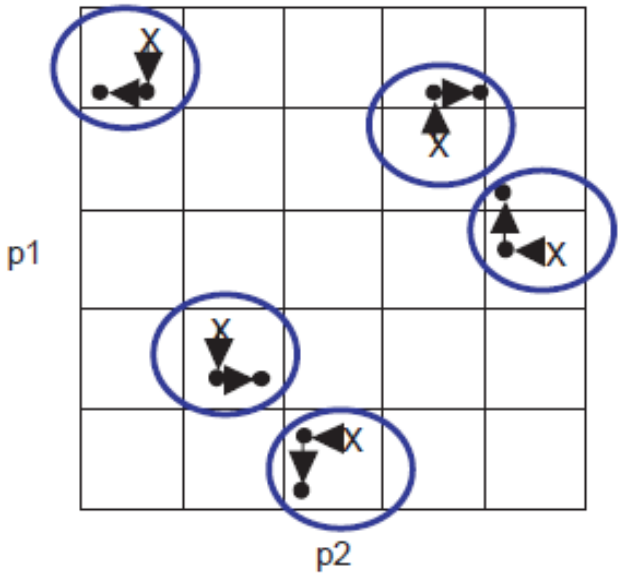

Figure 25 Illustration of LH-OAT sampling of values for two parameter model where X represent the LH point and • the OAT point (van Griensven et al., 2006)

Once the most sensitive parameters are selected, the calibration and uncertainty analysis is then performed. The calibration, in the SWAT model, can be performed using several approaches. Here, the description of two of them is reported, ParaSol (Van Griensven and Meixner, 2006) and SUFI-2 (Abbaspuor et al., 2004, 2007).

2.2.7 ParaSol (Parameter Solution Method):

ParaSol is based on a modification of the global optimization Shuffled Complex Evolution method developed at the University of Arizona algorithm (SCE-UA) (Duan et al., 1992). The method derive the prediction uncertainty using the simulation performed during optimization, as the algorithm explore the whole parameter space and focus on solution near the optimum/optima (van Griensven and Meixner, 2006).

The SCE-UA algorithm combines the direct search method of the simplex procedure with the concept of a controlled random search of Nelder and Mead (1965), a systematic evolution of points in the direction of global improvement, competitive evolution (Holland, 1975) and concept of complex shuffling.

The ParaSol procedure is as follows:

1. After the optimization made by the SCE-UA algorithm, the simulations are classified as "good" and "not good" by a threshold value of the objective function, as in GLUE, so that "good" and "not good" parameter sets are distinguished. The threshold in ParaSol is chosen on the basis of the χ^2-statistics, that compute a confidence region (CR), or on the basis of Bayesian statistics that are able to point out the high probability density region (HPD).
2. The prediction uncertainty is constructed by equally weighting all the "good" simulations.

The objective function used in ParaSol is the sum of the squares of the residuals (SSQ) or the sum of the squares of the difference of the measured and simulated values after ranking (SSQR). The latter method aims at the fitting of the frequency distributions of the observed and the simulated series. In this case the time of occurrence of a given value of a variable is not accounted for (van Griensven and Bauwens, 2001).

$$SSQ = \sum_{i=1,n}\left[x_{i,measured} - x_{i,simulated}\right]^2 \quad (32)$$

$$SSQR = \sum_{j=1,n}\left[x_{j,measured} - x_{j,simulated}\right]^2 \quad (33)$$

The χ^2-method, for the selection of the threshold, consist in finding the best parameter set, θ^* on the basis of the SSQ or the SSQR by the SCE-UA algorithm and then defining the threshold, c, for "good" parameter sets as following:

$$c = OF(\theta^*) * \left(1 + \frac{\chi^2_{p,0.95}}{n-p}\right) \quad (34)$$

Where *n* and *p* are the number of observations and of parameters respectively.

The Bayesian method is based on the Bayesian theorem: the probability $p(\theta|Y_{obs})$ of a parameter set θ is proportional to:

$$p(\theta|Y_{obs}) \propto exp\left[-\frac{\sum_{t=1}^{T}(y_{t,sim}-y_{t,obs})^2}{2\sigma^2}\right] \quad (35)$$

Where $\sigma^2 = \frac{SSQ_{MIN}}{nobs}$.

After normalizing the probabilities so that the integral over the entire parameter space is equal to 1, a cumulative distribution can be computed and the 95% confidence region can be computed. To prevent the problem of having the results dominated by the samples near the optimum that are more dense than in the other regions of the parameter space, the following procedure is used:

a) The parameter range is divided into m intervals
b) For each interval k, for every parameter j, the sampling density is calculated by counting the times the parameter j was sampled in the *kth* region.
c) Weight for the parameter set $\theta_i$is calcualted as:

$$W(\theta_i) = \frac{1}{\left[\prod_{j=1i}^{p} nsamp(k,j)\right]^{1/p}} \quad (36)$$

Where $nsamp(k,j)$ is the number of samples within the interval k for the parameter j.

d) Then the threshold is determined sorting the parameter sets according to decreasing probabilities, multiplying by the weights and normalizing the weighted probabilities by division by PT: $PT = \sum_{i=1}^{T} W(\theta_i) * p(\theta|Y_{obs})$
e) The normalized weighted probabilities are then summed starting from 1 until the sum is higher than the cumulative probability limit (95% or 97.5%). The objective function corresponding to the latest probability defines the threshold.

2.2.8 SUFI-2

SUFI-2 describes the parameter uncertainty by a multivariate uniform distribution in a parameter hypercube, while describe the output uncertainty by the 95% prediction uncertainty band (95PPU). Independent parameter sets are drawn by a LHS. The uncertainty rising from all the uncertainty sources is represented, similarly to GLUE.

The procedure is as following:

a) The objective function $g(\theta)$ and the parameter ranges $[\theta_{absmin}, \theta_{absmax}]$are defined
b) Latin Hypercube sampling is carried out in the hypercube $[\theta_{min}, \theta_{max}]$ and the corresponding objective functions are evaluated. The sensitivity matrix **J** and the covariance matrix **C** are computed according to:

$$J_{ij} = \frac{\Delta g_i}{\Delta \theta_j}, \quad i = 1 \ldots\ldots, C_2^m, \quad j = 1 \ldots\ldots, n. \tag{37}$$

$$C = s_g^2 (J^T J)^{-1} \tag{38}$$

Where s_g^2 is the variance of the objective function values resulting from m model runs. n is the number of columns, that is the number of parameters, and $C_2^m$is the number of rows of **J**, corresponding to the number of all possible combinations of two simulations.

c) The 95% predictive interval of each parameter θ_j is computed as follow:

$$\theta_{j,lower} = \theta_j^* - t_{v,0.025}\sqrt{C_{ij}} \ , \ \theta_{j,upper} = \theta_j^* + t_{v,0.025}\sqrt{C_{ij}} \tag{39}$$

Where θ_j^* is the value of the parameter θ_j that gives the best estimation and v is the number of degree of freedom (m-n).

d) After calculating the 95PPU, two indices are computed: the *p-factor* (percentage of observations bracketed by the 95PPU) and the r-factor:

$$r - factor = \frac{\frac{1}{n}\sum_{ti=1}^{n}(y_{ti,97.5\%}^M - y_{ti,2.5\%}^M)}{\sigma_{obs}} \tag{40}$$

Where $y_{ti,97.5\%}^M$ and $y_{ti,2.5\%}^M$ are the upper and the lower boundaries of the 95PPU, and σ_{obs} is the standard deviation of the measured data.

The goodness of the calibration and prediction uncertainty is judged on the basis of the closeness of p-factor to 100% and of r-factor to 1.

The procedure is then repeated updating the parameter distribution as follow: if the p-factor and the r-factor have satisfactory values, then a uniform distribution in the parameter hypercube $[\theta_{min}, \theta_{max}]$ is considered satisfactory and interpreted as the posterior parameter distribution. Otherwise $[\theta_{min}, \theta_{max}]$ is updated:

$$\theta_{j,min,new} = \theta_{j,lower} - \max\left(\frac{\theta_{j,lower} - \theta_{j,min}}{2}, \frac{\theta_{j,max} - \theta_{j,upper}}{2}\right) \tag{41}$$

$$\theta_{j,man,new} = \theta_{j,upper} + \max\left(\frac{\theta_{j,lower} - \theta_{j,min}}{2}, \frac{\theta_{j,max} - \theta_{j,upper}}{2}\right) \tag{42}$$

The aim of the project is to perform an uncertainty analysis integrating these methods, according to the structure of the model and the sources of uncertainty taken into account for, with the assessment of the uncertainty in observations, considering both, series of driving variables (e.g. rainfall) and series used for model calibration and validation.

The former series will be changed randomly within assumed boundaries of variability, based on literature values of error, to evaluate the effect on model output, while the modifications to Goodness-Of-Fit indicators (Nash-Sutcliff index is used to calibrate both the SWAT and the HEC-RAS model) proposed by Harmel et al. (2006) will be used to take into account for the uncertainty in observations. To assess the magnitude of the error in observations, for streamflow uncertainty, the model proposed by Di Baldassarre and Montanari will be used.

The calibration of the HEC-RAS model is performed by finding the Manning coefficient "n" and the value of a lateral flow, that is found to be well represented as the percentage (between 26% and 36%) of the upstream inflow (see description of the model for a better description), that make the simulated values of water stage fit the observed (see below). For this model the input streamflow series will be randomly modified within assumed boundaries of variability, based on Di Baldassarre and Montanari model and the uncertainty boundaries found in the SWAT model. The global uncertainty of the model will be considered as the cumulated uncertainty of the three single models.

3 The model codes

3.1 The SWAT model code

SWAT (Soil and Water assessment tool) is a river basin scale model developed by Dr. Jeff Arnold for the USDA Agricultural Research Service (ARS). The model was developed to predict the effect of land management practices on water, sediment, and agricultural chemical yields in large watersheds with varying soil, land use and management condition over long periods of time. This model has been validated in many studies and has proven to be an effective tool for assessing water resource and nonpoint source pollution problems for a wide range of scales and environmental conditions across the globe (Gassman et al. 2007).

To satisfy this objective, the model:

- Is physically based: SWAT requires specific information about weather, soil properties, topography, vegetation and land management practice occurring in the watershed.
- Is partly distributed.
- Uses readily available inputs.
- Is computationally efficient.
- Runs in continuous time (daily updating of the water balance, plant growth, nutrient and pesticide concentrations, etc.) and is capable of simulating long periods for computing the effects of management changes.

The time step is daily, but future development of the model, will be focused in modifying and evaluating the efficiency of an hourly or sub-hourly time step.

The water quality processes simulated by SWAT include precipitation, evapotranspiration, surface run-off and lateral, ground water and the percolation of the latter two. Nutrient transformation as well as crop growth and agricultural practices are also incorporated.

The simulator is incorporated in a GIS by ArcView preprocessor. SWAT divides the basin in sub-basins, by means of a Digital Elevation Map (DEM), and creates, within every sub-basin, hydrologic response units (HRUs) that are the result of the overlapping of three different maps: the Digital Elevation Model (DEM), the Land Use map and the soil map. Every HRU is thus a combination of slope, land use and soil and has a certain response to a rainfall event depending on this combination and the characteristic of soil and land cover: the runoff is calculated as the difference between the precipitation and the infiltration in the soil. In every sub-basin the contributions to runoff of every HRU is then summed to estimate the in-stream flow at the outlet of the sub-basin.

Next section describes the principal processes modeled in SWAT. For more detailed description of all the processes see Neitsch et al., 2005, Van Griensven, 2002.

3.1.1 Development of SWAT

SWAT was developed by the Agricultural Resource Service of the United States Department of Agriculture (ARS/USDA). It integrates the simulators:

- SWRRB: Simulator for Water Resources in Rural Basins.
- GLEAMS: Groundwater Loading Effects on an Agricultural Management System.
- CREAMS: Chemical, Runoff and Erosion from Agricultural Management Systems.
- ROTO: Routing Output To Outlet.
- EPIC: Erosion-Productivity Impact Calculator.

Originally SWRRB was linked to ROTO to take the output from several SWRRB models and route the flows through rivers and reservoirs. As this approach required several independent simulation runs and considerable computer storage, the two models were merged into a single model, SWAT.

There have been many releases of the SWAT model: SWAT94.2, SWAT96.2, SWAT98.1, SWAT99.2, SWAT2000, SWAT2005 and SWAT2009.

Also many tools and interfaces have been built for the SWAT model:

- AVSWAT (ArcView SWAT): it is a complete preprocessor, interface and post processor of the hydrological model SWAT.
- ArcSWAT: it is a ArcGIS-ArcView extension and a graphical user input interface for the SWAT
- SWAT-CUP: a computer program for calibration of SWAT models. It incorporates four different algorithms for calibration and uncertainty analysis of the SWAT model.
- VIZSWAT: a visualization and analysis tool.

3.1.2 Structure of SWAT:

SWAT allows a number of physical processes to be simulated in a watershed. For modeling purposes, a watershed may be partitions into number of sub-watersheds of subbasins.

Input information for each subbasin is grouped or organized into the following categories: climate; hydrologic response units or HRUs; ponds/wetlands; groundwater and the main channel or reach draining the subbasin. HRUs are lumped land areas within the subbasin that are comprised of unique land cover, soil and management combinations. The program calculation at first compute the fluxes in

each HRU, then these outputs are aggregated at the subbasin level. The subbasin output is then routed through river reaches according to the river network.

The input structure also reflects the structure of the model, as some of the inputs represent the whole basin, others the subbasins and the HRUs (see table 6).

BASIN		*SUB-BASIN*	
*.tmp	temperature (optional)	*.gw	groundwater parameters
*.pcp	precipitation (optional)	*.rte	river routing parameters
*.fig	model structure	*.swq	river water quality parameters
*.cod	model operation parameters	*.wgn	weather generator parameters
file.cio	all names of input files	*HRU*	
project.alo	Limit dimensions of the model (maximum number of reaches, subbasins, HRU's)	*.sub	Geometry and areal percentage of each HRU.
crop.dat	crop database	*.sol	soil characteristics
till.dat	tillage database	*.mgt	management practices
pest.dat	pesticide database	*.chm	initial chemical concentrations
ferst.dat	fertilizer database		

Table 6 Structure of SWAT model inputs (Van Griensven, 2002)

3.1.3 The water balance

Water balance is the driving force of everything that happens in the watershed. The simulation of the hydrology of the watershed can be separated into two major divisions: the land phase of the hydrologic cycle and the routing phase. The former controls the amount of water sediment, nutrient and pesticide loadings in the main channel in each subbasin. The latter is defined as the movement of water, sediments, etc. through the channel network of the watershed to the outlet.

The land phase processes are driven by the external forces of the weather, precipitation, temperature, wind speed, solar radiation and relative humidity. When rain reaches the surface, part can be retained by canopy interception. The remaining can either infiltrate or run off. The infiltrated water is then redistributed in the soil using a storage routing technique to predict flows among each layer in the root

zone. When the field capacity is exceeded and the layers below are not saturated, downward flow or percolation occurs.

The model take into account also for evapo-transpiration, lateral flow (flow from unsaturated zone in the soil to the stream), return flow (from the shallow aquifer to the stream), plant uptake and evaporation from the shallow aquifer in order to complete the water balance. The hydrologic model is based on the water balance equation:

$$SW_t = SW + \sum_{i=1}^{t} (R_i - Q_i - ET_i - P_i - QR_i) \tag{43}$$

where SW is the soil water content minus the 15-bar water content, t is time in days, and R, Q, ET, P, and QR are the daily amounts of precipitation, runoff, evapo-transpiration, percolation, and return flow; all units are in mm.

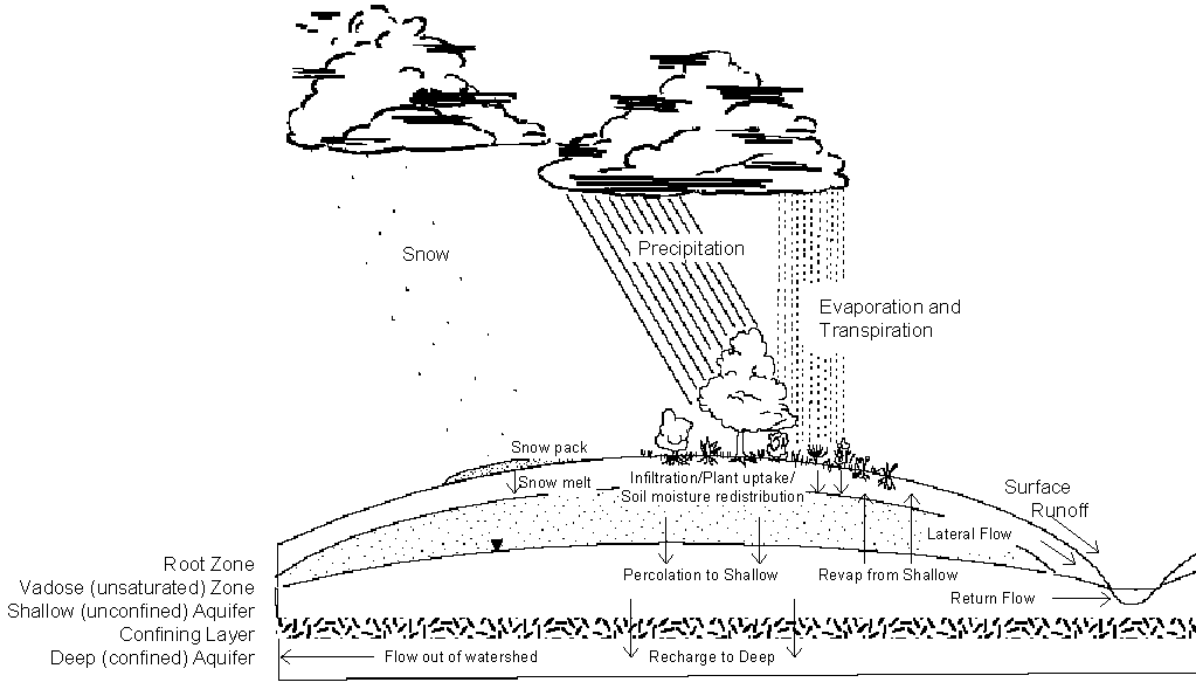

Figure 26 Schematic representation of the land phase of the hydrologic cycle (Neitsch et al., 2005).

Crop simulations are included in the model and consist in growth, growth limitations and uptake of water and nutrients. Land management practices may interact with these processes. Figure 26 represent the general sequence of processes used by SWAT to model the land phase of the hydrologic cycle. The next sections describe briefly the most important processes involved in the land phase of the hydrologic cycle.

Climate

The daily weather variables of a watershed are calculated with monthly average values and a weather generator. For precipitation, temperature (maximum and minimum), solar radiation, relative humidity, wind speed and potential evapotranspiration time series can be used.

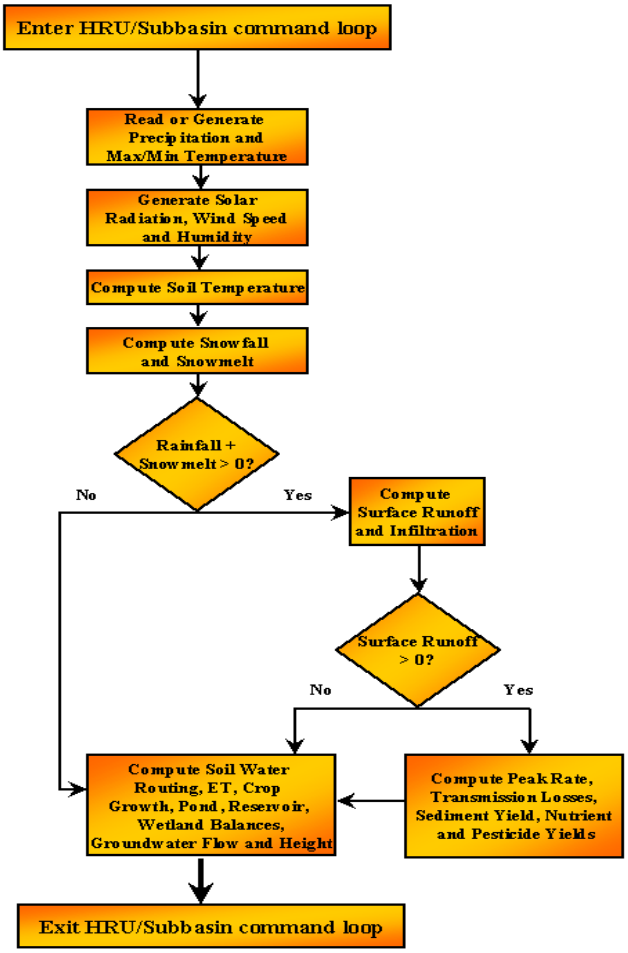

Figure 27HRU/Subbasin command loop (Neitsch et al., 2005).

Hydrology

As precipitation descends it may be intercept by the vegetation canopy or fall to the soil surface and either infiltrate in the soil profile or flow overland as runoff and reach relatively quickly the stream channels and contribute to short term stream response. Water that infiltrate is redistributed in the soil profile and can either evapotranspirate or move slowly to the surface system via underground paths, in figure 28 a schematic representation of the modeled possible pathways of water in SWAT is reported.

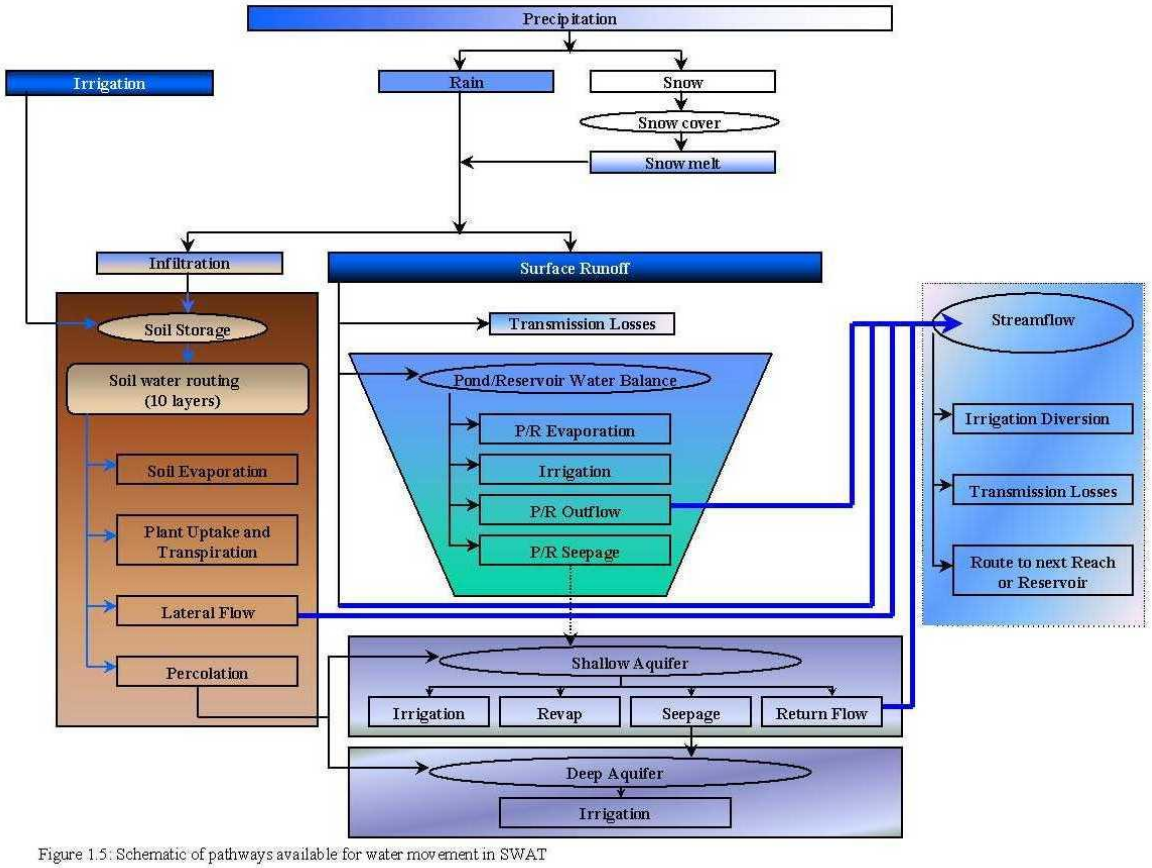

Figure 28 Available pathways for water in SWAT (Neitsch et al., 2005).

Canopy storage

Plant canopy can significantly affect infiltration, surface runoff and evapotranspiration by intercepting and storing the water falling as precipitation: as rain falls, canopy interception reduces the erosive energy of droplets and traps a portion of the rainfall within the canopy. The influence the canopy exerts on these processes is a function of the density of the plant cover and the morphology of the plant species. If the SCS curve number method is used to calculate the surface runoff, canopy interception is computed in term of initial abstraction. SWAT allows the user to input the maximum amount of water that can be stored in the canopy at the maximum leaf area index for the land cover. This value and the leaf area index are used by the model to compute the maximum storage at any time in the growth cycle of the land cover/crop. When evaporation is computed, water is first removed from the canopy storage. If the Green Ampt model is used to compute the surface runoff and infiltration, the interception of rainfall by canopy must be calculated separately.

Infiltration/Surface runoff

Infiltration refers to the entry of water in the soil profile from the soil surface. As infiltration continues, the soil becomes increasingly wet, so the infiltration rate decrease until it reaches a steady state. The

initial infiltration rate depends on the initial moisture content of the soil prior the introduction of water in the profile. The final infiltration rate corresponds to the saturated hydraulic conductivity of the soil.

If using the SCS curve number method (CN), as SWAT works on daily time-step, the infiltration is calculated as the difference between the precipitation and the surface runoff. Surface runoff is calculated using the SCS curve number equation as:

$$Q = \frac{(R-0.2s)^2}{R+0.8s}, \quad R > 0.2s$$

$$Q = 0.0 \ , R \leq 0.2s \tag{44}$$

Where Q is the daily runoff, R is the rainfall and s is a retention parameter calculated with the CN (Curve Number) and water content of the soil. The parameter s varies among subbasins, because slope, soils, land use and management all vary, and with time because of changes in soil water content.

Peak runoff predictions are made with a modification of the rational method. The rational method is based on the idea that if a rainfall of intensity *i* begins instantaneously and continues indefinitely, the rate of runoff will increase until the time of concentration t_c, when the entire subbasin is contributing to flow at the outlet. In the modified Rational Formula, the peak runoff rare is a function of the proportion of daily precipitation that falls during the subbasin t_c, the daily surface runoff volume, and the subbasin time of concentration. The proportion of rainfall occurring during subbasin t_c is estimated as a function of total daily rainfall using a stochastic technique. The subbasin time of concentration is estimated using Manning's Formula considering both overland and channel flow.

The Rational Formula is:

$$q_{peak} = \frac{C \cdot i \cdot Area}{3.6} \tag{45}$$

Where $q_{peak}$is the peak runoff rate (m^3/s), C is the runoff coefficient, i is the rainfall intensity (mm/hr), Area is the subbasin area (km^2) and 3.6 is a unit conversion factor.

The time of concentration is the amount of time from the beginning of a rainfall until the entire subbasin is contributing to flow at the outlet. It is calculated as the sum of the overland flow time and the channel flow time.

SWAT2005 is provided also of a module that can calculate the infiltration using a modification of the Green Ampt method. This method assumes that the soil profile is homogeneous and antecedent moisture is uniformly distributed in the profile. As water infiltrates into the soil, the model assumes the soil above the wetting front is completely saturated and there is a sharp break in moisture content at the wetting front. The method incorporated in SWAT was developed in 1973 by Mein and Larson. The

Green-Ampt Mein Larson (GAML) excess rainfall method requires sub-daily precipitation data supplied by the user. The infiltration rate in this method is defined as:

$$f_{inf} = K_e \cdot \left(1 + \frac{\Psi_{wf} \cdot \Delta\theta_v}{F_{inf,t}}\right) \quad (46)$$

Where f_{inf} is the infiltration rate at time *t* (mm/hr), K_e is the effective hydraulic conductivity (mm/hr), Ψ_{wf} is the wetting front matric potential (mm), $\Delta\theta_v$ is the change in volumetric moisture content across the wetting front (mm/mm) and $F_{inf,t}$ is the cumulative infiltration at time *t* (mm H_2O).

When the rainfall intensity is less than the infiltration rate, all the rainfall will infiltrate during the time period and the cumulative infiltration for that time period is calculated:

$$F_{inf,t} = F_{inf,t-1} + R_{\Delta t} \quad (47)$$

Where $F_{inf,t}$ is the cumulative infiltration for a given time step (mm H_2O), $F_{inf,t-1}$ is the cumulative infiltration for the previous time step (mm H_2O), and $R_{\Delta t}$ is the amount of rain falling during the time step (mm H_2O).

The infiltration rate is a function of the infiltrated volume, which in turn is a function of the infiltration rate in previous time step. The Green-Ampt effective hydraulic conductivity parameter K_e is approximately one-half the saturated hydraulic conductivity of the soil, K_{sat}:

$$K_e = \frac{56.82\ {K_{sat}}^{0.286}}{1+0.051\exp\left(0.062CN\right)} - 2 \quad (48)$$

Wetting front matrix potential is calculated as function of porosity, percent sand and percent clay.

The change in volumetric moisture content across the wetting front is calculated at the beginning of each day as function of the soil water content of the entire profile excluding the amount of water held in the profile at wilting point (mm H_2O), the amount of water in the soil profile at field capacity (mmH_2O) and the porosity of the soil (mm/mm).

King et al. (1999) compared the results of two SWAT models using the CN method and the Green-Ampt method on the same case study. They concluded that the GAML method, as drainage area increases, stream flow peaks tend to smooth out and the use of the GAML becomes ineffective, but in watersheds in which the stream peak response is quick, the use of the GAML coupled with a sub-daily routing step becomes beneficial in estimating direct runoff hydrographs. As streams get larger they do not respond as rapidly and CN should produce satisfactory results. CN provides a simple, yet robust, means of estimating excess rainfall. The major limitation of the CN is the inability to account for rainfall intensity and duration. GAML considers the intensity/duration and is advantageous when flood routing and peak discharges are needed. The parameters required by GAML are physically measurable

while CN is empirical. The drawbacks of GAML, include the need for breakpoint rainfall data and the intensive and time consuming soil test required for parameterization.

Ponds

Ponds are water storage structures located within a subbasin which intercepts surface runoff. The catchment area of a pond is defined as a fraction of the total area of the subbasin, Ponds are assumed to be located off the main channel in a subbasin and will never receive water from upstream subbasin, Pond water storage is a function of pond capacity, daily inflows and outflows, seepage and evaporation, required inputs are the storage capacity and surface are of the pond when filled to capacity, Surface area below capacity is estimated as a non-linear function of storage.

Tributary channels

Two types of channels are defined within a subbasin; the main channel and tributary channels, Tributary channels are minor or lower order channels branching off the main channel within the subbasin. Each tributary channel within a subbasin drains only a portion of the subbasin and does not receive groundwater contribution to its flow. All flow in the tributary channels is released and routed through the main channel of the subbasin. SWAT uses the attributes of tributary channels to determine the time of concentration for the subbasin.

Transmission losses

Transmission losses are losses of surface flow via leaching through the streambed. This type of loss occurs in ephemeral or intermittent streams where groundwater contribution occurs only at certain times of the year, or not at all. In SWAT water losses from the channel are a function of channel width and length and flow duration. Both runoff volume and peak rate are adjusted when transmission losses occur in the tributary channel.

Redistribution

Redistribution refers to the continued movement of water that has infiltrated in the soil. Redistribution is caused by differences in the water content in the profile. Once the water content throughout the entire profile is uniform, redistribution will stop. The redistribution component of SWAT uses a storage routing technique to predict flow through each soil layer in the root zone. Downward flow or percolation occurs when field capacity of a soil layer is exceeded and the layer below is not saturated. The flow rate is governed by the saturated conductivity of the soil layer. Movement of water from a subsurface layer to an adjoining upper layer may occur when the water content of the lower layer exceeds field capacity. The upward movement of water is regulated by the soil water to field capacity ratios of the two layers. Redistribution is also affected by soil temperature. If the temperature in a particular soil layer is below the freezing temperature, no redistribution is allowed from the layer.

The storage routing technique is based on the equation:

$$SW_i = SW_{oi}\exp\left(-\frac{\Delta t}{TT_i}\right) \quad (49)$$

Where SW_{oi} and SW_i are the soil water content at the beginning and the end of the day in mm, Δt is the time interval (24h) and TT_i is the travel time through the layer in h. Thus, the percolation can be computed by subtracting SW_i from SW_{oi}.

The travel time, TT_i, is computed for each soil layer with the linear storage equation:

$$TT_i = \frac{(SW_i - FC_i)}{H_i} \quad (50)$$

where H_i is the hydraulic conductivity in mm/h and FC is the field capacity minus wilting point water content for layer i in mm. The hydraulic conductivity is varied from the saturated conductivity value at saturation to near zero at field capacity.

$$H_i = SC_i\left(\frac{SW_i}{UL_i}\right)^{\beta_i} \quad (51)$$

where SC_i is the saturated conductivity for layer i in mm/h , UL_i is soil water content at saturation in mm/mm. β_i is a parameter that causes H_i to approach zero as SW_i approaches FC_i:

$$\beta = \frac{-2.655}{log_{10}\left(\frac{FC_i}{UL_i}\right)} \quad (52)$$

Flow through a soil layer may be limited by a saturated lower soil layer. If the layer immediately below the layer being considered is saturated, no flow can occur. The effect of lower layer water content is expressed in the equation:

$$O_{ci} = O_i\sqrt{1 - \frac{SW_i+1}{UL_i+1}} \quad (53)$$

Where O_{ci} is the percolation rate for the layer i in mm/d, corrected for the water content of layer i+1 and O_i is the percolation computed above.

Evapotranspiration

The evapotranspiration includes the processes of evaporation from water bodies and streams, bare soil and the sublimation from ice and snow cover and vegetative surface. It includes also the transpiration from the leaves of plants. The model computes evaporation from soils and plants separately. Potential soil water evaporation is estimated as a function of evapotranspiration and leaf area index (are of plant leaves relative to the area of the HRU). Actual soil water evaporation is estimated by using exponential functions of soil depth and eater content. Plant transpiration is simulated as a linear function of potential evapotranspiration and leaf area index.

Potential evapotranspiration (PET) is the rate at which evapotranspiration would occur from a large area completely and uniformly covered with growing vegetation which has access to an unlimited supply of

water. The model offers the possibility to evaluate the PET using three approaches: Hargreaves, Priestley-Taylor and Penman-Montheith. There is also the possibility to provide directly daily values of PET as input data series.

Evapotranspiration is the primary mechanism by which water is removed from a watershed. As roughly the 62% of the precipitation that falls on the continents is evapotranspired. Evapotranspiration exceeds runoff in most river basins and on all continents except for Antarctica.

Lateral Subsurface Flow

Lateral subsurface flow or interflow is streamflow contribution which originates below the surface but above the zone where rocks are saturated with water. Lateral subsurface flow in the soil profile (0-2m) is calculated simultaneously with redistribution. A kinematic storage model is used to predict lateral flow in each soil layer. The model accounts for variation in conductivity, slope and soil water content. SWAT incorporates a kinematic storage model for subsurface flow taken from Sloan and Moore (1984). The model simulates subsurface flow in a two dimensional cross section along a flow path down a steep hillslope. The kinematic approximation was used in its derivation. The model is based on mass continuity equation or mass water balance, with the entire hill slope segment used as the control volume.

The mass continuity equation used is:

$$\frac{S_2 - S_1}{t_2 - t_1} = iL - \frac{q_{lat1} - q_{lat2}}{2} \tag{54}$$

where S is the drainable volume of water stored in the saturated zone m/m (water above field capacity), t is time in hours, q_{lat} is the lateral flow in m^3/h, *i* is the rate of water input to the saturated zone in m^2/h, *L* is the hillslope length in m, and subscripts *1* and *2* refer to the beginning and end of the time step, respectively.

Return Flow

Return flow or base flow is the volume of streamflow originating from groundwater into two aquifer systems: a shallow, unconfined aquifer which contributes return flow to streams within the watershed and a deep, confined aquifer which contributes return flow to streams outside the watershed. Water percolating past the bottom of the root zone is partitioned into two fractions-each fraction becomes recharge for one of the aquifers. In addition to return flow, water stored in the shallow aquifer may replenish moisture in the soil profile in very dry conditions or be directly removed by plant uptake (only trees may uptake water from the shallow aquifer). Water in the shallow aquifer may also seep into the deep aquifer or be removed by pumping. Water in the deep aquifer may be removed by pumping.

The main objective of the groundwater model developed in SWAT is to predict the impact of management changes on total water supplies. The model is intended for general use where extensive field-work to obtain inputs is not feasible. Thus the groundwater component must use readily available inputs.

The water balance for the shallow aquifer is described by the equation:

$$aq_{sh,i} = aq_{sh,i-1} + w_{rchrg,sh} - Q_{gw} - w_{revap} - w_{pump,sh} \tag{55}$$

Where $aq_{sh,i}$ is the amount of water stored in the shallow aquifer during day *i*, $aq_{sh,i-1}$ is the amount of water stored in the shallow aquifer during day *i-1*, $w_{rchrg,sh}$ is the amount of recharge entering the

shallow aquifer on day *i*, Q_{gw} is the groundwater flow, or base flow, entering into the channel, w_{revap} is the amount of water moving into the soil zone in response to water deficiencies on day *i* and $w_{pump,sh}$ is the amount of water removed from the shallow aquifer by pumping on day *i*. All the variables are measured in mm H_2O.

The steady state response of groundwater flow to recharge is:

$$Q_{gw} = \frac{8000 \cdot K_{sat}}{{L_{gw}}^2} h_{wtbl} \tag{56}$$

Where Q_{gw} is the groundwater flow, or base flow, on day *i* in mm H_2O, K_{sat} is the hydraulic conductivity of the aquifer (mm/day), L_{gw} is the distance from the ridge or the subbasin divide for the groundwater system to the main channel (m) and h_{wtbl} is the water height (m).

Water table fluctuations, due to non-steady-state response of groundwater flow to periodic recharge, due to seepage from the stream channel, reservoirs or the soil profile (rainfall and irrigation), and depletion, due to return flow to stream, is calculated as:

$$\frac{dh_{wbhl}}{dt} = \frac{w_{rchrg,sh} - Q_{gw}}{800 \cdot \mu} \tag{57}$$

Where $\frac{dh_{wbhl}}{dt}$ is the change in water table height with time (mm/day), $w_{rchrg,sh}$ is the amount of recharge entering the shallow aquifer on day *i* (mm H_2O), Q_{gw} is the groundwater flow into the main channel on day *i* (mm H_2O) and μ is the specific yield of the shallow aquifer (mm/mm). Variation in return flow with time is related to the changes in water table height:

$$\frac{dQ_{gw}}{dt} = 10 \frac{K_{sat}}{\mu {L_{gw}}^2} \left(w_{rchrg,sh} - Q_{gw}\right) = \alpha_{gw} \left(w_{rchrg,sh} - Q_{gw}\right) \tag{58}$$

where α is the constant of proportionality or the reaction factor. The integration of the equation 58 gives the return flow:

$$Q_{gw,i} = Q_{gw,i-1} e^{-\alpha_{gw} \Delta t} + w_{rchrg,sh} \left(1 - e^{-\alpha_{gw} \Delta t}\right) \quad if\ aq_{sh,i} > aq_{shthr,qi}$$
$$Q_{gw,i} = 0 \quad if\ aq_{sh,i} \leq aq_{shthr,qi} \tag{59}$$

Where $aq_{shthr,qi}$ is a user specified threshold.

The relation for the water table height is derived by combining the equations 56 and 59:

$$h_{wtbl,i} = h_{wtbl,i-1} e^{-\alpha_{gw} \Delta t} + \frac{w_{rchrg}}{800 \cdot \mu \alpha} (1 - e^{-\alpha_{gw} \Delta t}) \tag{60}$$

. Groundwater movements are:

- Recharge: the delay time for return flow is estimated by using an exponential decay weighting function

$$w_{rchrg,i} = \left(1 - e^{-1/\delta_{gw}}\right) w_{seap} + e^{-1/\delta_{gw}} w_{rchrg,i-1} \tag{61}$$

  Where δ_{gw} is the delay time or drainage time of the overlying geologic formation (days) and w_{seap} is the total amount of water exiting the bottom of the soil profile on day *i* (mm H_2O).

- Revap is the movement of water into overlying unsaturated layers as a function of water demand for evapotranspiration. The maximum amount of water that will be removed from the aquifer via revap on a given day is:

$$w_{revap,mx} = \beta_{rev} E_0 \quad (62)$$

Where $w_{revap,mx}$ is the maximum amount of water moving into the soil zone in response to water deficiencies (mm H_2O), β_{rev} is the revap coefficient and $E_0$is the PET for day *i.*

The actual amount of revap is:

$$w_{revap} = 0 \qquad if \;\; aq_{sh} \leq aq_{shthr,rvp}$$
$$w_{revap} = w_{revap,mx} - aq_{shthr,rvp} \qquad if \;\; aq_{shthr,rvp} < aq_{sh} < (aq_{shthr,rvp} + w_{revap,mx})$$
$$w_{revap} = w_{revap,mx} \qquad if \;\; aq_{sh} \geq (aq_{shthr,rvp} + w_{revap,mx}) \quad (63)$$

Where $aq_{shthr,rvp}$is a user defined threshold level in the shallow aquifer for revap to occur.

- Seepage to deep aquifer:
The water balance for the deep aquifer is

$$aq_{dp,i} = aq_{dp,i-1} + w_{deep} - w_{pump,dp} \quad (64)$$

Where $aq_{dp,i}$ is the amount of water stored in the deep aquifer on day *i*, $aq_{dp,i-1}$ is the amount of water stored in the deep aquifer on day *i-1*, w_{deep} is the amount of water percolating from shallow aquifer on day *i* and $w_{pump,dp}$ is the amount of water removed by pumping from the deep aquifer on day *i.* All the variables in the equation are measured in mm H_2O.

The return flow will indirectly depend on the infiltration and the previous soil parameters as it is fed by the seepage of the soil profile to the shallow aquifer. The direct parameters set consist of 2 parameters that express delay or lag effects, 2 that define fractions and 2 threshold depths for the storage of the shallow aquifer to have "revap" or return flow to occur.

3.1.4 Land Cover/Plant Growth

SWAT utilises plant growth model to simulate all types of land cover. The model is able to differentiate between annual and perennial plants. Annual plants grow from the planting date to the harvest date or until the accumulated heat units equal the potential heat units for the plant. Perennial plants maintain their root systems throughout the year, becoming dormant after frost. They resume growth when the average daily air temperature exceeds the minimum or base, temperature required. The plant growth model is used to assess the removal of water nutrients from the root zone, transpiration and biomass/yield production.

Potential Growth

The potential increase in plant biomass on a given day is defined as the increase in biomass under ideal growing conditions. The potential increase in biomass for a day is a function of intercepted energy and

the plant's efficiency in converting energy to biomass. Energy interception is estimated as a function of solar radiation and the plant's leaf area index.

Potential and Actual Transpiration

The process used to calculate potential plant transpiration is described the section on evapotranspiration. Actual transpiration is a function of potential transpiration and the soil water content.

Growth constraints

Potential plant growth and yield are usually not achieved due to constraints imposed by the environment. The model estimates stresses caused by water, nutrients and temperature.

Nutrient uptake

Plant use of nitrogen and phosphorus are estimated with a supply and demand approach where the daily plant nitrogen and phosphorus demands are calculated as the difference between the actual concentration of the element in the plant and the optimal concentration. The optimal concentration of the element varies with growth stage.

3.1.5 Erosion

Erosion and sediment yield are estimated for each HRU with the Modified Universal Loss Equation (MUSLE). MUSLE is a modified version of the Universal Soil Equation (USLE). While the USLE uses rainfall as an indicator of erosive energy, MUSLE uses the amount of runoff to simulate erosion and sediment yield. The MUSLE equation is:

$$sed = 11.8 \cdot (Q_{surf} \cdot q_{peak} \cdot area_{HRU})^{0.56} K_{USLE} \cdot C_{USLE} \cdot P_{USLE} \cdot LS_{USLE} \cdot CFRG \quad (65)$$

Where *sed* is the sediment yield on a given day (metric tons), Q_{surf} is the surface runoff volume (mm H_2O/ha), q_{peak} is the peak runoff rate (m^3/s), $area_{HRU}$ is the area of the HRU (ha), K_{USLE} is the USLE soil erodibility factor, C_{USLE} is the USLE cover and management factor, P_{USLE} is the USLE support practice factor, LS_{USLE} is the USLE topographic factor and $CFRG$ is the coarse fragment factor.

3.1.6 Water quality

The water quality module in SWAT calculate the amount of algae, dissolved oxygen and carbonaceous biological oxygen demand (CBOD) entering the main channel with surface runoff. The in-stream water quality module for is based on the QUAL2E model (Brown and Barnwell, 1987).

Nitrogen

SWAT tracks the movement and transformation of nutrients (nitrogen and phosphorus) in the watershed. The ways nutrients can be introduced in the main channel are: surface runoff and lateral subsurface flow. Other point and nonpoint sources can be introduced manually in the model.

Nitrogen is modeled using five different pools: two pools are mineral (ammonium NH4 and nitrates NO3) and three of them are Organic (active, stable and fresh). NO3 can be removed by plant uptake or denitrification and NH4 by volatilization, while fresh nitrogen come from plant residue. The nitrogen can be transformed from one to another pool

The different processes modelled by SWAT in the HRU's and the various pools of nitrogen in the soil are shown in Fig. 16. Plant use of nitrogen is estimated using the supply and demand. In addition to plant use, nitrate and organic N may be removed from the soil via mass flow of water. Amounts of NO_3-N contained in runoff, lateral flow and percolation are estimated as products of the volume of water and the average concentration of nitrate in the layer. Organic N transport with sediment is calculated with a loading function. The loading function estimates the daily organic N runoff loss based on the concentration of organic N in the top soil layer, the sediment yield, and the enrichment ratio. The enrichment ratio is the concentration of organic N in the sediment divided by that in the soil.

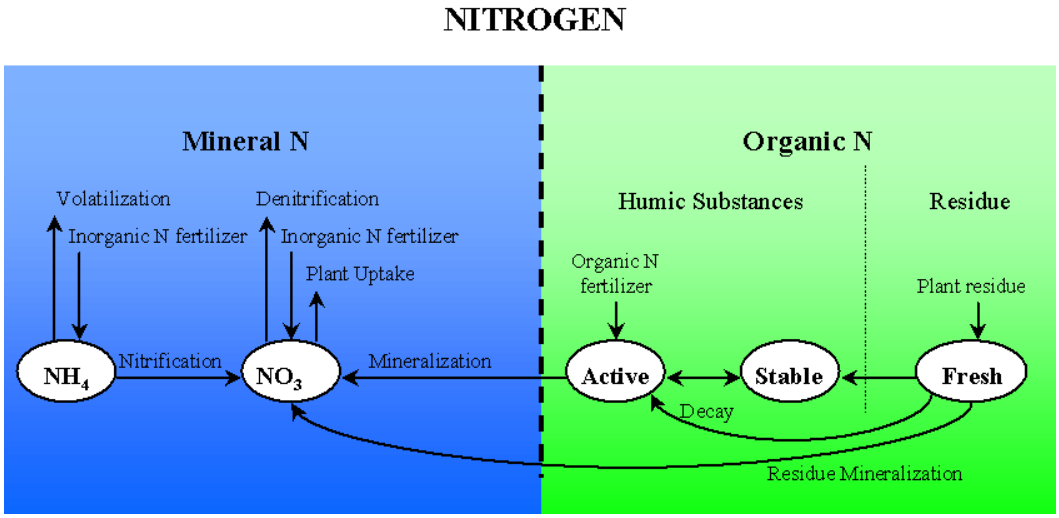

Figure 29 Partitioning of Nitrogen in SWAT (Neitsch et al. 2002)

Phosphorus

The Phosphorus module (independent from the nitrogen one) is modeled using five pools: three are mineral and two of them are organic.

The different processes modelled by SWAT in the HRU's and the various pools of phosphorus in the soil are depicted in Fig. 17. Plant use of phosphorus is estimated using the supply and demand approach described in the section on plant growth. In addition to plant use, soluble phosphorus and organic P may be removed from the soil via mass flow of water. Because, phosphorus is not very soluble, the loss of phosphorus dissolved in surface runoff is based on the concept of partitioning pesticides into the solution and sediment phases. The amount of soluble P removed in runoff is predicted using labile P concentration in the top 10 mm of soil, the runoff volume and a partitioning factor. Sediment transport of P is simulated with a loading function as described in organic N transport.

Pesticides

Although SWAT does not simulate stress on the growth of a plant due to the presence of weeds, damaging insects and other pests, pesticides may be applied to an HRU to study the movement of the chemical on the watershed, SWAT simulated pesticides movement into the stream network via surface runoff and into soil profile and aquifer by percolation. The movement of the pesticides is controlled by its solubility, degradation half-life, and soil organic carbon adsorption coefficient. Pesticide on plant foliage and in the soil degrades exponentially according to the appropriate half-life. Pesticide transport by water and sediment is calculated for each runoff event and pesticide leaching is estimated for each soil layer when percolation occurs.

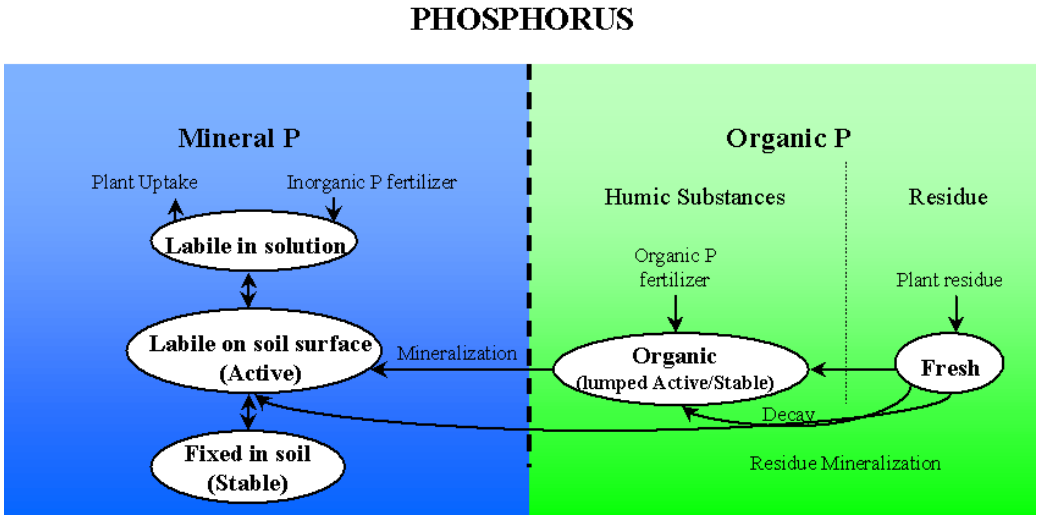

Figure 30 Partitioning of Phosphorus in SWAT (Neitsch et al. 2005)

3.1.7 Management

SWAT allows the user to define management practices taking place in every HRU. The user may define the beginning and the ending of the growing season; specify timing and amounts of fertiliser, pesticide and irrigation applications as well as timing of tillage operations. At the end of the growing season, the biomass may be removed from the HRU as yield or placed on the surface as residue.
In addition to these basic management practices, operations such as grazing, automated fertiliser and water applications, and incorporation of every conceivable management option for water use are available.

3.1.8 Routing Phase of the Hydrologic Cycle

Once SWAT determines the loading of water, sediment, nutrients and pesticides to the main channel, the loadings are routed through the stream network of the watershed. In addition to keeping track of mass flow in the channel, SWAT models the transformation of chemicals in the stream and streambed. Fig. V-7 illustrates the different in-stream processes modelled by SWAT. As water flows downstream,

a portion may be lost due to evaporation and transmission through the bed of the channel. Another potential loss is removal of water from the channel for agricultural or human use. Flow may be supplemented by the fall of rain directly on the channel and/or addition of water from point source discharges. Once SWAT determines the loading of water, sediment, nutrients and pesticides to the main channel, the loadings are routed through the stream network of the watershed.

3.2 The HEC-RAS model code

HEC-RAS is an integrated system of software that performs one-dimensional hydraulic calculations for a network of natural and constructed channels. The one-dimensional river analysis components are:

1. Steady flow water surface profile computations;
2. Unsteady flow simulation;
3. Movable boundary sediment transport computations;
4. Water quality analysis

The four components use a common geometric data representation (i.e. river cross sections) and hydraulic computation routines.

The next section presents briefly the components of the model. For further information about the theory behind the model see the HEC-RAS hydraulic reference manual (US Army Corps of Engineers, 2008).

The current HEC-RAS version can perform river water quality analysis taking into account for Temperature and transport of Algae, Dissolved Oxygen, Carbonaceous Biological Oxygen Demand, Dissolved Orthophosphate, Dissolved Organic Phosphorus, Dissolved Ammonium Nitrate, Dissolved Nitrite Nitrogen and Dissolved Organic Nitrogen.

HEC-RAS is designed to perform one-dimensional hydraulic calculations for a full network of natural and constructed channels. The major hydraulic capabilities of HEC-RAS are reported below.

3.2.1 Steady flow water surface profiles

This component of the modeling system is intended for calculating water surface profiles for steady gradually varied flow. The system can handle a single river reach, a dendritic system, or a full network of channels. The steady flow component is capable of modeling subcritical, supercritical, and mixed flow regime water surface profiles. The basic computational procedure is based on the solution of the one-dimensional energy equation. Energy losses are evaluated by friction (Manning's equation) and contraction/expansion (coefficient multiplied by the change in velocity head). The momentum equation is utilized in situations where the water surface profile is rapidly varied. These situations include mixed flow regime calculations (i.e., hydraulic jumps), hydraulic of bridges, and evaluating profiles at river confluences (stream junctions). The effect of various obstructions such as bridges, culverts, weirs, spillways and other structures in the flood plain may be considered in the computations. The steady flow system is designed for application in flood plain management and flood insurance studies to evaluate floodway encroachments. Also, capabilities are available for assessing the change in water surface due to channel improvements, and levees. Special features of the steady flow component include: multiple plan analyses; multiple profile computations; multiple bridge and /or culvert opening analysis, and split flow optimization at stream junctions and lateral weirs and spillways.

Water surface profiles are computed from one cross section to the next by solving the Energy equation with an iterative procedure called the standard step method. The energy equation is:

$$Z_2 + Y_2 + \frac{a_2 {V_2}^2}{2g} = Z_1 + Y_2 + \frac{a_1 {V_1}^2}{2g} + h_e \tag{66}$$

Where Z_1 and Z_2 are the elevation of the main channel inverts; Y_1 and Y_2 are the depth of water at cross sections; V_1 and V_2 are the average velocities (total discharge/total flow area); a_1 and a_2 are velocity weighting coefficients, g is the gravitational acceleration and h_e is the energy head loss. The energy head loss between two cross sections is comprised of friction losses or expansion losses. The equation is:

$$h_e = L\bar{S}_f + C\left|\frac{a_2 {V_2}^2}{2g} - \frac{a_1 {V_1}^2}{2g}\right| \tag{67}$$

Where L is the discharge weighted reach length, $\bar{S}_f$ is the representative friction slope between two sections and C is the expansion or contraction loss coefficient.

The L is calculated as the weighted sum of the lengths of the overbanks (left, right and main channel) of the reach. The weights are the arithmetic average of the flows between sections for each overbank.

The calculation of the total conveyance and the velocity coefficient for a cross section require the flow be subdivided into units for which the velocity is uniformly distributed. The approach used in HEC-RAS is to subdivide flow in the overbank areas using the input cross section Manning's n-value break points as the basis for the subdivision. Conveyance is calculated using the Manning's equation:

$$Q = K{S_f}^{1/2}$$

$$K = \frac{1}{n}AR^{2/3} \tag{68}$$

Where K is the conveyance for the subdivision n is the Manning's roughness coefficient for the subdivision. A is the flow area for the subdivision and R is the hydraulic radius for the subdivision (area / wetted perimeter).

The program will sum-up all the conveyance for each of the subdivision (left bank, right bank and main channel) or each of the subdivisions of the river bed in which the Manning's "n" changes.

Because HEC-RAS is one dimensional water surface profiles program, only a single water surface and therefore a single mean energy are computed at each cross section as the mean energy obtained by computing flow weighted energy from the three subsection of a cross section (left and right overbank and main channel). In order to compute the mean kinetic energy it is necessary to obtain the velocity head weighting coefficient alpha, in case of two subdivisions, as:

$$a\frac{\overline{V}^2}{2g} = \frac{Q_1\frac{{V_1}^2}{2g}+Q_2\frac{{V_2}^2}{2g}}{Q_1+Q_2} \tag{69}$$

In general:

$$a = \frac{\left[Q_1{V_1}^2+Q_2{V_2}^2+\cdots+Q_N{V_N}^2\right]}{Q\overline{V}^2} \tag{70}$$

Friction losses are computed from Manning's equation as follow:

$$S_f = \left(\frac{Q}{K}\right)^2 \tag{71}$$

Other alternative options are available as: the Average Conveyance Equation; the Average Friction Slope Equation; the Average Mean Friction Slope Equation and the Harmonic Mean Friction Slope Equation.

The contraction and expansion losses in HEC-RAS are evaluated by the equation 72:

$$h_{ce} = C\left|\frac{\alpha_2{V_2}^2}{2g} - \frac{\alpha_1{V_1}^2}{2g}\right| \tag{72}$$

Where C is the contraction or expansion coefficient. The contraction is assumed to be occurring whenever the velocity head downstream is greater than the velocity head upstream. The expansion is assumed to occur whenever the velocity downstream is smaller than the velocity upstream.

The model is capable of calculate the critical depth. Whenever the water surface passes through critical depth, the energy equation is not applicable anymore, as the transition from supercritical to subcritical flow is a rapidly varying flow situation, and the energy equation is applicable only in situation of gradually varied flow. In case of transition from supercritical to subcritical flow occurs, empirical equations (for drop structures or weirs) or the momentum equation can be used. The latter is used for hydraulic jumps, low flow hydraulics at bridges and stream junctions. Applying the Newton's second law of motion to a body of water between two cross sections at locations 1 and 2, the following expression for the change in momentum over a unit time can be written:

$$P_2 - P_1 + W_x - F_f = Q\rho\Delta V_x \tag{73}$$

Where P is the hydrologic pressure force at location 1 and 2; W_x is the force due to weight of water in the X direction; F_f is the force due to external friction losses from 2 and 1; Q is the discharge; ρ is the density of water; andΔV_x is the change on velocity from 2 to 1, in the X direction.

The principal limitations linked to the Steady Flow Program are the following assumptions: the flow is steady; the flow is gradually varied; the flow can be modeled as one dimensional and the channel have small slopes (less than 1:10).

- ### *3.2.2 Unsteady Flow Simulation*

This component of the HEC-RAS modeling system is capable of simulating one-dimensional unsteady flow through a full network of open channels. The hydraulic calculations for cross sections, bridges, culverts and other hydraulic structures that were developed for the steady flow component are incorporated into the unsteady flow module. The unsteady flow component has the ability to model storage areas and hydraulic connections between storage areas, as well as between stream reaches.

The physical laws which govern the flow of water in a stream are: (1) the principle of conservation of mass (continuity), and (2) the principle of conservation of momentum. These laws are expressed mathematically in the form of partial differential equations. Conservation of mass for a control volume states that the net rate of flow into the volume is equal to the rate of change of storage inside the volume. The change in mass in the control volume is equal to:

$$\rho \frac{\partial A_T}{\partial t} \Delta x = \rho \left[\left(Q - \frac{\partial Q}{\partial x} \frac{\Delta x}{2} \right) - \left(Q + \frac{\partial Q}{\partial x} \frac{\Delta x}{2} \right) + Q_l \right] \quad (74)$$

Where ρ is the fluid density; $\frac{\partial A_T}{\partial t} \Delta x$ is the rate of change in storage, $\left(Q - \frac{\partial Q}{\partial x} \frac{\Delta x}{2} \right)$ and $\left(Q + \frac{\partial Q}{\partial x} \frac{\Delta x}{2} \right)$ are the inflow and the outflow respectively and Q_l is the lateral inflow.

Conservation of momentum is expressed by Newton's second law (as for the steady flow regime) as:

$$\sum F_x = \frac{dM}{dt} \quad (75)$$

Conservation of momentum for a control volume states that the net rate of momentum entering the volume (momentum flux) plus the sum of all external forces acting on the volume are equal to the rate of accumulation of momentum. This is a vector equation applied in the x-direction. The momentum flux is the fluid mass times the velocity vector in the direction of flow. Three forces are considered in the momentum calculation: pressure, gravity and boundary drag, or friction force.

The one-dimensional unsteady flow equation solver used in HEC-RAS is the four-point implicit scheme, or box scheme. Space derivates and function values, under this scheme, are evaluated at an interior point, $(n+\theta)\Delta t$. Thus values at $(n+1)\Delta t$ enter into all terms in the equations. For a reach of river, the result is a system of simultaneous equations. The simultaneous solution is an important aspect of this scheme because it allows information from entire reach to influence the solution at any one point. The implicit scheme is demonstrated to be unconditionally stable for values of the θ factor $0.5 < \theta \leq 1.0$ and conditionally stable for $\theta = 0.5$ and unstable for $\theta < 0.5$. The solution scheme can be, thus unstable: the sources on instability are, along with the θ factor value, dramatic changes in channel

cross-sectional properties, abrupt changes in channel slope, characteristic of the flood wave itself, and complex hydraulic structures such as levees, bridges, culverts, weirs and spillways.

The scheme is represented in figure 31.

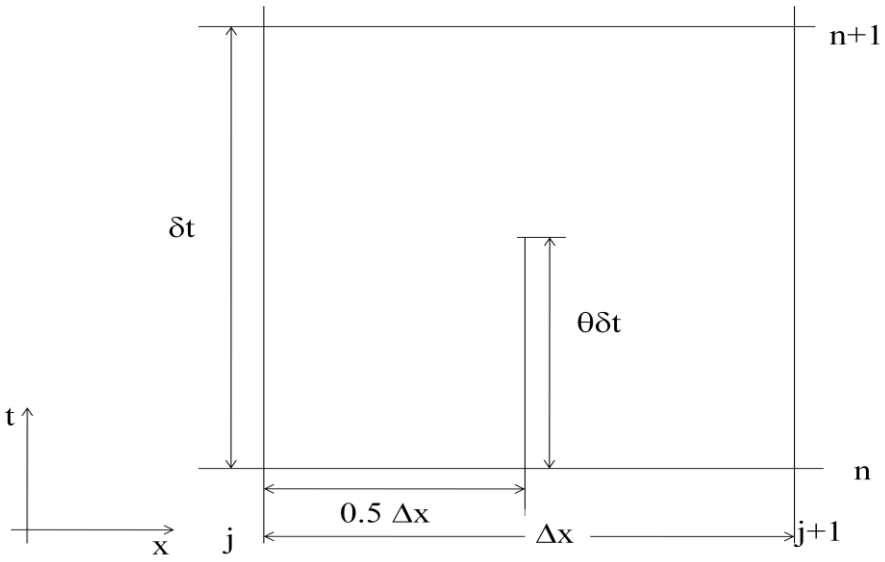

Figure 31 Representation of the Implicit Finite Different Scheme

The following notation is defined: $f_j = {f_j}^n$

And $\Delta f_j = {f_j}^{n+1} - {f_j}^n$. Then: ${f_j}^{n+1} = {f_j}^n + \Delta f_j$.

The general implicit finite difference forms are:

1. Time derivate:

$$\frac{\partial f}{\partial t} \approx \frac{\Delta f}{\Delta t} = \frac{0.5(\Delta f_{j+1} \Delta f_j)}{\Delta t} \tag{76}$$

2. Space derivate:

$$\frac{\partial f}{\partial x} \approx \frac{\Delta f}{\Delta x} = \frac{(f_{j+1} f_j) + \theta(\Delta f_{j+1} \Delta f_j)}{\Delta x} \tag{77}$$

3. Function value:

$$f \approx \bar{f} = 0.5\left(f_j + f_{j+1}\right) + 0.5\theta(\Delta f_j + \Delta f_{j+1}) \tag{78}$$

3.2.3 Sediment Transport/Movable Boundary Computations

This component of the modeling system is intended for the simulation of one-dimensional sediment transport/movable boundary calculations resulting from scour and deposition over moderate time periods (typically years, although applications to single flood events will be possible). The model is

designed to simulate long-term trends of scour and deposition in a stream channel that might result from the modifying in the frequency and duration of the water discharge and stage, or modifying the channel geometry. The system can be used to evaluate de deposition in reservoirs, design channel contractions required to maintain navigation depths, predict the influence of dredging on the rate of deposition, estimate maximum possible scour during large flood events, and evaluate sedimentation in fixed channels.

3.2.4 Water Quality Analysis

The current HEC-RAS version can perform river water quality analysis taking into account for Temperature and transport of Algae, Dissolved Oxygen, Carbonaceous Biological Oxygen Demand, Dissolved Orthophosphate, Dissolved Organic Phosphorus, Dissolved Ammonium Nitrate, Dissolved Nitrite Nitrogen and Dissolved Organic Nitrogen.

3.3 The KOSIM model code

KOSIM is a continuous simulation model for combined sewer systems developed by ITWH, Hannover. It was developed for long simulations of flows and quality variables of combined sewer systems.

The model simulates four processes: dry-weather flows, dry-weather pollutants loads, storm flows and storm pollutant loads. The pollutants loads are simulated in the model as BOD, suspended solids, ammonia and phosphorus.

4 The case study: the Zenne River

4.1 Overview

The Zenne river basin (figure 32) is located in Belgium over the Flemish, Walloon and Brussels region. The river sources are in the Walloon region. The river then flows toward the Flemish and Brussels region. The outlet of the river is in the north of Brussels, in correspondence of the town of Mechelen, in the Dijle River, a tributary of the river Scheldt. The source of the latter is in the north of France and the estuary is in the south of Netherlands.

Figure 32 map of Belgium - overview of the Zenne River

Some general information about the river and the territory are reported below:
Area: 1011 km^2

- 564 km^2 in the Walloon region
- 162 km^2 in Brussels
- 286 km^2 in Flemish region

Average flow: 8 m^3/sec
Average velocity: 0.2 – 0.3 m/sec
Bed slope: 0.2-0.5% (Van Griensven, 2002).

The Zenne River, upstream Brussels, has a natural meandering course. In the Brussels region, the river has been deviated over a distance of 10.5 km and has been almost completely covered and canalized. A canal, the canal Brussels-Charleroi, which is fed by former tributaries of the Zenne, the Hain, Maalbeek, Thines and Samme, flows parallel to the river. The canal and the river are then connected by four diversions (Hiver, 1979; Cosyn, 1983; Bauwens et al., 1992; Van Griensven, 2002):

- Lembeek: overflow from the Zenne to the Channel (Q_{max} = 66 m^3/s);

- Anderlecht (Aa): overflow from the Zenne to the Channel (Q_{max} = 24 m^3/s);
- Ninoofse Poort: overflow from the Zenne to the Channel (Q_{max} = 15 m^3/s);
- Vilvoorde (dock): self-priming siphon from the Channel to the Zenne (Q_{max} = 90 m^3/s)

The connections have been made mostly to prevent flooding in the city of Brussels.

The tributaries of the Zenne are listed in the table 7. The table reports the tributaries name, the location of the mouth in the Zenne and the area of the sub-basin. In the table are also shown the tributaries that have been disconnected from the river to feed the canal Brussels-Charleroi.

	Tributary	*Mouth in Zenne at*	*Area (km²)*
Walloon region			
I	Thines	Disconnected	49
II	Samme	Disconnected	86
II	Zennette	Soignies	120
IV	Zenne (Source-Tubize)	-	130
VI	Brainette	Steenkerke	31
V	Gageolle	Soignies	31
VII	Hain	Disconnected	83
VIII	Stincup-Loobeek		40.4
Flemish Region			
IX	Molenbeek	Lot	46
X	Zenne (Tubize-Lot)	-	35
XII	Zenne (Lot-Drogenbos)	-	44
XI	Zuunbeek	St. Pieters Leeuw	89
XIII	Maalbeek	Disconnected	41
XIV	Aabeek	Leest	30
	Trawool	Vilvoorde	8
XV	Woluwe+Trawool	Vilvoorde	94
XVI	Zenne (Vilvoorde-Mouth)	-	50
Brussels region	160		
	TOTAL		**1160**

Table 7 Tributaries of the Zenne river. Some of them have been disconnected from the river to feed the canal Brussels-Charleroi (Bauwens, 2009)

The analysis of precipitation and observed series of flows in the station of Vilvoorde, at the outlet of the modeled area of the basin shows that approximately the 30% of the inflow (precipitation and discharges from the sewer system) arrives at the outlet as outflow. It can be seen from table 8 that the annual rainfall is generally between 650 mm and 850 mm per year. The precipitation, summed to the contribution of the discharges from the combined sewer system in Brussels and the sewer system all over the basin generate an inflow of approximately 0.17 km^3 per year. The average annual flow in Vilvoorde, during the years 1995-1998, is between 6 and 8 m^3/sec.

Year	1995	1996	1997	1998
Annual outflow in Vilvoorde [km3]	0.25	0.21	0.19	0.24
Basin area [km2] (excluding Brussels)	791.17	791.17	791.17	791.17
Annual precipitations (mm)	789.60	648.00	684.00	858.10
Sewers inflow [km3]	0.17	0.16	0.17	0.20
Annual inflow [km3]	0.79	0.67	0.71	0.87
Average annual flow in Vilvoorde [m3/sec]	7.93	6.60	6.01	7.72
Runoff coefficient (total outflow/total inflow)	0.32	0.31	0.27	0.28

Table 8 Inflow and outflow quantities in the Zenne basin

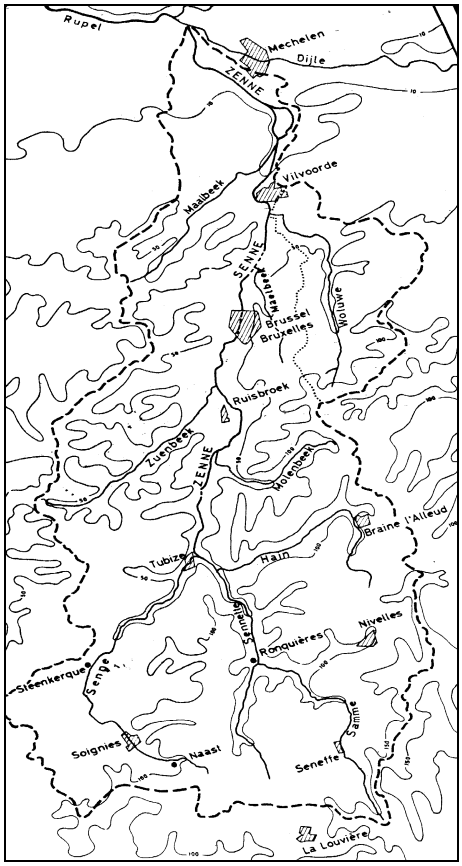

Figure 33 The Zenne River basin (Hiver, 1979)

4.1.1 Topography

The topography map used in the study is a digital elevation map (DEM) obtained by the National Geographic Institute. The map has a resolution of 50m x 50m. The elevation of the basin ranges approximately between 9 m above mean sea level (AMSL) and 170 m AMSL.

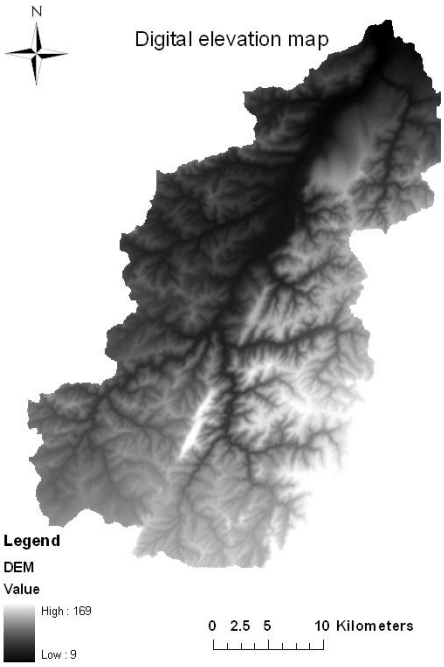

Figure 34 Digital elevation map of the Zenne River

4.1.2 Land use and soil type

Information about the soil type is taken from a map obtained from Corrine land cover (satellite) with a scale of 1:250000 and a resolution of 20m x 20m. Due to lack of data it has not be possible to build a model of the whole basin, since only the land use and soil map of the Flemish region were available. The model of the subbasins located in the Walloon region is built by a research group in the Vrije Universitet in Brussels. The figures below show the land use map of the modelled area of the basin. As it can be seen the most of the soil type in the area is loam or sandy loam. Four main different land uses can be distinguished. The percentage values of land dedicated to the different uses are reported in table 9. The second column reports the values for the entire Zenne basin. The third column reports the values only for the modelled part. As it can be seen the urbanized area occupies the largest part of the territory.

	Entire basin	Modeled area
Agricultural	48%	31%
Urbanized	38%	60%
Pasture	8%	2%
Forest and natural	6%	8%

Table 9 Land use in the Zenne River basin

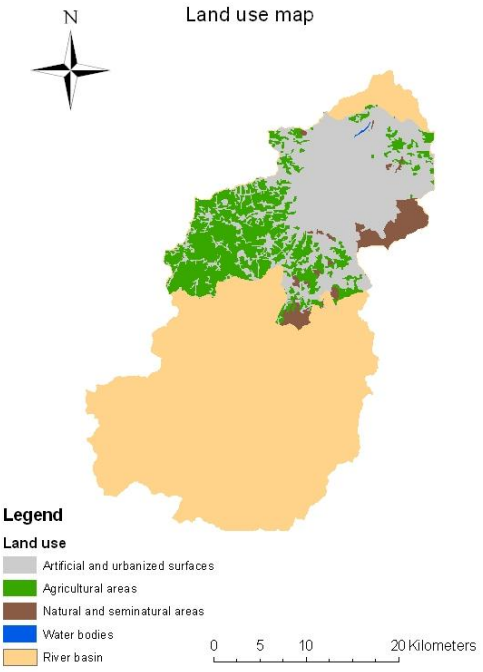

Figure 35 Land use map of the modeled area of the basin

4.1.3 Weather data

Weather data series are provided by the Royal Meteorological Institute: sub-hourly precipitation data for the years from 1995 to 1998, temperature, solar radiation, wind speed, potential evapo-transpiration and humidity daily data, for the years from 1970 to 2000. The weather station is located in Ukkel, Brussels (see table 10).

Station	Variable	Period	Time step
Ukkel	Precipitation	1970-1979, 1982-1999	10 minutes
Ukkel	Min and Max daily Temperature	1970-1999	daily
Ukkel	Wind speed	1970-1998	daily
Ukkel	Relative Humidity	1970-1999	daily
Ukkel	Solar radiation	1970-1994	daily
Ukkel	Potential Evapotranspiration	1970-2000	daily

Table 10 Meteorological data at Ukkel

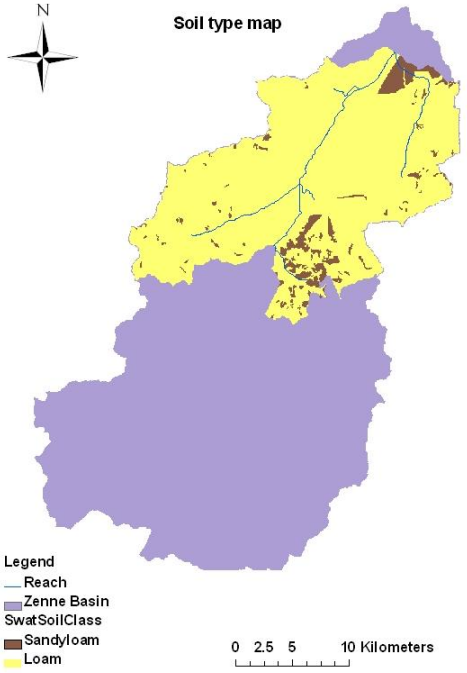

Figure 36 Soil type map of the modeled area of the basin

4.1.4 Hydrology

Hydrological data of discharges in Lot, Vilvoorde, Eppegem, Zemst and Hombeek are provided by the Hydrologisch InformatieCentrum - HIC.

The stations used in this study are Lot, upstream Brussels region; Vilvoorde, downstream the Brussels region; Epppegem, Zemst and Hoombeek. In figure 37 the location of the stations in the basin is shown. In table 11 all the available hydrological data series are reported.

Station	Variable	Period	Time step
Vilvoorde	Water stage	1975-1979,1984-1992, 1994-2004	
Vilvoorde	Flows	2004-2008	15 minutes
Vilvoorde	Water stage	2004-2009	15 minutes
Lot	Flows	1985-2002	1 hour
Lot	Flows	2003-2008	15 minutes
Eppegem	Water stage	2005-2008	15 minutes
Eppegem	Water stage	1971-2004	1 hour
Eppegm	Flows	1988-2000	daily
Zemst	Water stage	2003-2008	1 minute
Hombeek	Water stage	2003-2008	1 minute

Table 11 Water flow and water stage available data from HIC

In table 12 the variables and the period of the data series used for the project for each station are reported.

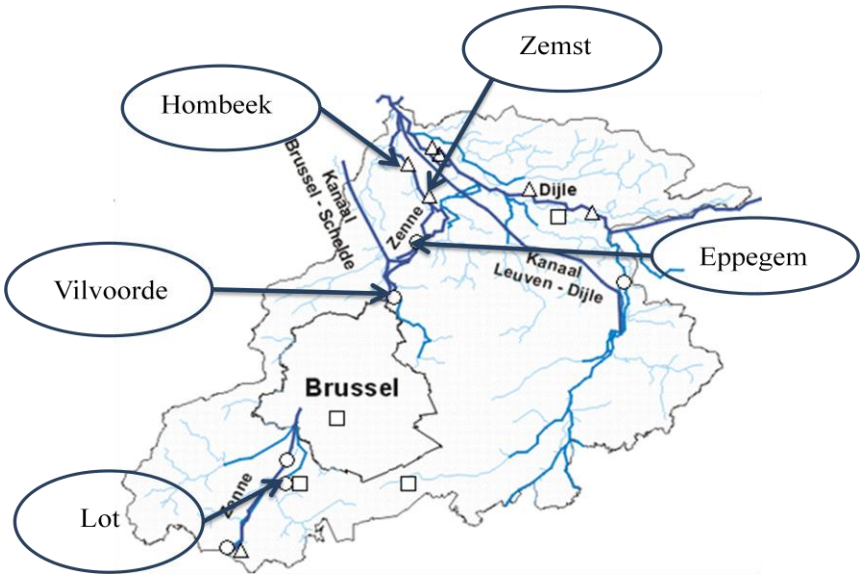

Figure 37 Overview of the hydrological stations used in this study. Image taken from http://www.lin.vlaanderen.be/awz/waterstanden/hydra/images/hic_dijle04.gif

Station	Variable	Period	Time step
Lot	Flows	1995-1998	daily
Vilvoorde	Flows	1995-1999	daily
Vilvoorde	Water stage	2010	15 minutes
Eppegem	Water stage	2010	15 minutes
Eppegem	Flows	2010	1 hour
Zemst	Water stage	2010	1 minute
Hoombek	Water stage	2010	1 minute

Table 12 measurement stations from HIC used for the study

The flows in Vilvoorde, Lot and Eppegem are calculated by means of a rating curve. The HIC provided the equations of the rating curve used in Vivoorde:

Q = a0 + a1.H + a2.H^2 + a3.H^3			H in m relative --- Zero level = 9.00 mAMSL						
Validity period		h1	h2	h1	h2	a0	a1	a2	a3
Begin	End	(m)	(m)	(mAMSL)	(mAMSL)				
24/10/2003		-1.00	0.00	8.00	9.00	7.2051	12.92	5.7867	0
		0.00	3.50	9.00	12.50	7.2051	12.92	2.2775	0
12/01/1994	20/06/2002	0.60	1.00	9.60	10.00	-1.0671	0.2752	7.4411	0
		1.00	4.20	10.00	13.20	-3.2426	4.2648	5.9884	-0.3614

Table 13 Rating curves for the gauge station in Vilvoorde

Two rating curves are available: one used in the period from 1994 to 2002 and the other used from 2003 on. For each rating curve two different curves are provided: one for values of the water stage greater than 9 m above mean sea level and the other for values below 9 m above mean sea level.

4.1.5 The Brussels region

The Brussels region is mainly an urbanized region. The runoff and the water flows that feed the Zenne River are mainly generated by runoff over impervious areas and discharges from the combined sewer system. The sewer system is divided in three main subsystems: Sewers South, Sewer North, and Sewer Woluwe. These three subsystems are modelled using the KOSIM model.

KOSIM is a continuous simulation model for combined sewer systems developed by ITWH, Hannover. It has been designed for long term simulations of flows and quality variables of combined sewers systems. A new model of the Brussels city system is being built by professor Willy Bauwens research group in Vrije Universiteit Brussel The new codes and input data of the model are not available, but output of the model, discharges in the Zenne River, are available for the years 1995-1998. These series are used as data input of the model built for this study.

Point discharge	Variable	Period	Time step
South	Wastewater Flows	1995-1998	1 hour
Woluwe	Wastewater Flows	1995-1998	1 hour
North	Wastewater Flows	1995-1998	1 hour

Table 14 Available KOSIM model output

Other discharges from the sewer system are modelled as constant daily discharges. The constant point sources of the whole basin are listed in table 15.

Point source code (KOSIM model)	Inhabitants	Flow [m^3/day]
1	21461	3219.15
2	28961	4344.15
3	24954	3743.10
4	9620	1443.00
5	2054	308.10
6	13150	1972.50
7	10127	1519.05
8	27303	4095.45
9	183	27.45
10	37000	5550.00
11	33350	5002.50
12	66493	9973.95
13	12131	1819.7025

Table 15 Point source list. The number of inhabitants and the value of flows correspond to the values modeled by A. Van Griensven (2002) and are valid for the years 1995-1998.

4.1.6 Water quality

The Zenne is one of the most polluted rivers in Belgium. Pollution comes mostly from domestic waste water. All this pollution is carried in the Scheldt River. The water of the Zenne is quoted as polluted and heavily polluted by the Flemish Environmental Protection Agency. The Zenne is anyway not biologically dead (Verbeiren, 2001; Van Griensven, 2002).

Before 2000 the waste water of 1.4 million people came untreated directly in the Zenne River from the Brussels region combined sewers system (Van Griensven, 2002). Two big Wastewater Treatment Plants (WWTP) have been built after 2000:

- Brussels South, started up in 2000: it treats 360,000 Inhabitants Equivalent (IE). The 70% of the treated wastewater come from households, while the rest is industrial water.
- Brussels North, started up in 2007: The WWTP treats water from the communes in the Brussels region not treated by Brussels South and 90,000 IE from the Flemish region.

Water quality data for dynamic point sources area are provided by KOSIM model. Other water quality data, for the constant point sources listed in table 15, have been calculated using coefficients of average daily discharges in sewers by the population.

The Flemish Environmental Agency (VMM) provides also data from the stations in Lot and Vilvoorde. These data are concentrations of Oxygen, BOD5, COD, nitrites, nitrates, ammonia measured approximately once a month.

4.2 The models

The model built for the Zenne River integrates three models built using the model codes described previously: SWAT is used to model the area of the watershed located in the Flemish region and part of the Brussels region, KOSIM is used for the city of Brussels. The HEC-RAS model is used to model the river downstream Brussels till the outlet in the Dijle River. A KOSIM model for the urbanized area of Brussels was built in previous researches by Demuynck and Bauwens (1996). The output of this model is used as input for the SWAT model. Another research group is building a SWAT model for the Walloon region and a new version of the model of the city of Brussels. The outcome of these works will be integrated in one model. Figure 38 shows a scheme of the different component of the composite model.

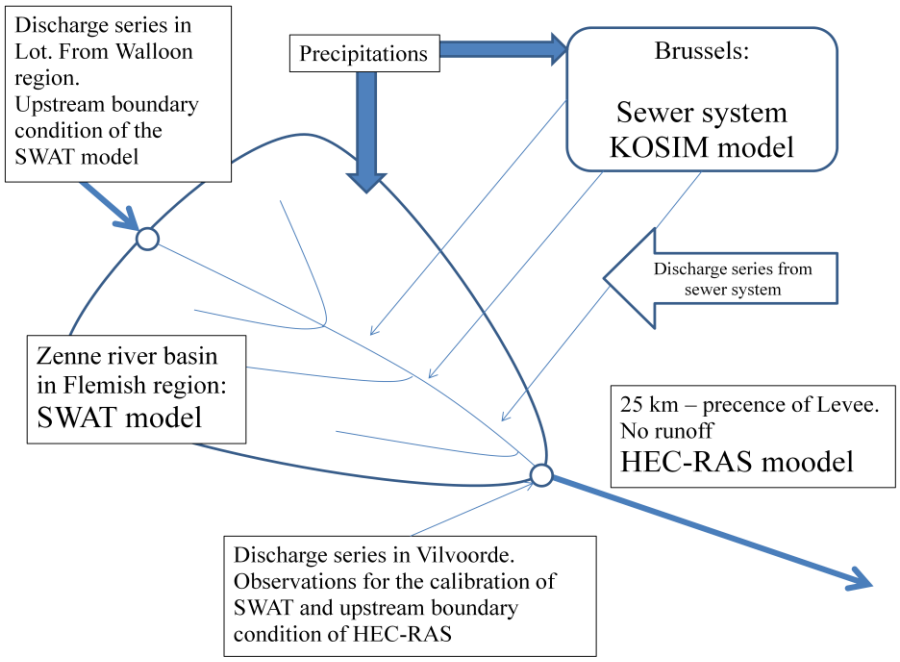

Figure 38 Structure of the composite model of the system.

4.2.1 The SWAT model

The upstream boundary of the SWAT model is located in correspondence of the city of Lot, downstream the overflow in Lembeek, where a gauge station registers water stage and flows. These data series is used as boundary condition. Twelve subbasins have been built to model this area of the Zenne basin. The characteristics of these sub-basins and of the river are summarized in table 16:

Subbasin	Area (km2)		Channel width (m)	Channel length (km)	Corrected channel length (km)	Distance
1	0.12	ZENNE	81.95	0.12		
2	0	*Zenne (KOSIM)*	20		**1.**	Sewer North - Woluwe
4	0	*Zenne (KOSIM)*	9	3.25		
3+5	0	*Zenne (KOSIM)*	20		12.8	Anderlecht – Sewer North
6	41	Maalbeek	10		**6**	
7	0	*Zenne (KOSIM)*	20		**1**	Zuunbeek – Anderlecht
8	2.8	Zenne	65.52	0.44	**0.49**	
9	30.5	Linkebeek	10.03	2.5		
10	78.9	Zuunbeek	17.73	11.78		
11	20.1	Zenne	63.62	6.86	**10.24**	
12	46.4	Molenbeek	12.9	4.61	**5.49**	

Table 16 Subbasin and reaches description

Six point sources have been added to the SWAT model: the upstream boundary in Lot, three constant point sources and three dynamic point sources. The constant and dynamic point sources are used to model the inflow coming from the sewer system. The dynamic point sources represent the combined sewer system of Brussels and are modeled by KOSIM. The constant point sources flows are calculated based on Inhabitant Equivalents and daily loads discharged on average by a person The area of the sub-basins that are in the Brussels region and that are modeled by KOSIM is changed and set to zero. In figure 39 a map of the modeled basin is shown. In table 17 the point sources and the basins to which they belong are reported.

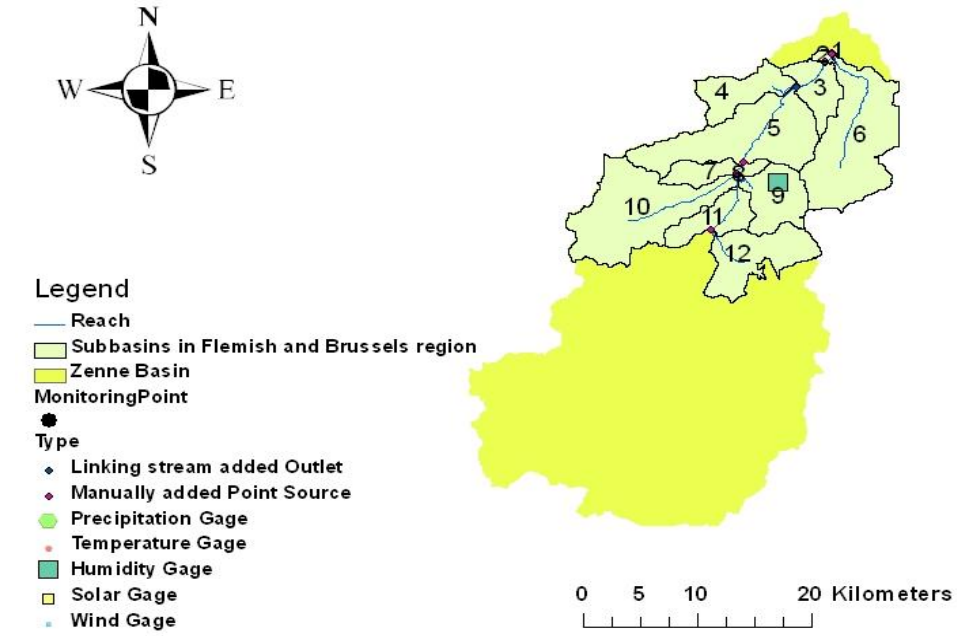

Figure 39 Image of the basin of the Zenne River in the Walloon and the Flemish region. In light green the subbasin of the model built for the Flemish region are visible

4.2.2 Connections between canal Brussels-Charleroi and Zenne River

The area modeled in SWAT includes one of the overflows that connect the river and the canal: the overflow in Anderlecht is added modifying the codes in SWAT and adding the following equations:

$$\begin{aligned} &\text{If } Q_i<Q_{lim} \\ &Q_o=0 \\ &Q_t=Q \\ &\text{If } Q_i>Q_{lim} \\ &Q_o=(Q-Q_{lim})*(1-f_o) \\ &Q_t=Q_{lim}+(Q-Q_{lim})*f_o \end{aligned} \tag{79}$$

Where Q_o is the overflow, Q_t the remaining throughflow and Q_{lim} the threshold value (Van Griensven 2002).

Point source code	Subbasin	Dynamic flows	Constant flows code in KOSIM model
1p	1	Woluwe (Kosim)	
2p	2	Sewers North (Kosim)	
5p	5	Swers South (Kosim)	
7p	7		10 (KOSIM)
8p	8		9 (KOSIM)
11p	11	Lot (HIC)	8 (KOSIM)

Table 17 Constant and dynamic point sources introduced in the model

From Anonymous (1986) it can be derived that for flows in the Zenne upstream of the Anderlecht between 0 and 80 m^3/s, a fairly constant fraction of 31% of the flow is diverted to the canal. This fraction holds from September 1981 onwards, after the recalibration works on the river Zenne near the Anderlecht (Bauwens, 2009). The study provides also information on the situation before this date. Anyway this information is not confirmed and introduces in the model a source of uncertainty. Two versions of the model are, thus, built: one in which the overflow is introduced, with a constant flow from the river of 31% of the flow in the river. A second version of the model in which the overflow doesn't work is built and compared with the first one.

4.2.3 The HEC-RAS model

The HEC-RAS model has been built using the cross section data provided by the Department for Environment and Infrastructure of the Flemish Community. A total of 211 cross sections have been used. The average distance between them is 125 m (figure 40). It can be noticed in the figure that the river divides into two streams; one is the natural river, the other an artificial canal, which some kilometers downstream join together again before the Zenne discharges in the Dijle River.

The upstream boundary of the HEC-RAS model is located in the same point where the SWAT model downstream boundary is located, in correspondence of the city of Vilvoorde, as shown in the figure 40. HEC-RAS doesn't take into account for any runoff from the watershed. In this part of the river there is actually no runoff entering the river because of the presence artificial dykes. In the HEC-RAS model has been also introduced one of the overflow: the one in Vilvoorde dock, which transfer water from the canal Brussels-Charleroi to the Zenne. A description of the overflow model used for the overflow is reported in the chapter about the calibration of the HEC-RAS model. As for the SWAT model, also for the HEC-RAS model two versions are built: one in which the overflow is working and one in which the overflow is not working. Uncertainty about the presence and the entity of an overflow from the canal to the river rise from the fact that if on one side the analysis of flow data in Vilvoorde and in Eppegem shows an increment in flow that ranges between the 21% and the 38%, from the other side water quality indexes do not show significant changes upstream and downstream the location of the overflow: water quality in the canal is very different from the one in the Zenne: the former is in fact less polluted, so the presence of the overflow should make the concentration of pollutants decrease. A deeper description of the analysis of the case is reported in the chapter relative to the building and the calibration of the HEC-RAS model.

Boundary conditions for the model are hourly flow data (upstream) and water stage hourly data (downstream) provided by the Hydrologic Information Center (HIC) of the Flemish region. The observations downstream show a strong tide effect in the river, so water stage data are the most appropriate boundary condition, in this case. Data for the calibration are water stage data series in two stations located downstream of the overflow in Vilvoorde and some kilometers upstream the downstream boundary condition.

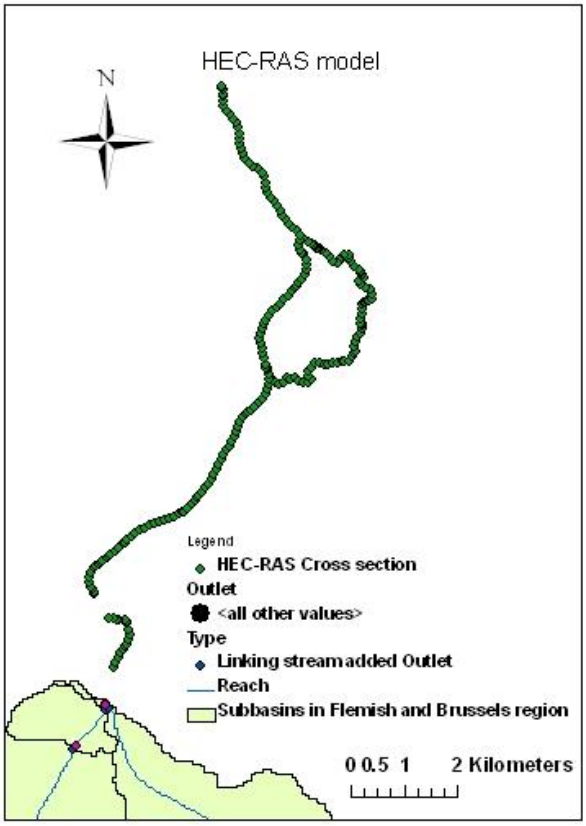

Figure 40 Points where cross section of the river Zenne are available and used for modeling are showed. They start where there is the outlet of the SWAT model

4.2.4 The composite model

The composite model is the result of the integration of the three models, KOSIM, SWAT and HEC-RAS. The outputs of the KOSIM model, as described previously, are used as input in different points of the SWAT model. The output of the SWAT model in Vilvoorde is used as upstream boundary of the HEC-RAS.

In figure 41 every model is represented and connected to the others by the cascade of input-output. Also the input data series are represented. As it can be seen precipitation records are used to feed both the KOSIM and the SWAT model. SWAT receives also daily discharge series from the output of the

KOSIM model in three different point sources and daily discharges records from the upstream region of the basin. The latter records are provided by the HIC. The SWAT output, that is daily series of discharges in Vilvoorde are then used as input of the HEC-RAS model.

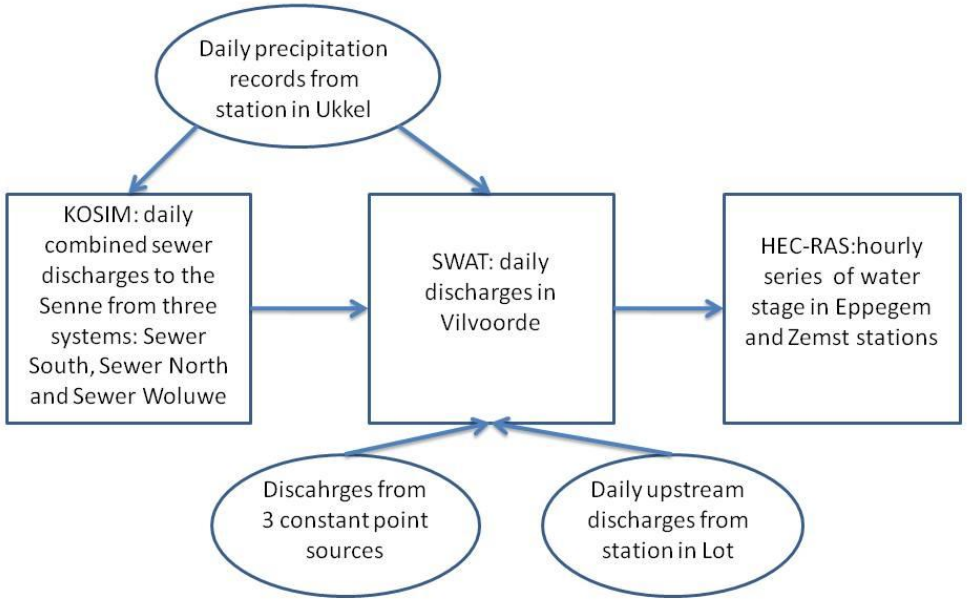

Figure 41 Structure of the composite model and input data.

5 Sources of uncertainty

In order to assess the uncertainty affecting the model the sources of uncertainty are identified: SWAT model needs many input data. It has been chosen to analyze model's behavior when an error affects some of them: the upstream boundary condition in Lot and the series of discharges from the sewer system modeled by KOSIM. Very important sources of uncertainty that are not taken into account in this study are the precipitation data. The reason of this choice is that only one gauge station is used to generate input data for the model. This means that the spatial variability of the rainfall, that is one of the most important sources of uncertainty in rainfall data (Chaubey et al., 1998; Carpenter and Georgakakos , 2004), cannot be analyzed. A non-complete analysis of the rainfall uncertainty would result. It has been, thus, chosen to focus on the uncertainty in the aforementioned input data series. The model used for the analysis is the one that uses the GAML method for runoff generation.

5.1 Error in KOSIM output

As the entity and the nature of the error affecting the KOSIM output are unknown, a random error with uniform distribution is added to the discharge data for each time step. This error is proportional to the discharge value itself and ranges from $Q - \beta \cdot Q$ to $Q + \beta \cdot Q$, where β is a proportionality coefficient.

Not all the input of the SWAT model coming from the sewage system are considered in this study as being affected by this error: the error is applied only to the dynamic point sources. These are, actually the most interesting to be studied, both because, they are dynamic and affected by rainfall, so they are responsible for the flood events entity and time of occurrence and because they have higher magnitude in discharge values: the average value is for the three sewer sub-systems, Woluwe, North and South, respectively, 109000 m^3/day, 255000 m^3/day and 66000 m^3/day, while the daily discharges from the constant point sources ranges from 27 m^3/day to 4000 m^3/day.

5.2 Error in river discharge observations

The method for the identification of uncertainty in river discharge observations proposed by Di Baldassarre and Montanari (2009) consider the following sources of uncertainty:

1. $\varepsilon_1(Q(x,t))$ In the measurement of Q'(x,t) obtained with the velocity-area method
2. $\varepsilon_2(Q(x,t))$ due to ranting curve uncertainty.
    a. $\varepsilon_{2.1}(Q(x,t))$: interpolation and extrapolation of the rating curve
    b. $\varepsilon_{2.2}(Q(x,t))$: presence of unsteady flow conditions
    c. $\varepsilon_{2.3}(Q(x,t))$: seasonal changes of roughness

The aggregation of the error is computed using the equations 80 and 81.

$$\varepsilon(Q(x,t)) = \varepsilon_1(Q(x,t)) + \varepsilon_2(Q(x,t)) \quad (80)$$

$$|\varepsilon_2(Q(x,t))| = |\varepsilon_{2.1}(Q(x,t))| + |\varepsilon_{2.2}(Q(x,t))| + |\varepsilon_{2.3}(Q(x,t))| \quad (81)$$

The errors $\varepsilon_{2.1}\big(Q(x,t)\big)$, $\varepsilon_{2.2}\big(Q(x,t)\big)$ and $\varepsilon_{2.3}(Q(x,t))$ are summed taking the absolute values because the sign of these errors is not known, so a conservative approach is used to take into account for the worst case, in which the three errors have the same sign.

The method is based on some assumptions about the nature of the errors:

1. Observations in river stage are neglected as they are usually small, around 1-2 cm and of the same order of magnitude of the topographic error.
2. The geometry of the cross is constant in time. Due to this assumption one of the most important sources of uncertainty is not considered, that is the fact that cross section geometry changes in time due to sediment transport and erosion.
3. The total error can be obtained by adding the different sources of error.
4. The uncertainties affecting Q'(x,t) are independent and systematic errors are excluded.
5. ε_1(Q(x,t)) is a Gaussian random variable.
6. ε_2(Q(x,t)) is a binary random variable inferred by means of numerical simulations which can assume values $+|\varepsilon_2(Q(x,t))|$ and $-|\varepsilon_2(Q(x,t))|$ with equal probability and can be computed accordingly to an absolute additive error model.

ε_1, according with Di Baldassarre and Montanari (2009) is assumed to be about 5,3% of Q'(x,t) at the 95% confidence level.

The uncertainty induced by interpolation and extrapolation of the rating curve is mainly due to the fact that rating curves are usually derived by using river discharge measurements in ordinary flow conditions and then extrapolated for high flow conditions.

The uncertainty induced by the presence of unsteady conditions will be discussed in the chapter dedicated to the calibration of the HEC-RAS model, as, for the generation of the flow series in Vilvoorde, the upstream boundary condition of the model, has been reduced by using the Jones equations. This reduction of the error could not be done for the flow series in Lot, as the equation of the rating curve in that station was not provided.

The uncertainty induced by seasonal changes in roughness of the river bed depends on the state of the vegetation.

5.2.1 Uncertainty induced by interpolating and extrapolating the rating curve

The interpolation and extrapolation error $|\varepsilon_{2.1}\big(Q(x,t)\big)|$ was estimated as follows. For each cross section, a total of 20 (Q'(x,t); h(x,t)) points corresponding to river discharge values in the range 2–20 m^3/s, by steps of 2 m^3/s, were obtained through steady flow simulations. Then, rating curve was estimated using a polynomial function with three degrees to interpolate these (Q'(x,t); h(x,t)). This methodology reflects the fact that rating curves are usually derived by using river discharge measurements related to ordinary flow conditions (for obvious practical reasons) and then extrapolated to estimate river discharge for high flow conditions also. Specifically, in the river reach under study, river discharges in the range 2–20 m3/s correspond to ordinary flow conditions (from low flow values

to ordinary floods), while river discharges in the range 22–42 m3/s correspond to exceptional flow conditions. Finally, for each cross section, errors were computed by comparing the steady flow rating curve to the estimated one both in the ranges 2-20 m3/s, interpolation error, and 22– 42 m3/s, extrapolation error. Assuming that the percentage errors with respect to Q(x,t) are Gaussian, the average $|\varepsilon_{2.1}(Q(x,t))|$ along the river reach was found to be equal to 1.14% of Q(x,t).

5.2.2 Uncertainty induced by the presence of unsteady flow conditions

It is well known that in unsteady flow conditions there is not a one-to-one relationship between the river stage and the river discharge. Actually, during a flood the same river stage corresponds to different river discharges in the two limbs of the hydrograph, the higher one occurring in the raising limb. In order to assess the magnitude of the error that can be induced by the presence of unsteady flow, the model was used to simulate the flood event occurred between the 17 and the 22 of February 2010 and estimate the unsteady flow rating curve. Then, for each cross section, river discharge values simulated by the model were compared to the corresponding values estimated by using the steady flow rating curve. For each value of Q(x,t) in the range 2- 42 m^3/s, with step of 2 m^3/s, and each cross section the largest absolute errors were taken in order to obtain a one-to-one relationship between $|\varepsilon_{2.2}(Q(x,t))|$ and Q(x,t). By assuming that the percentage (with respect to Q(x,t)) $|\varepsilon_{2.2}(Q(x,t))|$ are Gaussian, the average $|\varepsilon_{2.2}(Q(x,t))|$ along the river reach was found to be equal to 7.7% of Q(x,t).

5.2.3 Uncertainty induced by seasonal changes of the river roughness

Floodplain and river banks roughness depends on the state of the vegetation, which is affected by seasonal variations. This causes changes in the rating curve and therefore may affect the river discharge estimation. A representative value of the Manning's roughness coefficient value for the winter-autumn period is 0.043 (see chapter 7.1), while a representative value of the roughness in spring and summer is 0.048. For each value of Q(x,t) in the range 2– 42 m^3/s, with step of 2 m^3/s, and each cross section, the error $|\varepsilon_{2.3}(Q(x,t))|$ was computed. By assuming that the percentage (with respect to Q(x,t)) $|\varepsilon_{2.3}(Q(x,t))|$ are Gaussian the average of $|\varepsilon_{2.3}(Q(x,t))|$ was found to be equal to 10.03 % of Q(x,t).

The computation of the total error give as result an error in terms of percentage with respect to the flow *Q(x,t)*, assumed to be Gaussian, has an average value of 24.1%. This value is assumed to be the order of magnitude of the error. The objective of this study is to evaluate the influence of the error in input data of a model on the output of the model and the influence of uncertainty in output of models when this output is used as input in another model. To evaluate the influence of the computed discharge error on the output of the hydraulic model, in this case study, the error affecting the input series, as a simplified assumption and using a conservative approach, is assumed to have a normal distribution with zero mean and standard deviation proportional to the discharge.

$$\varepsilon = N(0, \beta Q_{obs}) \tag{82}$$

where β is a coefficient of proportionality. This random error assumes a value that affects the discharge of each time step of the inflow series for a flood event.

To simplify the computation of the uncertainty induced by the presence of this error, twenty different input series are created, each affected by an error characterized by the same probability of occurrence than the others. The cumulate probability function of the error is used to calculate the value of the error affecting each element of the series, starting from a cumulate probability equal to 0.025, with a step of 0.05 until a probability of 0.975. For each time step of the original series a new value, affected by this error, is calculated.

6 Calibration of the SWAT model and uncertainty analysis

The calibration of the SWAT model is done following this procedure:

1. Perform sensitivity analysis to identify the most sensitive parameters
2. Find, for the most sensitive parameters the good parameter sets as described previously

Two algorithms are used for the calibration: ParaSol and SUFI2.

Three different models have been built and evaluated in this study:

- A model in which the overflow in Anderlecht is present. The method for runoff generation is the Green-Ampt Mein Larson (GAML).
- A model without overflow that uses the GAML method for runoff generation.
- A model without overflow that uses the Curve Number method for the generation of the runoff.

The description of the two runoff generation methods is reported in chapter 3.1 along with the description of the whole SWAT model. The performance of the runoff model depends on the single case, so both the models have been modeled and calibrated.

6.1 Sensitivity analysis and calibration

The sensitivity analysis is performed over all the parameters involved in the hydrologic processes. Table 18 shows the parameters analyzed, their description, the boundaries and the changing mode. The changing mode can be:
1: substituting the initial value with one in the range.
2: adding a value comprised in the range specified to the initial value.
3: multiplying the initial value for $(1+\alpha)$, where α is a percentage value comprised between the lower and upper specified values.

The values of the boundaries and the changing mode have been chosen basing on a study made by van Griensven et al. (2006). This parameters and ranges will be used for the sensitivity analysis of all the models. The sensitivity has been performed analyzing the changing in the output, in the sum of square of the error and the sum of the square of the error after ranking (see chapter 2). The parameter to be calibrated are the ones that have a value of the average sensitivity index from medium to very high, as indicated by Lenhart et al. (2002), thus for parameter with a sensitivity index greater than 0.05.

#	Parameter	Description	Lower boundary	Upper boundary	Changing mode
1	Alpha_Bf	Baseflow alpha factor (days)	0	1	1
2	Biomix	Biological mixing efficiency	0	1	1
3	Blai	Leaf Area Index	-50	50	3
4	Canmx	Maximum canopy index	0	10	1
5	Ch_Cov	Channel cover factor	-0.001	1	1
6	Ch_Erod	Channel erodibility factor	-0.05	0.6	1
7	Ch_K2	Effective hydraulic conductivity in main channel alluvium (mm/hr)	0	150	1
8	Ch_N2	Manning coefficient for channel	-50	50	1
9	Cn2	SCS runoff curve number for moisture condition 2	-50	50	3
10	Epco	Plant evaporation compensation factor	-50	50	1
11	Esco	Soil evaporation compensation factor	0	1	1
12	Gw_Delay	Groundwater delay (days)	0	50	2
13	Gw_Revap	Groundwater 'revap' coefficient	-0.02	0.2	1
14	Gwqmn	Threshold depth of water in the shallow aquifer for return flow to occur (mm)	-1000	1000	2
15	Rchrg_Dp	Groundwater recharge to deep aquifer (fraction)	0	1	1
16	Spcon	Linear parameter for calculating the channel sediment routing	0.0001	0.01	1
17	Spexp	Exponent parameter for calculating the channel sediment routing	1	2	1
18	Usle_C		-25	25	3
19	Usle_P	USLE equation support practice (P) factor	-25	25	3
20	Revapmn	Threshold depth of water in the shallow aquifer for 'revap' to occur (mm).	0	500	1
21	Sftmp	Snowfall temperature (8C)	0	5	1
22	Slope	Average slope steepness (m/m)	-50	50	3
23	Slsubbsn	Average slope length (m).	-50	50	3
24	Smfmn	Minimum melt rate for snow during the year (occurs on winter solstice) (mm/8C/day)	0	10	1
25	Smfmx	Maximum melt rate for snow during (mm/8C/day)	0	10	1
26	Smtmp	Snow melt base temperature (8C)	-25	25	3
27	Sol_Alb	Soil albedo	-50	50	3
28	Sol_Awc	Available water capacity of the soil layer (mm/mm soil)	-50	50	3
29	Sol_K	Soil conductivity (mm/h)	-50	50	3
30	Sol_Z	Soil depth	-25	25	3
31	Timp	Snow pack temperature lag factor	0	1	1
32	Surlag	Surface runoff lag coefficient	0	10	1
33	Tlaps	Temperature laps rate (8C/km)	-50	50	3

Table 18 Parameters used in calibration

Class	Index	Sensitivity
I	$0:00 \leq \lvert I \rvert < 0:05$	Small to negligible
II	$0:05 \leq \lvert I \rvert < 0:20$	Medium
III	$0:20 \leq \lvert I \rvert < 1:00$	High
IV	$\lvert I \rvert \geq 1:00$	Very high

Table 19 Sensitivity index interpretation

Calibration is performed using the Nash Sutcliff Efficiency Index as index of goodness of fit. The observed data series is daily flow data series observed in Vilvoorde. The Calibration period is the 1995, while validation period is 1996. Despite also years 1997 and 1998 could be used as all the necessary

data series are available, it has been noticed that the results are not good, both in calibration and validation, using 1997 for calibration and 1998 for validation. The reason of the bad performance in that period can be:

- Changes in the cross section in Lot and Vilvoorde and in the parameter of the rating curves due to deposition and sedimentation.
- Initial condition of the soil moisture and soil water content in the model not corresponding to the observed ones. A warm period for the model, before performing the calibration and validation, is usually. A warm-up period is used to run the model without using the output to evaluate the performance to make all the variables of the hydrologic cycle fully functioning. Unfortunately the SWAT model don't allow to perform warm up periods smaller than one year and the warm-up period options cause a not proper functioning of the calibration algorithm.

The calibration algorithms used are ParaSol and SUFI2. These two algorithms are compared: at first calibration is performed by ParaSol which finds a wide ensemble of good parameter sets. A maximum of 20000 simulations for the Shuffled Complex Evolution algorithm is imposed. Then the boundaries drawn by the maximum and the minimum value of each parameter for all the good parameter sets are used in SUFI2 for a Latin Hypercube sampling. 2000 Latin Hypercube samples are found by the SUFI2 in the parameter space. If the SUFI2 performs better than the Parasol, the calibration using the Parasol is re-performed updating the range of values of the parameters.

6.2 Model with overflow and Green-Ampt Mein Larson method

6.2.1 Sensitivity analysis

The results from the sensitivity analysis for this model are shown in table20.

OBJECTIVE FUNCTION 1			OBJECTIVE FUNCTION 2			OUTPUT 1		
SSQR for flow (m^3/s) at Vilvoorde			SSQ for flow (m^3/s) at Vilvoorde			Aver. for flow (m^3/s) at Vilvoorde		
Rank	Parameter name	mean	rank	Parameter name	mean	#	par	mean
1	Ch_K2	7.29E-01	1	Alpha_Bf	6.28E-01	1	Gwqmn	3.17E-01
2	Alpha_Bf	6.26E-01	2	Ch_K2	5.14E-01	2	Rchrg_Dp	1.57E-01
3	Cn2	6.22E-01	3	Ch_N2	3.21E-01	3	Revapmn	7.42E-02
4	Ch_N2	4.20E-01	4	Esco	1.37E-01	4	Alpha_Bf	5.50E-02
5	Esco	3.15E-01	5	Cn2	1.35E-01	5	Sol_Awc	5.04E-02
6	Sol_K	2.15E-01	6	Gwqmn	9.75E-02			
7	Canmx	1.71E-01	7	Sol_K	7.74E-02			
8	Gwqmn	1.19E-01	8	Canmx	6.16E-02			
9	Sol_Z	1.08E-01	9	Rchrg_Dp	5.46E-02			
10	Rchrg_Dp	1.06E-01						
11	Revapmn	9.66E-02						
12	Sol_Awc	7.29E-02						

Table 20 Sensitivity index values for the most sensitive parameters

In calibration the hydraulic conductivity in the channel has not been calibrated, as it is expected that is very close to 0. The Manning's coefficient, n, for the channel, instead has been calibrated differently for the basins belonging to the Brussels region and the other basins, as in the Brussels region the river have been almost completely canalized and covered.

The calibration performed using the ParaSol algorithm presented really bad performance: using the same boundaries of the parameter space than in sensitivity analysis, the value of the Nash Sutcliff Efficiency Index is 0.14. After changing the values of the boundaries of the parameters the NSE index improves to 0.18. Despite the improvement in the performance indicated by the NSE, the performance is not sufficiently good. The new boundaries are shown in the following table:

Name	Minimum	Maximum
v__ALPHA_BF.gw	0	1
r__CN2.mgt	-0.5	0.25
v__CH_N2.rte_____1-5	0.02	0.06
v__CH_N2.rte_____6-12	0.02	0.06
v__ESCO.hru	0	1
r__SOL_K(1).sol	-0.75	0
v__CANMX.hru	30	100
v__GWQMN.gw	0	100
v__SOL_Z(1).sol	0	300
v__RCHRG_DP.gw	0	0.5
v__REVAPMN.gw	0	100
r__SOL_AWC(1).sol	-0.75	0

Table 21 New parameter boundaries for second step of calibration

As the results of this model are really bad, this one has not been further used in this study.

6.3 Models without overflow

6.3.1 Green-Ampt Mein Larson method

The sensitivity analysis results for the model are shown in table 22. Eight parameters result to be sensitive.

OBJECTIVE FUNCTION 1			OBJECTIVE FUNCTION 2			OUTPUT 1		
SSQR for flow (m^3/s) at Vilvoorde			SSQ for flow (m^3/s) at Vilvoorde			Aver. for flow (m^3/s) at Vilvoorde		
rank	Parameter name	mean	rank	Parameter name	mean	#	par	mean
1	Rchrg_Dp	9.35E-01	1	Rchrg_Dp	4.45E-01	1	Rchrg_Dp	1.02E-01
2	Gwqmn	5.06E-01	2	Gwqmn	2.33E-01			
3	Sol_Awc	2.89E-01	3	Sol_Awc	1.58E-01			
4	Sol_Z	1.35E-01	4	Cn2	1.20E-01			
5	Cn2	1.09E-01	5	Gw_Delay	7.77E-02			
6	Esco	1.06E-01	6	Sol_Z	7.46E-02			
7	Gw_Delay	9.24E-02						
8	Sol_K	5.68E-02						

Table 22 Sensitivity analysis results.

Anyway also other parameters are added to these for the calibration, basing on experience of other versions of the model built previously: the parameters CANMX, ALPHA_BF, CH_K2, SURLAG and CH_N2 (see table 18) have been added to the parameter to be calibrated.

In table 23 the parameters and the values of the boundaries are reported.

Name	Minimum	Maximum
r__CN2.mgt	-0.5	0.5
v__CANMX.hru	0	100
v__GWQMN.gw	0	5000
r__SOL_AWC(1).sol	-0.5	0.5
r__ESCO.hru	-0.01	1
v__ALPHA_BF.gw	0	1
v__CH_K2.rte	0	50
v__RCHRG_DP.gw	0	1
r__SOL_K(1).sol	-0.5	0.5
v__SOL_Z(1).sol	0	3000
v__GW_DELAY.gw	0	50
v__SURLAG.bsn	1	24
v__CH_N2.rte_____1-5	0.02	0.06
v__CH_N2.rte_____6-12	0.02	0.06

Table 23 calibrated parameters

ParaSol algorithm

The results of the ParaSol algorithm are, in this case, good: the algorithm stopped after 5596 simulations. Of these 5597 simulations, 4830 simulations are considered good basing on the χ^2 method (see chapter 2). The best parameter set give a good performance: the value of the NSE is 0.899.

An overview of the results of the calibration is shown in table 24. The p-factor is the percentage of measured data bracketed by the 95% prediction uncertainty (95PPU).

The r-factor is the ratio between the average distance between the lower and the upper 95PPU and the standard deviation of the measured data, which is a good indicator of the width of the 95PPU. A desirable value for the r-factor is below 1, while a desirable value for the p-factor is close to 1. Anyway generally the smaller the r-factor is, the smaller the p-factor become. Actually the results show a very narrow 95PPU. This is one of the main reasons why the p-factor is small. In figure 42 the simulated and the measured hydrographs are shown. Also the 95PPU are shown. It can be noticed that the 95PPU become smaller during peaks, when the errors become bigger.

Calibration: results of 4830 simulations				
Variable	n	p-factor	r-factor	NS
q_1.out	365	0.119	0.49	0.899

Table 24 Results of the calibration

All the good parameter sets have been run and on the basis of all the simulations the 95PPU have been computed. The hydrographs are shown in figure 43. It can be noticed that the simulated runs tend to underestimate the baseflow and the peaks.

Anyway, both the calibration and the validation give a good representation of the observations, in particular the frequency of the peaks is well represented.

Validation: results of 4830 simulations				
Variable	n	p-factor	r-factor	NS
q_1.out	366	0.22	0.17	0.756

Table 25 Results of the validation

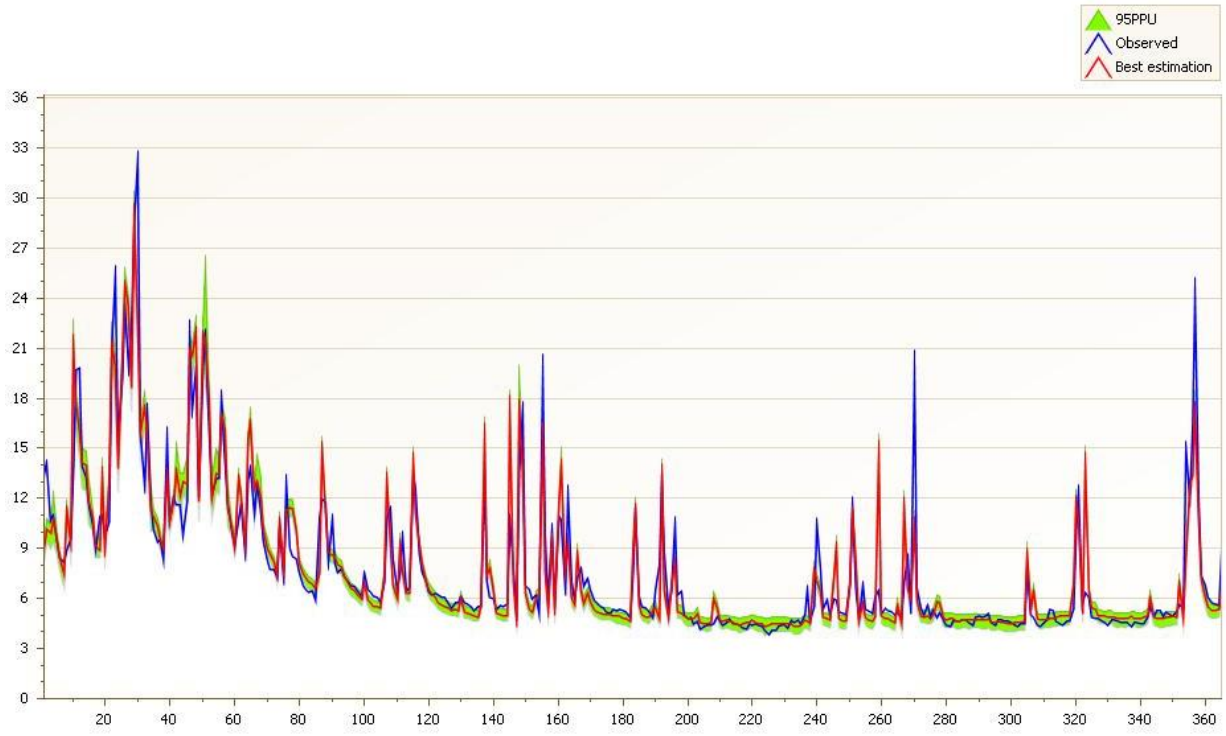

Figure 42 Calibration: Hydrographs of the observed and simulated flows in Vilvoorde for the year 1995

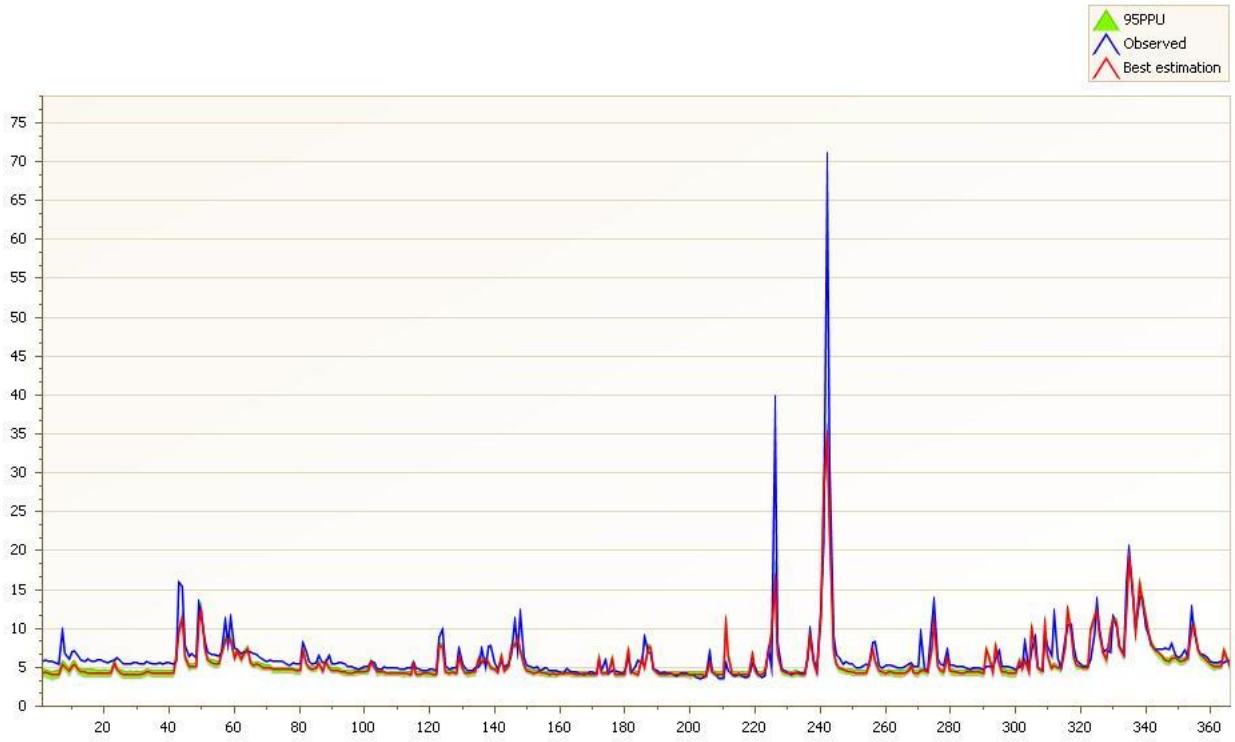

Figure 43 Validation: Hydrographs of the observed and simulated flows in Vilvoorde for the year 1995

SUFI2 Algorithm

SUFI2 algorithm has been performed both for calibration and validation period. Despite the results are better in Parasol it can be noticed that the p-factor is much higher in both calibration and validation. The r-factor is, anyway low.

Calibration: Goal type= Nash Sutcliffe		Best sim no= 216	Best goal = 8.49E-01
Variable	p_factor	r-factor	NS
q_1	0.87	0.5	0.85

Figure 44 Calibration results of the SUFI2 algorithm

Validation: Goal type=Nash Sutcliffe		Best sim no= 34	Best goal =7.68E-01
Variable	p_factor	r-factor	NS
q_1	0.72	0.39	0.77

Figure 45 Validation results of the SUFI2 algorithm

In figure 46 and 47 the hydrographs of the calibration and the validation period are represented. It can be noticed that the 95PPU are wider than in the ParaSol iteration. In validation period it can be noticed that again the base-flow is almost always underestimated.

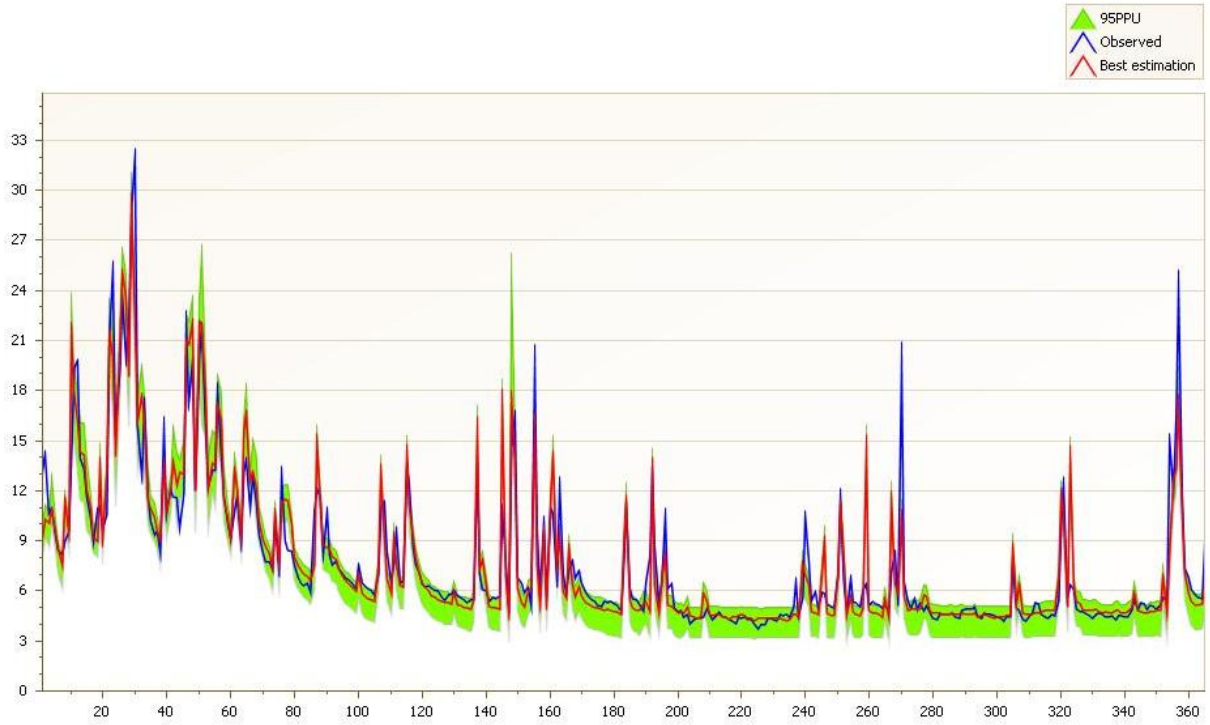

Figure 46 Calibration: observed and simulated hydrographs

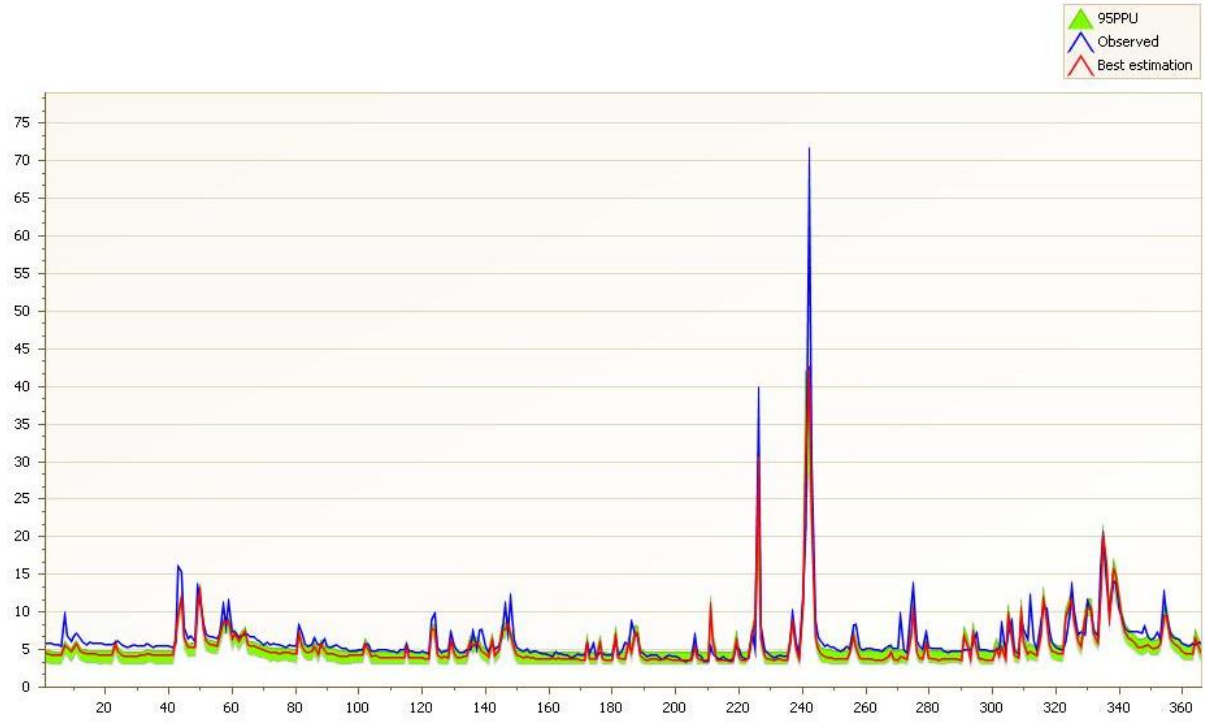

Figure 47 validation: observed and simulated hydrographs

Water balance

The water balance can be made on three components of the hydrologic system:

- Surface runoff: The water yield, which is the total amount of water leaving the HRUs and entering the main channel, is equal to the surface runoff, summed to the lateral flow and the groundwater contribution to streamflow, subtracted by the transmission losses in the main channel and the pond abstraction.

$$WYLD = SURQ + LATQ + GWQ - TLOSS - pond\ abstraction \quad (83)$$

- Channel routing: the water entering from the basins upstream summed to the water coming from the sewer system must be equal to the water flowing out of the basin summed to the water yield.

$$\sum Qin = Qout + WYLD \quad (84)$$

- Water content in the soil:

$$SW_t = SW + \sum_{i=1}^{t} (R_i - Q_i - ET_i - P_i - QR_i) \quad (85)$$

where SW is the soil water content minus the 15-bar water content, t is time in days, and R, Q, ET, P, and QR are the daily amounts of precipitation, runoff, evapotranspiration, percolation, and return flow; all units are in mm.

Figure 48 give a better idea of the balance.

Tables 19 and 20 report the water balance for the modelled sub-basins. The balance for water yield and water content in the soil are done summarizing the amount of water in each HRU of the sub-basin. As it can be seen in table 26 the water yield balance, for the years 1995-1996 is correct: the last column is the water yield calculated as sum of the variables in the other columns. It is equal to the water yield given as input by the SWAT model. The water balance for the channel routing is affected by a small error in some of the subbasins. The water content in the soil is affected by a non-negligible error, of the same order of magnitude of the variables involved in the balance.

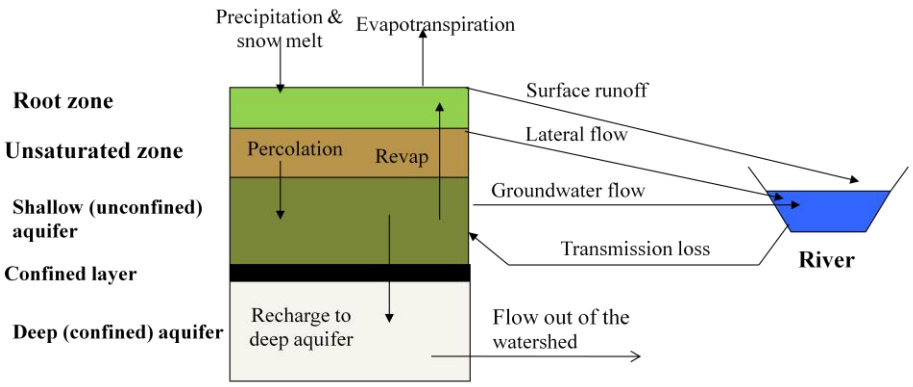

Figure 48 Representation of the water balance in the soil layers

Basin	AREAkm2	SURQ_GENmm	TLOSSmm	LATQmm	GW_Qmm	WYLDmm	WYLDcalc
1	6.25E-02	8.03E+00	6.78E-02	4.01E+00	0.00E+00	1.20E+01	1.20E+01
2	9.76E-02	1.03E+01	8.14E-01	2.83E+00	0.00E+00	1.23E+01	12.27441
3	1.01E-01	5.54E+00	3.57E+00	2.41E+00	0.00E+00	4.38E+00	4.38223
4	1.01E-01	2.59E+00	1.93E+00	3.26E+00	0.00E+00	3.92E+00	3.917175
5	1.01E-01	2.36E+00	2.32E+00	2.72E+00	0.00E+00	2.76E+00	2.7546
6	4.10E+01	2.31E+00	4.75E-02	4.41E+00	0.00E+00	6.68E+00	6.677947
7	1.01E-01	3.08E+00	2.04E+00	2.38E+00	0.00E+00	3.42E+00	3.422866
8	2.80E+00	1.34E+01	1.00E-03	6.00E-03	0.00E+00	1.34E+01	13.358
9	3.05E+01	6.89E-01	7.54E-03	5.64E+00	0.00E+00	6.32E+00	6.3217
10	7.90E+01	6.90E-01	2.87E-02	2.43E+00	0.00E+00	3.09E+00	3.089825
11	2.01E+01	1.90E+00	2.59E-02	3.91E+00	0.00E+00	5.78E+00	5.779703
12	1.01E-01	4.71E-01	4.71E-01	9.25E+00	0.00E+00	9.25E+00	9.253255

Table 26 Water yield balance

Reach	Flow in [m3/sec]	Flow out [m3/sec]	Flow out - Flow out from upstream reaches [m3/sec]	Flow in from sewer system [m3/sec]	Water yield [m3/sec]	Error
1	7.15200	7.14300	1.15684	1.26	0.00	0.10
2	6.05300	5.98100	2.69600	2.92	0.00	0.23
3	3.36800	3.28500	-0.08300		0.01	0.09
4	0.00001	0.00000	0.00000		0.00	0.00
5	3.56000	3.36800	0.51400	0.77	0.00	0.26
6	0.00867	0.00516	0.00516		0.00	0.00
7	2.87100	2.85400	0.06535	0.06	0.00	0.00
8	0.00150	0.00055	0.00055	0.00	0.00	0.00
9	0.00611	0.00293	0.00293		0.00	0.00
10	0.00772	0.00372	0.00372		0.00	0.00
11	3.40500	2.79900	2.79900	2.28	0.00	-0.52
12	0.00003	0.00000	0.00000		0.00	0.00

Table 27 Channel routing water balance

6.3.2 Curve Number method

Sensitivity analysis

The results of the sensitivity analysis for this model are reported in table 28. Eight parameters have been identified as to be sensitive. These eight parameters have been calibrated using the two algorithms as it has been done for the previous model.

OBJECTIVE FUNCTION 1			OBJECTIVE FUNCTION 2			OUTPUT 1		
SSQR for flow (m^3/s) at Vilvoorde			SSQ for flow (m^3/s) at Vilvoorde			Aver. for flow (m^3/s) at Vilvoorde		
rank	Parameter name	mean	rank	Parameter name	Mean	#	par	mean
1	Cn2	4.82E+00	1.00E+00	Cn2	2.85E+00	1.00E+00	Cn2	2.36E-01
2	Surlag	8.11E-01	2.00E+00	Surlag	4.55E-01			
3	Sol_Awc	5.91E-01	3.00E+00	Sol_Awc	2.93E-01			
4	Esco	3.23E-01	4.00E+00	Canmx	1.82E-01			
5	Canmx	2.95E-01	5.00E+00	Esco	1.75E-01			
6	Sol_Z	1.44E-01	6.00E+00	Sol_Z	7.63E-02			
7	Rchrg_Dp	9.51E-02	7.00E+00	Rchrg_Dp	5.35E-02			
8	Slope	6.42E-02						

Table 28 Sensitivity analysis results

Name	Minimum	Maximum
r__CN2.mgt	-0.5	0.5
v__SURLAG.bsn	1	24
r__SOL_AWC(1).sol	-0.5	0.5
r__ESCO.hru	-0.01	1
v__CANMX.hru	0	100
v__SOL_Z(1).sol	0	3000
v__RCHRG_DP.gw	0	1
r__HRU_SLP.hru	-0.5	0.5

Table 29 Calibrated parameters and their boundaries

Parasol Algorithm

The results of the ParaSol algorithm are, in this case, less good than in the previous model: the algorithm stopped after 3909 simulations. Of these 3909 simulations, 3523 simulations are considered good basing on the χ^2 method (see chapter 2).. The best parameter set give a value of the NSE equal to 0.68. An overview of the results of the calibration is shown in table 30. Both the p-factor and the r-factor are very small. This means that the 95PPU has really narrow boundaries. It can be noticed from figure 49 that the 95PPU are almost not visible.

Calibration: Results of 3523 simulations				
Variable	n	p_factor	r-factor	NS
q_1.out	365	0.01	0.02	0.76

Table 30 Calibration results

The results of the validation are surprisingly much better than the results of the calibration. In table 31 the results of the validation are shown. The NSE increases and the mean square error decreases. Not big differences can be seen in the p-factor and the r-factor. The hydrographs are reported in figure 50. It can be noticed that the results are in this case much better that the results of calibration. The main difference with the previous model is that the baseflow and the peaks are generally overestimated.

Validation: Results of 3523 simulations				
Variable	n	p_factor	r-factor	NS
q_1.out	365	0.04	0.02	0.79

Table 31 Validation result

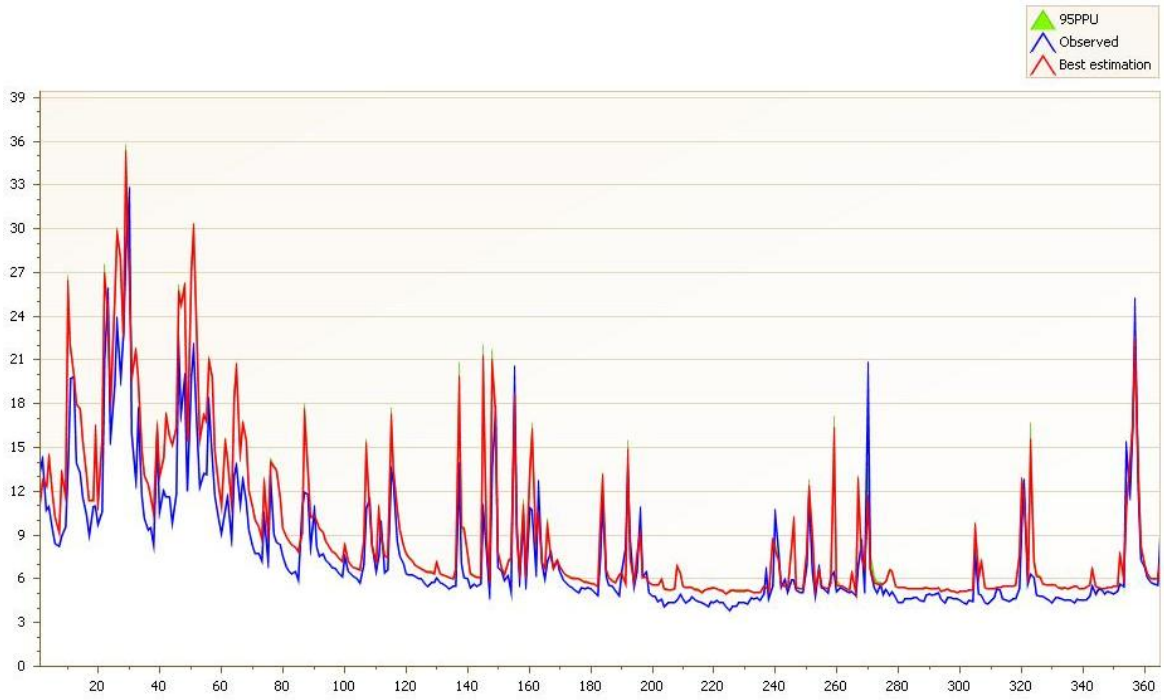

Figure 49 Calibration observed and simulated hydrograohs

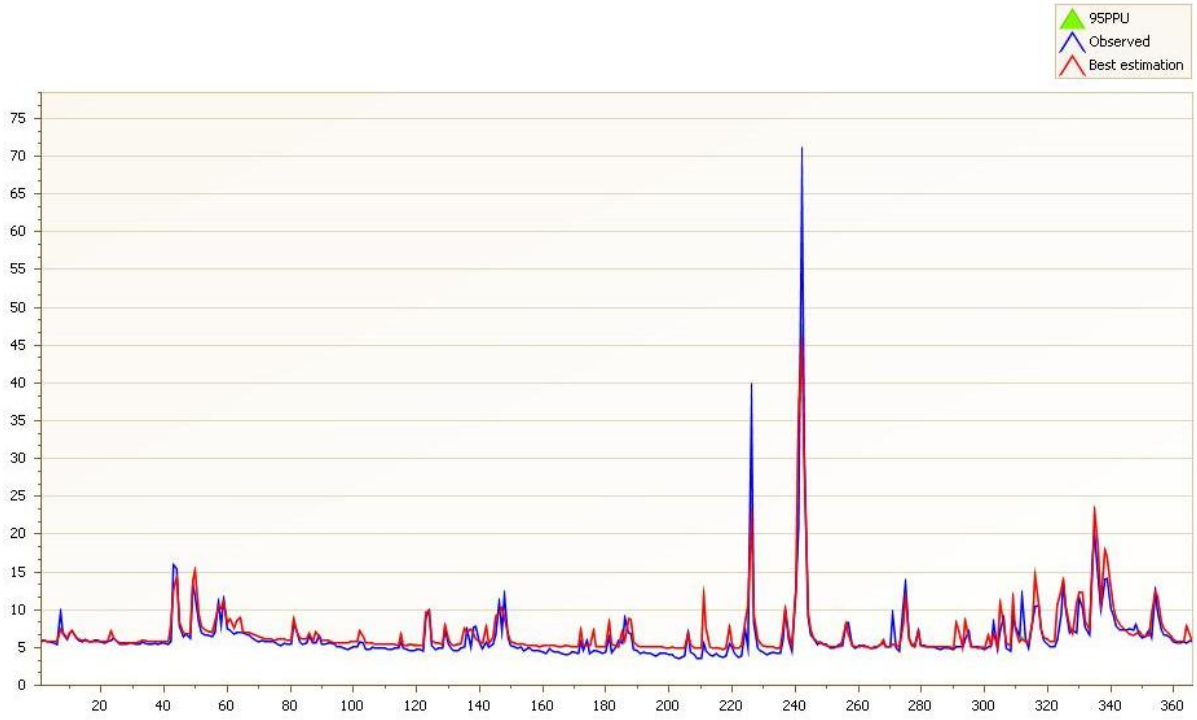

Figure 50validation observed and simulated hydrographs

SUFI2 algorithm

As it has been done with the previous model, the next step of the calibration is using the SUFI2 algorithm with parameter space boundaries in the drawn by the good parameter sets found by the SCE-UA algorithm of ParaSol method.

The results of the calibration don't show great improvements compared to the previous step of the calibration. The 95PPU are wider and the p-factor is, thus, higher, anyway the NSE is even smaller than the previous.

Surprisingly the validation gives much better results than the calibration: not only the NSE is higher, but the p-factor also, even if the r-factor is smaller than in calibration. Table 33 and figure 50 show the results.

Calibration: Goal type= Nash Sutcliffe		Best sim no= 1534	Best goal =6.73E-01
Variable	p_factor	r-factor	NS
q_1	0.29	0.24	0.67

Table 32 Calibration results

Validation: Goal type = Nash Sutcliffe		Best sim no =188	Best goal= 8.10E-01
Variable	p_factor	r-factor	NS
q_1	0.35	0.17	0.81

Table 33 Validation results

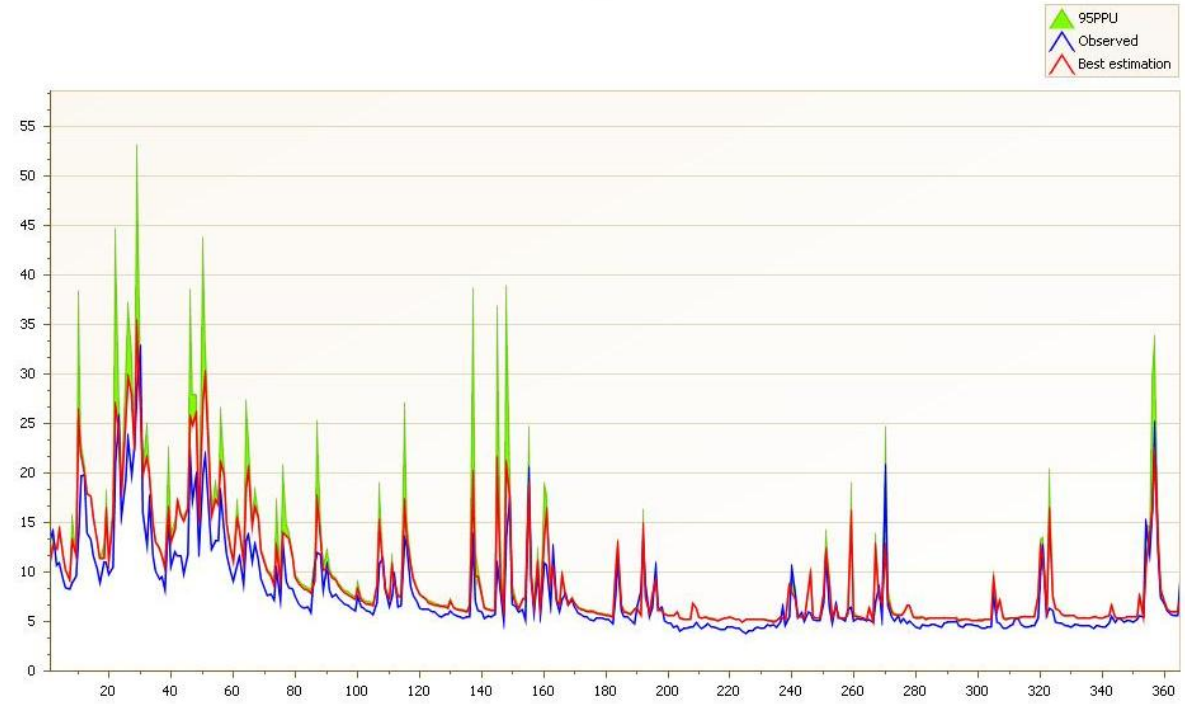

Figure 51 Calibration: observed and simulated hydrographs

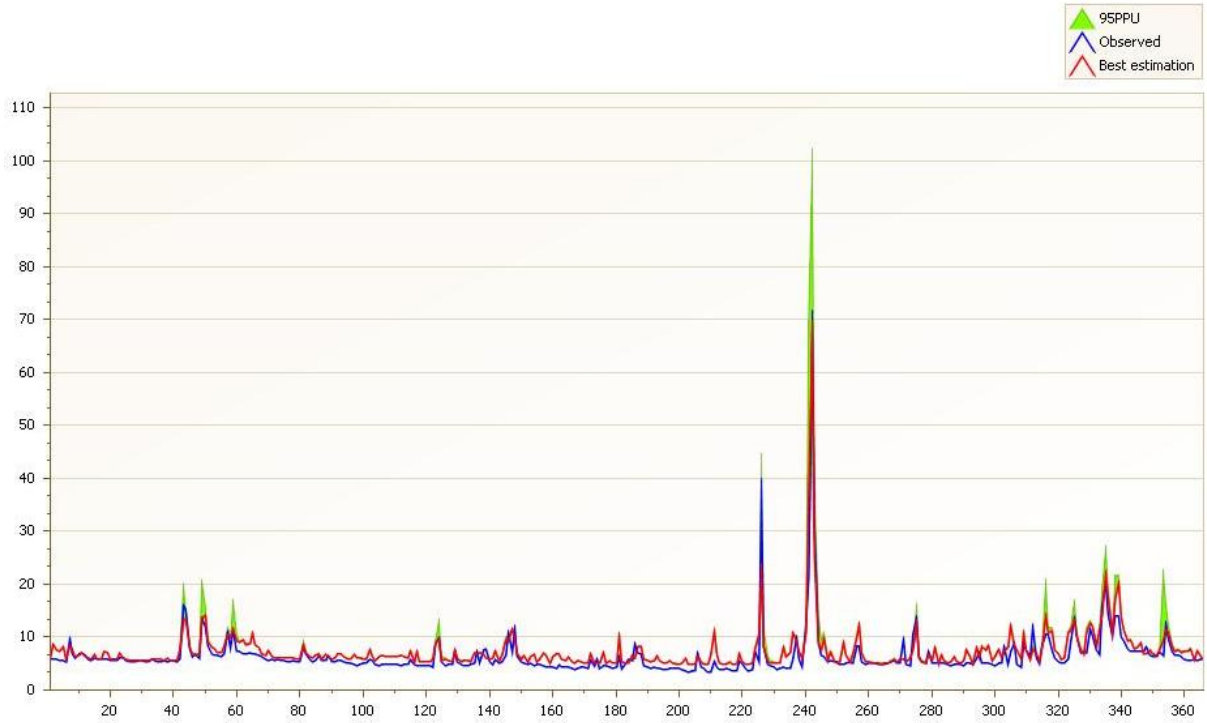

Figure 52 Validation: observed and simulated hydrographs

Water balance

The results of the water balance are reported in the tables 28 and 29. As for the previous model the water yield balance is good and the water yield calculated as the sum of the other variables is equal to

the one given as input of the SWAT model. The water balance of the channel routing is affected by a small error, while the water balance of the soil water content is affected by an error with the same order of magnitude of the variables involved in the balance.

Basin	AREAkm2	SURQ_GENmm	TLOSSmm	LATQmm	GW_Qmm	WYLDmm	WYLDcalc
1	6.25E-02	1.45E+02	2.43E+00	1.12E+00	2.49E-01	1.44E+02	1.44E+02
2	9.76E-02	1.80E+02	1.63E+01	6.09E-01	2.31E-01	1.65E+02	164.7799
3	1.01E-01	1.14E+02	6.56E+01	8.68E-01	5.08E-01	4.98E+01	49.79988
4	1.01E-01	6.64E+01	4.29E+01	7.92E-01	5.07E-01	2.48E+01	24.80436
5	1.01E-01	7.34E+01	5.06E+01	6.71E-01	5.20E-01	2.40E+01	23.98482
6	4.10E+01	5.61E+01	2.99E+00	1.28E+00	3.50E-01	5.47E+01	54.72248
7	1.01E-01	6.45E+01	3.67E+01	5.86E-01	4.80E-01	2.89E+01	28.87929
8	2.80E+00	2.39E+02	1.50E-02	1.00E-03	6.10E-02	2.39E+02	238.656
9	3.05E+01	4.48E+01	1.52E+00	1.87E+00	3.69E-01	4.55E+01	45.51198
10	7.90E+01	1.13E+01	5.02E-01	5.78E-01	4.31E-01	1.18E+01	11.8386
11	2.01E+01	4.05E+01	7.87E-01	1.93E+00	3.86E-01	4.20E+01	42.02723
12	1.01E-01	2.39E+01	1.89E+01	4.46E+00	4.63E-01	9.92E+00	9.920405

Table 34 Water yield balance

Reach	Flow in [m3/sec]	Flow out [m3/sec]	Flow out - Flow out from upstream reaches [m3/sec]	Flow in from sewer system [m3/sec]	Water yield [m3/sec]	Error
1	8.44800	8.44800	1.33771	1.26	0.00	-0.08
2	7.04000	7.04000	2.76800	2.92	0.02	0.17
3	4.27300	4.27200	-0.00103		0.02	0.03
4	0.00008	0.00003	0.00003		0.01	0.01
5	4.27600	4.27300	0.70400	0.77	0.01	0.08
6	0.07105	0.07029	0.07029		0.01	-0.06
7	3.57000	3.56900	0.08516	0.06	0.01	-0.01
8	0.02147	0.02077	0.02077	0.00	0.00	-0.02
9	0.04396	0.04355	0.04355		0.01	-0.03
10	0.02958	0.02729	0.02729		0.00	-0.03
11	3.42800	3.41400	3.41400	2.28	0.00	-1.13
12	0.00003	0.00000	0.00000		0.00	0.00

Table 35 Channel routing water balance

Presence of heteroscedasticity

Once the uncertainty boundaries are computed, the presence of heteroscedasticity can be verified: Heteroscedasticity occurs when the distribution of the residual is dependent on the indicator variable. Variance heterogeneity is usually detectable by examining the observed residuals plotted against the indicator variable (Petersen-Øverleir, 2004; Beven, 2006).

By plotting the uncertainty boundaries against the best estimation made and by computing the equations of the regression lines of the uncertainty boundary values versus the best estimation one can notice that the error in the model does not have a constant variance. The width of the uncertainty boundaries is, actually, proportional to the value of the flow in the best estimation. This phenomenon is not very visible in this case. Once the uncertainty due to the presence of an error in the input data is computed, this effect will become more important. An indicator of the goodness of the fitting of the regression lines is the coefficient of determination, that is the ratio between the sum of squares due to regression (SSR), that is the sum of the squares between the predicted values and the mean, and the total sum of squares (SST), that is the sum of the squares between actual values and the mean. It assumes values between 0 and 1, with values closer to 1 implying a better fit. R^2 = SSR/SST.

The coefficient of determination of the regression lines is for both the curves higher than 0.99. This means that the regression lines represent quiet well the computed boundaries.

The equation parameters of the two regression lines are reported in table 36.

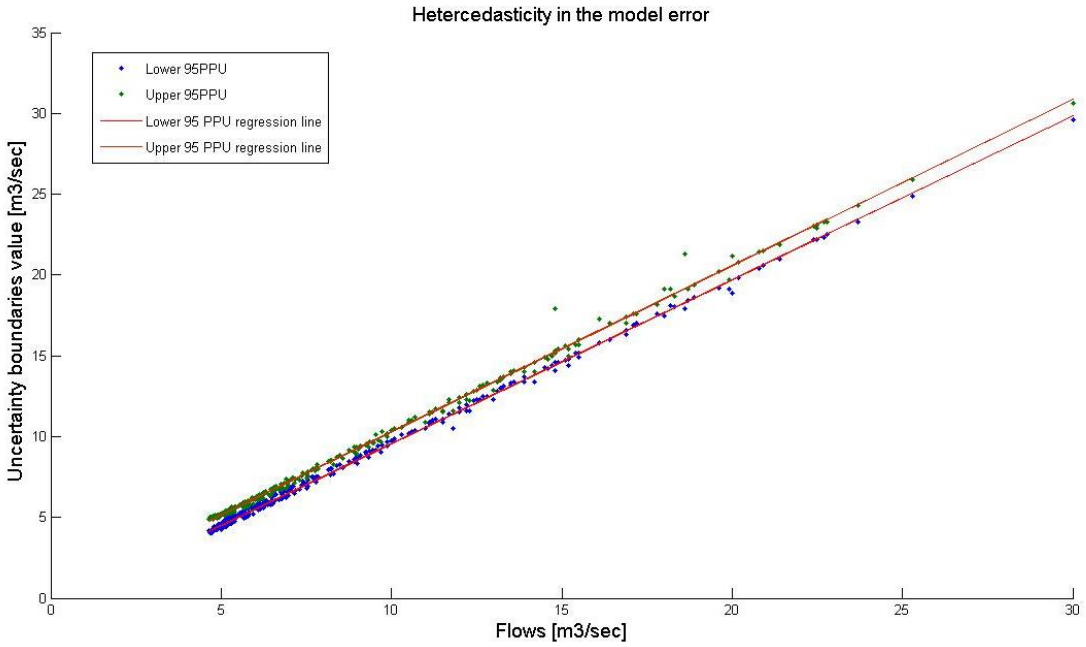

Figure 53 Heteroscedasticity of the uncertainty boundaries of the SWAT model

	Angular coefficient	Y-Intercept
Lower boundary	1.0135	-0.57419
Upper boundary	1.0276	0.022177

Table 36 Values of the parameters of the regression lines of the 95PPU of the model

6.3.3 Discussion

The comparison between the Curve Number and the Green Ampt model shows that, for this case study, the Green Ampt gives much better results, despite the flow is most of the time underestimated.

The Curve Number method, from the other side is as well affected by a bias effect, as the base flow is always over estimated. Another difference between the two models is that the Green Ampt method reproduces better the peaks. It can be noticed also that the Curve Number method is more affected, than the GAML by the initial conditions of the soil: the calibration period, the year 1995, starts with a period of high flows. The model that employs the GAML method gives a better response than the other to this initial period of high flows. Generally anyway a warm-up period of one year is recommended to make the hydrologic cycle fully operational and avoid this kind of problems.

The validation period give sometimes better results than the calibration. Looking at the hydrographs the reason can be identified in the fact that the validation year is characterized by less flood events, while the calibration period is characterized by long periods of floods, most of all in the first period of the year, when the model needs a warm-up period.

The comparison between the two calibration algorithms ParaSol and SUFI2 show that the Parasol give better results. The main difference is in the width of the uncertainty boundaries: Parasol performs better, but the width of the uncertainty boundaries is so small that only a very small percentage of the observation is included. SUFI2, instead, has better results in terms of percentage of observations within the boundaries, but also the width of the boundaries is much higher

From now on in this study, the model that employs the Green Ampt method without overflow is used, as the results are better than the one that uses the Curve Number method.

The last analysis of the uncertainty boundaries showed that the uncertainty boundaries can be approximated by means of regression.

6.4 Uncertainty analysis due to input data

To analyze the influence of the input error on the model the uncertainty analysis using the GLUE approach has been performed with different combinations of the error:

- The error in the rating curve has been applied to the model using only the best parameter set;
- The error in the rating curve has been applied to the model using all the good parameter sets;
- The error in the KOSIM output has been applied on the model using only the best parameter set;
- The error in the KOSIM output has been applied on the model using all the good parameter sets;
- Both the errors in the rating curve and in the KOSIM output have been applied together to the model using only the best parameter set;
- Both the errors in the rating curve and in the KOSIM output have been applied together to the model using all the good parameter set.

The purpose of using all these combinations is to analyze the different influences of the errors on the model.

The uncertainty boundaries are built basing on the GLUE approach: for each time step, for the good simulations, a cumulate probability distribution is built weighting the values using the NSE as a measure of the probability of the parameter set of being behavioral. Basing on Bayesian theory, the probability of the error should be multiplied to the value of the probability of the parameter set. The likelihood updating is (Beven and Binley 1992):

$$L_p(\Theta|y) \propto L_y(\Theta|y)L_o(\Theta) \tag{86}$$

Where $L_o(\Theta)$ is the prior likelihood weight of the parameter set; $L_y(\Theta|y)$ is the calculated likelihood of the parameter sets and $L_p(\Theta|y)$ is the posterior likelihood weight. The error applied to the input has been chosen so that it has the same occurrence probability for each cumulate probability, which is 1/20. So no updating of the likelihood weight is necessary.

6.4.1 Uncertainty in KOSIM output

The uncertainty analysis of the model due to the error in the KOSIM output has been performed first applying the error in the input series generated by the KOSIM model and then running the model with the best parameter set, to assess the uncertainty due to only the error in the input data, and all the good parameter sets, to assess the combination of uncertainties due to the parameters and the input. For each parameter set 50 run with 50 different random error series have been performed. When performing the uncertainty analysis to the model using only the best parameter set two different errors have been applied: one with a value of the parameter β equal to 0.1 and one with β equal to 0.25. Then the value 0.25 has been kept for the rest of the analysis.

The best parameter set performance obtained in calibration gave a value of the coefficient of efficiency equal to 0.899.

The result of 50 simulations with a random error ranging from -10% of the flow to +10% and of 50 simulations with a random error in the input ranging from -25% to +25% of the flow are reported in table 37.

	Model not affected by input error	Model affected by error in the input from the sewer system model	
		β=0.1	β=0.25
Lower NSE	0.89	0.56	0.55
Maximum NSE	0.9	0.58	0.855
Smallest width of uncertainty boundaries [m3/s]	0.4	0.35	0.878
Largest width of uncertainty boundaries [m3/s]	3.8	2.45	8.81
r-factor	0.15	0.16	0.47
p-factor [%]	34.25	3.56	68.7
Lower PPU regression line equation	1.014x - 0.57	0.976x - 0.133	0.78x + 0.336
Upper PPU regression line equation	1.028x + 0.022	1.02x + 0.154	1.06x + 0.263

Table 37 Evaluation of the uncertainty of the model with respect to the error in the input from the sewer system.

The model results to be affected by the error in the input for β equal to 0.1, as it can be seen from the value of the NSE. Anyway the r-factor has a very low value. Due to the small width of the boundaries, anyway, only a small percentage of the observations are included in the boundaries. The same cannot be said in the case of a larger error: in this case the range of the NSE gets higher. Also the r-factor and the p-factor become greater. Actually it can be seen that the r-factor is three times the one resulting from only parameter uncertainty and the p-factor is the double. In this case the error has been applied only to the best parameter set. This means that the uncertainty in the parameter affects the results less than the uncertainty in the input data.

Figure 55 shows the uncertainty boundaries versus the value of flow in the best simulations and their regression lines. It can be noticed that a relation can be found between the value of the simulated flow with the best parameter set and the uncertainty boundary width. It can also be noticed that the width of the uncertainty boundaries gets greater with the magnitude of the random error. The fitted curves have very high value of the coefficient of determination R^2: for the value of β equal to 0.1 the R^2, for both the lower and the upper 95PPU are equal to 0.99, while for β equal to 0.25, they are equal to 0.97 for the lower boundary and 0.98 for the upper boundary.

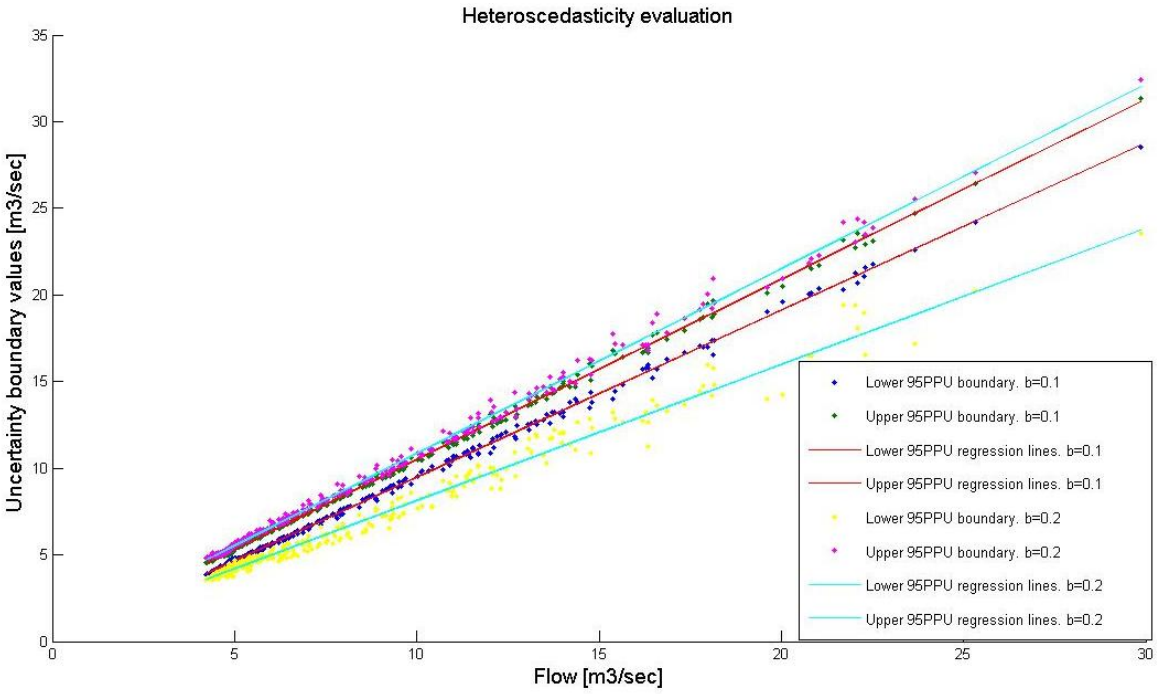

Figure 54 Comparison of 95PPU boundaries for different magnitudes of the random error in the input

The effect of the parameter uncertainty combined with the input uncertainty is shown in table 38 and in figure 56.

	Model not affected by input error	Model affected by error in the input from the sewer system model	
		β=0.25	β=0.25 and parameter uncertainty
Lower NSE	0.89	0.55	0.70
Maximum NSE	0.9	0.855	0.86
Smallest width of uncertainty boundaries [m3/s]	0.4	0.878	2.15
Largest width of uncertainty boundaries [m3/s]	3.8	8.81	11.90
r-factor	0.15	0.47	0.62
p-factor [%]	34.25	68.7	80.82
Lower PPU regression line equation	1.014x - 0.57	0.78x + 0.336	0.90x - 0.68
Upper PPU regression line equation	1.028x + 0.022	1.06x + 0.263	1.09x + 0.55

Table 38 Evaluation of the uncertainty of the model due to parameter uncertainty and input uncertainty from the sewer system. Comparison with uncertainty due to parameters and due to input error separately.

It can be noticed that, introducing the parameter uncertainty, the values of the NSE are more similar to those found in calibration. In this case the uncertainty due to parameters combined with the uncertainty in the input has been computed simulating the model with 161 good parameter sets, including the best

one, sampled randomly among those behavioural found with the Parasol algorithm, and feeding each simulation with corrupted inputs from the sewer system.

It must be noticed that the uncertainty boundaries become wider than those found computing the uncertainty analysis due to parameters. From the figure it can be also noticed that the lower boundary regression line found in the previous step is lower than the last computed. The regression lines still have very high R^2 values: in both cases, lower and upper boundaries, they are approximately 0.98.

The p-factor is greater than the one calculated for the parameter uncertainty solely, as the 88% of the observations are lay within the uncertainty boundaries.

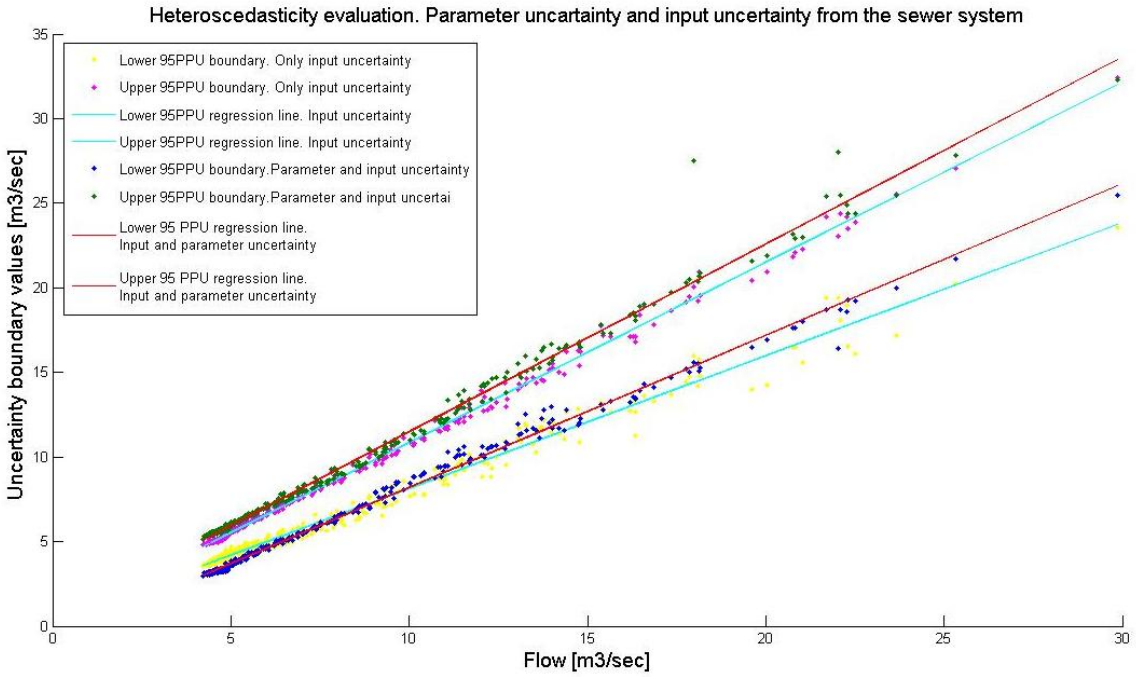

Figure 55 Comparison of 95PPU boundaries for solely input uncertainty and combination of input and parameter uncertainty.

6.4.2 Uncertainty in river discharge series: upstream boundary

A similar analysis can be done for the error in the upstream boundary of the model. At first the results of the analysis of the uncertainty due to the input with the best parameter set is presented, then the results of the combined uncertainty, parameters and input, is discussed.

Figure 57 and table 39 show that, compared to the parameter uncertainty and the input uncertainty from the sewer system, the uncertainty grows: the boundaries get wider, as it can be seen from the r-factor. It can be also seen that the p-factor, is higher than in the previous analysis. The error in the upstream boundary in Lot generates uncertainty boundaries wider than those of the random error uniformly distributed in the sewer system output. Actually the average daily discharge from the upstream boundary is 375'680 m^3/day, while the total discharge from the sewer system is 430'000 m^3/day: as the two inputs have the same order of magnitude, the different width of the uncertainty boundaries is due to the structure of the error.

The uncertainty boundaries still show heteroscedasticity: the regression lines are shown in the figure 57 and their equations are reported in the table 39. Their coefficients of determination are still very high: 0.95 for the lower boundary and 0.98 for the upper boundary.

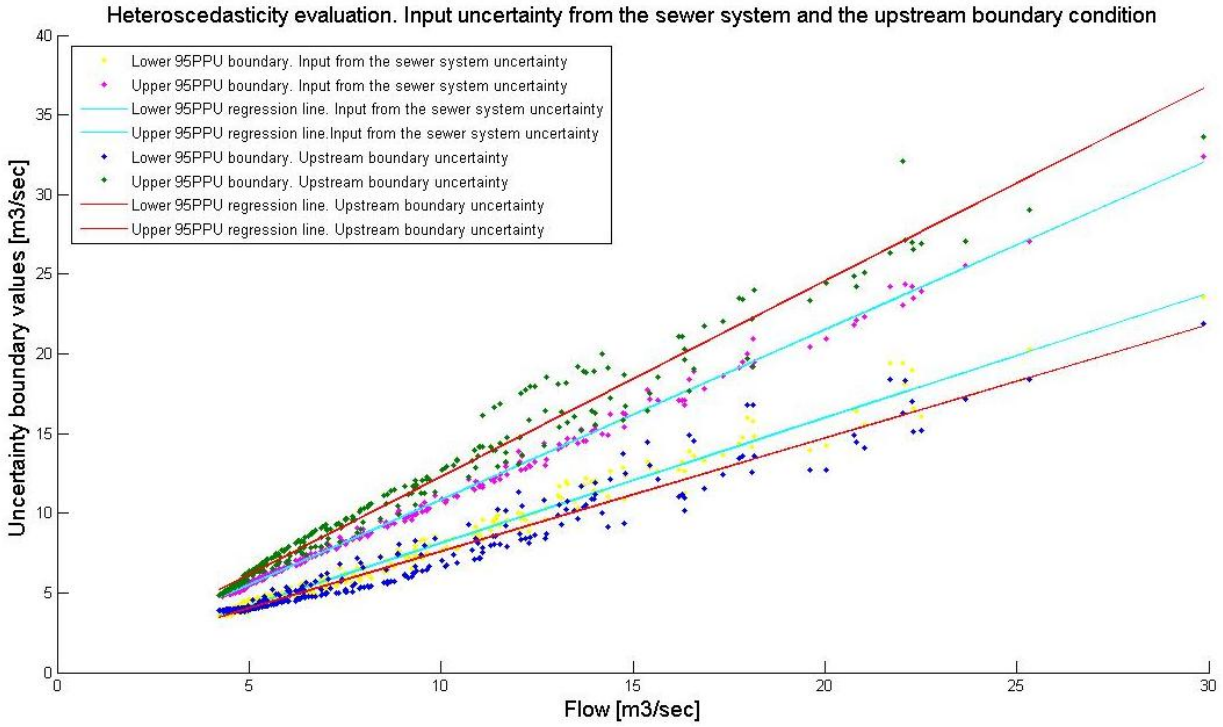

Figure 56 Comparison of 95PPU boundaries for input uncertainty from the sewer system and the upstream boundary condition.

	Model not affected by input error	β=0.25	Error in the upstream boundary
Lower NSE	0.89	0.55	0.55
Maximum NSE	0.9	0.855	0.85
Smallest width of uncertainty boundaries [m3/s]	0.4	0.878	0.97
Largest width of uncertainty boundaries [m3/s]	3.8	8.81	15.76
r-factor	0.15	0.47	0.79
p-factor	34.25	68.7	84.66
Lower PPU regression line equation	1.014x - 0.57	0.78x + 0.336	0.704x + 0.51
Upper PPU regression line equation	1.028x + 0.022	1.06x + 0.263	1.21x + 0.023

Table 39 Evaluation of the uncertainty of the model due to input from the upstream boundary in Lot. Comparison with uncertainty due to parameters.

The uncertainty analysis is done, then combining the input uncertainty with the parameter uncertainty. The value of the NSE have a wider range than before: the smallest value found is 0.41, while the greatest is 0.81. The width of the boundaries is lower than that found before, when analyzing only the uncertainty due to the input without combining it with the uncertainty in the parameter sets. Anyway the average width of the boundaries is more than 5 times the one of the uncertainty boundaries of the parameters solely. The r-factor is very high: 0.85. This means that the average width of the uncertainty boundaries is not sensitively smaller than the standard deviation of the observations. The p-factor is 76.7%. The regression curves representing the uncertainty boundaries in function of the discharge in the best simulation have a coefficient of determination very high: 0.95 and 0.97 for the lower and upper boundary respectively.

	Model not affected by input error	Error in the upstream boundary	Combined uncertainty
Lower NSE	0.89	0.55	0.41
Maximum NSE	0.9	0.85	0.81
Smallest width of uncertainty boundaries [m3/s]	0.4	0.97	1.05
Largest width of uncertainty boundaries [m3/s]	3.8	15.76	12.4
r-factor	0.15	0.79	0.85
p-factor	34.25	84.66	76.7
Lower PPU regression line equation	1.014x - 0.57	0.704x + 0.51	0.68x - 0.705
Upper PPU regression line equation	1.028x + 0.022	1.21x + 0.023	1.22x + 0.33

Table 40 Evaluation of the uncertainty of the model due to input from the upstream boundary in Lot and parameters. Comparison with uncertainty due to parameters and solely input.

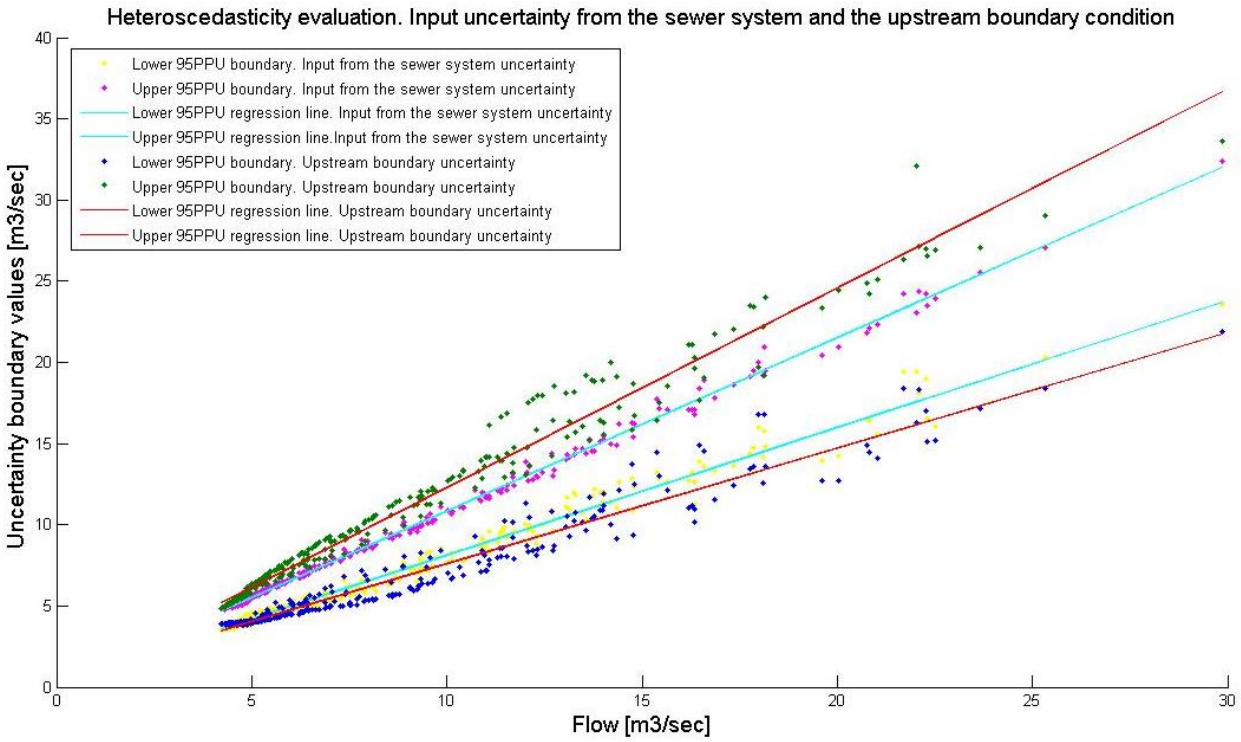

Figure 57 Comparison of 95PPU boundaries for solely the input uncertainty from the upstream boundary and the combined uncertainty in the input and in the parameters.

In figure 59 parts of the observations and of the uncertainty boundaries is represented. It can be noticed that the width is very high.

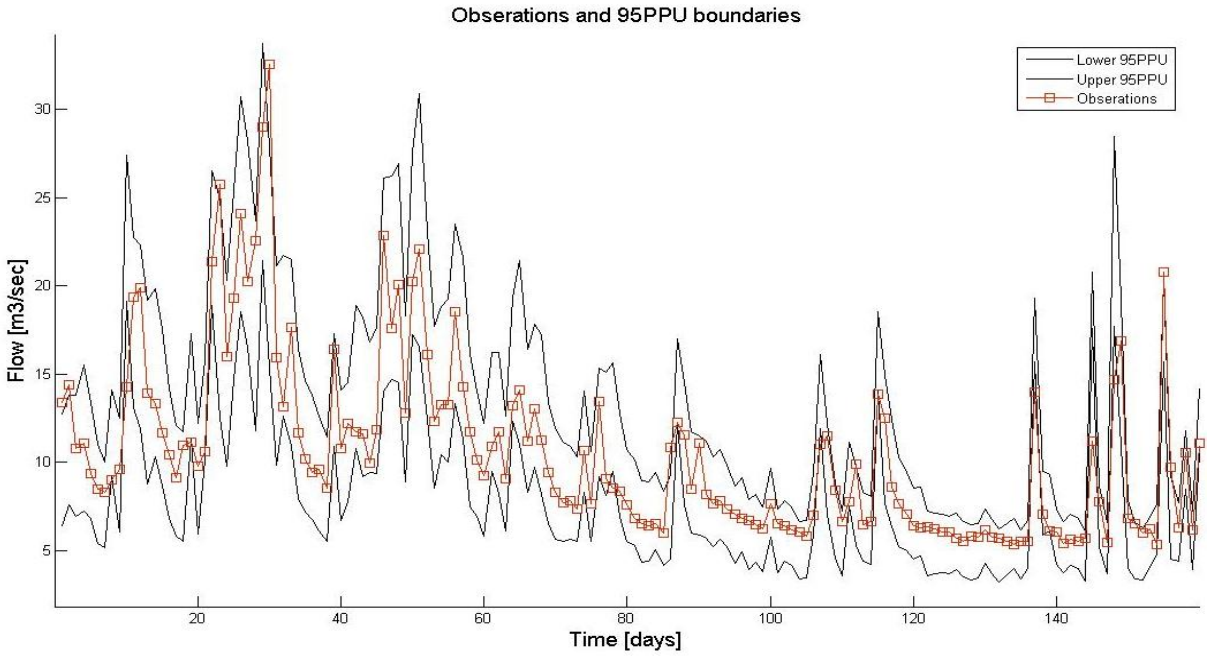

Figure 58 95PPU boundaries and observations

6.4.3 Uncertainty in all the input hydrographs

Finally the uncertainty due to all the considered input is computed: as it was done before, at first the uncertainty boundaries due to solely the input are calculated, then the combination of input and parameter uncertainty is computed. In table 41 the evaluation of the uncertainty in both cases is reported, while figure 60 shows the uncertainty boundaries against the simulated flows for the combination of uncertainty due to parameter sets and input data. It can be seen from the table and the graph that the new uncertainty boundaries do not change much between the uncertainty due to solely the input and the combined uncertainty of input and parameters.

	Model not affected by input error	Error only in the inputs	Combined uncertainty
Lower NSE	0.89	0.46	0.52
Maximum NSE	0.9	0.84	0.85
Smallest width of uncertainty boundaries [m3/s]	0.4	1.57	1.77
Largest width of uncertainty boundaries [m3/s]	3.8	12.1	1.18
r-factor	0.15	0.94	0.94
p-factor [%]	34.25	89.8	90.4
Lower PPU regression line equation	1.014x - 0.57	0.7x + 0.43	0.711x - 0.257
Upper PPU regression line equation	1.028x + 0.022	1.26x + 0.3	1.27x + 0.15

Table 41 Evaluation of the uncertainty of the model due to inputs and parameters. Comparison with uncertainty due to parameters.

The most interesting thing to be noticed is that the uncertainty boundaries are now very wide, with values of the r-factor very close to 1. The width of the uncertainty boundaries is, thus, comparable with the standard deviation of the observations.

Again the uncertainty boundaries present heteroscedasticity: the variance is heterogeneous and, in particular, the boundaries can be approximated with regression lines whose coefficient of determination is 0.95 and 0.96 for the lower and the upper boundaries for both cases: uncertainty due to only input data and combined uncertainty due to parameter sets and input data..

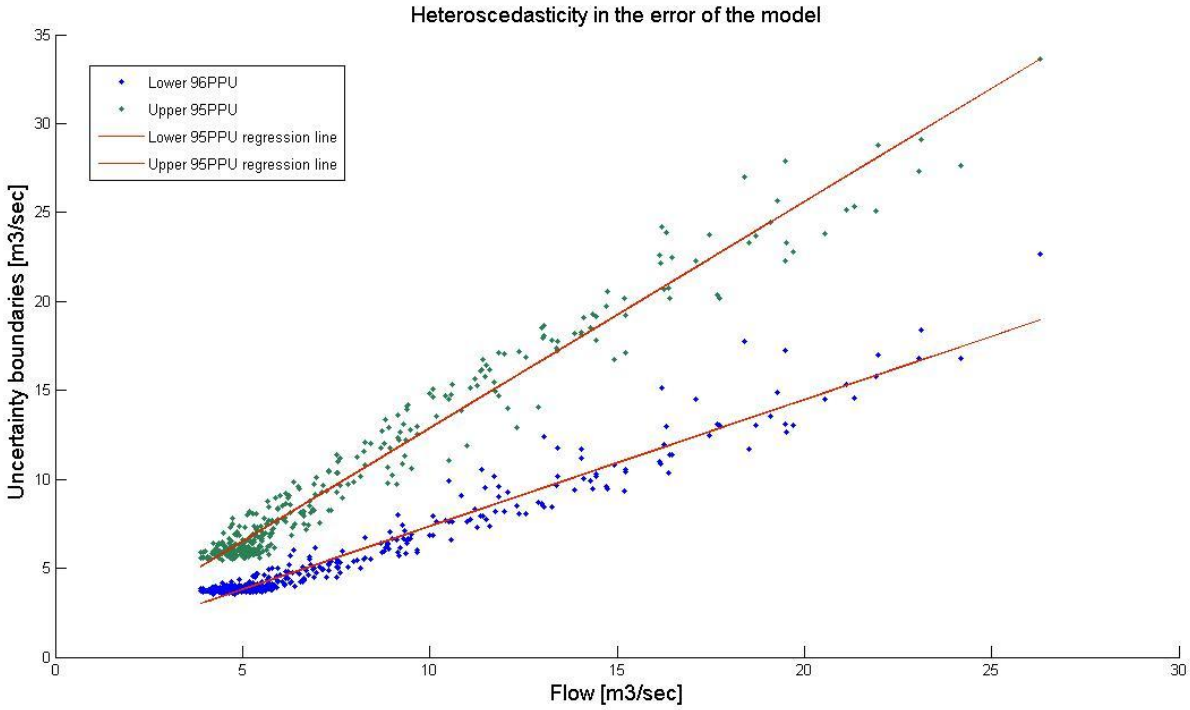

Figure 59 Bande di confidenza del 95% in funzione della migliore simulazione e rette di regressione.

Figure 61 shows a tract of the observations hydrograph and of the 95PPU. It can be noticed that the width of the uncertainty boundaries is very big also for the baseflow, not only for the high values of the flow.

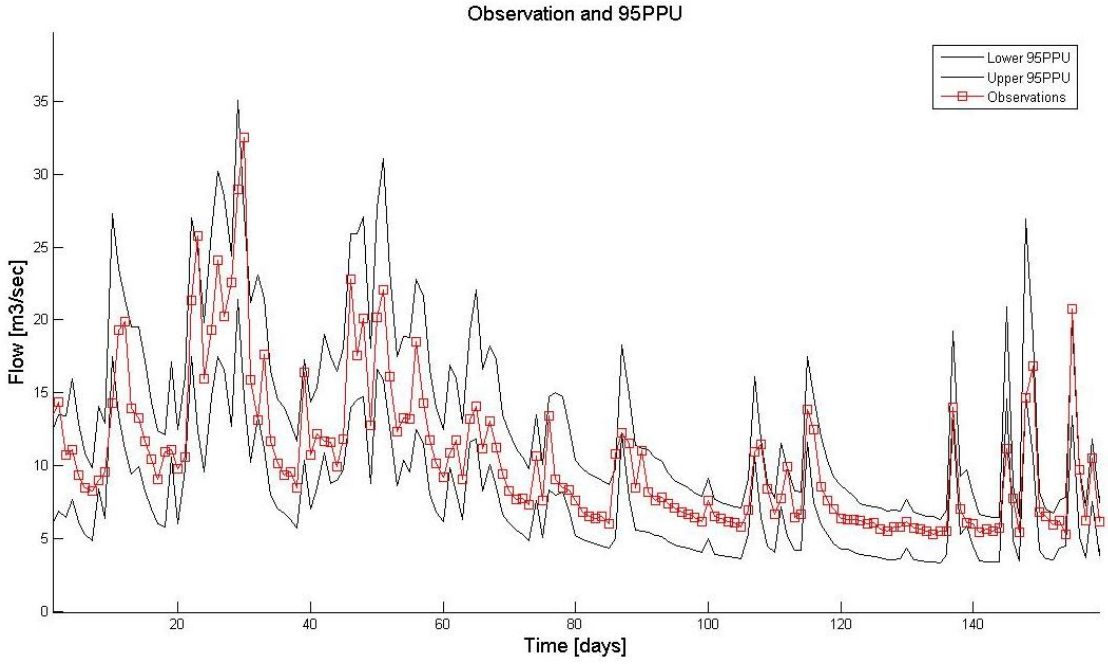

Figure 60 Uncertainty boundaries and observations for input and parameters uncertainty

6.4.4 Discussion

The uncertainty analysis of the parameters has been compared and combined with the uncertainty due to input. The effect is that the uncertainty boundaries get very wide. The r-factor, the ratio between the average width of the uncertainty boundaries and the standard deviation of the observations, for the combined uncertainty in all the input and in the parameter sets, is equal to 0.94 [m3/s] for the combined uncertainty in all the input and in the parameter sets. The performances are in general good: the lowest values of the NSE are found when combining the uncertainty in the input and the uncertainty in the parameters. In particular, in those cases, very good performance are found (the highest NSE is never smaller than 0.84), but also bad performances are common, with values around 0.4. These low performances, in particular, are responsible for the very wide uncertainty boundaries.

This analysis will be used to evaluate the cascading uncertainty from the hydrological model to the hydraulic model. In figure 62 it is reported an example of the cumulate probability of the simulations, in terms of probability of the parameter sets combined with the probability of the error, computed by means of the likelihood function. This distribution can be used to create input series for the HEC-RAS model with different cumulate probabilities, to evaluate the effect of the uncertainty due to the cascading of models, combined with the uncertainty in the parameter sets.

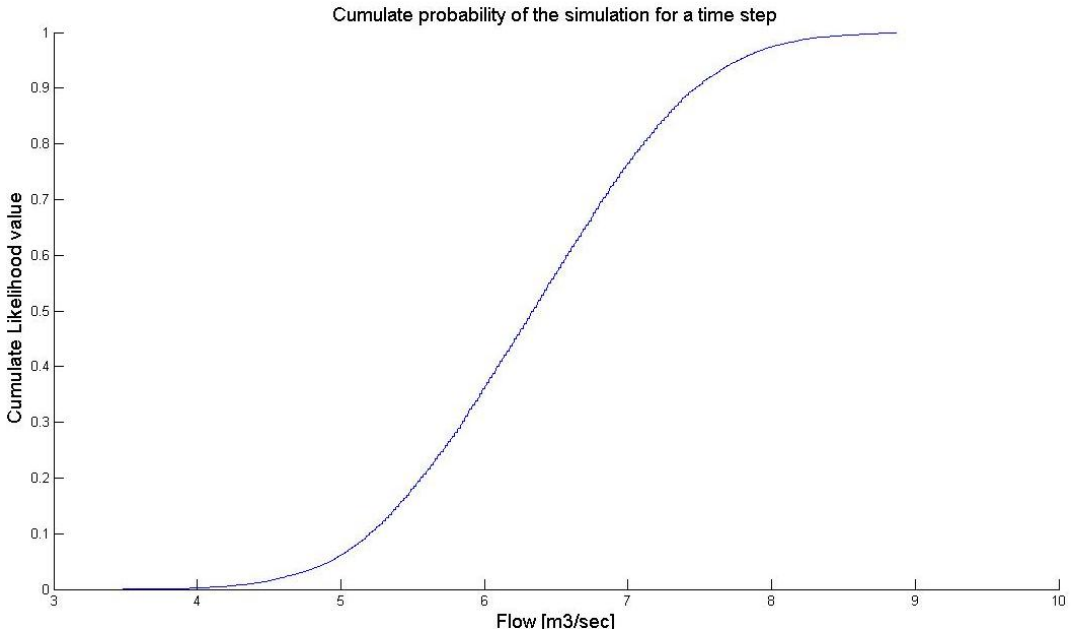

Figure 61 Cumulate probability of the simulation computed for one time step by means of the likelihood function

7 HEC-RAS model calibration and uncertainty analysis

7.1 Calibration

Calibration of the HEC-RAS model is performed comparing the values of water stage simulated by the model with the observed ones provided by the Hydrologisch Informatie Centrum (HIC) in two stations in Eppegem and in Zemst. Boundary conditions of the model are hourly flows in the station of Vilvoorde and water stage records downstream in the station of Hombeek (see figure 63). In the map in figure 63 the lateral inflow in Vilvoorde dock is also represented.

The data available from the HIC that are used for the analysis of the system and for the calibration of the model are:

- Sub-hourly (15 minutes) water stage data in Vilvoorde;
- Sub-hourly (15 minutes) water stage data in Eppegem;
- Hourly flow data in Eppegem;
- Sub-hourly (1 minute) water stage data in Zemst;
- Sub-hourly (1 minute) water stage data in Hoombek..

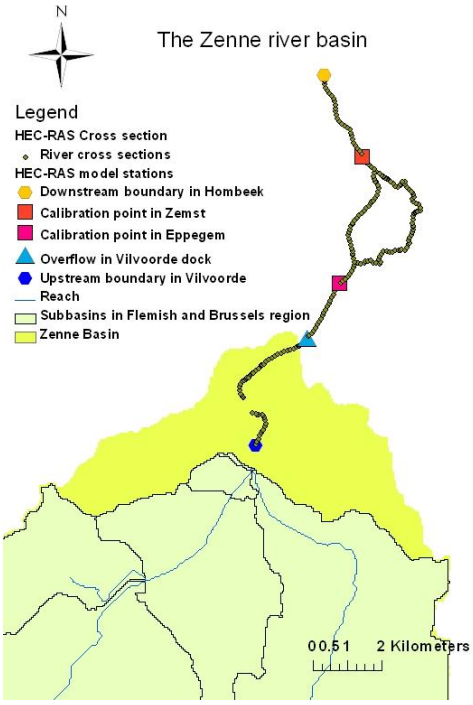

Figure 62 River stations for boundary conditions and calibrations point in the Zenne River

Flows in Vilvoorde are generated using the rating curve provided by the HIC modified using the Jones formula. The data of the 15 minutes time-step series are then aggregated to a one hour time step series,

by averaging the values. The choice of aggregating the data raise from the fact that the SWAT model that will be built in future will work with hourly time-step and will provide hourly data series to the HEC-RAS model. So the calibration must be made in the same condition of work of the composite model that is being built.

7.1.1 Jones formula correction

The Jones formula is used to correct the error induced by the presence of unsteady flow conditions (Pietersen Overlier, 2006). In case of presence of unsteady state there is not a one-to-one relation between the river stage and the discharge: same water stage values in the rising and the recession limb have, in fact, different discharges, and the rising one has the higher (Di Baldassarre, Montanari, 2009). Unsteady flow is concerned with flood wave propagation. When a flood wave passes through a given cross section, the effect of the wave front, when it's upstream the cross section, is to increase the velocity, while, when the peak passes downstream the cross section, the effect is to reduce the velocity. The result is that for the same stage, the discharge is higher during rising limb and lower during recession limb (Pietersen Overlier, 2006). In some streams the effect is manifested as distinctive loops in the stage-discharge relationship, as it can be seen in figure 64, where a comparison between a rating curve without Jones formula correction and with Jones formula correction is showed.

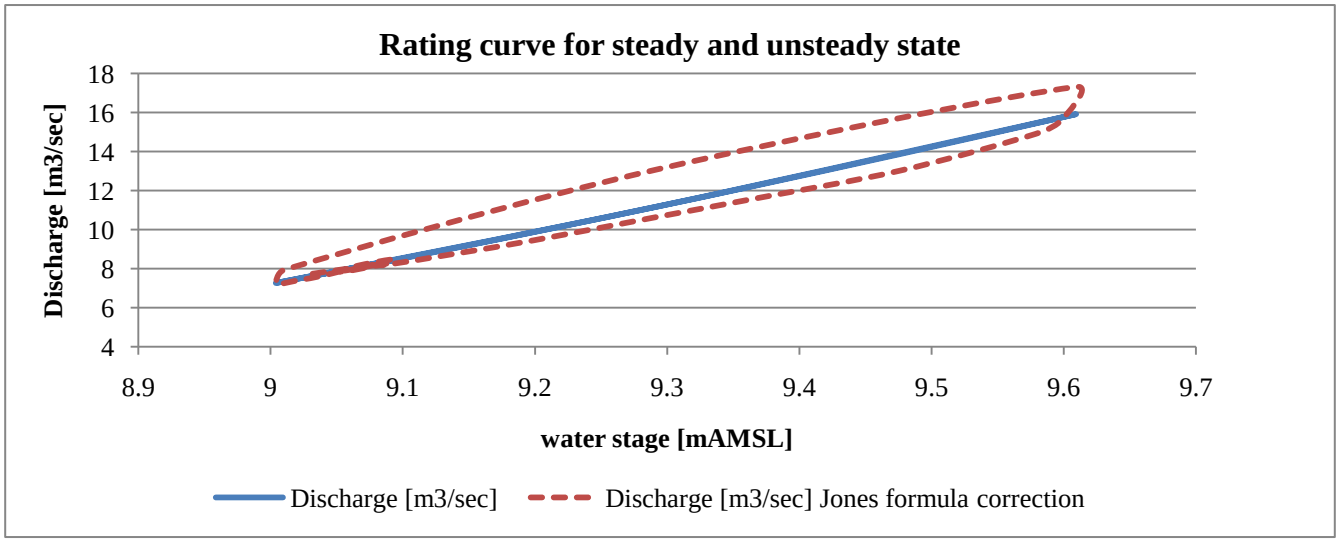

Figure 63 Stage discharge relationship calculated using the rating curve corrected and not corrected by the Jones formula

The consequence is that, if the Jones formula is not used, the simulated flows, in the HEC-RAS model have a delay of about one hour compared to the observations. In figure 65, two hydrographs generated using the rating curve corrected and not corrected by the Jones formula are used. As it can be seen, the peak of the wave built using the Jones formula is anticipated of one hour compared to the other one.

The graphs in figures 64 and 65 have been drawn using discharge values calculated using the rating curve and the stage values of a flood event occurred between the third and the fourth of April 2010, applying and not applying the Jones formula.

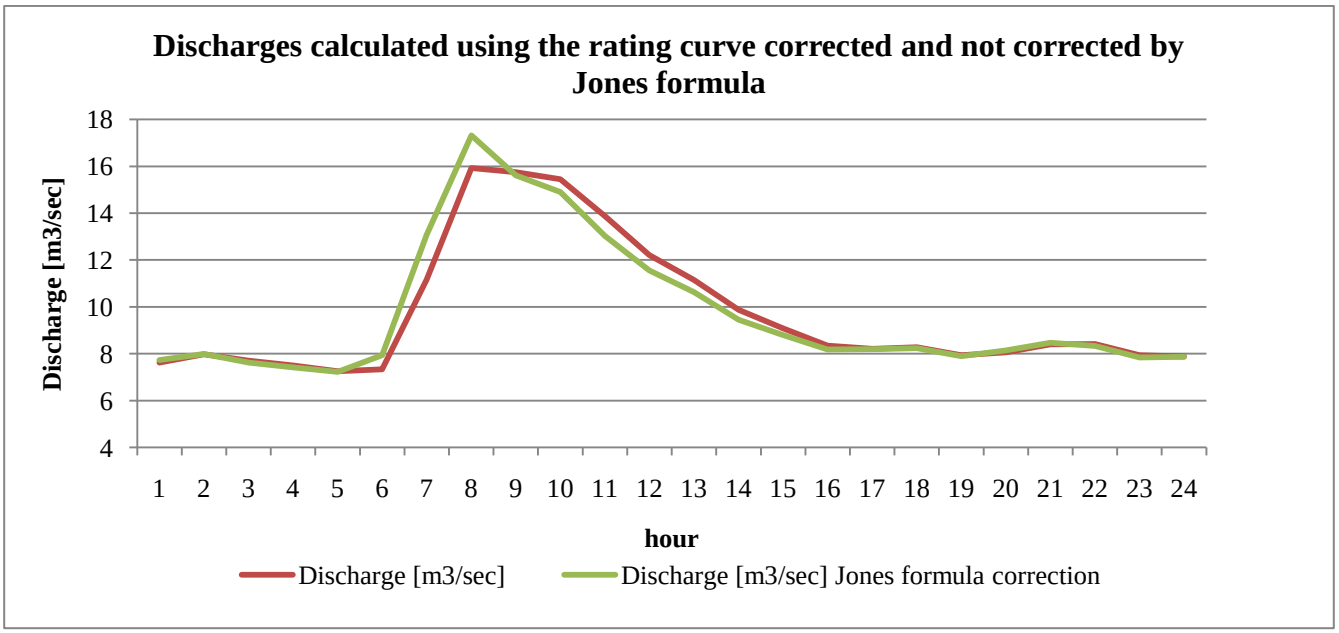

Figure 64 Hydrographs computed using the rating curve with and without the Jones formula correction

To apply the Jones formula, some initial simplifying assumptions for a short cross section are needed:

a. The flow is uniform when steady.
b. The channel section is prismatic.
c. There is negligible outflow or inflow.
d. No backwater effects are present (Pietersen Overlier, 2006).

The Jones formula discharge equation is:

$$Q = Q_n \sqrt{1 + \frac{1}{S_0 c} \frac{\partial h}{\partial t}} \tag{86}$$

Where Q_n is the discharge at steady and uniform flow, S_0 is the bottom slope, h is the depth of flow in the cross-section and c is the celerity of the wave. In order to apply the formula these terms have to be calculated:

- The celerity of the flood wave is calcualted analyzing the travelling time of the peaks in the flood events, comparing the water stage data in the stations of Vilvoorde and Eppegem and the distance between the two stations: the distance between the stations is 6572 m, while a delay of about three hours for the flood wave peak is found. The celerity is, thus, 0.61 m/sec, approximately.
- The bottom slope is calculated as the average bottom slope for the first 400 meters after the Vilvoorde station. It is approximately 0.12%.
- The derivate of the water depth with respect to time is calculated as:

$$\frac{\Delta h_i}{\Delta t} = \frac{h_{i+1} - h_{i-1}}{2\Delta t} \tag{87}$$

Equation 86 is considered suitable if the term $|(1/S_0)(\partial h/\partial t)|$ is less than 0.5 (Pietersen Overlier, 2006). If in some time step this condition is not respected, the Jones formula is not applied, in that time step.

7.1.2 Presence of overflow

An analysis of the flows calculated in Vilvoorde and the flow data provided by HIC in Eppegem shows that there is an increment of flow between the two stations that ranges approximately between the 22% and the 38%. It has been found that the ratio between the flow in Vilvoorde at the time t and the flow in Eppegem at the time t+3hours is approximately constant for each flood event analyzed. In table 42 the average, the standard deviation and the coefficient of variation of this ratio for some events is reported.

	Flood events			
	13 FEB - 22 FEB	**9 MAR -18 MAR**	**3 APR - 13 APR**	**17 APR - 27 APR**
Average ratio for the event	1.22	1.27	1.38	1.23
Standard deviation	0.12	0.07	0.21	0.25
Coefficient of variation	0.10	0.05	0.15	0.20

Table 42 Average values of the ratio between the flows in Vilvoorde and in Eppegem and their deviation from average value

This increment of flow can be due to two different reasons:

- The overflow in Vilvoorde dock is working and a lateral inflow, from the canal to the river, discharges a volume proportional to the volume derived from the Zenne to the canal in the overflows upstream.
- There is an error in the rating curve equation used to estimate the flows in Eppegem.

This last hypothesis rises from the fact that it is known that the overflows works during flood events when the water level in the canal is higher than 13.31 mAMSL. Unfortunately no data of water stage in the canal in Vilvoorde are available. Also the analysis of the water quality data, upstream and downstream the diversion, in the river and in the canal suggest the presence of a certain grade of uncertainty: the difference in water quality in the canal and in the river is really high, despite that, the water quality in the Zenne river does not show particular changes upstream and downstream the diversion. It can be due to the presence of the tributary Maalbeek. Table 43 shows some example of water quality indexes upstream and downstream the overflow. It can be seen that in many cases the indexes don´t change, for example for the BOD, NO2 and NO3. Figure 66 shows the river in the point where the overflow discharges from the canal into the river. It can be distinguished also the last stream of the tributary Maalbeek, which has been disconnected from the Zenne river due to the presence of the canal. Despite the Maalbeek has been disconnected from the Zenne to feed the canal Brussels Charleroi (figure 67), its last stretch might be still discharging in the river wastewater as it is part of the sewer system Brussels North. The presence of the discharges coming from sewers, the Maalbeek and the wastewater treatment plant, that affect significantly the water quality makes really difficult to explain what happens in the stream.

Date	BOD Zenne upstream [mgO2/L]	BOD Canal upstream [mgO2/L]	BOD Zenne Downstream [mgO2/L]	Date	NO2 Zenne upstream [mgN/L]	NO2 Canal upstream [mgN/L]	NO2 Zenne Downstream [mgN/L]
28/02/2003	33	2	30	28/02/2003	0.01	0.17	0.01
				28/02/2003	0.01	0.18	0.01
31/03/2003	104	2	77	31/03/2003	0.01	0.18	0.12
30/04/2003	21	4	17	30/04/2003	0.13	0.73	0.01
28/05/2003	87	2	87	28/05/2003	0.01	0.31	0.01
30/06/2003	62	2	51	30/06/2003	0.01	0.16	0.01
Date	**NO3 Zenne upstream [mgN/L]**	**NO3 Canal upstream [mgN/L]**	**NO3 Zenne Downstream [mgN/L]**	**Date**	**NH4 Zenne upstream [mgN/L]**	**NH4 Canal upstream [mgN/L]**	**NH4 Zenne Downstream [mgN/L]**
28/02/2003	0.07	6.46	0.07	28/02/2003	14.3	1.03	10
28/02/2003	0.07	6.4	0.07	28/02/2003	14.3	1.1	10
31/03/2003	0.12	5.92	0.07	31/03/2003	19	1.97	18.1
30/04/2003	0.13	7.29	0.07	30/04/2003	10.9	0.56	11.5
28/05/2003	0.07	6.06	0.07	28/05/2003	22.8	0.18	21.2
30/06/2003	0.07	4.84	0.07	30/06/2003	19.6	0.32	13.7

Table 43 Comparison of water quality indexes upstream and downstream the overflow in Vilvoorde

Due to this structure uncertainty two models are built: one in which the overflow is working, for which the discharge from the overflow is a parameter to be found, and one in which the overflow is not working at all.

Figure 65 Overview of the overflow in Vilvoorde dock and the measurement station of the VMM used to analyze the difference in water quality upstream and downstream the overflow

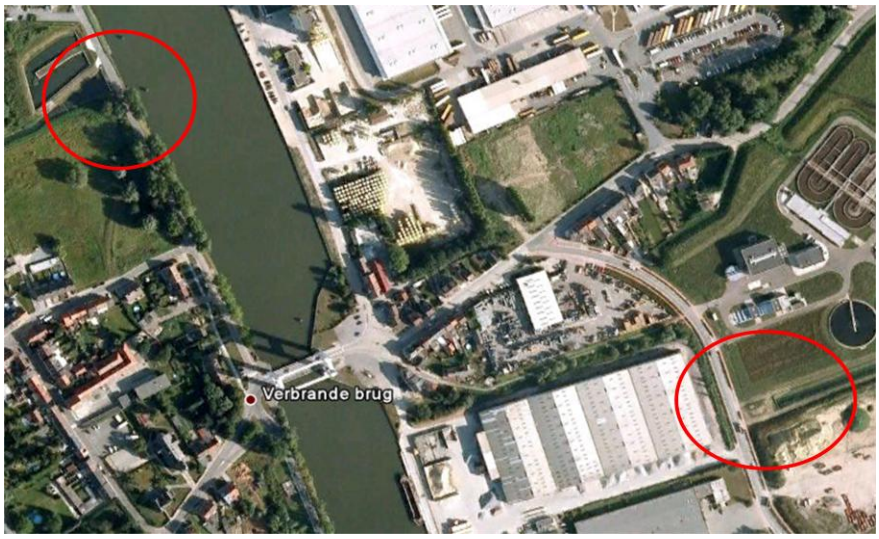

Figure 66 The Maalbeek, former tributary of the Zenne, has been disconnected from the river, to feed the Sea Canal in Grimbergen

7.1.3 Numerical scheme

The time step of the computation and the θ factor have been chosen in order to find a good compromise between accuracy of the simulation and stability: it has already been mentioned that larger values of the θ factor produce robust simulation at the cost of accuracy (US Army Corps of Engineers, 1998; Pappenberger 2004). Whenever possible, the θ factor has been set to 0.6, but many simulations needed higher values of the factor in order to be stable.

The choice of the computation time step has to be done either using a value that is the 20th of the time of the rise of the inflow hydrograph or to ensure that the Courant condition is met (US Army Corps of Engineers, 1998; Pappenberger 2004):

$$\Delta x \geq c \cdot \Delta t \tag{88}$$

where Δx is the space step, c is the speed of the flood wave and Δt is the time step.

A time step of 15 seconds or of 20 seconds has been found as being good, as the simulations are stable and accurate. For calibration and validation a time step of 15 seconds has been used whenever the simulation was stable. In case the simulation was not stable, the time step was changed to 20 seconds.

7.1.4 The calibration

The parameters to be calibrated for the HEC-RAS model are the Manning coefficient n and the percentage to be multiplied to the flow in Vilvoorde to generate the lateral inflow, α.

The Manning's coefficient n is the parameter governing the Manning's equation:

$$Q = \frac{1}{n} R^{2/3} S^{1/2} A \tag{89}$$

Where Q is the flow [m^3/sec], R is the hydraulic radius [m], S is the slope of the water surface or the hydraulic head loss and A [m^2] is the cross-section area.

As the inflow in Vilvoorde is dependent on the flow abstracted from the overflows upstream in Anderlecht and in Lembeek, the parameter α could be, apparently more reasonably, defined as a proportion of the flow abstracted from the river. The choice of defining α as a percentage of the flow in Vilvoorde rise from the following reasons:

- It has been found that, in different episodes, the ratio between the flow in Eppegem and in Vilvoorde is proportional with a good approximation.
- If α is relationed to the flow in Vilvoorde, then the HEC-RAS model can be calibrated independently from the results of the SWAT and the KOSIM models, otherwise a new source of uncertainty due to input from other models would be introduced.
- The SWAT model built for this study does not include all the overflows, i.e. the overflow in Lembeek that is upstream the boundary.

Two different models are built and calibrated: one in which the overflow is constantly working and one in which the overflow is not working, so the value of α is kept equal to 0.

The approach used for the calibration is GLUE. The goodness of fit indicator for calibration used is the Nash-Sutcliff coefficient of efficiency (NS). The Nash Sutcliff coefficient of Efficiency has been chosen as it is really intuitive and widely used for the GLUE approach. The threshold used for the selection of the behavioural parameter sets is 0.75. Moriasi et al. (2007) consider the performance of models as being very good for values of the NS higher than this threshold.

Four historic flood episodes are available for the calibration and the validation of the model (table 44):

	Flood events			
	17 FEB - 22 FEB	9 MAR -18 MAR	3 APR - 12 APR	17 APR - 26 APR
Max flow in Vilvoorde	8.917	7.27	16.19	6.25
Min flow in Vilvoorde	4.134	5.10	4.51	3.92

Table 44 Flood events for calibration and validation of the HEC-RAS model.

For calibration of the model the events of the 17-22 of February and 17-27 of April have been used, while for the validation the events of 9-18 March and 3-13 of April are used. The latter presents the highest values of flow in Vilvoorde.

At first, for the calibration, these pairs of events have been treated as single episodes putting together the series. This way about 15 days of hourly data are used.

The choice of combining two different events for calibration and validation was also taken to find a parameter set that can give good result with different conditions due to seasonal change of the roughness of the bed. In fact it is expected that in winter (February) and in spring (April) the roughness of the river bed changes because of the growth of vegetation.

The result of the calibration is a series of parameter sets with a value of the NS that ranges from -21, for a value of the α equal to 0.21 and a value of the Manning's n equal to 0.02, to 0.66 for a value of the α equal to 0.21 and a Manning's n equal to 0.038 for the station of Eppegem.

The Zenne River is influenced by tidal effect from the outlet downstream. Due to the tidal effect, in Zemst the effect of the flow from the upstream boundary in Vilvoorde is almost negligible and sometimes the flow is even negative. As a consequence the performance of the model in Zemst is

always very good with values of the NS most of the times higher than 0.9. Anyway the maximum is not higher than 0.922. The performance of the model in Eppegem is, thus, the one considered more important for the model evaluation. The good parameter sets are, thus chosen, basing on the performance in the station of Eppegem.

The values in green are the ones with the highest values: higher than 0.6 in the station of Eppegem and more than 0.92 in the station of Zemst.

The model has been re-run using all the parameter sets with values of the parameters between 0.21 and 0.39 for the α and between 0.032 and 0.038 for the Manning's n taking the two events of February and April separately to analyze the behaviour of the model in the two seasons and find a parameter set that give good performance in both cases.

While the event of February give good results, the event of April never give good results as the value of the NS index is almost always under the value of 0.4, with a maximum equal to 0.4074.. This big difference in the result can be due to different conditions of the river bed and changing in the rating curve due to changes in the cross section caused by erosion and sediment transport.

The model is, thus re-calibrated using only the event of February. 38 behavioural parameter sets have been found (table 45). In the following table the values of the parameters and of the NS are reported.

The best simulation has a value of the NS equal to 0.9361. The values of the parameters are:

α: 24; Manning's n: 0.035.

α	n	NS	α	n	NS
0.2100	0.0350	0.8409	0.3000	0.0340	0.8543
0.2100	0.0360	0.9345	0.3100	0.0330	0.9243
0.2200	0.0350	0.8947	0.3100	0.0340	0.7708
0.2200	0.0360	0.8971	0.3200	0.0320	0.7969
0.2300	0.0350	0.9309	0.3200	0.0330	0.9295
0.2300	0.0360	0.8364	0.3300	0.0320	0.8610
0.2400	0.0340	0.7905	0.3300	0.0330	0.8919
0.2400	0.0350	0.9361	0.3400	0.0320	0.9029
0.2500	0.0340	0.8693	0.3400	0.0330	0.8467
0.2500	0.0350	0.9168	0.3500	0.0320	0.9204
0.2600	0.0340	0.9138	0.3500	0.0330	0.7571
0.2600	0.0350	0.8664	0.3600	0.0310	0.7750
0.2700	0.0340	0.9242	0.3600	0.0320	0.9267
0.2700	0.0350	0.7952	0.3700	0.0310	0.8365
0.2800	0.0330	0.8077	0.3700	0.0320	0.8943
0.2800	0.0340	0.9287	0.3800	0.0310	0.8837
0.2900	0.0330	0.8716	0.3800	0.0320	0.8537
0.2900	0.0340	0.9000	0.3900	0.0310	0.9143
0.3000	0.0330	0.9154	0.3900	0.0320	0.7780

Table 45 Behavioral parameter sets and NS values

From the values of the behavioural parameter sets it can be seen that there is a high correlation between them: high values of the α correspond to low values of the Manning's coefficient. Actually the whole parameter space of the prior parameter distribution is covered: the values of the α range from 0.21 to

039 and the values of the Manning's coefficient ranges from 0.31 to 0.39. This means that the effect of the two parameters compensate each other and that, in the proper range of values, any value of the Manning's coefficient or of the α can be chosen, using an appropriate value of the other parameter, to obtain good results (figure 68).

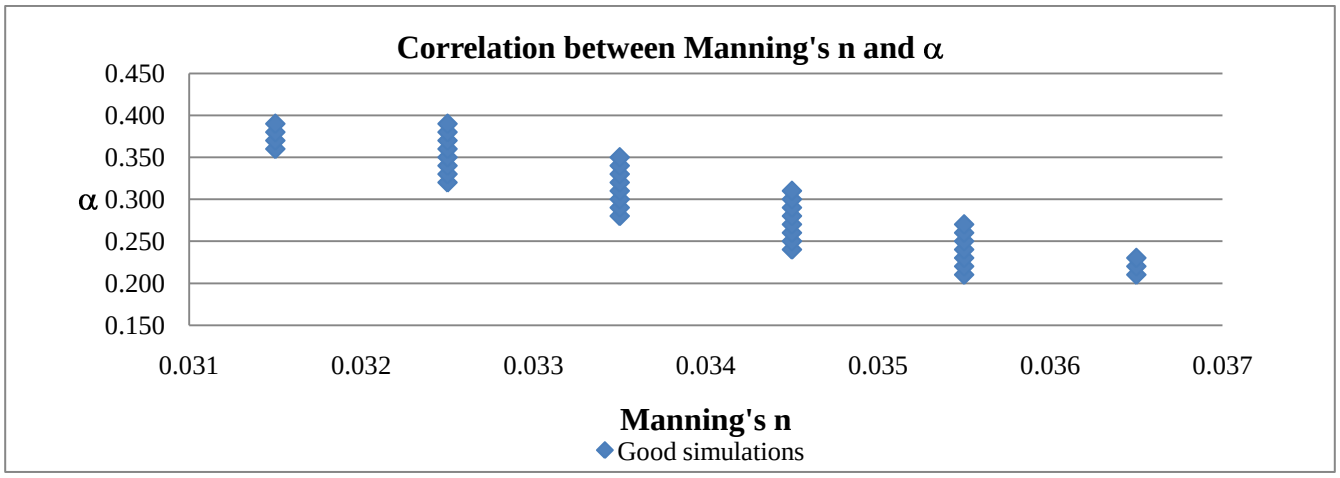

Figure 67 Correlation between the Manning's coefficient and the parameter α

Figure 69 shows the water stage values over time for the best parameter set simulation, the observed water-stage series and the boundaries of the 95% confidence region. Table 46 reports the NS values, the uncertainty boundaries values, the percentage of observations in the uncertainty boundaries and the r-factor for the calibration events and the validation events.

The minimum width of the confidence region is 0.03 m, while the maximum is 0.04 m. The percentage of observed values that is not included in the confidence region is 12.38%. The r-factor is 0.81, which is a rather high value (figure 69, table 46).

The NS value, for the chosen parameter set, in Zemst is 0.9868. Among the good parameter sets, the parameter set that give the best performance in Zemst give a value of NS equal to 0.9885. The values of the two parameters are different from the ones that give the best performance in Eppegem. Anyway the difference in performance is really low among all the parameter sets (the lowest value is 0.985). This can be noticed also from the uncertainty boundaries: the maximum width is equal to 0.21 m and the r-factor is equal to 0.14. However, despite the really high value of the NS, the 55.7% of the observed data is out of the uncertainty boundaries (table 46).

In figure 70 the simulated and the observed water stage series are reported. As it can be seen, they don't differ much. Actually as the tidal effect is dominant in Zemst, the performance of the model in that station is always very good: of all the parameter sets used, the worst performance give a value of the NS equal to 0.9636.

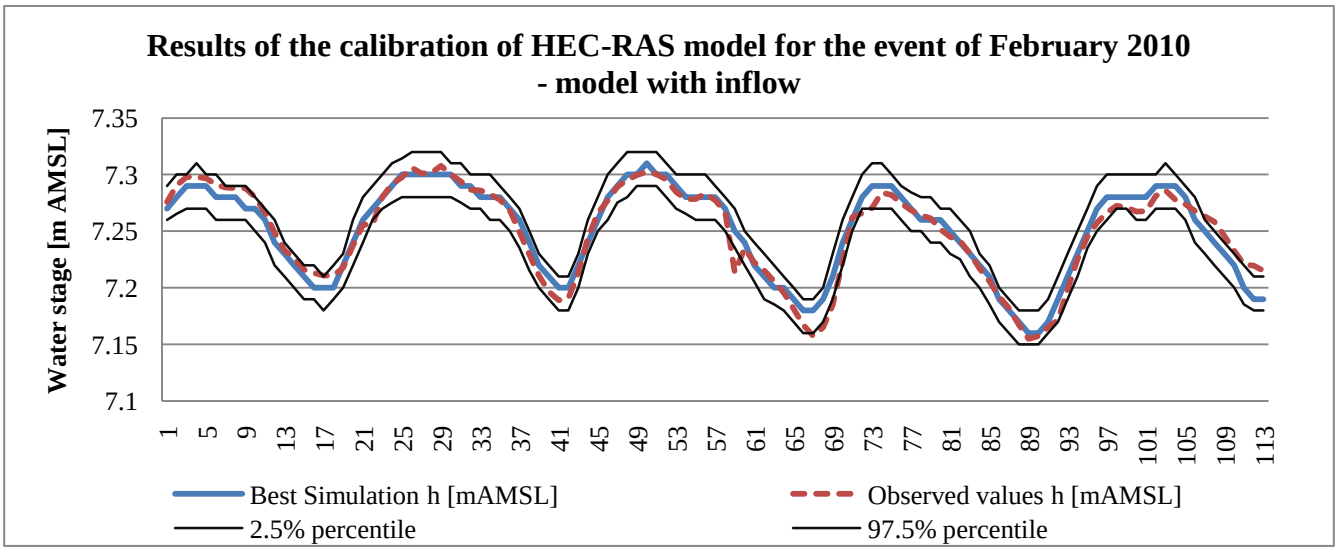

Figure 68 Results of the calibration of HEC-RAS. The blue line is the hydrograph of the best simulation in Eppegem, while the red line is the measured data. In the image the uncertainty boundaries are also reported.

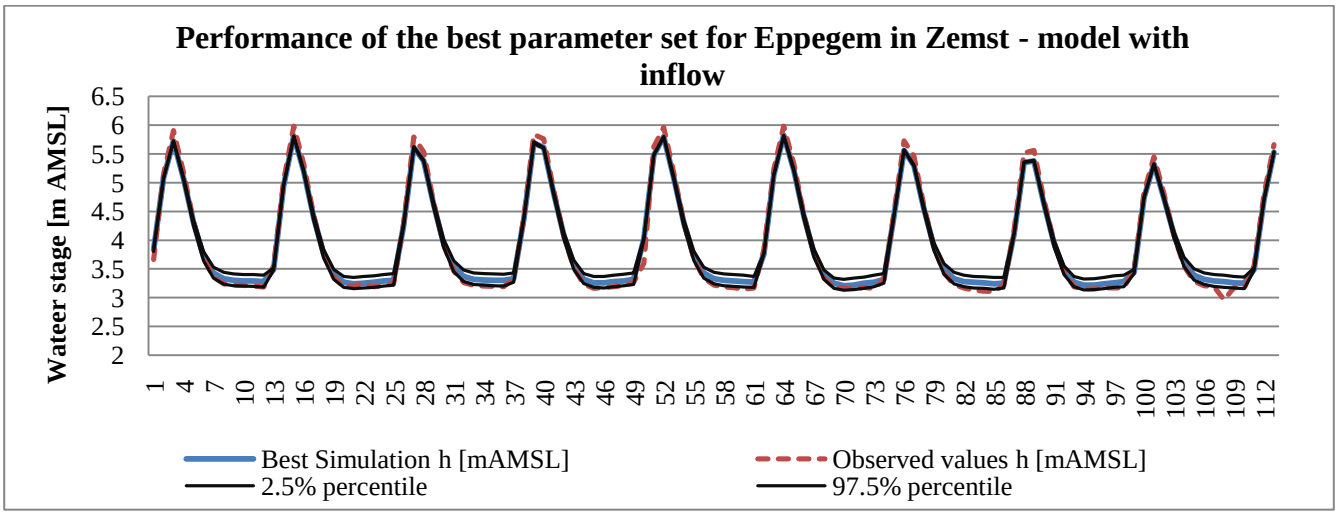

Figure 69 Results of the calibrated model in Zemst

The validation of the model is made running the model for the period of 9-18 March and 3-13 of April separately with all the good parameter sets. The second event is characterized by a maximum value of the flow in Vilvoorde equal to 16.19 [m^3/sec], that is almost the double of the one in the calibration period (8.917 [m^3/sec]). For each event and gauge station, the best parameter set and performance are identified and the 95% prediction boundaries computed. The first event give a relatively low performance, with a maximum value of the NS equal to 0.658, for α equal to 0.23 and n equal to 0.036, and a minimum value of the NS of 0.112. This low performance can be attributed to the effect of the tide in the first hours that dominate the water stage in the station of Eppegem. The second period, instead, give a better performance, as the maximum NS is equal to 0.79, for α equal to 0.35 and n equal to 0.033, and the minimum is 0.656. This good performance is, furthermore, for an event in which the maximum flow value is almost the double the one chosen for the calibration.

The following figures show the results of the simulations in Eppegem and in Zemst for both the periods. As it can be seen, for both the validation periods, in Zemst the results are really good, while the simulated water stage series in Eppegem, for the event of March, does not give good results. The event of April, instead, despite some wave is not perfectly reproduced, the result is good. It can be noticed also, from the graphs and from the simulated series, that the 97.5% boundary and the best simulation for the validation periods are, often, equal. This phenomenon is due to the fact that the good parameter sets tend to underestimate the water stage in Eppegem during both the validation events. Another thing to be noticed is that the r-factor is much smaller during the validation events (tab. 35): only for the event of March, in Eppegem, the value is rather high (0.71), the rest of the events have values lower than 0.2. This, along with the underestimation of the water stage is the cause of low values of the p-factor (percentage of observed values within the uncertainty boundaries).

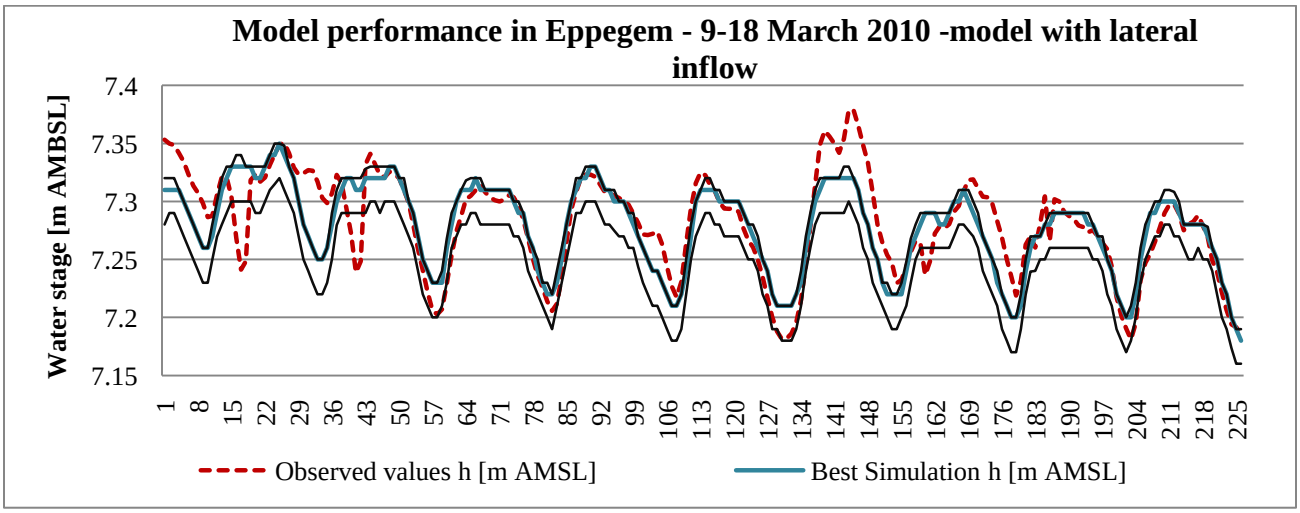

Figure 70 Results of the simulation with the validation data set in Eppegem for the event of 9-18 March 2010

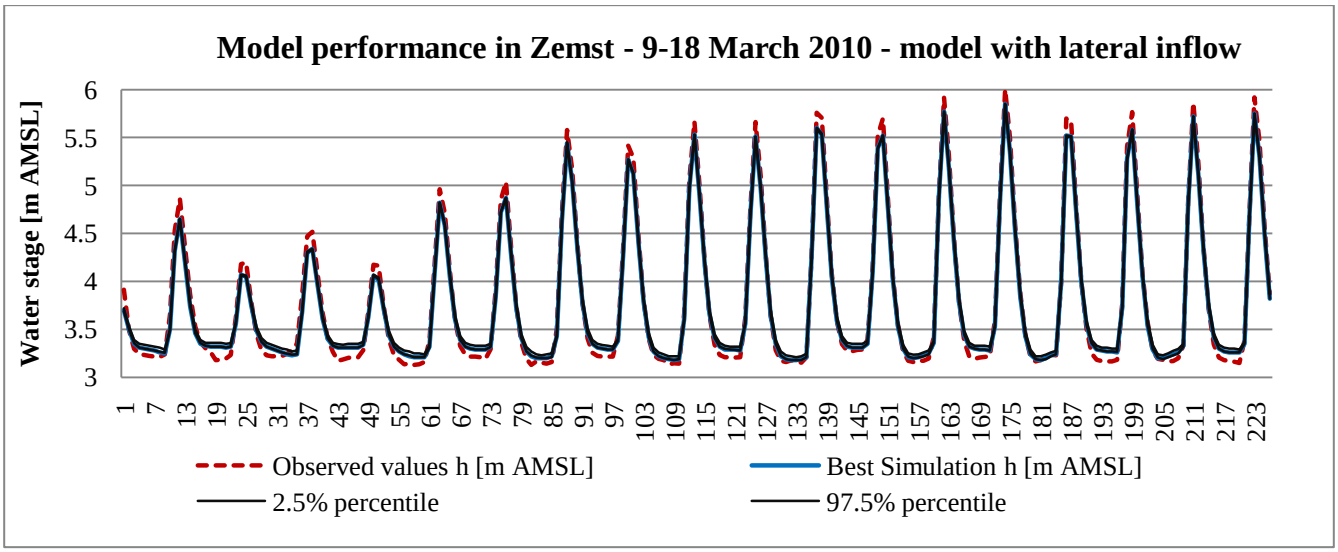

Figure 71 Results of the simulation with the validation data set in Zemst for the event of 9-18 March 2010

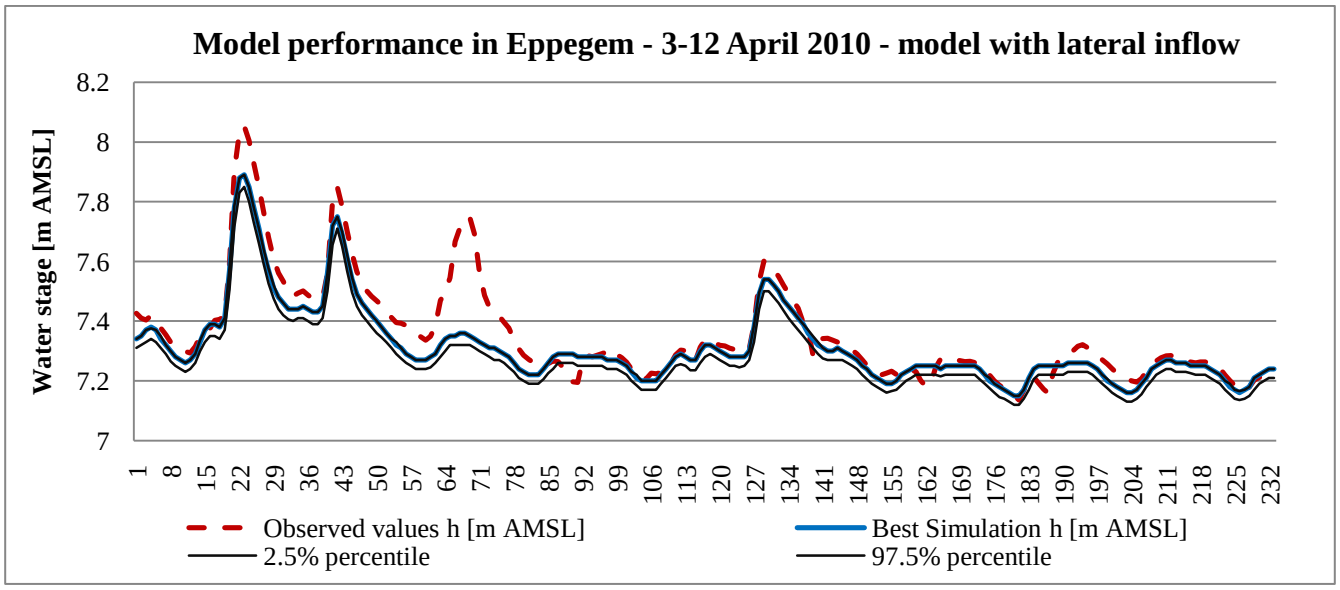

Figure 72 Results of the simulation with the validation data set in Eppegem for the event of 3-12 April 2010

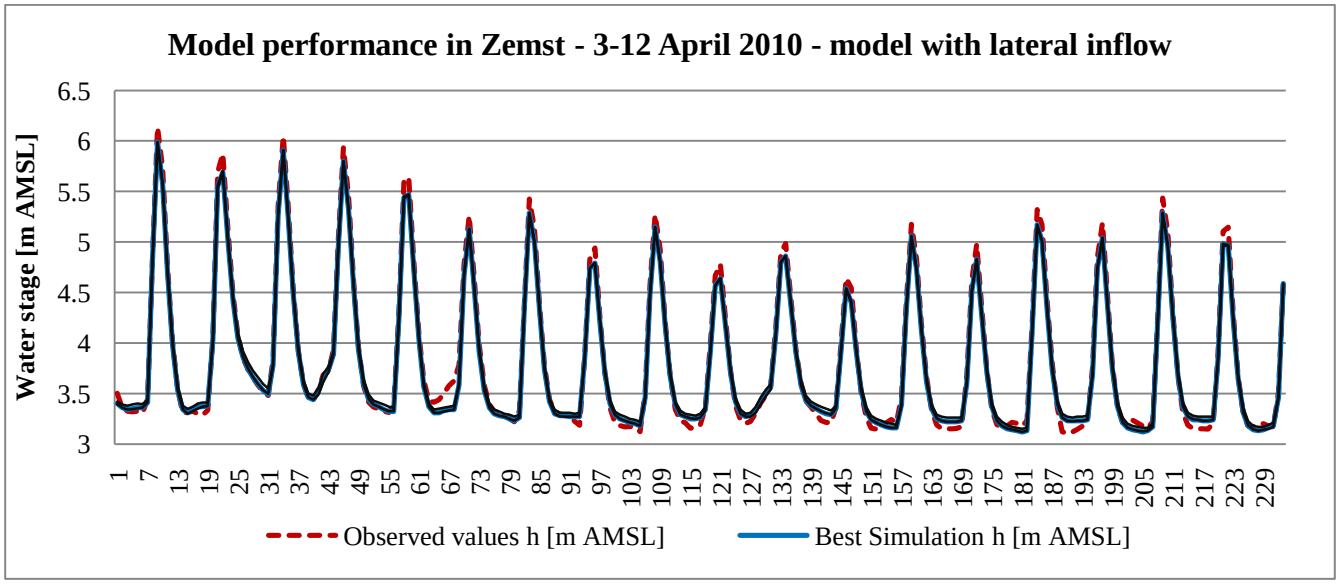

Figure 73 Results of the simulation with the validation data set in Zemst for the event of 3-12 April 2010

Best parameter set	Calibration period		Validation period			
	February-2010		March-2010		April-2010	
	Eppegem	Zemst	Eppegem	Zemst	Eppegem	Zemst
α	0.24	0.32	0.23	0.36	0.35	0.36
n	0.035	0.032	0.036	0.031	0.033	0.031
NS	0.9361	0.9885	0.658	0.987	0.79	0.989
Largest width of uncertainty boundaries [m]	0.0400	0.2100	0.02	0	0.075	0.081
Smallest width of uncertainty boundaries [m]	0.0300	0.0000	0.04	0.051	0.025	0
Percentage of observations in the uncertainty boundaries [p-factor]	87.61	44.25	52.65	8.4	7.5	1.5
r-factor	0.81	0.139	0.701	0.04	0.2	0.04

Table 46 Calibration and validation evaluation indexes for the model with working overflow

The model has then been recalibrated keeping the overflow downstream Vilvoorde equal to 0.

The result is a model with α equal to 0 and the Manning's coefficient equal to 0.43. Five behavioral parameters have been individuated for the station in Eppegem, while all the parameter sets in the prior distribution of the parameter have been found to be behavioral in the station of Zemst. The uncertainty analysis has been performed on the basis of these behavioral parameter sets.

n	NS		n	NS	
	Eppegem	Zemst		Eppegem	Zemst
0.0300	-20.6389	0.981297	0.0390	-1.07806	0.989807
0.0310	-17.1125	0.983875	0.0400	-0.24476	0.988784
0.0320	-14.2046	0.986109	0.0410	0.389642	0.987529
0.0330	-11.4519	0.987678	0.0420	0.766598	0.98603
0.0340	-9.0952	0.989027	0.0425	0.862553	0.984995
0.0350	-6.9000	0.989939	0.0430	0.921175	0.984089
0.0360	-5.1181	0.990413	0.0435	0.920436	0.982951
0.0370	-3.50034	0.990606	0.0440	0.865296	0.98198
0.0380	-2.17735	0.990365	0.0450	0.580785	0.979315

Table 47 Values of the Nash Sutcliff coefficient for the prior parameter distribution used for calibration. The values in green are the ones considered as being behavioral

The figures 75-80 show the simulated water stage series, the observed ones in Eppegem and in Zemst and the 95% uncertainty boundaries, for the calibration event and the two validation events. Table 47 reports the NS values, the uncertainty boundaries values, the percentage of observations in the uncertainty boundaries and the r-factor for the calibration events and the validation events. Similar observations, as for the model with overflow, can be done for this model: the event in April give better performance than the one in March; the good parameter sets tend to underestimate the water stage; the r-factor is really small causing low values of the p-factor (percentage of observed values within the 95% uncertainty boundaries).

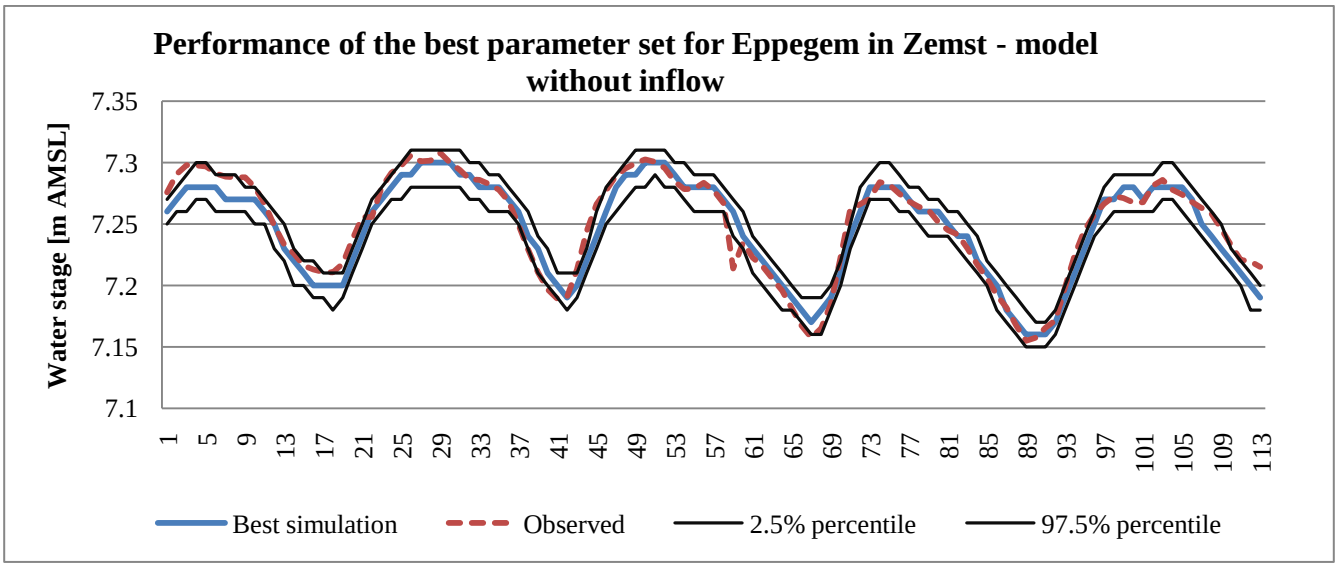

Figure 74 Best parameter set run, uncertainty boundaries and observed water stage in Eppegem for the calibration event.

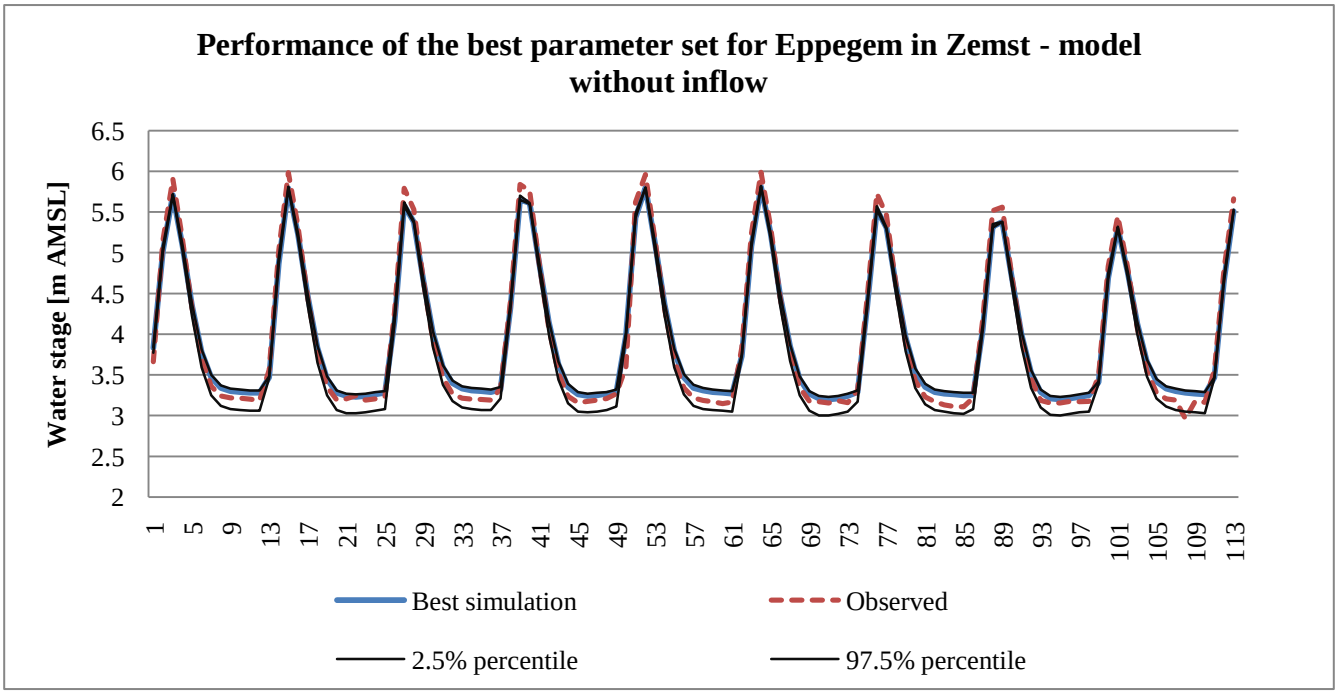

Figure 75 Best parameter set run, uncertainty boundaries and observed water stage in Eppegem for the calibration event.

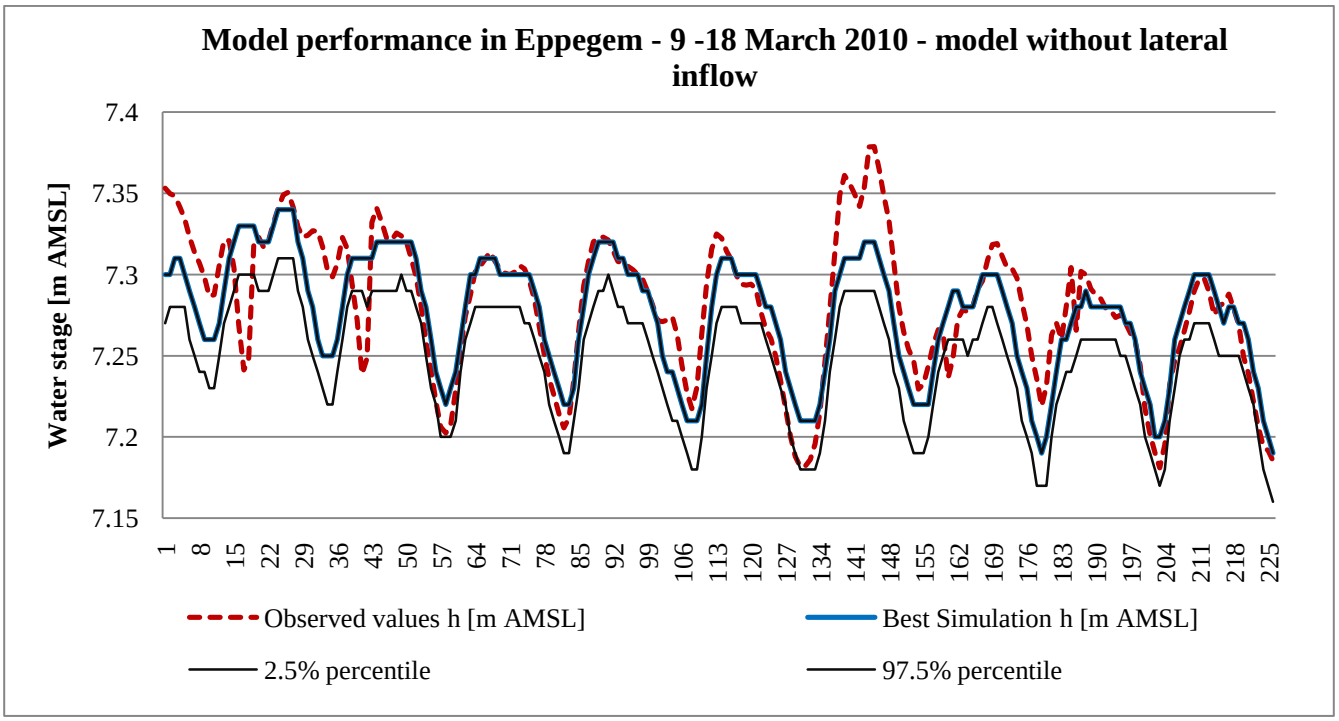

Figure 76 Best parameter set run, uncertainty boundaries and observed water stage in Eppegem for the validation event of March

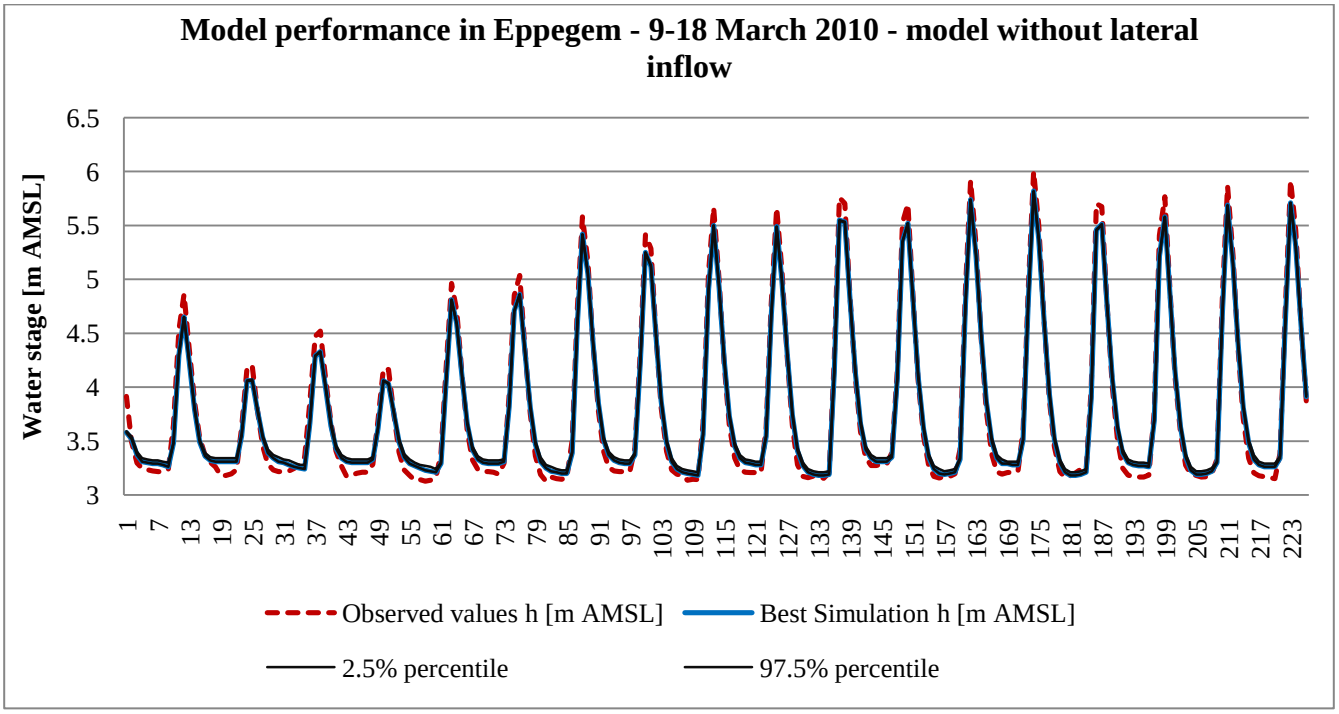

Figure 77 Best parameter set run, uncertainty boundaries and observed water stage in Zemst for the validation event of March

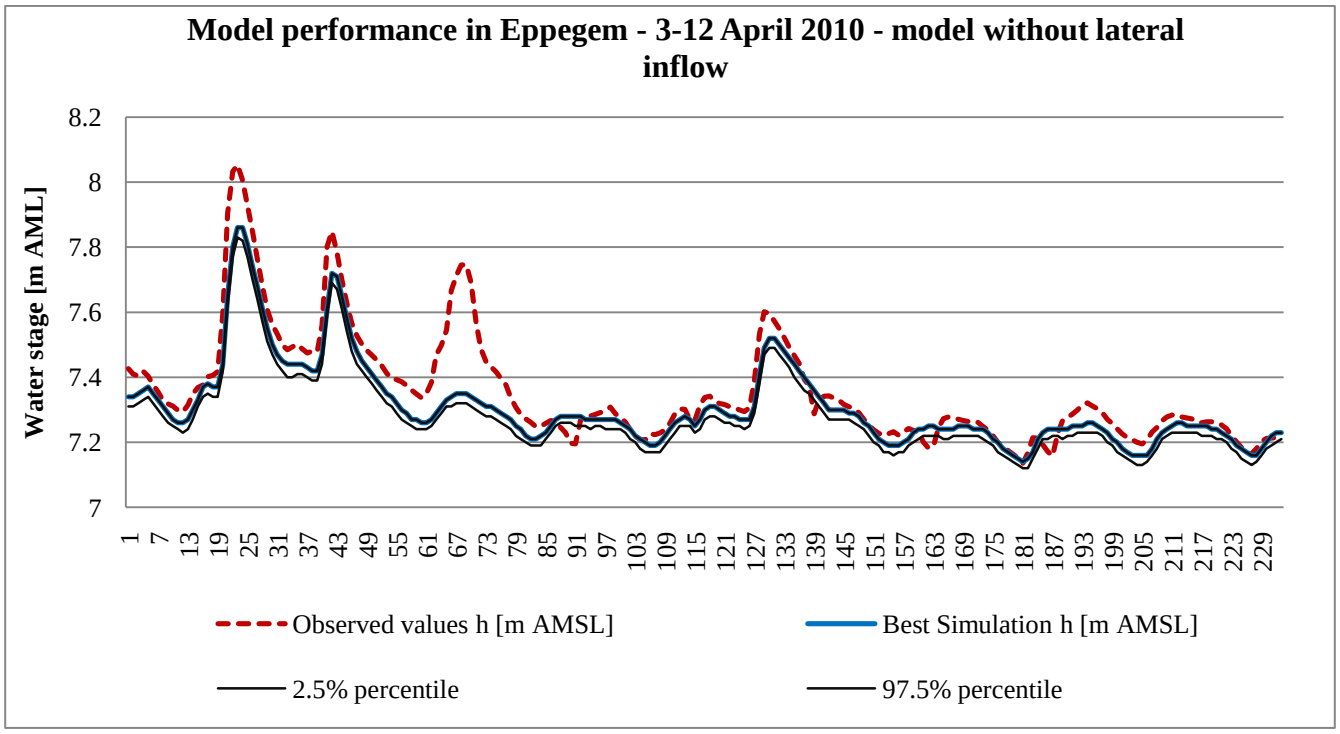

Figure 78 Best parameter set run, uncertainty boundaries and observed water stage in Eppegem for the validation event of April

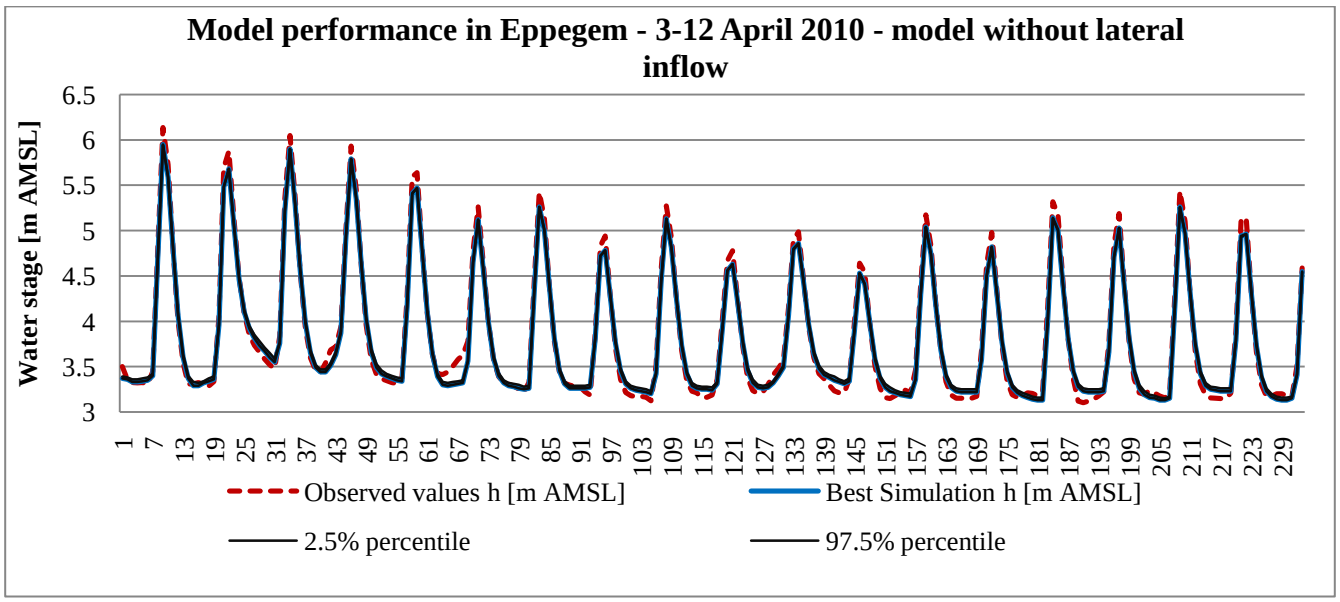

Figure 79 Best parameter set run, uncertainty boundaries and observed water stage in Zemst for the validation event of April

Best parameter set	Calibration period		Validation period			
	February-2010		March-2010		April-2010	
	Eppegem	Zemst	Eppegem	Zemst	Eppegem	Zemst
α	0.00	0.00	0.00	0.00	0.00	0.00
n	0.043	0.042	0.044	0.042	0.044	0.042
NS	0.9212	0.986	0.6417	0.983	0.762	0.985
Largest width of uncertainty boundaries [m]	0.0300	0.2600	0.03	0.04	0.04	0.05
Smallest width of uncertainty boundaries [m]	0.0200	0.0000	0.02	0	0.02	0
Percentage of observations in the uncertainty boundaries	73.45	66.37	38.93	3.98	3.98	3.5
r-factor	0.645	0.178	0.609	0.028	0.159	0.03

Table 48 Calibration and validation evaluation indexes for the model with non-working overflow

It can be noticed that in the validation series the flows are underestimated and that one of the peaks is not computed at all. The reasons can be:

- A different value of the Manning's coefficient characterizes the bed of the river in April, with respect to February.
- Some of the peaks are not well predicted because of the overflow in Vilvoorde, whose functioning is not known.

7.2 Uncertainty analysis and Manning's coefficient sensitivity

As it is done with the SWAT model, also HEC-RAS model behaviour is analyzed after applying an error to the input data. In particular the effect of the error in the rating curve used to generate the upstream boundary condition of the model (flow series in Vilvoorde) is analyzed. It has been already discussed in chapter 5.2 the form of the error affecting the rating curve. It is assumed to have a normal distribution with zero mean and standard deviation proportional to the discharge.

$$\varepsilon = N(0, \beta Q_{obs}) \tag{90}$$

where β is a coefficient of proportionality. Each flood event is affected by this error. For the entire flood event it is assumed that an error with same probability of occurrence affect every element of the input series. To simplify the computation of the uncertainty boundaries, twenty different input series are created, each affected by a different error characterized by a probability of occurrence that is the same for each time steps. The error is computed using the cumulate probability function, starting from a cumulate probability equal to 0.025, with a step of 0.05, until a cumulate probability of 0.975. For each time step of the original series a new value, affected by this error, is calculated. To analyze the influence of this error on the output of the model and the sensitivity of the model itself and of the behaviour of the parameter sets, five different values of the coefficient β are used, from 0.05 to 0.25 (fig. 52). The latter value is chosen accordingly with the results found by Di Baldassarre and Montanari, as the average value of the error affecting the rating curve is 25.6%. Figure 81 shows the cumulate probability of the error versus the value of the average flow value for the event.

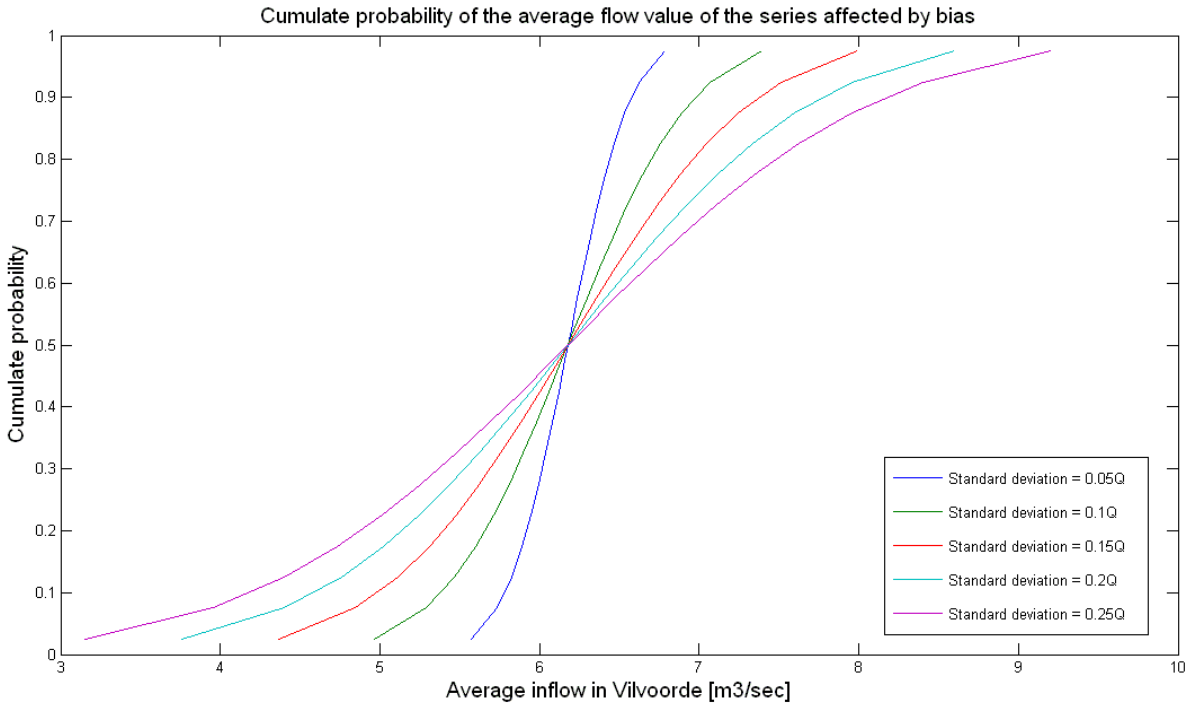

Figure 80 Cumulate probabilities and average flows of the input in Vilvoorde

The effect of this variation on the input results in variations in the output of the model and, thus, in different behavioural parameter sets. The model without overflow has been used to evaluate the sensitivity of the Manning's coefficient due to errors in the input data. The prior distribution of the Manning's coefficient ranges from 0.028 to 0.080. So for each combination of Manning's n and error, the model has been run and the Nash Sutcliff coefficient of Efficiency value has been calculated. The Manning's values have been chosen with a step of 0.001. In total, for each value of the parameter β, 1060 simulations have been performed, for a total of 5300 simulations. The event used for the simulations is the same used for calibration, the flood event from 17/02/2010 to 22/02/2010. The uncertainty boundaries are built basing on the simulations which gave a value of the NSE greater than 0.75.

Roughness coefficient is considered to have, together with the geometry, the most important impact on predicting flow characteristics: whether the model is more sensitive to either or both of the roughness and geometry uncertainty is in part result of the dimensionality of the model structure (Pappenberger et al., 2005). All the model geometry is an approximation of the real geometry, with all its downstream variations, and therefore will have an implicit effect in the values of the effective roughness parameters. This means that it should be possible to compensate to a certain degree for geometrical uncertainty by varying the effective roughness values (Aronica et al., 1998; Marks and Bates, 2000; Pappenberger et al., 2005). Many modellers see the main problem in practical applications as a problem of choosing the correct roughness. Some studies have, instead, demonstrated discrepancies between calibrated effective model values and roughness's which have been estimated based only on the nature of the channel. Effective roughness values include all the effects of variable cross-sections, heterogeneous slopes and vegetation cover, as it is impossible to quantify all the energy losses separately. These parameters also have to compensate for the effects of manmade structure neglected in the specifications of the reach geometry and possibly numerical algorithms (Pappenberger et al., 2005). Pappenberger et al. (2005) reports that many studies have been made to compare different model codes and it was found that all the models performed equally well, although different responses to changes in the friction parameterization.

The objective of this chapter is to discuss how the error in the input of the model influences the output of the model and the value of the behavioural roughness coefficients. It will be shown that roughness coefficient not only can compensate the effect of different energy losses, manmade structures and numerical algorithms, but also eventual errors in the rating curve used to generate the input hydrographs.

At first, an analysis the uncertainty boundaries and their characteristics and a sensitivity of the uncertainty boundaries related to the introduction of the error in the model are done. Then a sensitivity analysis of the Manning's coefficient versus the difference between the original flow value and the flow value affected by the error and a global analysis are reported to analyze the influence of the magnitude of the error in the inflow in the output of the model and the choice of the behavioural parameters.

7.2.1 Uncertainty Boundaries

An analysis similar to the one made in the calibration and uncertainty analysis chapter is now made: the GLUE procedure has been used to compute the uncertainty boundaries basing on the result of the simulations performed. A number of behavioral parameter sets between 41 and 54, for each standard deviation, are found, with values of the NSE ranging from 0.75 to 0.94 (table 49). Figure 82 shows the values of the Manning coefficient for which the model is considered behavioral versus the cumulate probability of the error of the model with standard deviation equal to *0.05Q*. It can be noticed that for negative errors the Manning coefficient grows, while, for positive values of the error, the value of the parameter gets lower: in the first case the value of the inflow get smaller, while, in the second case, the value of the inflow grows. It must be noticed that for values of the cumulate probability of the error equal to 0.5, the flow doesn't change, as the mean and the median of the error are 0. The effect of the roughness of the river bed is, for increasing values, to increase the water stage. As a consequence, in order to have good simulations, when the inflow gets smaller, n gets greater and vice versa.

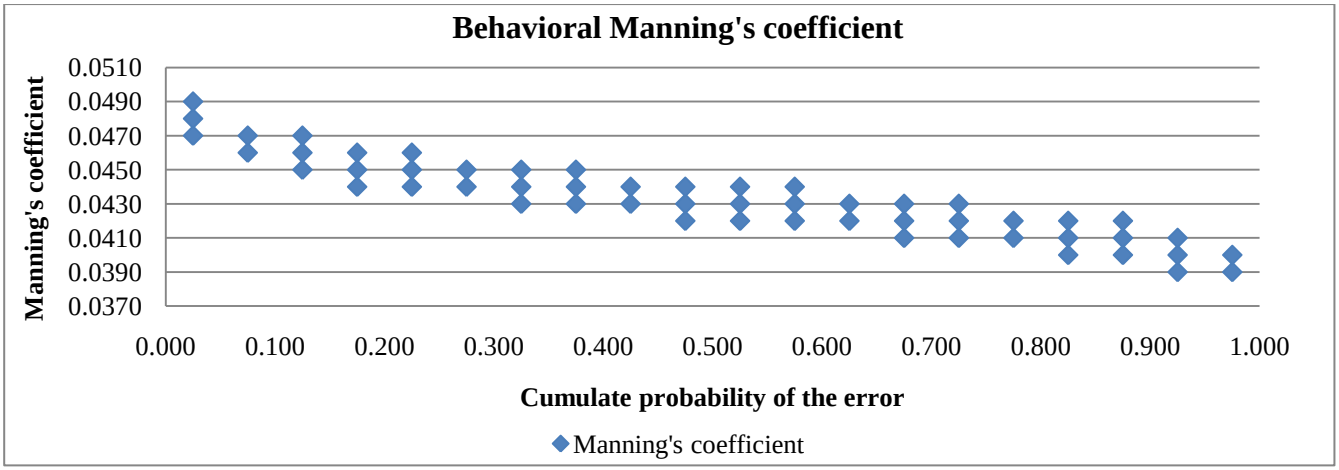

Figure 81 Distribution of the behavioral Manning's coefficient values versus the cumulate probability of the error. Standard deviation equal to 0.05Q

Figure 83 shows the distribution of the behavioral Manning's coefficients versus the cumulate probability of the error for all the standard deviations considered. It can be noticed that the range of the behavioral Manning's coefficients, for bigger values of the standard deviation, and thus of the error, is bigger. It can be also noticed that, for high standard deviations and small cumulate probabilities of the error, no behavioral Manning's coefficient is found: for these values of the error, the upstream inflow is very small and, even for very high values of the roughness; the observed water stage cannot be reached by the model. For very high values of the inflow, so for high values of the standard deviation and high values of the cumulate probability, instead, very small values of the roughness can make the model reach water stage values similar to the observed ones. Later in the chapter this fact will be better discussed.

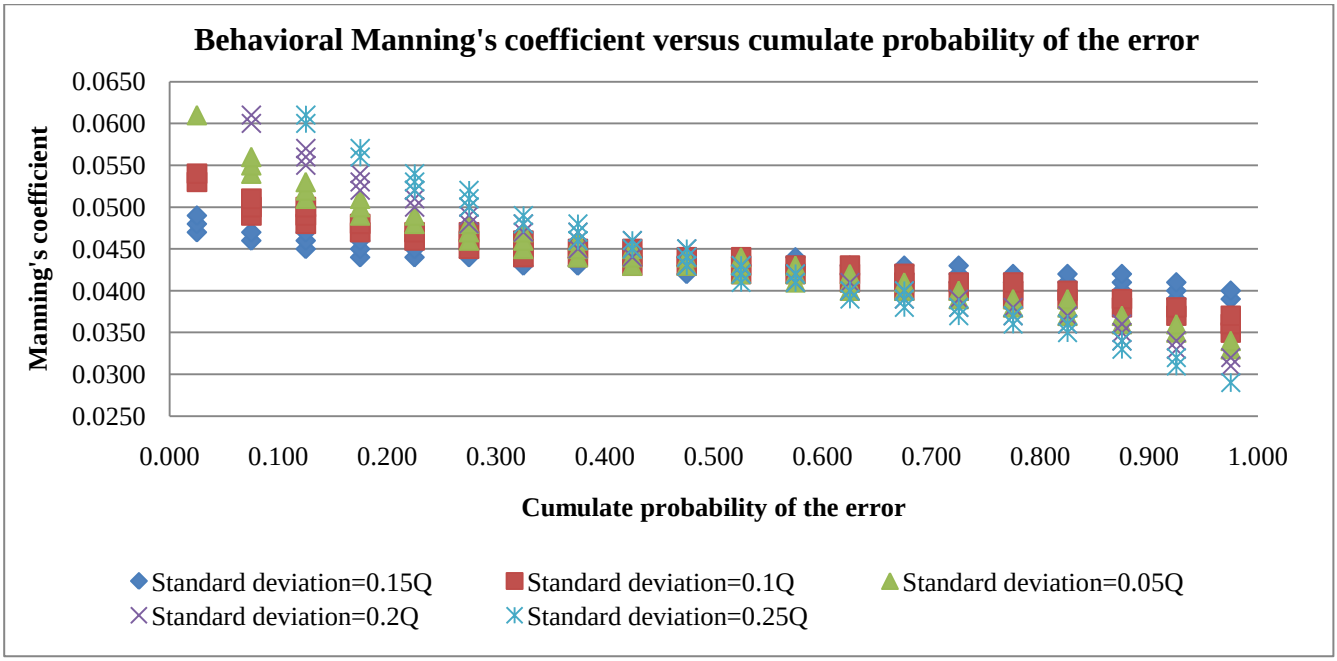

Figure 82 Distribution of the Manning's behavioral coefficient versus the cumulate probability of the error. Overview for all the standard deviations used in the study.

In order to simplify the analysis, only the results in the station of Eppegem are analyzed: it has been already showed that the results in Zemst are, in the most of the cases, very good, as there is no influence by the upstream flows, but mainly by the tide effect. This makes the value of the Manning's coefficient almost ineffective on the results of the model and the analysis less interesting. Figure 84 reports the uncertainty boundaries, the observed stage values and the best simulation of the calibrated model (see chapter 7.1). As the difference among the uncertainty boundaries graphs for the different standard deviation is barely appreciable, only the graph representing the uncertainty boundaries of the model with standard deviation in the error equal to *0.25Q* is reported.

The uncertainty boundaries are built basing on the GLUE approach: for each time step, for the good simulations, a cumulate probability distribution is built weighting the values using the NSE as a measure of the probability of the parameter set of being behavioral. Basing on Bayesian theory, the probability of the error should be multiplied to the value of the probability of the parameter set. The likelihood updating is (Beven and Binley 1992):

$$L_p(\Theta|y) \propto L_y(\Theta|y)L_o(\Theta) \tag{91}$$

Where $L_o(\Theta)$ is the prior likelihood weight of the parameter set; $L_y(\Theta|y)$ is the calculated likelihood of the parameter sets and $L_p(\Theta|y)$ is the posterior likelihood weight. The error applied to the input has been chosen so that it has the same occurrence probability for each cumulate probability, which is 1/20. So no updating of the likelihood weight is necessary.

In table 49 a comparison between the uncertainty boundaries found in calibration and after applying the error to the input data is reported, for each of the standard deviation applied. It can be seen that the main result is that the uncertainty boundaries are wider, as the r-factor from a value of approximately

0.65 grows to a value of 0.8 for σ equal to *0.05Q* and 0.9 for σ equal to *0.25Q*. The consequence is that the percentage of the observed values included in the uncertainty boundaries passes from a value of 73.5% to values among the 89% and the 95%.

It can be argued that, including the error in the input, in the uncertainty analysis, the model increased his capacity of explaining the observations. The cost for this is an increase in the width of the uncertainty boundaries.

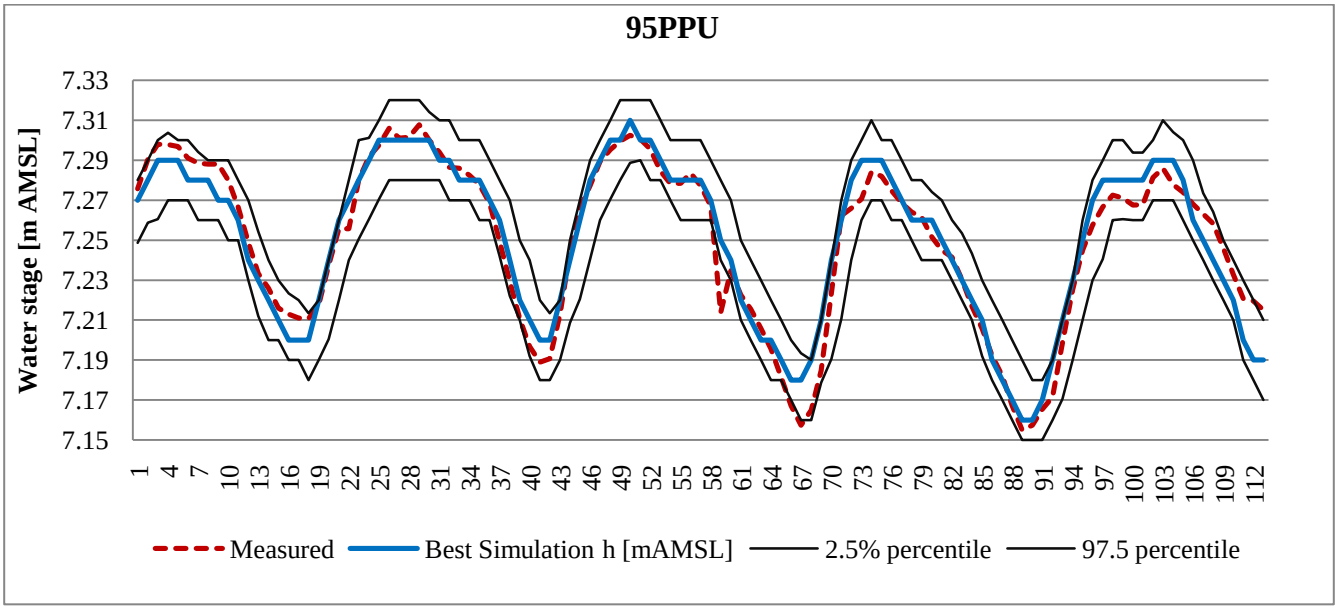

Figure 83 Uncertainty boundaries: standard deviation equal to 0.25Q

	Model not affected by input error	Model affected by error in the input				
		σ=0.05Q	σ=0.1Q	σ=0.15Q	σ=0.2Q	σ=0.25Q
Number of behavioral parameters	3	54	50	50	45	41
Lower NSE	0.77	0.76	0.75	0.76	0.75	0.75
Maximum NSE	0.92	0.93	0.94	0.94	0.94	0.94
Largest width of uncertainty boundaries [m]	0.03	0.04	0.04	0.05	0.05	0.06
Smallest width of uncertainty boundaries [m]	0.02	0.03	0.03	0.03	0.02	0.03
r-factor	0.65	0.80	0.80	0.84	0.80	0.90
p-factor	73.45	90.27	89.38	92.04	90.27	95.58

Table 49 Results of the uncertainty analysis

It can be also observed that the difference in the width of the 95PPU among the models with the different standard deviation of the error is not as high as the difference of them with the model in which no error has been applied to the input. Sensitivity of the p-factor and of the r-factor is reported in table 49.

The sensitivity index is calculated as:

$$I = \frac{\Delta(r-factor)}{r-factor_i} \Big/ \frac{\Delta\sigma}{\sigma_i} \tag{92}$$

$$I = \frac{\Delta(p-factor)}{p-factor_i} \Big/ \frac{\Delta\sigma}{\sigma_i} \quad (93)$$

where $r - factor_i$, $p - factor_i$ and σ_i are the initial values of the r-factor, p-factor and of the standard deviation. In case the sensitivity index is calculated considering the model without the error in the input, that is a model with a standard deviation of the error equal to $0 \cdot Q$, the sensitivity index is $I = \frac{\Delta(x-factor)}{x-factor_i}$, where the x is either r or p, as the standard deviation of the model without error is equal to 0. Table 50 reports the value of the sensitivity analysis of the 95% prediction uncertainty boundaries. The first two rows report the values of the p-factor and r-factor. The third and the fourth rows report the sensitivity with respect to the model without error in the input and the last two rows report the values of the sensitivity index calculated considering as initial condition, the model with an error in the input with standard deviation equal to 0.05Q. It can be noticed that the sensitivity indexes reported in rows 3 and 4 are at least one order of magnitude greater than the others. This means that the introduction of the error in the model input caused a quiet big increase of the average width of the uncertainty boundaries, while the increasing of the error does not affect it as much as not having the error at all.

	Model not affected by input error	Model affected by error in the input				
		σ=0.05Q	σ =0.1Q	σ =0.15Q	σ =0.2Q	σ =0.25Q
r-factor	0.65	0.80	0.80	0.84	0.80	0.90
p-factor	73.45	90.27	89.38	92.04	90.27	95.58
Sensitivity index for r-factor with respect to the model without error		0.24	0.25	0.29	0.24	0.40
Sensitivity index for p-factor with respect to the model without error		0.23	0.22	0.25	0.23	0.30
Sensitivity index for r-factor with respect to the model with standard deviation 0.5Q			0.002649	0.021101	0.00024	0.031125
Sensitivity index for p-factor with respect to the model with standard deviation 0.5Q			-0.0098	0.009804	0	0.014706

Table 50 Sensitivity of the 95 PPU

It can be, thus, argued that neglecting the error in the observations when building a hydraulic model can be the cause of a not satisfying result. On the other hand, the introduction of the error helped the model to include in the uncertainty boundaries a high percentage of observations, compensating also part of the structural uncertainty of the model.

7.2.2 Sensitivity analysis

The first thing that can be noticed, analyzing the sensitivity of the Manning's coefficient with respect to the error introduced in the input series, is how the range of values of behavioral parameters change with the standard deviation of the error. In figure 85 for each value of β, the coefficient multiplied to the flow value to obtain the standard deviation, the behavioral coefficients are showed. It can be noticed that, not only the number of behavioral coefficient increases (as it has already been shown in the previous paragraph), but also the difference between their maximum and minimum value.

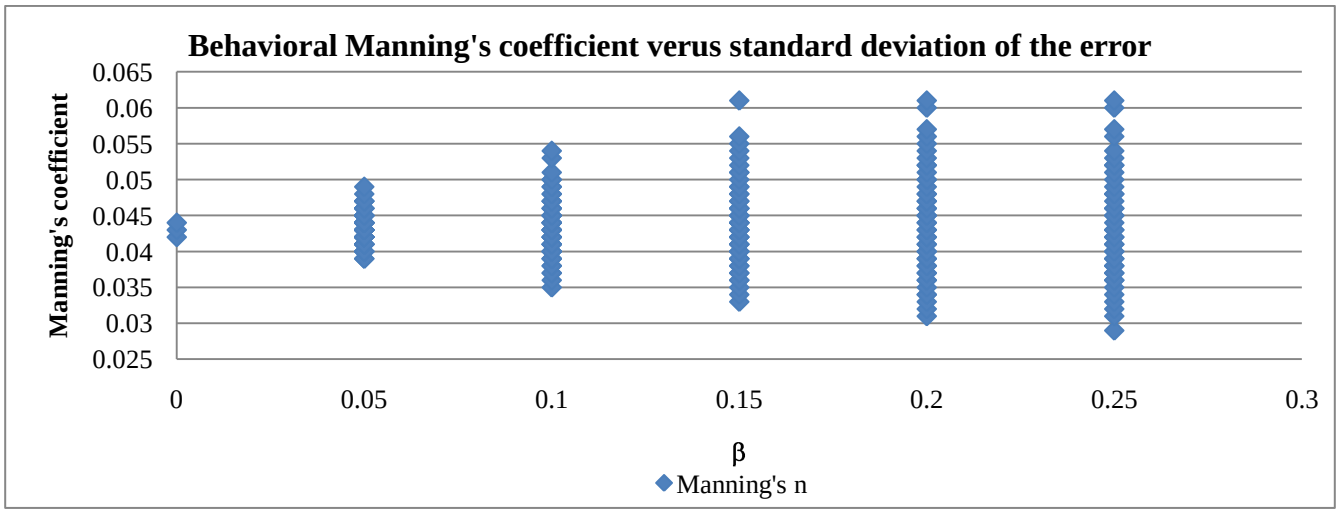

Figure 84 Variation of the range of the behavioral Manning's coefficient versus the standard deviation of the error.

Table 51 shows the sensitivity index of the difference between the highest and the lowest behavioural Manning's coefficient, Δn, with respect to the changing in the standard deviation of the error, computed as:

$$I = \frac{\Delta(\Delta n)}{\Delta n_i} \Big/ \frac{\Delta \sigma}{\sigma_i} \tag{94}$$

Where Δn is the difference between the maximum and the minimum values of the behavioral n and Δn_i is the value of the range of behavioral parameters of the reference model: from the fourth row on, the reference model are: the one with standard deviation equal to 0, the model with the standard deviation equal to 0.05Q, and so on for all the standard deviations used in the analysis. It can be noticed that the index reported in the first row is one order of magnitude higher than the others. As observed in the previous paragraph, the introduction of the error in the input increased visibly the uncertainty of the model. This reflects not only in the width of the uncertainty boundaries, but also in the range of behavioural roughness coefficients. It can be argued, thus, that the presence of an error in the input series can be compensated by the roughness coefficient, when it is a series of discharges values generated by means of a rating curve, as it is already done with other uncertainties in the model, like geometry and presence of manmade structures. It can be also noticed that the index value decreases when referred to the models with standard deviation equal to 0.2Q and 0.25Q. This happens because the range of behavioural roughness's doesn't grow linearly: it has already been said that for very low values of the inflow, even very high values of the roughness cannot compensate the error, as the water stage in the station where the observations are registered cannot be reproduced: the maximum value of behavioural Manning's coefficient is 0.61 and is never over passed. In figure 86 the maximum values of the NSE versus the average inflow are reported. It can be noticed that for very high negative errors, that is very low inflows, the maximum NSE cannot reach satisfactory values.

	Model without error	Standard deviation = 0.05Q	Standard deviation = 0.1Q	Standard deviation = 0.015Q	Standard deviation = 0.2Q	Standard deviation = 0.25Q
Lowest Behavioral n	0.042	0.039	0.035	0.033	0.031	0.029
Greatest Behavioral n	0.044	0.049	0.054	0.061	0.061	0.061
Difference between highest and lowest n	0.002	0.01	0.019	0.028	0.030	0.032
Sensitivity indexes	Model without error	4	8.5	13	14	15
	Standard deviation = 0.05Q		0.9	0.9	0.667	0.55
	Standard deviation = 0.1Q			0.947	0.579	0.4569
	Standard deviation = 0.015Q				0.2149	0.044
	Standard deviation = 0.2Q					0.095

Table 51 Sensitivity of the range of behavioral Manning's values with respect to the standard deviation of the error

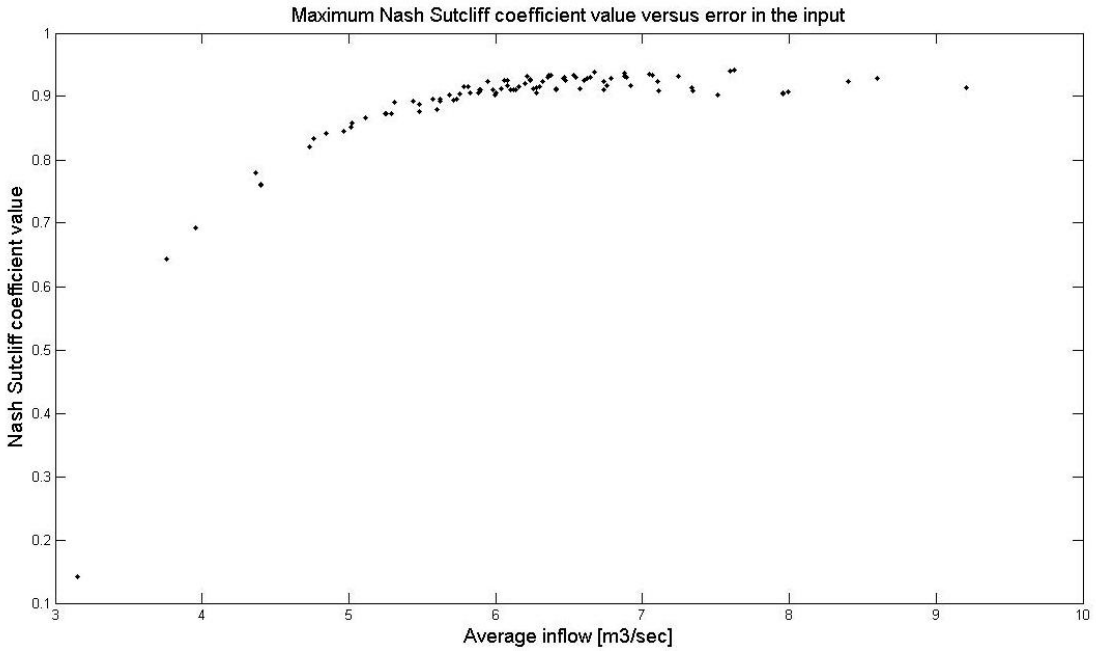

Figure 85 Maximum values of the Nash Sutcliff coefficient of efficiency obtained with the calibration, versus average inflow.

Figure 87 shows the surface obtained from the relation between the values of the average inflow in the model, the roughness parameter and the coefficient of Nash Sutcliff. On the XY plane contour lines are drawn: these iso-lines project on the XY plane the limits of regions of the surface delimited by constant values of the NSE. Figure 88 show the behavior of the good roughness coefficients versus the average inflow. The curve is obtained by plotting the Manning's coefficient that give the maximum NSE for each of the considered average inflow of the model, obtained applying the error to the original series. From both the graphs it can be noticed that the curves (the contours and the curve in figure 87) have a hyperbolic behavior: for very high values of the average inflow, the roughness asymptotically goes to

0, while for very small values of the average inflow the curve tends to grow asymptotically towards infinite. This fact raise directly from the Manning's formula:

$$V = \frac{1}{n} A R^{2/3} {S_f}^{1/2} \tag{95}$$

Where Q is the cross-sectional average flow [m^3/sec], A is the flow area for the subdivision, R is the hydraulic radius for the subdivision (area / wetted perimeter [m]) and S_f is the hydraulic head loss [m/m]. If we consider a rectangular cross section in which the width is much greater than the height, so the perimeter can be approximated to the width, the hydraulic radius can be approximated to the water stage:

$$\frac{w \cdot h}{w+2h} \approx \frac{w \cdot h}{w} = h \tag{96}$$

Where w is the width and the h is the water stage. It can be noticed that, if we consider the water stage as a constant, n is inversely proportional to the flow and directly proportional to the head loss. The head loss between two cross sections can be, also, considered approximately not varying between two behavioral models with different inflows, as it is determined by the water stage in the two cross sections.

$$n = \frac{h^{5/3} w {S_f}^{1/2}}{Q} \tag{97}$$

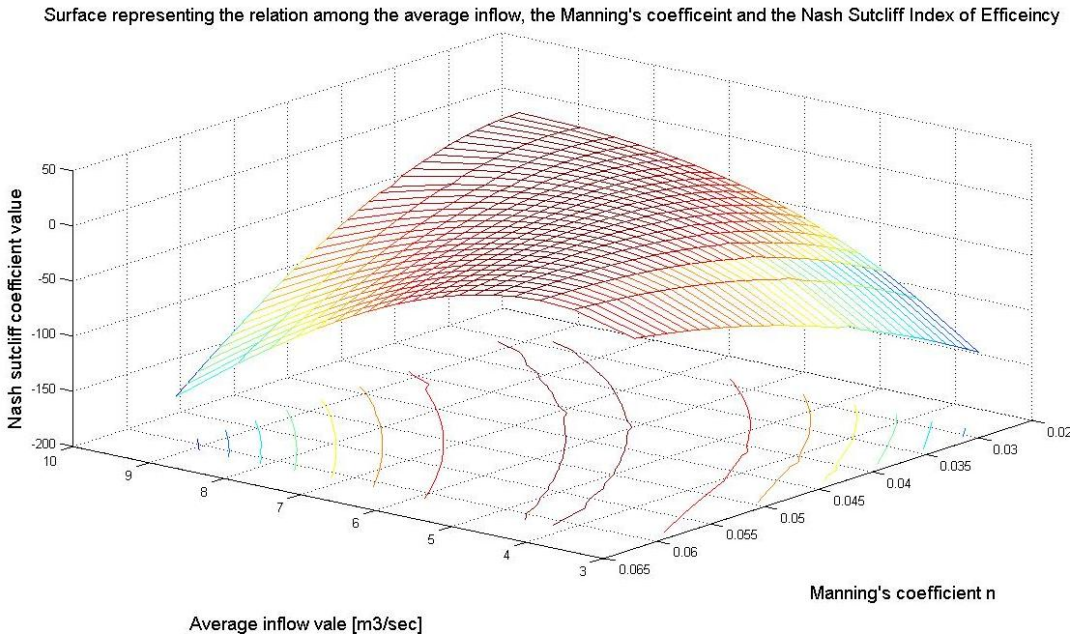

Figure 86 Surface representing the relation between the roughness, the average inflow and the NSE

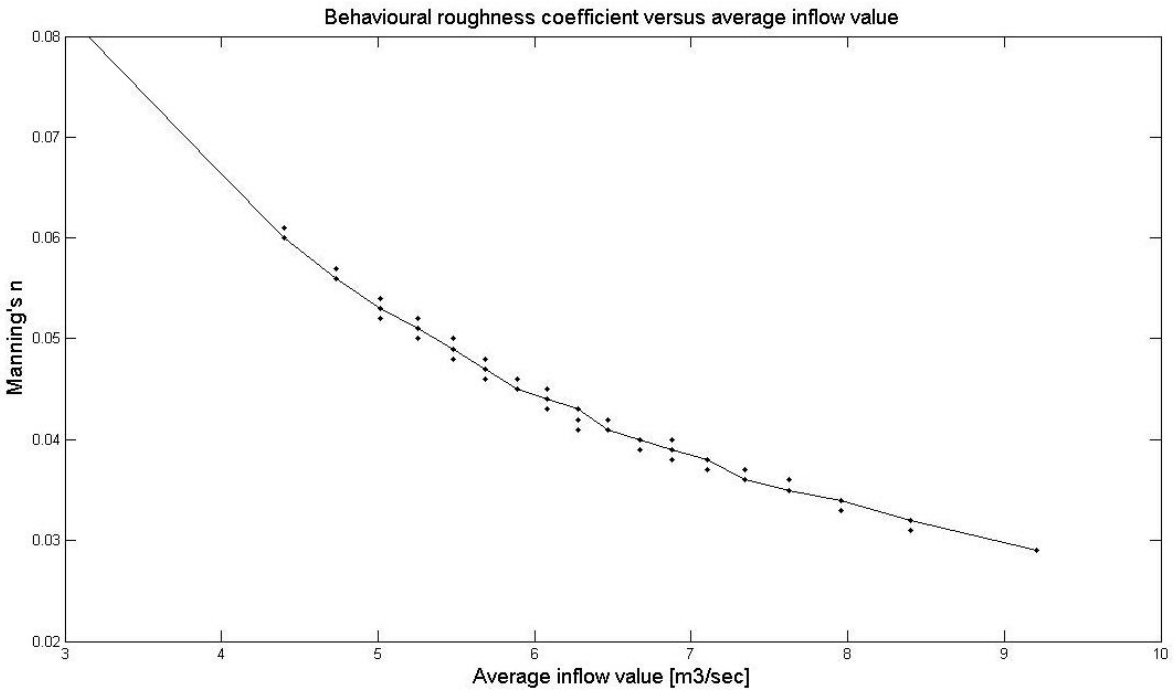

Figure 87 Behavioral Manning's coefficient versus average inflow.

Despite the fact that for very high negative errors the compensating capacity of the Manning's coefficient loses effectiveness, in this case it must be noticed that if the error in the rating curve has a standard deviation of 0.25Q and a cumulate probability of 0.125, that is in percentage an error equal to the 28.76% of the original inflow, a value of the *n* equal to 0.61 make the model simulation give a good performance, that is a value of NSE greater than 0.75. So the compensation capacity of the Manning's coefficient is able to compensate the average error magnitude found by Montanari and Di Baldassarre method (see chapter5.2).

A sensitivity index can be also computed to analyze the relative difference of the Manning's behavioral coefficient with respect to the relative error introduced in the inflow:

$$I = \left| \frac{\Delta n}{n_i} \Big/ \frac{\Delta \bar{q}}{\bar{q}_i} \right| \tag{98}$$

Where n_i is the roughness coefficient of the behavioral models found in calibration, $\bar{q}$ is the average inflow and $\bar{q}_i$ is the average inflow of the original series. The index has been computed for all the combination of behavioral models with error in the input and all the behavioral models without error in the input. The average value of the index is: 1.1075. That is, according with Lenhart et al. (2002) a very high value. One can notice that when the behavioral model does not change the Manning's coefficient, the index is equal to 0. Figure 89 shows the sensitivity index for all the behavioral roughness coefficients. The vertical line in the figure represents the average flow value of the input series not affected by the error. It can be noticed that for relatively small error, the sensitivity index is equal to zero, so the initial values of *n* are still behavioral. It must also be noticed that for each value of the error, the maximum value of the sensitivity index decreases, apparently, hyperbolically: for very small errors a small changing in the Manning's coefficient generate a high value of the sensitivity index,

while for higher error, the relative changing in the Manning's coefficient is, in comparison with the relative change in the inflow value, much smaller.

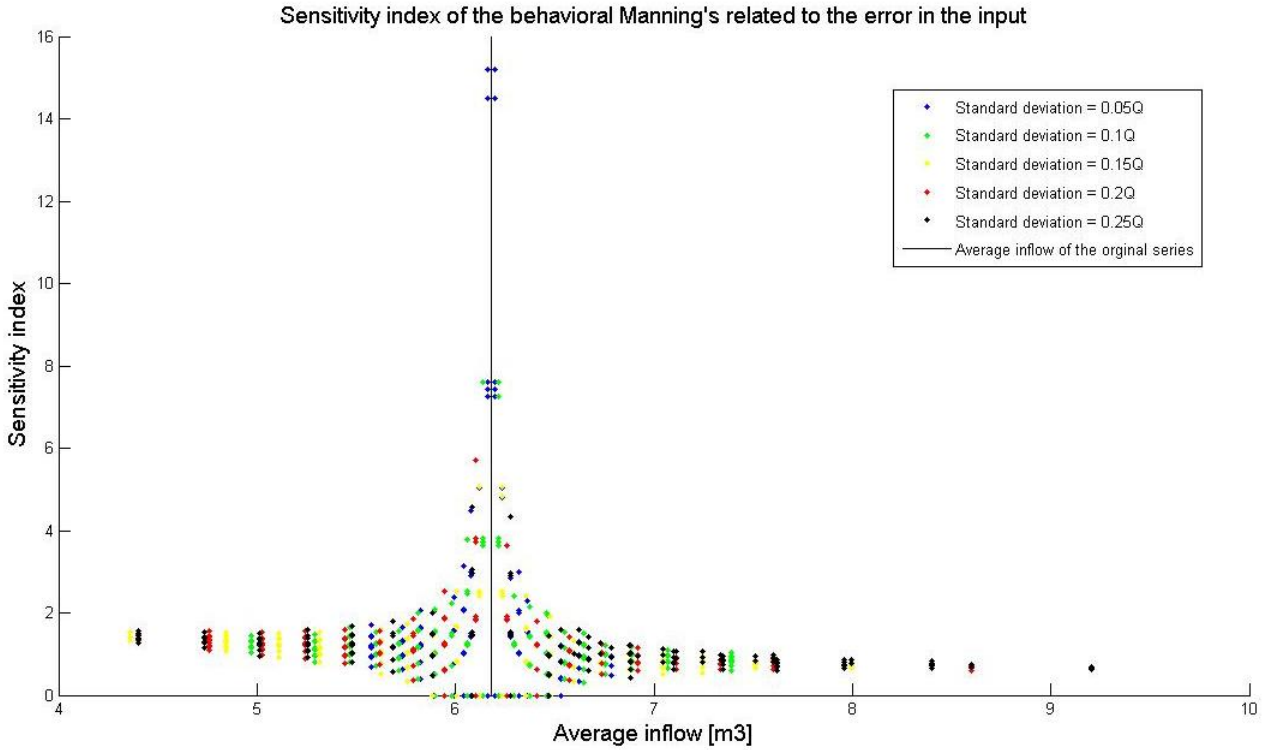

Figure 88 Sensitivity index of the behavioral Manning's coefficient

Analyzing the data one can find that for error ranging between -4.78% and +5.75% the behavioral Manning's coefficients are the same of the model in which the error has not been introduced. This means that for this value of the error the model performance is not affected (table 52).

Error for which the behavioral Manning's does not change		
	Average inflow [m3/sec]	% error
Original value	6.18	
Minimum	5.88	-4.78
Maximum	6.53	+5.75

Table 52 Error in terms of percentage of the original inflow series, for which the behavioral Manning's does not change

Model of the uncertainty boundaries

Finally, basing on all the simulations performed a model of the uncertainty boundaries can be built. At first, basing on all the 5300 simulations made, new uncertainty boundaries are built. Then a relation between the water stage and the difference between the best simulation and the lower and upper boundaries is found. In the end a validation of the uncertainty boundaries using the validation event of 3-12 April 2010 is used. This event is the one that present the highest peaks of all the events used in calibration and validation.

Once the uncertainty boundaries are built using the GLUE methodology, three different methodologies have been used to build the model of the uncertainty:

- A function of the water stage built using a regression curve to fit all the values of the upper and lower boundaries computed;
- A function of the water stage built using a regression curve to fit the maximum and the minimum upper and lower value of the boundaries found in simulation;
- The absolute maximum difference between the best simulation and the boundaries.

In the first and the second case two linear functions have been found. In figures 90 and 91 the regression curves and the equations are shown. In validation it has been found that for high values of the water stage the best simulation does not lay in between the boundaries. In figures 92 and 93 the validation series and the model of the boundaries applied are shown.

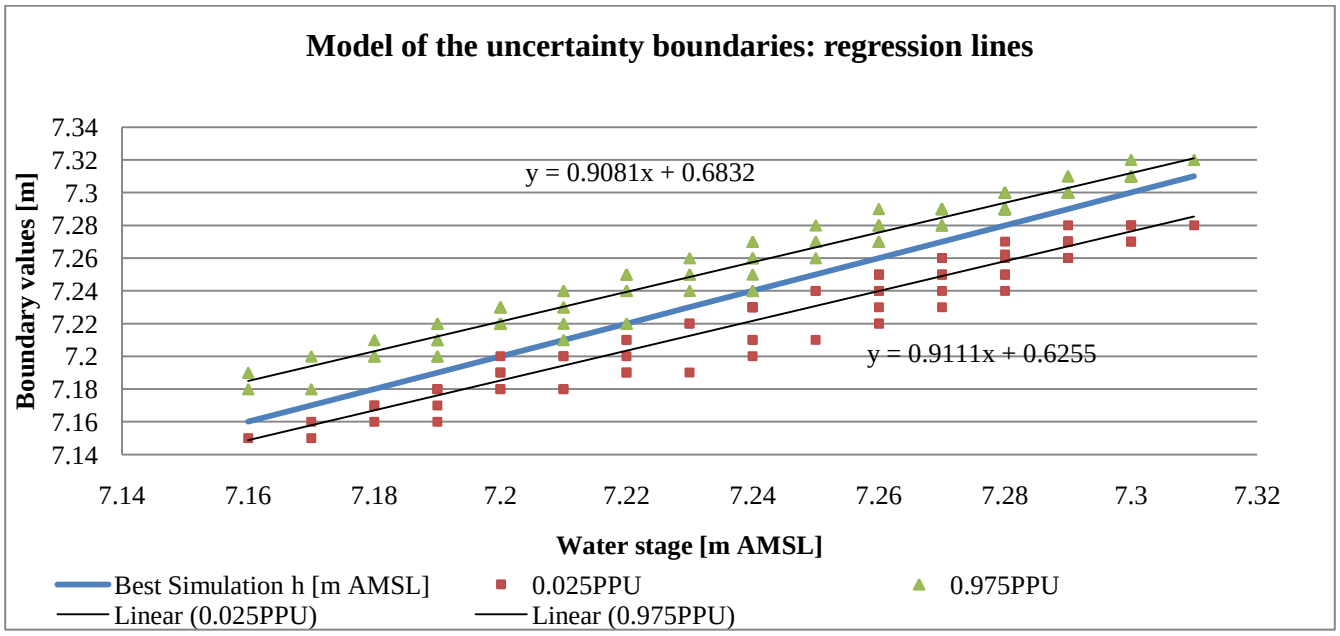

Figure 89 Uncertainty boundaries model: regression line of the boundary values in function of the water stage. The equations of the regression lines are reported on chart.

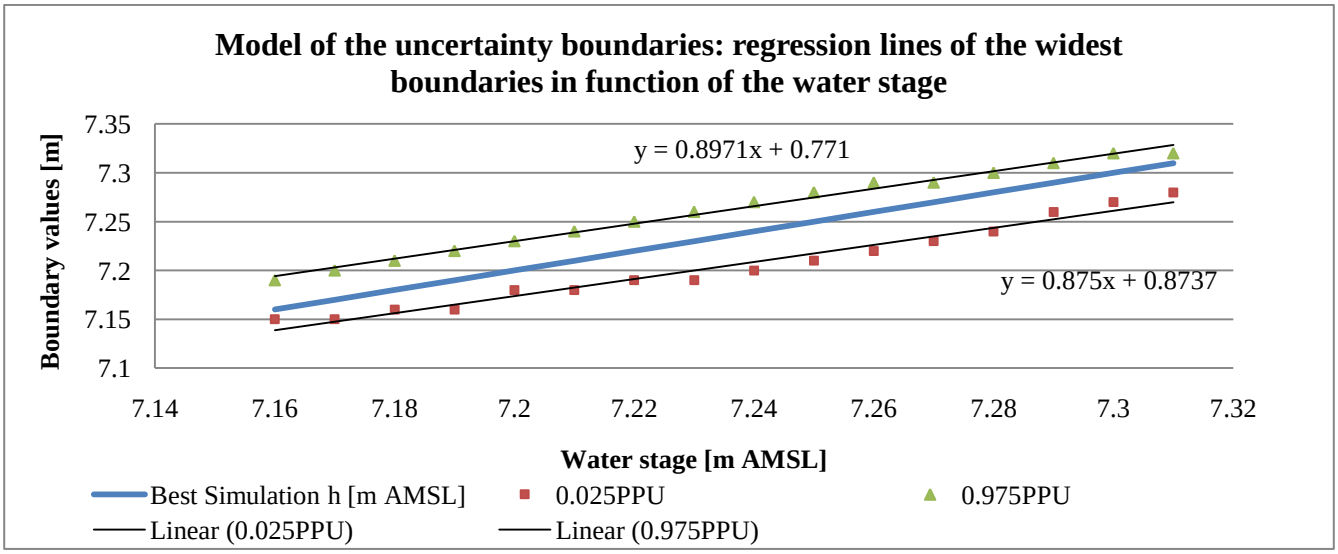

Figure 90 Uncertainty boundaries model: regression line of the widest boundary values in function of the water stage. The equations of the regression lines are reported on chart.

The last solution, the simplest and the most robust, as it takes the worst case and use it for the whole output series is finally chosen. It has been found that the difference between the best simulation and the lower boundary is 0.04 m, while the difference between the upper boundary and the best simulation is 0.03 m. Figures 92 and 93 show the best simulation in the validation period, the boundaries and the observations. The 54% of the observations is included in the boundaries and the r-factor is 0.41. In validation the p-factor and the r-factor were 4% and 0.16. The uncertainty boundary model built can explain much better the uncertainty of the model and include a much higher percentage of observations if applied to the validation series then the uncertainty boundaries found in validation without including the uncertainty of the input.

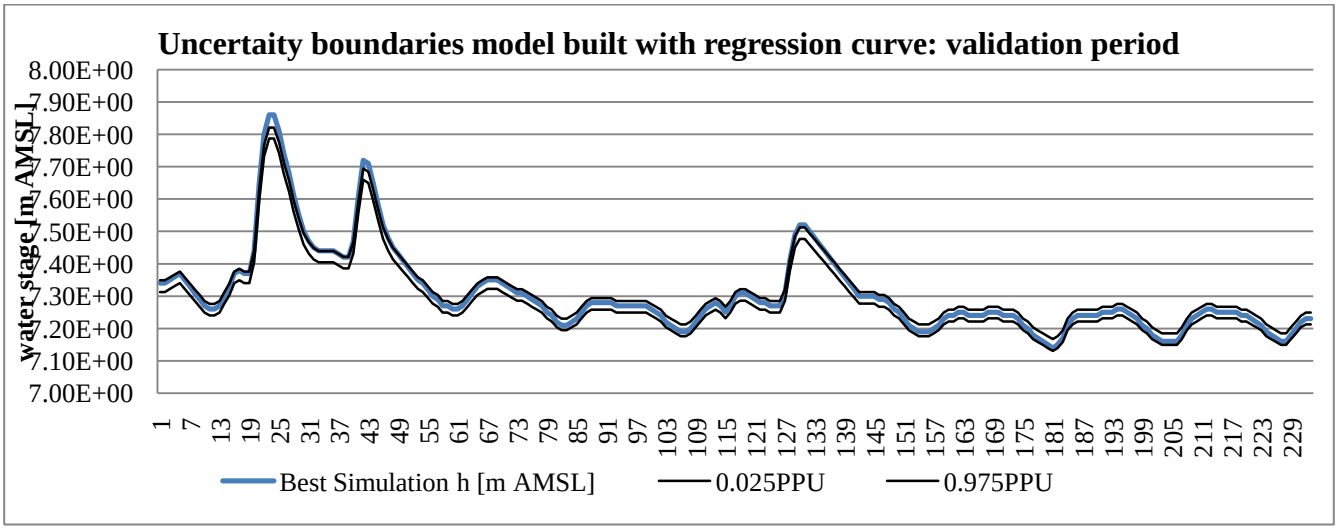

Figure 91 Graph of the uncertainty boundary model built using the regression lines applied to the validation series. When peaks occur the uncertainty boundaries don't include the simulation.

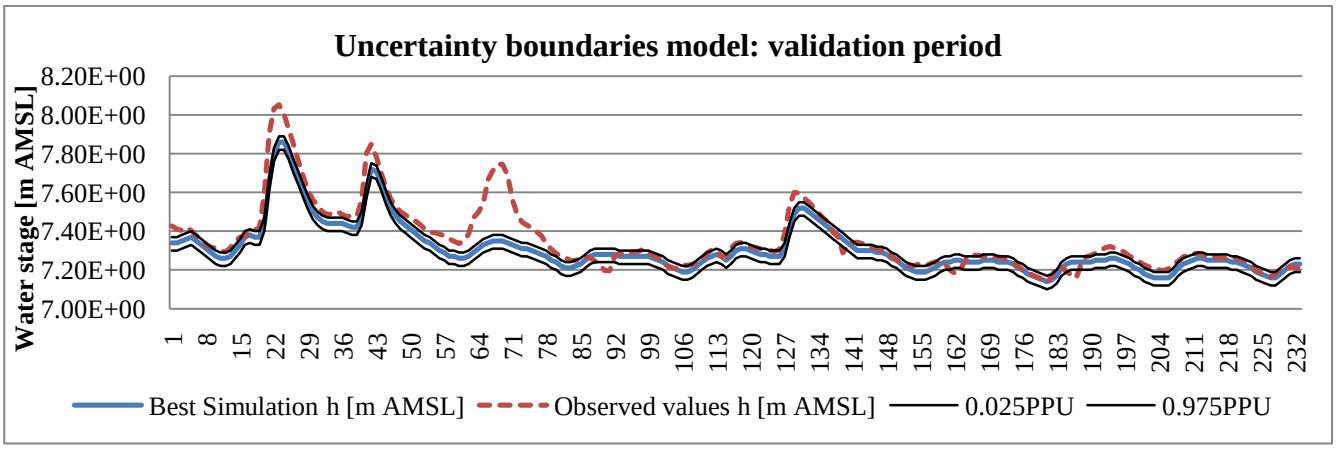

Figure 92 Uncertainty boundaries model built using the widest difference between the best simulation and the 95PPU. On chart also the observation are reported.

7.2.3 Discussion

In this chapter, the influence of the error in the input data of the HEC-RAS model and the sensitivity of the Manning's coefficient have been analyzed.

The Manning roughness coefficient, *n*, is the parameter governing the Manning equation that is an empirical formula to determine the velocity and the flow in a stream used in many models and codes, like HEC-RAS. This coefficient is used, often, to compensate geometrical uncertainty in the models. The result of this is that calibrated roughness values do not correspond to the values found by basing on the nature of the channel.

It has been shown that not only geometrical uncertainty influence the choice of the value of the roughness parameter, but also the error affecting the input data. In case the input data are discharges calculated by means of a rating curve, the introduced error affecting the rating curve equation has the same probability of occurrence for each element of the inflow series of the flood event. It has been shown that for errors greater than the 5% of the discharge, the roughness coefficient is not affected, but for higher errors, the roughness coefficient can range between 0.029 and 0.061, in this case, while in case no error affects the input, the calibrated roughness values range between 0.042 and 0.044.

This result indicates that when simulating different flood episodes, the effective value of the Manning's coefficient can assume very different values, depending on the error present in the rating curve for that episode. Being conscious of the order of magnitude of the error and of the range of values that the rating curve can assume is very important to make the results of a model reliable.

It has been shown, also, that including the uncertainty in the input has the effect of enlarging the uncertainty boundaries, so that the model can explain better the observations: a greater percentage of observations, the 95%, versus the 73%, are included in the new uncertainty boundaries. Basing on all the simulations performed, a model of the uncertainty boundaries has been built and has been validated. The result is that also in the validation period the percentage of observations that lay within the uncertainty boundaries raise from 4% to 54%.

8 Cascading uncertainty

The first step for the evaluation of the cascading uncertainty consist in the calibration of the HEC-RAS model using, as input, the output of the SWAT model. Then the method used in the previous chapter to evaluate the uncertainty in HEC-RAS due to the input is used to evaluate the uncertainty due to the cascade of models.

The output series of the whole 1995 has been used to simulate the model. For this period (1995) no data for the stations of Hombeek and Zemst are available. As it has been demonstrated widely that there is no influence of the downstream boundary in Hombeek on the behavior of the flow in Eppegem, a value representing the water stage daily average in Hombeek is used as boundary condition. This value is kept equal to 3.5 meters above mean sea level.

The output of SWAT is a series of daily average flows. The computation is made, so, with a time step of 1hour for a period of 365 days. The input data and output of the simulations have both daily time step. The evaluation of the model performance is then made using daily average water stage values in Eppegem.

The fact that the computation time step is hourly and that the input series has daily time step make difficult to really assess the goodness of the HEC-RAS model and the influence of the input uncertainty when they are affected by the uncertainty in the upstream model. Despite that, a SWAT version that provides hourly output is being built, so this analysis can be extended in the future by using the new SWAT codes.

8.1 Calibration and validation of the model

The results of the calibration of the model are summarized in table 53. Four behavioral parameter sets have been found. The selection of the behavioral parameter sets has been done using the χ^2 method. The maximum value of the NSE is 0.75.

The values of the behavioral Manning's roughness are 0.044, 0.045, 0.046 and 0.047. They are different from those found in previous calibration because of the influence of the error in the upstream model. Despite the calibrated SWAT model performs well, it does not represent perfectly the observations in Vilvoorde. This reflects even more when using the model to simulate one single event: the SWAT model has been calibrated for long term simulations. The error in one single event can be compensated by good performance in other events of the simulated period. Anyway a long term simulation for HEC-RAS demonstrates that good performances can be achieved even for this cascade of models.

This fact can be noticed looking at the water stage hydrograph in figure 91: the first part of the graph is not well represented by the model, and the water stage is always underestimated. The uncertainty boundaries are really narrow and can be hardly distinguished from the simulation.

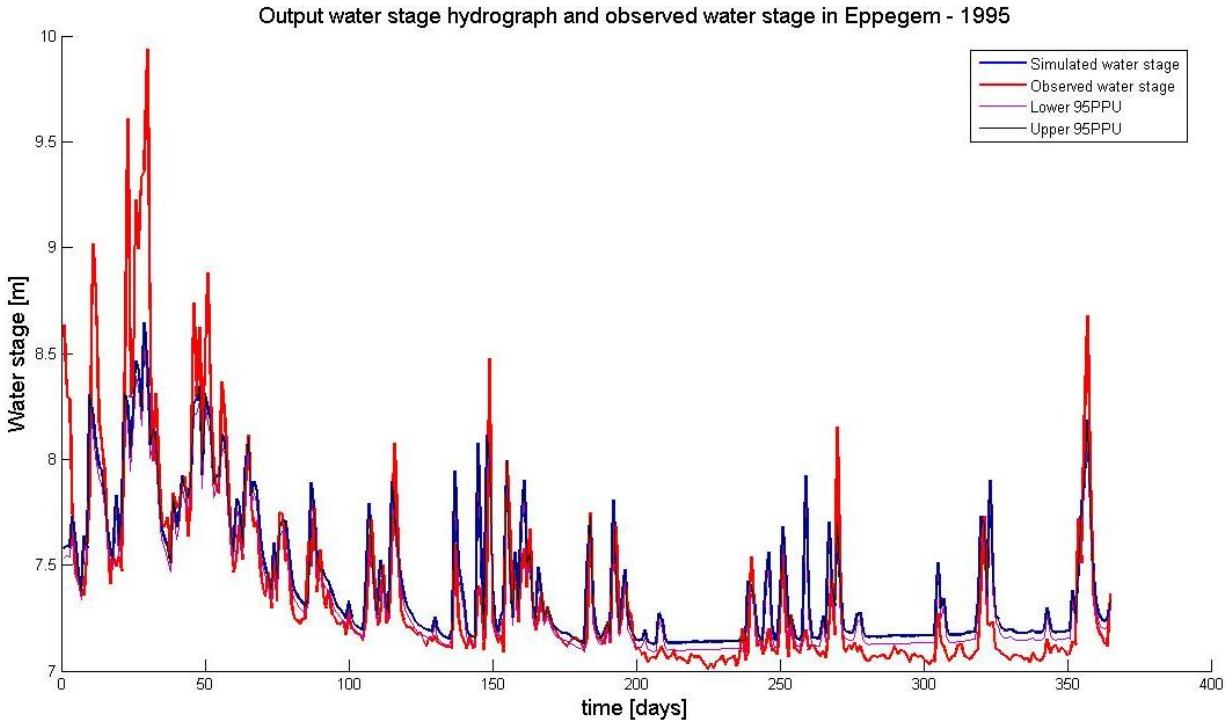

Figure 93 Observed and simulated water stage and uncertainty boundaries due to parameter estimation

The uncertainty boundaries due to parameter uncertainty have been built. The highest value of the width of the boundaries is0.08 m, while the smallest is 0.03 m.

Figure 92 instead shows the best simulation versus the uncertainty boundaries. It can be noticed that, again, a function can be built to represent the boundaries by regression. The equations of the regression lines are reported in table 53.

The model performs well also in the validation period: all the good parameter sets have been used to simulate and validate the model. In table 53 the results

for the validation period are reported in the last column. In figure 91 the hydrograph of the best simulation, the observations and the uncertainty boundaries are represented.

	Calibration	Validation
Minimum value of NSE	-1.30	0.68
Maximmum value of NSE	0.75	0.70
Minimum width of uncertainty boundaries [m]	0.03	0.03
Maximum width of uncertainty boundaries [m]	0.08	0.09
r-factor	0.09	0.13
p-factor [%]	10.41	17.53
Lower 95PPU regression line equation	0.972x+0.16	0.97x+0.173
Coefficeint of determination of lower 95PPU regression line	0.99	0.99
Upper 95PPU regression line equation	x	x
Coefficeint of determination of upper 95PPU regression line	1.00	1.00

Table 53 Results of calibration and validation of the cascading model

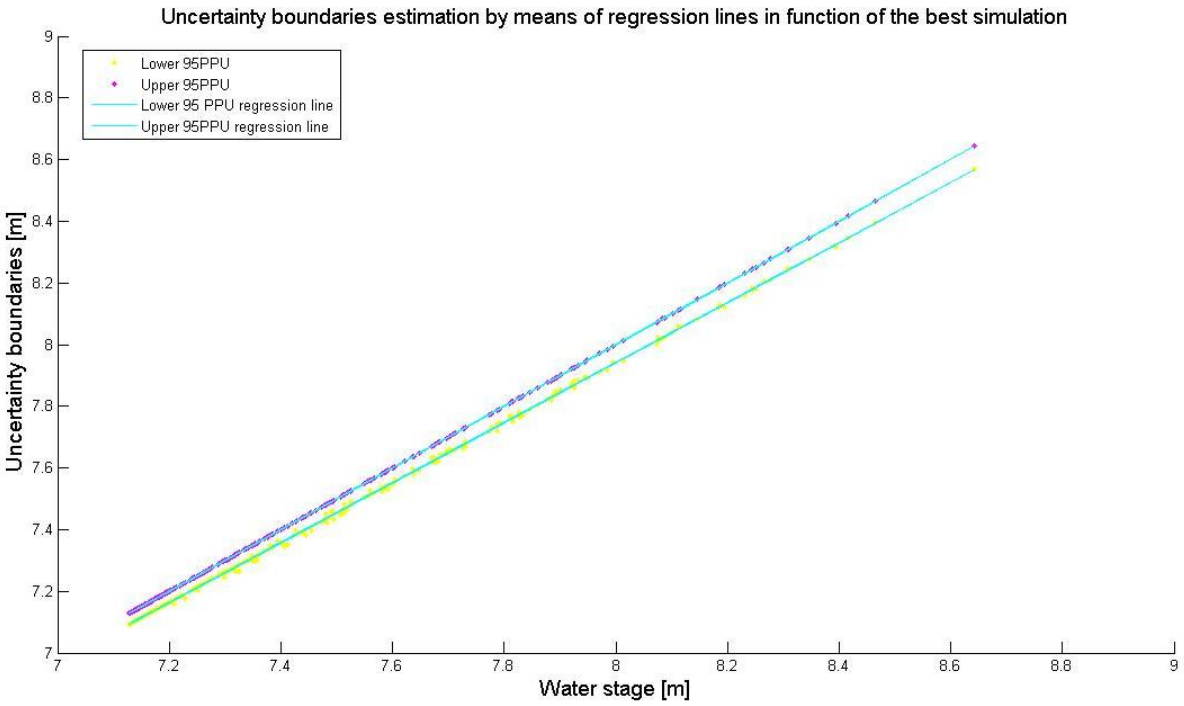

Figure 94 Uncertainty boundaries estimation by means of regression lines

8.2 Uncertainty due to input

As it has been done previously the uncertainty due to the input data has been assessed by simulating the model with an ensemble of input series. Each series has been built from the output of the SWAT model: each series is generated from a different percentile of the distribution of the uncertainty in the SWAT model. Each series has been used to simulate the model with those values of the Manning's coefficient that performed well in calibration. All the simulations have been used to build the uncertainty boundaries.

The updated uncertainty boundaries are wider than those found in the previous step, when evaluating only the uncertainty due to the parameter sets. In figure 93 the simulated and the observed water stage series are represented with the uncertainty boundaries. In figure 94 the uncertainty boundaries versus the best simulation are represented. Also the regression lines are reported. From these two graphs it can be noticed that the boundaries are wider than those found assessing the uncertainty only due to parameters. It can be seen that again the regression fits well the calculated boundaries and that the error in the model is affected by heteroscedasticity: the equations of the regression lines are reported in table 54. They show that the effect of the propagation of the error from the rating curve, through the SWAT model, to the HEC-RAS have important consequences on the reliability of the model.

The table reports also the r-factor and the p-factor. It can be noticed that the r-factor is very high, 0.69 and that the p-factor, the percentage of observations included in the boundaries is quiet high too. Despite that, from figure 93 one could notice that the observations, in the first period, characterized by

important precipitations, the model does not perform well, but the uncertainty boundaries, updated with the uncertainty in the input, include more observations than in the previous step.

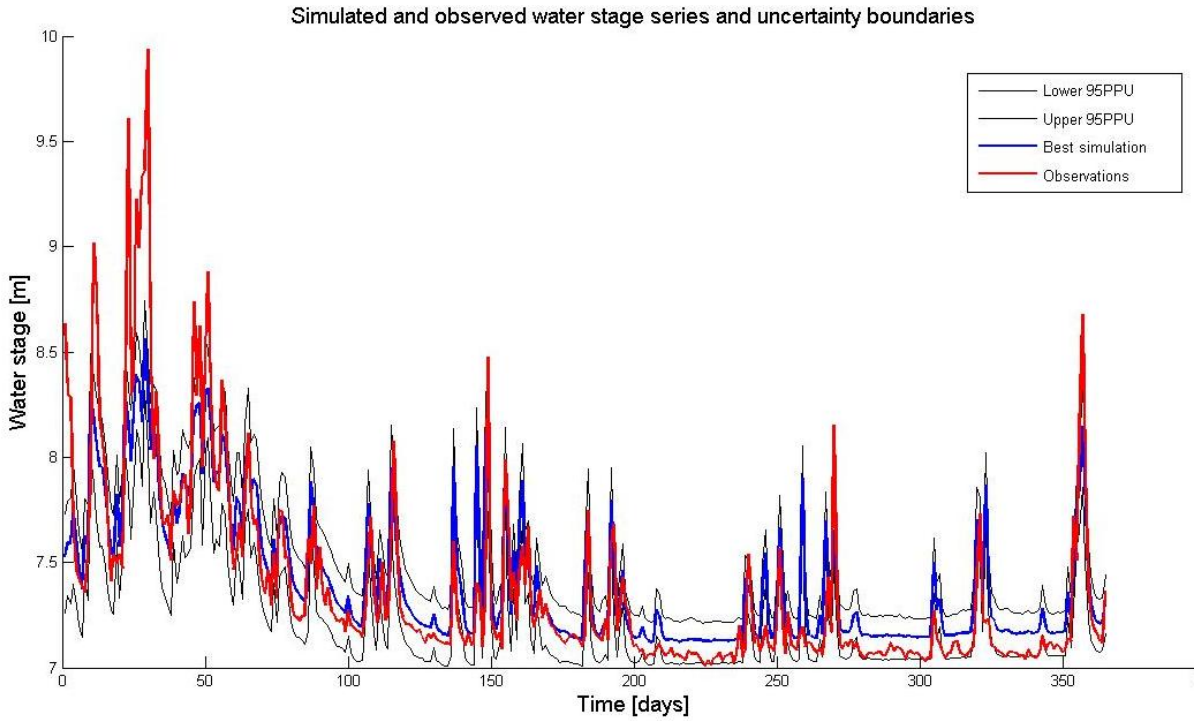

Figure 95 Observed and simulated water stage series and uncertainty boundaries

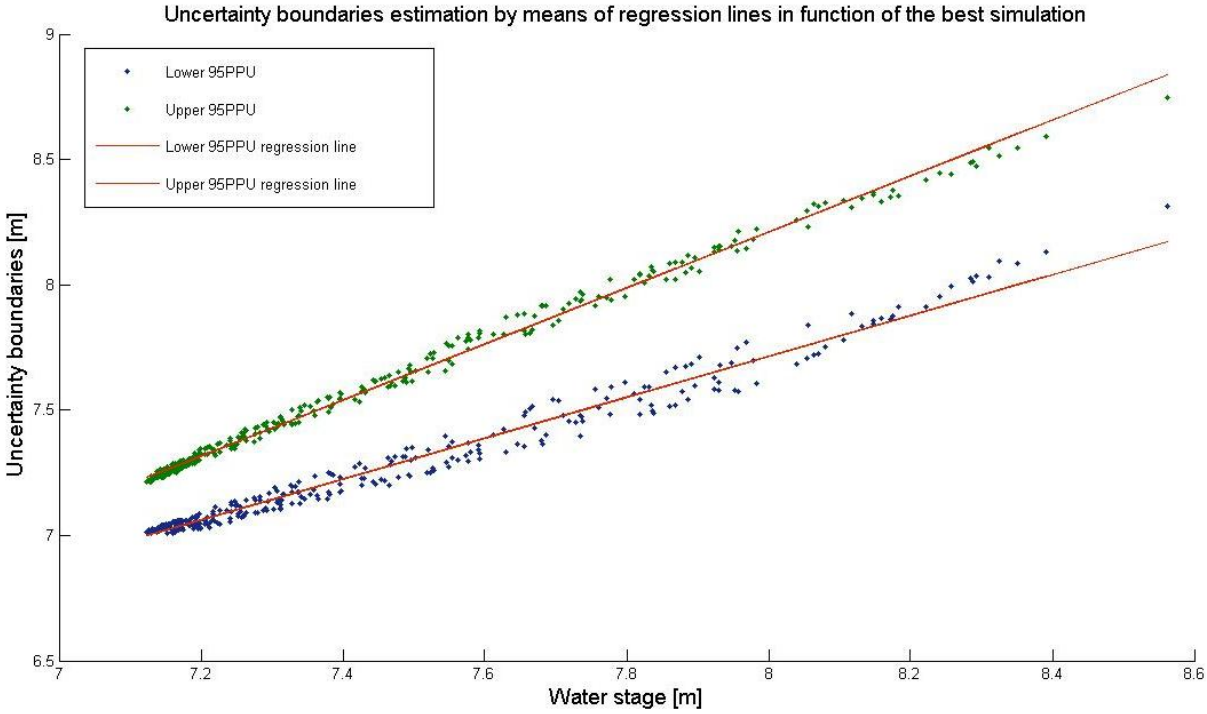

Figure 96 Uncertainty boundaries model by means of regression lines

	Calibration	Uncertainty due to input data
Minimum value of NSE	-1.30	0.55
Maximmum value of NSE	0.75	0.73
Minimum width of uncertainty boundaries [m]	0.03	0.19
Maximum width of uncertainty boundaries [m]	0.08	0.64
r-factor	0.09	0.69
p-factor [%]	10.41	76.99
Lower 95PPU regression line equation	0.972x+0.16	0.82x+1.2
Coefficeint of determination of lower 95PPU regression line	0.99	0.98
Upper 95PPU regression line equation	x	1.12x-0.73
Coefficeint of determination of upper 95PPU regression line	1.00	0.99

Table 54Results of the uncertainty analysis. Comparison with the results of the calibratino

9 Conclusions and recommendations

This study has presented a proposal of procedure for the computation of the uncertainty analysis of a cascade of Rainfall-Runoff and one-dimensional hydraulic models: the Zenne River have been modeled using two different model codes, SWAT and HEC-RAS for two different regions of the river basin. SWAT have been used for that portion of the territory where the influence of the runoff on the stream flow is important, while HEC-RAS has been used to model the last reach of the river, where no runoff is present to feed the streamflow. A third model, KOSIM, has been used to model the city of Brussels. The output of this model has been used to feed SWAT in the subbasins located where the city of Brussels is.

Both the uncertainty due to the parameters of the models and in the input data have been taken into account. The methods used for the calibration and uncertainty analysis computation are the GLUE method (Beven and Binley, 1992), based on the concept of equifinality (Beven, 2006) and ParaSol, an evolutive algorithm, and SUFI2, based on Monte Carlo and Latin Hypercube sampling, both based on the principle of equifinality: due to the uncertainty in the model structure it is impossible to find an optimum parameter set, so a selection of behavioral parameter sets is identified by these procedures. The model is run with many parameter sets and the performance is assessed by means of a goodness of fit index. In this study the Nash Sutcliff coefficient of efficiency has been used. Then a selection criterion is used to identify the behavioral parameter sets.

The input uncertainty has been computed using the same procedure: the input series of the model have been corrupted with an error and the model has been run. Then the performance calculated and the influence of the error on the output of the model analyzed.

The uncertainty in the two models has been at first assessed independently, taking into account for the different sources of uncertainty. An analysis of the influence of the input error over the behavior of the parameter sets could be done. The uncertainty boundaries of the SWAT model show that, for this type of model, the variance in the output value is heterogeneous and that grows with the value of the computed output. In particular linear regression curves could be computed to represent the growth of the 95% prediction uncertainty boundaries. The width of the uncertainty boundaries grows with the entity of the error. In particular the error affecting the rating curve with normal distribution around the flow value has very important influence over the width of the uncertainty boundaries. The representation of the uncertainty boundaries by means of regression curves in function of the best simulation is an effective and simple way of representing the uncertainty of the model. The distribution of the uncertainty boundaries computed, furthermore, permits to build an ensemble of output series, each from a different percentile of the distribution. These series permit to propagate in a simple way the uncertainty from one model to the other: by simulating the downstream model with all the output series generated, many behavioral parameter sets for the downstream model can be identified and by means of them new uncertainty boundaries can be drawn, taking into account for the uncertainty generated by the parameter sets and by the cascade of models.

Finally the uncertainty of the cascade of models is computed feeding the downstream model (HEC-RAS) with the output of the upstream model (SWAT). A new calibration of the model is done feeding the model with the best simulation output provided by the SWAT model, then an uncertainty analysis due to input error is performed feeding the HEC-RAS model with different input series, each with the same probability of occurrence, generated using the percentiles of the distribution of the SWAT model output, calculated in the previous step. The influence of the parameter and input uncertainty in the upstream model results in new behavioral parameter sets.

It has been also analyzed the effect of the input uncertainty over the Manning's roughness coefficient in the hydraulic model HEC-RAS. It has been concluded that small errors within the range of 5% of the flow value, do not affect the performance of the model and the choice of the behavioral roughness. For greater errors, the value of the behavioral roughness changes sensitively.

The uncertainty assessment is a very complex issue: due to lack of time many sources of uncertainty and other analysis could not be done. According to this some recommendations must be done, in order to suggest future studies to make a more complete analysis:

1. Uncertainty over the system structure, that is the uncertainty in the functioning of the connections between the Zenne River and the canal Brussels-Charleroi, must be reduced. Information about the functioning of these connections is fundamental in order to make a proper model of the entire system.
2. One of the most important sources of uncertainty for hydrological models was not taken into account because of lack of data: the uncertainty in precipitation and in precipitation spatial distribution. Future studies should take into account for this important source of uncertainty.
3. Another important source of uncertainty to be analyzed is the change in land use for the hydrological model and the influence of spatial resolution of the input maps on the hydrological model.
4. HEC-RAS computations are very time consuming and output files are very space consuming: the computation of a 15 days event with 20 seconds time step and hourly output needs approximately 5 minutes and the result of 5300 simulations occupies approximately 500 giga bytes. One of the main reasons is the number of cross sections used to model the river. A sensitivity analysis of the model due to the change in the number of cross sections should be performed, so that the minimum number of cross necessary for good performance can be found.
5. The SWAT model works on daily time step and provides daily output, while the HEC-RAS model works with different time steps (in this study, 20 seconds) and provides output with different time steps (in this study, 1 hour). The cascade of models has been made feeding the HEC-RAS model with the daily average flow value provided by SWAT and analyzing the daily average output value. A new analysis of the cascade of model uncertainty should be performed again with new codes of SWAT that work with hourly or sub-hourly time step, and that are being developed nowadays.

BIBLIOGRAPHY

Abbaspour, K.C., J. Yang, I. Maximov,., R. Siber, K. Bogner, J. Mieleitner, J. Zobrist, R. Srinivasan. 2007. Modeling hydrology and water quality in the pre-alpine/alpine Thur watershed using SWAT. *Journal of Hydrology,* 333:413-430.

Abbaspour, K.C., Johnson, A., van Genuchten, M.Th, 2004. Estimating uncertain flow and transport parameters using a sequential uncertainty fitting procedure. Vadose Zone Journal 3(4), 1340-1352.

Bates, P.D. and de Roo, A. P. J., 2000. A simple raster-based model for flood inundation simulation. *J. Hydrol.*, 236, 54-77.

Bauwens, W. (ed.), 1992. Studie voor het beheer en de modellering van het toekomstig waterbehandelingssysteem van Brussel Noord, Report for the Government of the Brussels' Region, Laboratory of Hydrology, Vrije Universiteit Brussel.

Bauwens, W., 2009. Towards the "good ecological status" in the river Zenne: re-evaluating Brussels' wastewater management, The Zenne river system. Impulse Programme, Project GESZ. The Vrije Universiteit Brussel and the Université Libre de Bruxelles.

Beck, M.B., 1987. Water quality modeling: a review of the analysis of uncertainty. *Water Resour. Res.* 23 (8), 1393–1442.

Beven, K., 1989. Changing ideas in hydrology - the case of physically-based models. Journal of hydolo. , 105, 157-172.

Beven, K.J. and Binley, A.M., 1992. The future of distributed models: model calibration and uncertainty prediction, Hydrological Processes, 6, p.279–298.

Beven, K. J.: A manifesto for the equifinality thesis, J. Hydrol., 320, 18–36, 2006.

Carpenter, T. M., Georgakakos, K. P., 2004. Impacts of parametric and rainfall uncertainty on the ensemble streamflow simulation of a distributed hydrologic model. *Journal of Hydrology,* 298 (2004) 202–221

Chaubey, I., Haan, C.T., Grunwald, S. and Salisbury, J.M., 1999. Uncertainty in the models parameters due to spatial variability of rainfall. *J. Hydrol.* **220**, pp. 46–61. Cosyn, J., 1983. Waterbeheersingswerken in de Zennevalei afwaarts van Brussel, Water nr. 9, p. 48-55.

Cullen, A.C., Frey, H.C., 1999. Probabilistic techniques in exposure assessment, A Handbook for Dealing with Variability and Uncertainty in Models and Inputs. Plenum Press, New York, London. 335 pp.

de Roo, A.P.J., 2000. LisFlood: A rainfall-runoff model for large river basins to assess the influence of land use changes on flood risk.

de Roo, A., Odijk, M., Schmuck, G., Koster, E. and Lucieer, A. (2001). "Assessing the Effects of Land Use Changes on Floods in the Meuse and Oder Catchment", *Physics and Chemistry of the Earth, Part B – Hydrology, Ocean and Atmosphere*, 26, 593–599.

Di Baldassarre G., Montanari A., 2009. Uncertainty in river discharge observations: a quantitative analysis. *Hydrol. Earth Syst. Sci*., 13, 913-921, 2009. www.hydrol-earth-syst-sci.net/13/913/2009

Duan, Q., Sorooshian, S. & Gupta, V. K. (1994) Optimal use of the SCE-UA global optimization method for calibrating watershed models. *J. Hydrol.* 158, 265-284.

Gassman P. W., Reyes M. R., Green C. H., Arnold J. G., 2007. The soil and water assessment tool: historical development, applications, and future research directions. *Transactions of the ASABE*. 50(4): 1211-1250

Georgakakos, K.P., Carpenter, T.M., 2003. A methodology for assessing the utility of distributed model forecast applications in an operational environment, In: Tachikawa, Y., Vieux, B.E.,

Harmel R.D., Cooper R.J., Slade R.M., Haney R.L., Arnold J.G., 2006. Cumulative uncertainty in measured streamflow and water quality data for small watershed. *Transactions of the ASABE*. 49(3):689-701.

Harmel R.D., Smith P.K., 2007. Consideration of measurement uncertainty in the evaluation of goodness-of-fit in hydrologic and water quality modeling, *Journal of Hydrology* (2007), 337, 326-336

Helton, J.C. and F.J. Davis. (2003). Latin hypercube sampling and the propagation of uncertainty in analyses of complex systems. *Reliability Engineering and System Safety* 81: 23-69.

Hiver, J., 1979. Applications de la télémesure et de la gestion sur le bassin de la Zenne (Troisième cycle en hydrorlogy: mesures, modèles et gestion en temps réel), Laboratoire de Recherche Hydraulique à Châtelet, pp. 21.

Holland, J.H., 1975. Adaptation in Natural and Artificial Systems. *The University of Michigan Press*, Ann Arbor, MI, 183 p.

Kelly, K.S. and Krzysztofowicz, R. (1997). "A Bivariate Meta-Gaussian Density for Use in Hydrology," *Stochastic Hydrology and Hydraulics*, 11(1), 17–31.

King, K.W., Arnold, J.G., Bingner, R.L., 1999. Comparison of Green-Ampt and curve number methods on Goodwin creek watershed using SWAT. Transactions of the ASAE 42(4), 919–925.

Legates, D.R., McCabe Jr., G.J., 1999. Evaluating the use of ‘‘goodness-of-fit’’ measures in hydrologic and hydroclimatic model validation. Water Resour. Res. 35 (1), 233–241.

Lei, J.H. and Schilling, W., 1996. Preliminary uncertainty analysis – a prerequisite for assessing the predictive uncertainty of hydrologic models. *Wat. science & techn*, 33 – 2.

Lenhart, T., Eckhardt, K., Fohrer, N., Frede, H.-G, 2002. Comparison of two different approaches of sensitivity analysis. *Physics and Chemistry of the Earth*, 27 (2002) 645-654.

Merz, B., Thieken, A., 2005: Separating aleatory and epistemic uncertainty in flood frequency analysis. Journal of Hydrology, 309(1-4), 114-132, doi:10.1016/j.jhydrol.2004.11.015

Montanari, A. and Brath, A. 2004. “A Stochastic Approach for Assessing the Uncertainty of Rainfall-Runoff Simulations,” *Water Resources Research*, 40, W01106.

Moriasi, D.N., Arnold, J.G., Van Liew, M.W., Bingner, R.L., Harmel, R.D., Veith, T., 2007. Model evaluation guidelines for systematic quantification of accuracy in watershed simulations. Trans. ASABE, 50(3): 885−900.

Neitsch, S.L., Arnold J.G., Kinry J.R. and Williams, J.R.. 2005. Soil and Water Assessment Tool. User's Manual. USDA, Agricultural Research Service and Blackland Research Center, Texas A&M University, USA.

Nelder, J.A. and Mead, R., 1965. A simplex method for function minimization, *Computer Journal*, 7, 308-313.

Pappenberger, F., Beven, M.,Horritt, S.,Blazkova, 2005 “Uncertainty in the calibration of roughness parameters in HEC-RAS using inundation and downstream level observaitons". Journal of Hydrology 302 (2005) 46-69.

Pappenberger, F., Beven, K.J.,Hunter, N.,Gouweleeuw, B., Bates, P., de Roo, A. and Thielen, J., 2005 “Cascading model uncertainty from medium range weather forecasts (10 days) through a rainfall-runoff model to flood inundation predictions within the European Flood Forecasting System (EFFS)”. *Hydrology and Earth System Science*, 9(4), 381-393.

Petersen-Øverleir, Asgeir(2006) 'Modelling stage—discharge relationships affected by hysteresis using the Jones formula and nonlinear regression / Modélisation des relations hauteur—débit affectées par de l'hystérésis en utilisant la formule de Jones et la régression non-linéaire', Hydrological Sciences Journal, 51: 3, 365 — 388

Petersen-Øverleir, A. Accounting for heteroscedasticity in rating curve estimates, J. Hydrol., 292, 173–181, 2004.

Sharpley, A.N., Kleinman, P.J.A., McDowell, R.W., Gitau, M., Bryant, R.B., 2002. Modeling phosphorus transport in agricultural watersheds: processes and possibilities. *J. Soil Water Conserv*. 57 (6), 425–439.

Shrestha, D. L. and Solomatine, D. P.: Data-driven approaches for estimating uncertainty in rainfall-runoff modelling, Int. J. River Basin Management, 6, 109–122, 2008.

US Army Corps of Engineers, HEC-RAS Hydraulic Reference Manual, Institute for Water Resources, Hydrologic Engineering Center, March 2008.

van Griensven, A. Developments towards integrated water quality modeling for river basins. Phd, Free University of Brussels, 2002.

van Griensven, A. and Bauwens W., 2001. Integral modeling of catchments. *Water Science abd Technol.,* 43(7), 321-328, 2001.

van Griensven A. and Meixner T. (2006). Methods to quantify and identify the sources of uncertainty for river basin water quality models, Water Sci. Technol., 53(1), 51-59.

van Griensven A., Meixner, T., Grunwald S., Bishop, T., Di Luzio, M. and Srinivasan, R. (2006). A global sensitivity analysis method for the parameters of multi-variable watershed models, J. Hydrol., 324(1-4), 10-23.

Yu, P.-S., Yang, T.-C., Chen, S.-J., 2001. Comparison of uncertainty analysis methods for a distributed rainfall-runoff model. *Journal of Hydrology,* 244(2001) 43-59.

Willmott, C.J., 1981. On the validation of models. Phys. Geograph. 2 (2), 184–194.